

EXPRESSION ANALYSIS OF THE REGENERATING UTRICLE SENSORY EPITHELIA:
FROM MICROARRAYS TO PARSING PATHWAYS

APPROVED BY SUPERVISORY COMMITTEE

Michael Lovett, Ph.D.

David Russell, Ph.D.

Deepak Srivastava, M.D.

Andrew Zinn, M.D., Ph.D.

*In memory of my mother
for expecting the most of me, but never pressuring me to be different from who I am*

*To my family
for all their support*

&

*To my wife
for always being there for me*

EXPRESSION ANALYSIS OF THE REGENERATING UTRICLE SENSORY EPITHELIA:
FROM MICROARRAYS TO PARSING PATHWAYS

by

RAYMOND DAVID HAWKINS

DISSERTATION

Presented to the Faculty of the Graduate School of Biomedical Sciences

The University of Texas Southwestern Medical Center at Dallas

In Partial Fulfillment of the Requirements

For the Degree of

DOCTOR OF PHILOSOPHY

The University of Texas Southwestern Medical Center at Dallas

Dallas, Texas

June, 2005

Acknowledgments

I want to thank all the people who have been there as I have traveled, literally, through graduate school. I would like to thank all the previous members from the Dallas group, but especially Andy Simmons, Dan Ratcliff, and Maurice Musy for helping me find my way around a research laboratory. After relocating to St. Louis, Bonnie Tam and Rose Tidwell, who actually helped me find a home, along with Rose Veile made me feel at home. Those three women along with Stavros Bashiardes and Yulia Kourshunova made up the core of our group as the lab got off to a new start. I thank them for all their support, their antics, and their camaraderie. More specifically, I would like to thank Stavros for all his help. We put in a lot of time establishing a microarray system in the lab, which meant a lot of late nights and early mornings. It was nice to have someone to commiserate with. I would also like to extend my thanks to other members of the lab, David Messina, Samin Sajan, David Alvarado, Veena Bhonagiri, Julia Winston, and Cindy Helms. They have all been very helpful with the research presented here, whether in scientific discussion, help analyzing my data, or discussing anything but science. All these people have made my stay in the Lovett Lab a very enjoyable one.

This brings me to my biggest debt of gratitude, which is owed to my mentor Michael Lovett. Working for Mike has been a great experience, and I would like to thank him for being a true mentor. He didn't just teach me how to think about and do an experiment, but allowed me to learn from failures as well as my successes. The latter being a case that I think is often

overlooked, as many only see your accomplishments as something that was expected of you. My most unfortunate graduate school experience has been knowing so many students who were unhappy about what they were doing, or at the least, they did not want to continue working in the same level of academia in which they were trained. However, when my projects were at their lowest, I always left Mike's office inspired to move forward, never told to move forward. I will miss those great anecdotal stories about successes and failures in science, as well as life. Mike has always allowed for (or demanded) a fun lab environment; from the occasional practical joke, to usurping our lab supplies for an "arts & craft day", to beer and food at journal club, and where else can you get your own lab T-shirt? I will take with me many valuable lessons about science; doing research, drafting manuscripts, giving talks, the politics of science. I am not only proud, but excited about the things I have accomplished during my dissertation research, and I look forward to expanding my knowledge as well as applying it.

I would like my family to know how much I appreciate all their love, their support, and their confidence in me. Finally, I would like to thank my wife from the depths of my heart for always being there for me through this whole process. I know it wasn't always easy, especially when I relocated to St. Louis and she was still in Dallas. She is a significant force behind all that I have accomplished.

EXPRESSION ANALYSIS OF THE REGENERATING UTRICLE SENSORY EPITHELIA:
FROM MICROARRAYS TO PARSING PATHWAYS

Publication No. _____

Raymond David Hawkins, Ph.D.

The University of Texas Southwestern Medical Center at Dallas, 2005

Supervising Professor: Michael Lovett, Ph.D.

I have used a human transcription factor microarray developed in the laboratory of Dr. Michael Lovett to study gene expression differences in the chicken inner ear sensory epithelia. In the initial study, the sensory epithelium from the utricle was compared to that of the cochlea. The purpose of this study was to identify gene expression differences between these two organs. The sensory epithelium from each organ is made up of hair cells and supporting cells. These hair cells are necessary for the detection of sound in the cochlea and for the detection of movement and acceleration in the utricle. The chicken sensory epithelia is of great research interest as it possesses the ability to fully regenerate hair cells that are damaged, whereas mammalian epithelia, once damaged, cannot regenerate. These two organs were compared because the utricle is in a constant state of hair cell turnover, and the cochlea remains quiescent, unless damaged. In order to carry out such microarray expression studies on a small number of cells, between 30,000-50,000 cells, a micro-cDNA amplification method, developed in the lab, was implemented and is described here as well. The experiments were carried out via cross-species

hybridizations, and subsequently, a number of genes were validated by quantitative PCR and *in situ* analysis. Additionally, a library subtraction was used to identify additional genes expressed in the utricle sensory epithelia.

In a second microarray expression study, the utricle sensory epithelia was damaged by two independent methods and allowed to recover for various time points for expression profiling on the same transcription factor array. The first method of damage was by laser microbeam to ablate the hair cells such that they die almost instantly. The second method of damage was using ototoxic antibiotics. In each time course, the time points were compared to time matched control epithelia (undamaged). The analysis of this data reveals some very important signaling cascades and developmental pathways involved in hair cell regeneration.

Finally, in an effort to functionally validate many of the genes identified during regeneration, gene transcripts were targeted by RNA interference to reduce the expression level and determine the effect on hair cell proliferation. Through this method, several genes were identified to reduce proliferation. Additionally, these experiments were profiled as a means for networking genes into pathways by identifying putative downstream targets in the expression data. An intersection of genes downregulated following inhibitory experiments reveals how several genes potentially lie downstream of one another and form a pathway containing some common regulatory elements.

Table of Contents

Chapter One: Inner Ear Development and Hair Cell Regeneration	1
Development	6
Developmental anatomy of AHCs	6
Notch Signaling	7
Math1	9
Cyclin Dependent Kinase Inhibitors	12
Pax-Eya-Six-Dach genes	12
Genes that affect Planar Cell Polarity	13
Hair cell maintenance	13
Ion flux	14
Stem cells	17
Genomic approaches to AHC function	18
Future Directions	19
Regeneration	20
Mitogenic Factors	24
Conclusion	27
 Chapter Two: Utricle-Cochlea Microarray Comparisons	 29
Introduction	30
Results	31
Feasibility and Design	31
Inner ear microarray	31
Preparation of target	32
Quantitative PCR	34
<i>In situ</i> hybridization and immunohistochemistry	34
The transcription factor microarray	38
Conclusion	46

Chapter Three: Utricle-Cochlea Library Subtraction	52
Introduction	53
Results	55
Subtraction Scheme	55
Primary subtraction	58
Reiterative subtraction	60
Sequence analysis	61
Conclusion	66
Subtraction efficiency	66
Interesting genes present in the subtracted library	67
 Chapter Four: Utricle Sensory Epithelia Time Courses of Regeneration	 71
Introduction	72
Results	73
Array analysis	74
Venn Diagrams: Genes that are "on"	75
Neomycin time course	78
Laser time course	80
Pathways	81
Commonalities	92
Conclusion	95
 Chapter Five: Functional Genomics: siRNA, Inhibitors, & Network Profiling	 99
Introduction	100
Proliferation Results	101
Beta-Catenin siRNA	101
JUND siRNA	106
96-well RNAi	107
JNK inhibitor	109
Expression Profile Results	114
Conclusion	123

Chapter Six: General Conclusions	127
 Chapter Seven: Materials and Methods	132
Sensory epithelia isolation	133
Antibiotic treatment	133
Laser microbeam ablation	134
Total RNA isolation	134
mRNA isolation, cDNA synthesis, and amplification	135
Micro-cDNA library construction	140
In vitro transcription	141
Target labeling	142
Microarray hybridizations	142
Microarray slide processing and printing	143
Design of custom cDNA and oligonucleotide microarrays	143
Quantitative PCR	145
In situ hybridizations and immunohistochemistry	146
Data analysis	147
Subtraction target preparation	153
Driver preparation	153
Subtraction hybridization	154
Subtraction target isolation after hybridization	155
Partial repair of ssDNA for transformation	155
Reiterative subtraction	156
Sequence analysis	156
siRNA generation	157
 Appendix	158
 References	197

Prior Publications

Lai, J.Y., Yu, J., **Hawkins, R.D.**, and Falck, J.R. (1995) Two-Carbon elongation/annulation of alcohols to nitriles. *Tetrahedron Lett.* 36: 5691-5694.

Hawkins, R.D., Bashiardes, S., Helms, C.A., Hu, L., Saccone, N.L., Warchol, M.E., and Lovett, M. (2003) Gene expression differences in quiescent versus regenerating hair cells of avian sensory epithelia: implications for human hearing and balance disorders. *Hum Mol Genet.* 12: 1261-1272.

Hawkins, R.D., and Lovett, M. (2004) The developmental genetics of auditory hair cells. *Hum Mol Genet.* 13 Spec No 2: R289-296.

Figures and Tables

Figure 1-1	Developmental anatomy of the mouse inner ear	4
Figure 1-2	Cross-sectional view of the macula within the utricle	5
Figure 1-3	The Notch and Math1 phenotypes of various knockdowns, knockouts, or overexpression constructs	8
Figure 1-4	The Notch and Math1 signaling cascades	11
Figure 2-1	BMP4, GATA3, GELSOLIN, and KIT RNA <i>in situ</i> hybridizations	36
Figure 2-2	Immunohistochemical staining with a GATA3 antibody	37
Figure 2-3	Differentially expressed TFs as candidate deafness loci	48
Table 2-1	Genes from the inner-ear array	33
Table 2-2	The 78 most significant changes in TF gene expression ranked by P-value	40
Table 2-3	The 50 highest changes in TF gene expression ranked by microarray fold changes	42
Table 2-4	TFs on in both the cochlea and utricle SE	43
Table 2-5	TFs uniquely on in the cochlea or utricle SE	45
Figure 3-1	Library Subtraction Flow Diagram	57
Figure 3-2	<i>GAPDH</i> Distribution	59
Figure 3-3	Database Venn Diagrams	64
Figure 3-4	Comparison of libraries for uniqueness	65
Table 3-1	<i>GAPDH</i> Distribution	60
Table 3-2	Reiterative Subtraction Enrichment	61
Figure 4-1	Venn diagrams illustrating the number of genes "on" at each time point	77
Figure 4-2	Array-qPCR comparisons for beta-catenin, KIAA0173, and TRIP15	80
Figure 4-3	Self-Organizing Maps	83

Table 4-1	Microarray validation by qPCR	79
Table 4-2	Cell Cycle - Proliferation affiliated TFs	85
Table 4-3	Apoptosis affiliated TFs	86
Table 4-4	List of genes differentially expressed during regeneration linked to TGF β signaling	88
Table 4-5	List of genes differentially expressed during regeneration that are linked to the PAX-EYA-SIX-DACH cascade	91
Table 4-6	Genes differentially expressed in the utricle and cochlea SE following neomycin damage	94
Table 4-7	Genes differentially expressed in the utricle and cochlea SE following laser treatment	94
Table 4-8	Genes differentially expressed in the cochlea and utricle SE and both laser and neomycin treatments	95
Figure 5-1	Increased Proliferation after laser damage	103
Figure 5-2	Beta-Catenin RNAi	104
Figure 5-3	Inhibition of proliferation after laser ablation and RNAi	105
Figure 5-4	Proliferation index for TFs - 96-well format	111
Figure 5-5	PAX2 immunohistochemistry following RNAi in 96-well primary cultures	112
Figure 5-6	JNK Signaling is required for sensory epithelial wound healing	113
Figure 5-7	Genes co-varying with <i>CEBPG</i> during regeneration and <i>CEBPG</i> RNAi	115
Figure 5-8	Venn diagram illustrating genes downregulated in multiple inhibitory treatments	116
Figure 5-9	Signaling/Genetic network of genes downstream of JNK, JUND, and <i>CEBPG</i>	119
Figure 5-10	IRX7 conserved motif	120
Figure 5-11	IRX7 and LRP5 conserved motif	121
Table 5-1	<i>CEBPG</i> siRNA, JUND siRNA, and JNK Inhibitor downregulated commonalities	117

Table 5-2	Genes downregulated following laser ablation and ID1 RNAi	122
Table 5-3	JNK and AP1 (JUN-FOS-ATF) related genes	125
Figure 7-1	Micro-cDNA amplification Part I	137
Figure 7-2	Micro-cDNA amplification Part II	139
Figure 7-3	R-I plots (ratio-intensity) showing the effect of LOWESS Normalization	149
Figure 7-4	Hierarchical Cluster of data from neomycin 24 vs control and neomycin 48 versus control	152

Abbreviations

All transcription factor gene names not found in the Appendix can be found on our website:

<http://hg.wustl.edu/lovet/projects/nohr/TFarray.html>

°C	degrees Celsius
1°	primary
50mer	50 base pair oligonucleotide
aFGF	acidic fibroblast growth factor
AHCs	auditory hair cells
AHL	age-related hearing loss
AP-1	activating protein 1 complex
aRNA	antisense RNA
BDNF	brain derived neurotrophic factor
bFGF	basic fibroblast growth factor
BMP4	bone morphogenic protein 4
bp	base pair
BrdU	5-bromo-2-deoxyuridine
cAMP	cyclic AMP
CDC	cell division cycle
CDH23	cadherin 23
cDNA	complementary DNA
CEBPG	CAAT element binding protein gamma
Ce tag	C. elegans control tag
cfu	colony forming units

chromatin IP	chromatin immunoprecipitation
cRNA	complementary RNA
CX26	connexin 26
Cy(3,5)	Cyanine
dsRNA	double stranded RNA
EGF	epidermal growth factor
EGFR	epidermal growth factor receptor
EGR1	early growth response 1
ES	embryonic stem (cells)
EST	expressed sequence tag
FGF	fibroblast growth factor
FGFR	fibroblast growth factor receptor
GAPDH	glyceraldehyde-3-phosphate dehydrogenase
GER	greater epithelial ridge
GFP	green fluorescent protein
hr	hour
IGF-1	insulin-like growth factor 1
IHCs	inner hair cells
IVT	in vitro transcription
JNK	Jun Kinase
min	minutes
MYAK-S	homolog of yeast protein kinase YAK1
MYO7A	myosin 7a

NCBI	National Center for Biotechnology Information
OHCs	outer hair cells
PCP	planar cell polarity
PCR	polymerase chain reaction
pfu	plaque forming units
PCs	pillar cells
qPCR	quantitative PCR
RNAi	RNA interference
rpm	rounds per minute
RT-PCR	reverse transcriptase PCR
SCs	supporting cells
SE	sensory epithelia
sec	seconds
SEM	scanning electron micrograph
siRNA	small interfering RNA
SNP	single-nucleotide polymorphism
SOM	self-organizing map
ssDNA	single stranded DNA
TFs	transcription factors
TGF α	transforming growth factor alpha
TGF β	transforming growth factor beta
TIGR	The Institute for Genome Research
UDG	uracil DNA glycosylase

USH	Usher's Syndrome
UTR	untranslated region

CHAPTER ONE

INNER EAR DEVELOPMENT AND HAIR CELL REGENERATION

Deafness is the world's second leading handicap with approximately 35 million Americans having some form of hearing loss. This is greater than 10 percent of the population. One in 1000 children are born deaf, and 6 in 1000 are born with some degree of hearing loss (Silverstein et al., 1992; National Institute on Deafness and Other Communication Disorders: <http://www.nidcd.nih.gov/health/statistics/hearing.asp>). Deafness is typically thought of as either hereditary or non-hereditary. Hereditary deafness is divided into 5 Groups: 4 are nonsyndromic; Autosomal Dominant, Autosomal Recessive, X-linked, Mitochondrial, and one Syndromic category (see Hereditary Hearing Loss Homepage (HHH) for categories containing a list of cloned and uncloned loci: <http://webhost.ua.ac.be/hhh/>). Congenital deafness is almost entirely defined as hereditary deafness. However, congenital deafness makes up a small proportion of the deaf and hard of hearing community. To date, 53 human genes have been cloned that cause hereditary deafness. Another 40 loci contain uncloned causative genes. However, the majority of those with hearing deficits suffer from presbycusis, or age-related hearing loss. While there may be a genetic component for susceptibility, it is primarily caused by repeated damage sustained by the hair cells of the inner ear. One in 3 people over the age of 65 suffer from age-related hearing loss. This rises to 1 in 2 over the age of 75 (Davies, 1993). If it were possible to regenerate new hair cells to replace those that have been damaged over the years, then this would be of great clinical and biological interest. Development of potential therapies will require an in-depth understanding of how hair cells (and other components of the inner ear) develop, as well as how other model organisms regenerate their own hair cells.

The cochlea is the hearing organ of the inner ear, and hair cells reside in the organ of Corti (Figure 1-1 C). Hair cells are named so for the stereocilia that protrude from the cell body. The stereocilia are mechano-electrical transducer that convert movement to an electrical impulse

that is sent to the brain through the VIIIth cranial nerve (for review see Hudspeth, 1997). Sound waves travel through the outer ear and vibrate the tympanic membrane (eardrum). The sound is relayed to the cochlea in the inner ear by vibration carried through the three bones of the middle ear. As the stapes moves it vibrates the membrane covering the round window of the cochlea. As sound wave vibrations move through the fluid-filled chamber of the cochlea, the underlying basal membrane vibrates. The membrane underlies the supporting cells and hair cells that make up the sensory epithelia of the organ of Corti. Overlying the stereocilia of the auditory hair cells is the tectoral membrane. Vibration of the basal membrane causes the stereocilia to move against the tectoral membrane. This deflection of the stereocilia, in turn leads to the opening of ion channels that allow an influx of ions (potassium), sending an electrical impulse through the afferent nerve attached to the base of each hair cell. There are two types of hair cells in the cochlea. The inner hair cells are a single row that serve as the primary "hearing cells" and are highly innervated. The three rows of outer hair cells act as amplifiers. As one moves from the base of the cochlea to the apex, hair cells change in length. The length is proportional to the frequency they detect, where the shorter the hair cell the higher the frequency it detects. Hair cells at the base detect high frequencies and those at the apex detect low frequencies.

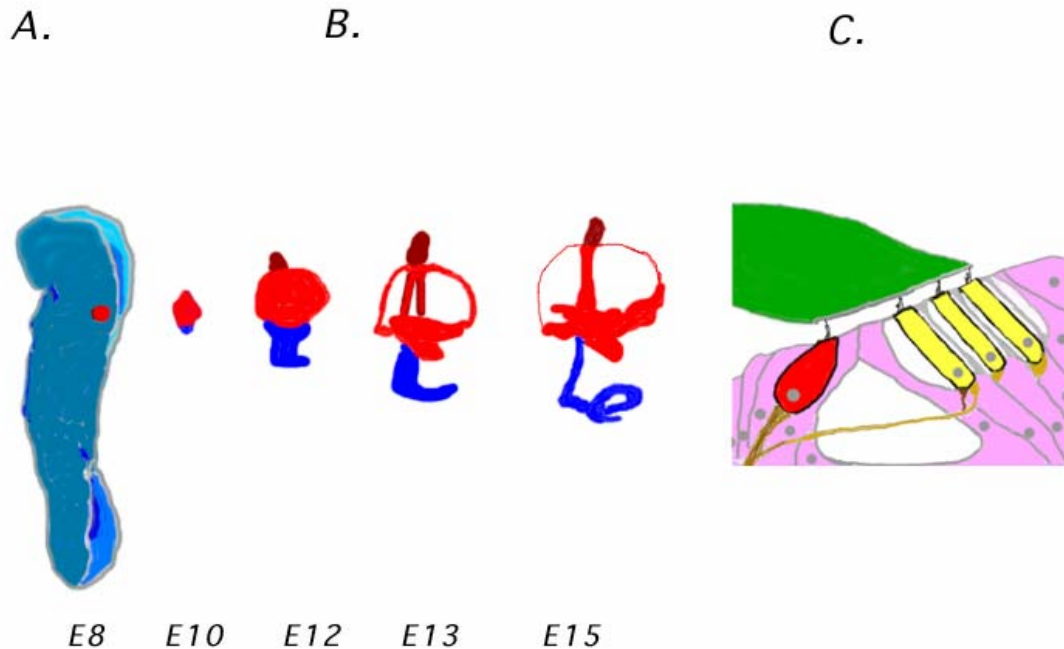


Figure 1-1. Developmental anatomy of the mouse inner ear. **A** shows a diagram of an embryonic day 8 mouse embryo. All of the structures of the inner ear arise from a small ectodermal thickening (the otic placode) shown highlighted in red. **B** shows diagrams of the structure of the dissected inner ear at days 10 through 15 of embryogenesis (modified from Morsli et al., 1998). Dorsal is to the top and anterior is to the right. The areas destined to become the cochlea are shown in blue. By E13 hair cells are beginning to differentiate, by E15 they are starting to acquire mechanotransduction capabilities. **C** shows a diagram of part of the organ of Corti within the adult cochlea. Four rows of AHCs are surrounded by supporting cells and have stereocilia imbedded into the overlying tectoral membrane (shown in green). The single row of inner hair cells (IHCs) is shown in red and the three rows of outer hair cells are shown in yellow. Movement of the basilar membrane (triggered by a sound wave) below the hair cells (not shown) results in hair cell movement and stereocilia deflection.

The hair cells of the utricle which detect movement and acceleration of the body work in a similar manner. The utricle is relatively flat compared to the cochlea. The hair cells of this organ are covered by an overlying matrix that stimulates the hair cells upon movement (Figure 1-2). The matrix contains pebble-like calcium objects called otoconia which are suspended in the gelatinous matrix. Again, there are two types of hair cells in the utricle, Type I and Type II, defined by their types of innervations (Jorgensen and Christensen, 1989).

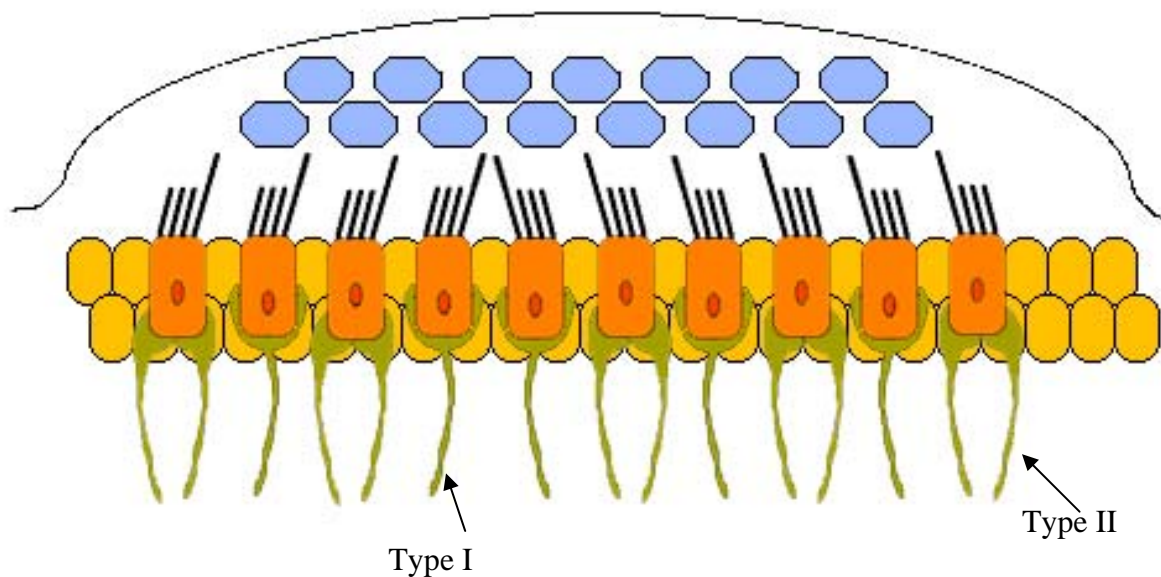


Figure 1-2. Cross-sectional view of the macula within the utricle. Hair cells are shown in orange. Type I and Type II hair cells are distinguished by their innervation (green). Type I hair cells have a nerve calyx. Type II hair cells have a afferent and efferent nerve. Supporting cells surround the hair cells (yellow). Cells are covered by the otolithic membrane. Embedded in the membrane are otoconia (blue). These "stones" are made up of calcium carbonate, the same composition as limestone.

Development

There is a vast literature on the anatomy and developmental genetics of the inner ear. In this section I deal only with those events that appear to directly impact upon auditory hair cell (AHCs) production and maintenance. After a brief description of AHC development, a description is given of some of the known genetic pathways that function in hair cell development and recent insights into how they may fit together. I then discuss attempts to either discover stem cells or engineer embryonic stem (ES) cells towards an AHC fate. Finally, genomics-based approaches to pathway discovery and manipulation of hair cell regeneration are discussed.

Developmental anatomy of AHCs.

Much of our current knowledge of the inner ear is derived from studies in the mouse and chicken (see below). Figure 1 illustrates some of the steps in the developmental anatomy of these complex structures. In the mouse, *bona fide* AHCs are not discernible until quite late in development (~E13) and they acquire mechanotransduction between E16 and E17 (Geloc and Holt, 2003). They arise, as do their surrounding supporting cells (SCs), from a sensory primordium. Eventually, two distinct types of hair cells are formed in the organ of Corti within the cochlea; a single row of inner hair cells (IHCs) and three rows of outer hair cells (OHCs). The hair cells, together with their surrounding supporting cells constitute the sensory epithelia (SE).

In the chicken the arrangement of AHCs and SCs is somewhat different, but the most striking difference in birds (and other lower vertebrates) is that, if their AHCs are damaged, they

can regenerate new ones from a population of supporting stem cells (Cruz et al, 1987; Cotanche, 1987; Warchol and Corwin, 1996). Discovering the molecular basis of this regenerative capability has been a major goal of auditory research for almost two decades.

Notch Signaling

The *Notch* and *Wingless* signaling cascades are important regulators of lateral inhibition. This occurs when one cell sends an inhibitory signal to its neighbor, preventing it from taking on the same fate. Figures 1-3 and 1-4 diagrammatically summarize a large body of work from the late 1990's showing that various components of the Notch pathway are important in AHC development. For example, in the mouse, loss of the *Notch* ligand *Jagged2* leads to two rows of IHCs and four rows of OHCs (Lanford et al., 1999). *Jagged2* appears to be necessary for lateral inhibition in supporting cells, expressing *Notch1*, to prevent the differentiation of excess AHCs. The expression of *Delta1*, another ligand of *Notch*, demarcates those cells that will give rise to differentiating AHCs in chickens and mice (Adam et al 1998, Morrison et al., 1999). *Delta1* expression in these nascent AHCs is eventually lost as the cells commit to their fate. *Delta1* is

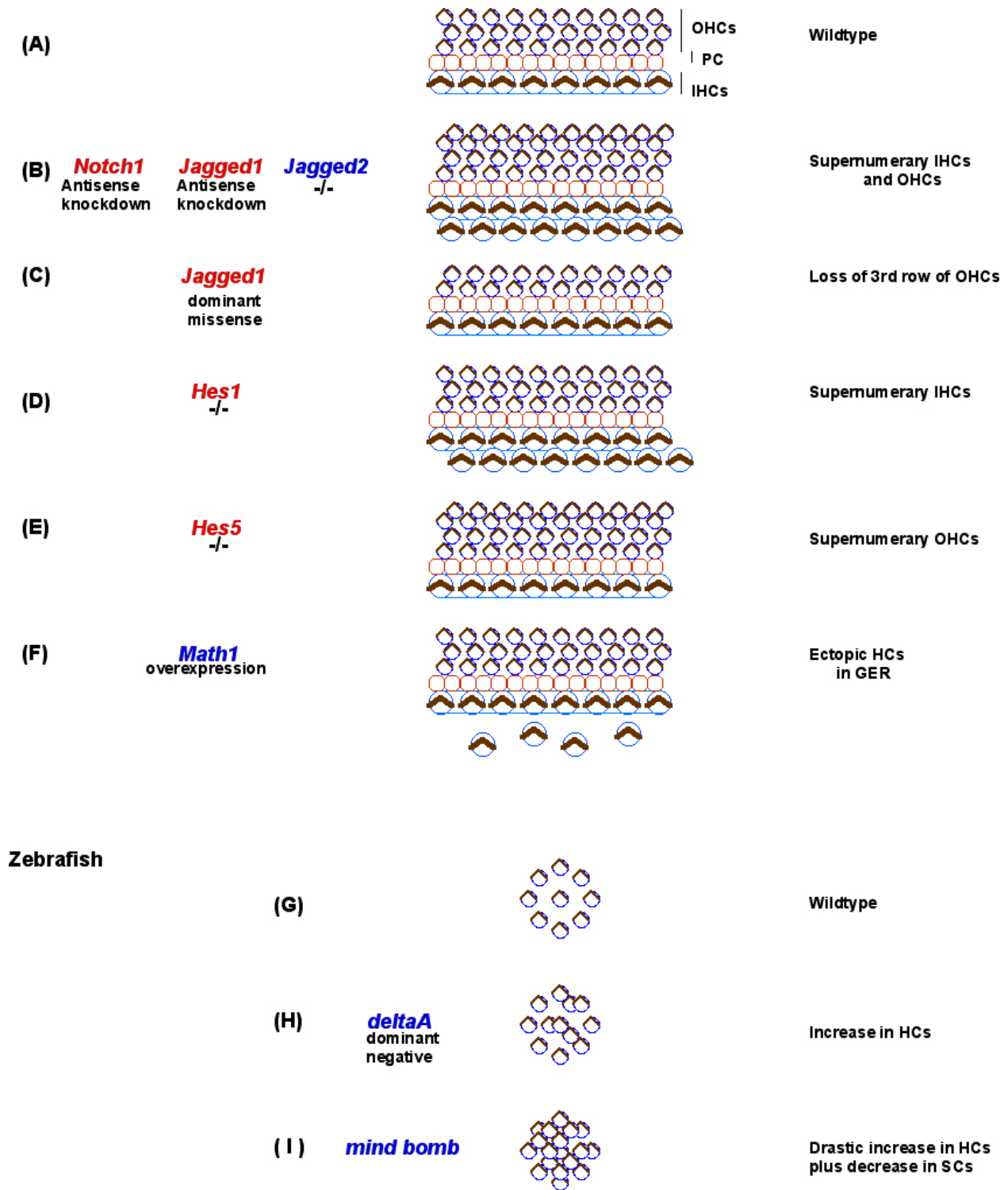


Figure 1-3. The Notch and Math1 phenotypes of various knockdowns, knockouts or overexpression constructs. Figure 1-3 summarizes work on mouse and zebrafish AHC phenotypes. The diagrams show outer hair cells (OHCs), pillar cells (PCs) and inner hair cells (IHCs) as seen from above. **A - F** list the

specific genes and the types of alterations (e.g. -/- indicates a homozygous null). In each case the effect upon AHCs is diagrammatically shown to the right and summarized at the far right. GER is the greater epithelial ridge. Genes are color coded according to the cell type within which they appear to be expressed. Blue is AHC-specific and red is SC-specific. **G - I** diagrammatically illustrate the effects of specific genes on the zebrafish sensory patch of AHCs. References are as follows: *Notch1* and *Jagged1* antisense knockdowns in rat explants cultures (Zine et al., 2000). *Jagged2* homozygous null mice (Lanford et al., 1999). *Jagged1* dominant missense mutation from an ENU screen (Tsai et al., 2001). *Hes1* homozygous null mice (Zheng et al., 2000a; Zine et al., 2001). *Hes5* homozygous null mice (Zine et al., 2001). *Math1* overexpression in rat explant cultures (Zheng et al., 2000b), and adenoviral mediated *in vivo* overexpression in guinea pigs (Kawamoto et al., 2003a). In the zebrafish an increase of hair cells in the sensory patch is seen for dominant negative allele of *deltaA* (Riley et al., 1999) and ten fold more hair cells in the *mind bomb* mutant (Haddon et al., 1998).

also expressed during AHC regeneration in the chicken inner ear (Stone and Rubel, 1999). Recently, Itoh et al., (2003) have added another piece to this complex pathway. They demonstrated that the zebrafish *mind bomb* locus (which affects numbers of hair cells) encodes a ubiquitin ligase that specifically acts upon DELTA1, targeting it for degradation.

Math1

The transcription factor (TF) *Math1* is specifically expressed in developing AHCs. *Math1* knockout mice fail to produce any AHCs (Bermingham et al., 1999). And overexpression of *Math1* leads to supernumerary hair cells. Recent work on the effects of *Math1* in other cell types has provided additional candidate downstream effectors for this pathway. For example, three transcription factors (*Lh2A(LHX2)*, *Lh2B(LHX9)*, and *Barhl1*) are no longer expressed in specific neuronal cell types in *Math1* null mice (Bermingham et al., 2001). The TF *Zic1* was recently shown to act as a repressor of *Math1* in the developing nervous system (Ebert et al., 2003). Additional *Zic* family members (e.g. *Zic2*) are expressed in the inner ear (Warner et al, 2003) and during avian HC regeneration (this thesis, Chapter 4).

Recent evidence indicates that the *Notch* and *Math1* pathways intersect. The TF gene *Hes1* is downstream in the *Notch* pathway (Ohtsuka et al, 1999) and suppresses the *Math1* overexpression phenotype of supernumerary hair cells when it is co-transfected into explants (Zheng et al., 2000b). *Hes1* appears to be a negative regulator of *Math 1*. While loss of *Hes1* leads to an increase in IHCs, loss of *Hes5*, a closely related member of the same TF gene family, leads to an increase in OHCs (Zine et al., 2001). Most recently, Gazit et al., (2004) have directly demonstrated (albeit in a different cell type) that Math1 binds to the *Hes5* promoter, thereby directly tying together these two important pathways. They propose that Math1 activates *Hes5*, which in turn inhibits *Math1* expression (see Figure 1-4).

Zheng and Gao (2000b) first showed that overexpression of *Math1* could lead to ectopic hair cells in rat cochlear explants, at least as measured by surrogate hair cell markers such as Myosin7a or immature stereocilia bundles. More recently, Kawamoto et al., (2003a) have shown that *Math1* overexpression *in vivo* has the same effect in the guinea pig inner ear. This study could not detect whether new hair cells arose in the sensory epithelium, but the putative new hair cells were able to attract axons. These first steps towards inner ear gene therapy are exciting and encouraging and many groups are pursuing these strategies towards eventual hair cell replacement.

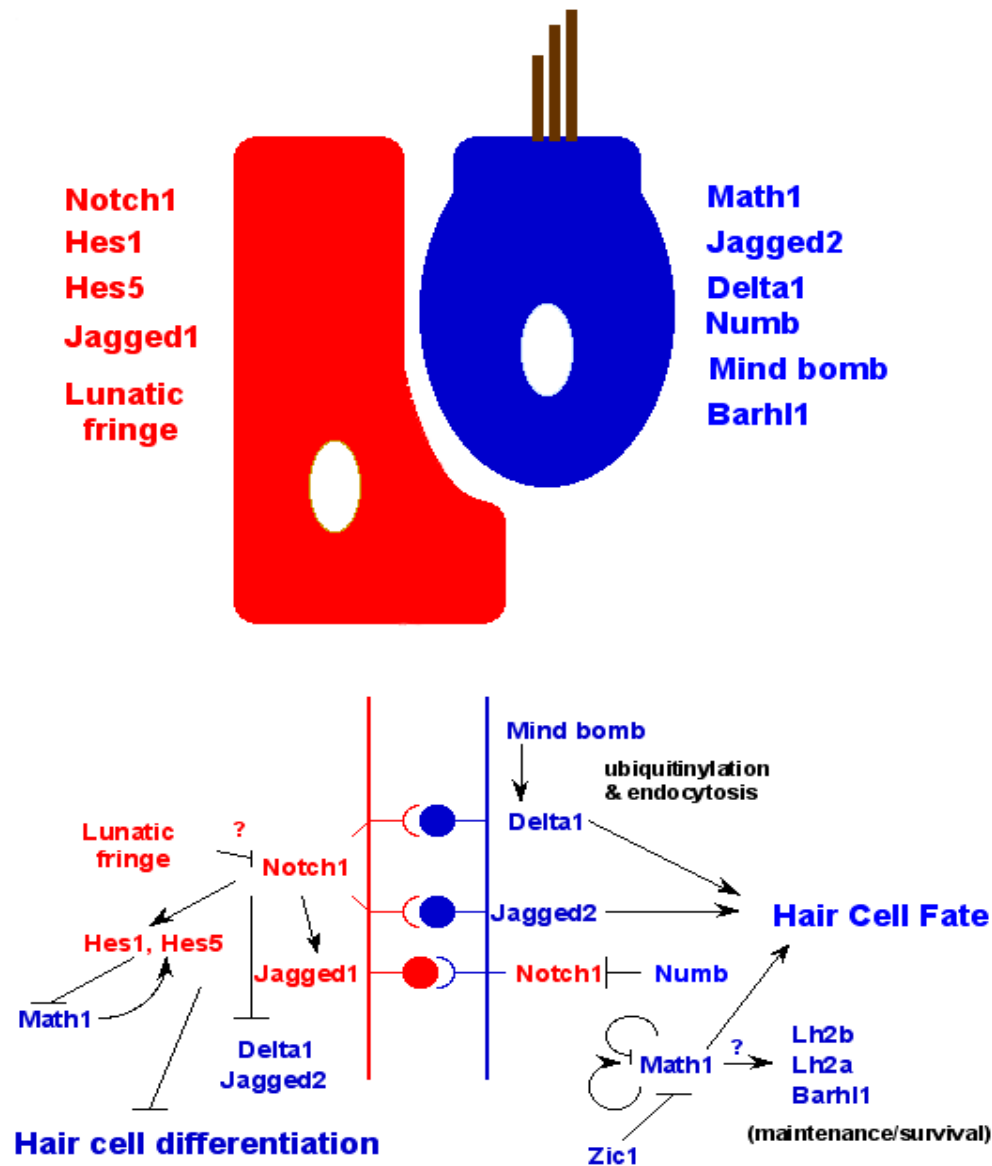


Figure 1-4. The Notch and Math1 signaling cascades. A supporting cell (red) and a hair cell (blue) are diagrammatically illustrated. Next to each cell is a list of color coded genes from the *Math1* or *Notch* pathways that are specifically active in one or other cell type. Shown in the lower part of the figure is a diagram illustrating the various interactions between components of these pathways. Again, the genes are color coded according to cell type. Ligands and receptors are also color coded with the red and blue vertical lines indicating the SC and AHC cell surfaces respectively. Lines ending with an arrow indicate induction, lines ending with a perpendicular line indicate repression. For a detailed review on *Notch1*, its ligands (*Delta1*, *Jagged1*, & *Jagged2*), and effectors (*Hes1* & *Hes5*) see Bryant et al., 2002. See the text for specifics on the interaction between *Math1* and *Notch* pathways. *Math1* is capable of positive autoregulation (Helms et al., 2000) and negative autoregulation (Gazit et al., 2004) and this is shown in the figure. It is also inhibited directly by *Zic1* (Ebert et al., 2003) and either directly or indirectly by *Hes1* and *Hes5* (Zine et al., 2000; Zine et al., 2001; Gazit et al., 2004).

Cyclin Dependent Kinase Inhibitors

Cyclin dependent kinases regulate transition through the cell cycle, while production of cyclin dependent kinase inhibitors (CKIs) leads to an exit from the cell cycle. Exit from the cell cycle coincides with expression of the cyclin dependent kinase inhibitor *P27/Kip1* in the developing mouse organ of Corti between E12 and E14 (Chen and Segil, 1999). *P27/Kip1* appears to be present in SCs, but absent from AHCs. Homozygous *p27/Kip1* knockout mice have supernumerary AHCs (both IHCs and OHCs), but they also retain SCs, indicating that this gene has some role in proliferation (would seem to have a role in suppressing AHCs), but not an absolute role in differentiation. Interestingly, heterozygote *p27/Kip1* knockouts only have additional IHCs. While *p27/Kip1* expression is one marker of SCs in the cochlear sensory epithelia, another cell cycle kinase inhibitor is specific to hair cells. *Ink4d/p19* is expressed in a similar temporal pattern to *p27/Kip1* before AHC and SC differentiation (Chen et al., 2003). However, *Ink4d/p19* knockout mice do not exhibit obvious morphological defects during embryonic development. At about five weeks after birth the mice show signs of progressive hearing loss, caused by AHCs reentering the cell cycle and dying through apoptosis.

Pax-Eya-Six-Dach genes

The *Pax*, *Eya*, *Six* and *Dach* gene families are important in otic development, but defining how they fit together has proved difficult. The recent derivation of *Six1* null mice is one step towards determining the complex epistatic relationships between these TF gene families (Zheng et al., 2003; Ozaki et al., 2004). *Six1* expression is lost in *Eya1* nulls (Zheng et al., 2003), which appears to place it downstream of *Eya1*. However, the relationship of *Pax* genes to *Six* and *Eya* expression is less clear. This may reflect functional redundancy in *Pax* genes (e.g.

Pax5 and *Pax2* [Bourchard et al., 2000]). Likewise, *Dach1* does not appear to be simply downstream of *Pax2* or *Eya1* (Heanue et al., 2002), unlike the situation in *Drosophila*. Defining these connections and functional redundancies is a continuing challenge.

Genes that affect Planar Cell Polarity

As AHCs differentiate, they reorient to their final arrangement (Dabdoub et al., 2003). The correct coordination of these reorientation events is necessary for hearing and this process can be disrupted by perturbations in *Wnt* signaling. At least eight *Wnt* genes are expressed in the organ of Corti. The primary receptors for these ligands are Frizzled proteins. *Frizzled* genes are expressed in the developing chick ear (Stevens et al., 2003), but not all *Frizzled* genes are necessary for this process. These types of orientation defects can also be caused by other genes that affect planar cell polarity (PCP). Mouse mutants in *Vangl2* (the ortholog to *Drosophila strabismus/van gogh*) and in *Scrib1* (Montcouquiol et al, 2003) have orientation defects in all rows of AHCs. The mouse mutants *Spin cycle* (*Scy*) and *Crash* (*Crsh*) also affect PCP (Curtin et al., 2003) and lead to misorientation of OHCs. While other mouse mutants, in genes such as *Myo7a* and *Cdh23* (see below), result in disorganized stereocilia bundles, they do not appear to be directly involved in PCP, which occurs before stereocilia develop.

Hair cell maintenance

Many human and *mouse* hearing and/or balance mutations lead to defects in the development or architecture of hair cell stereocilia. These specialized structures, when deflected by transmitted sound, directly lead to gating of AHC ion channels, potassium influx and cell depolarization. The genes that underlie the various forms of Usher's Syndrome (USH) have

provided particular insights into stereocilia development and/or maintenance. Of the eleven USH loci, seven have been molecularly cloned (several of these also cause nonsyndromic hearing loss). Most of these genes are "structural" in nature and include *MYO7A*, *HARMONIN*, *CDH23*, *PCDH15*, *USH2A*, and *USH3* (Weil et al., 1995; Verpy et al, 2000, Bitner-Glindzicz et al., 2000; Bork et al., 2001, Bolz et al., 2001; Ahmed et al., 2001, Alagramam et al., 2001; Eudy et al., 1998; Joensuu et al., 2001). Many of these proteins have recently been shown to interact with each other. For example, mutations in the *SANS* gene were recently identified as causing USH1G (Weil et al., 2003) and the *Jackson shaker* mutation in mice (Kikkawa et al., 2003). These alterations lead to stereocilia bundle disorganization. The *SANS* gene product interacts with another USH protein, *HARMONIN* (USH1C). *HARMONIN*, in turn, interacts with *MYOSIN7A* and *CADHERIN23* (*CDH23*), two additional USH proteins (Boeda et al., 2002). The *Deaf circler* and *Deaf circler 2* mouse mutants have also now been shown to result from mutations in *Harmonin* (Johnson et al., 2003). Most USH genes encode proteins with PDZ domains, (a common motif for protein-protein interaction). In this context it is interesting to note that the *Whirler* mouse mutant (in which hair cells degenerate) was recently shown to result from mutations in a PDZ protein, *Whirlin* (Holme et al., 2002; Mburu et al., 2003). This gene is also responsible for DFNB31 in humans and plays a role in stereocilia elongation through actin polymerization.

Ion flux

Ion flux is also critical for hearing and for AHC survival. Overexposure to K^+ leads to prolonged depolarization, and in time is toxic. Several hearing and/or balance mutations in mouse lead to hair cell death through ion toxicity. For example, mutations in tight junctions and

gap junctions are thought to lead to ion toxicity in HCs, resulting in postnatal hair cell death (Zenner 1986; Zenner et al., 1994; Ben-Yosef et al., 2003). The dynamics of these degenerative processes have been recently examined in a series of mouse models. Defects in the gap junction protein CONNEXIN 26 (CX26/GJB2, *DFNB1*) are the leading cause of sporadic nonsyndromic hearing loss in Caucasians (Kelsell et al., 1997; Zelante et al., 1997; Estivill et al., 1998). This gene has been targeted by conditional deletion in the mouse inner ear (Cohen-Salmon et al., 2002), and has also been overexpressed as a dominant-negative transgene (Kudo et al., 2003). In both of these models SCs die, followed by hair cell death around P14, and there is an eventual collapse of the organ of Corti, most likely due to problems in potassium homeostasis. A similar phenotype has been observed in *Connexin30* knockout mice (Teubner et al., 2003). Mouse models in which the gene encoding the tight junction protein Claudin14 (*DFNB26* in humans) is deleted also show progressive loss of AHCs by three weeks of age, possibly through loss of a cation barrier (Ben-Yosef et al., 2003).

Three TF genes have been implicated in hair cell maintenance/survival: When *Pou4f3* (*Brn3c*) is knocked out, it results in a failure of hair cell maturation late in embryonic development (Xiang et al., 1997). Mutations in *Gfi1* appear to result in a similar phenotype to *Pou4f3* (Wallis et al., 2003). *Gfi1* is the mouse ortholog of the *Drosophila* gene *senseless*, and its expression is dependent upon genes such as *atonal* (the ortholog of mouse *Math1*); The third of these TF genes is *Barhl1*, which was mentioned above as being potentially interconnected with the *Math1* pathway (Figure 1-4). Its expression is first detected in the cochlea at E14.5 and it is still expressed in AHCs at P2 (Li et al., 2002a). *Barhl1* null mice exhibit early and progressive hearing loss. However, these mice continue to express *Math1*, *Pou4f3*, *Myo6*, and *Myo7a*, indicating that *Barhl1* is more likely to play a role in HC maintenance than initiation of HC

differentiation. By P6, OHCs in the apical region of the null mutants show stereocilia misalignment and disorganization leading to progressive deafness.

Genes that are involved in Mendelian forms of hearing loss, such as those mentioned above, may provide insights into the more complex and common later onset forms. One interesting example is the *Cdh23* gene, mutations in which disrupt stereocilia in *USH1D*, *DFNB12*, and the *Waltzer* mouse mutant (Bork et al., 2001; Di Palma et al., 2001; Bolz et al., 2001). A single-nucleotide polymorphism (SNP) in *Cdh23* was found to act as a genetic modifier of the mouse *Deaf waddler* mutation in age-related hearing loss (AHL) (Noben-Trauth et al., 2003). This SNP (which leads to a synonymous codon substitution) is sufficient to cause exon skipping in the *Cdh23* gene. Subtle genetic alterations in known deafness loci, such as those found in *Cdh23*, may prove to be important discriminators of risk for late onset hearing loss in humans. Interestingly, Cadherin23 has now also been shown to be a component of hair cell stereocilia tip links (a filamentous linkage between the ends of adjacent stereocilia) (Siemens et al., 2004; Sollner et al., 2004). Defining the components of tip links has been a long sought after goal of auditory biologists that has at last been achieved.

We are beginning to gain insights into hair cell maintenance and stereocilia structure from mouse and human mutations. However, identifying the gene that encodes the hair cell-specific, mechanotransduction potassium channel has proved elusive. The presence of only a small number of channels on a small population of cells has made this biochemically difficult. However, recent work in zebrafish raises the hope that this might prove tractable. By employing a combination of molecular biology and bioinformatics approaches, Sidi et al., (2003) were able to isolate the zebrafish ortholog of the *Drosophila nompC* (no mechanoreceptor potential C) gene. This channel is expressed in all five sensory patches of the zebrafish embryonic inner ear.

Morpholino-directed knockdown of this gene leads to deafness, and failure to respond to acoustic stimuli. Hair cells appear morphologically normal, but lack channel activity. NompC is a member of the TRP superfamily of channels, transient receptor potential channels implicated in a variety of sensory processes. However, the zebrafish gene shares only 45% identity with its *Drosophila* ortholog, and conventional computational homology searches do not identify any unequivocal orthologs in the mouse or human genomes. Thus, the search for the mammalian channel continues.

Stem Cells

It is still unclear whether a stem cell population exists in the SE during late mammalian embryogenesis or in early postnatal life. Many, generally inconclusive, attempts have been made to identify such a cell type. Most recently, Li et al (2003a) reported a possible stem cell population in adult mouse utricles (a component of the inner ear that senses changes in movement). These cells appeared to have pluripotent potential and exhibited many of the characteristics that might be expected of inner ear stem cells. In a parallel study the same group took on the even more daunting task of differentiating embryonic stem cells (ES) toward a hair cell fate (Li et al, 2003b). ES cells were cultured in the presence of EGF and IGF-1, and subsequently in bFGF. Encouragingly, the resulting cultures contained cells that expressed a wide range of HC- specific markers, but these also showed expression of some SC markers. This may indicate that a mixed population is present and/or the cells were not fully differentiated. Transplantation of these mouse cells to the chick inner ear resulted in some hopeful signs of hair cell differentiation. The possibilities of stem cell therapies are exciting, but the current state of the art for inner ear ES cell differentiation seems rather hit-and-miss at present. Various

combinations of treatments are used in the hope that one will produce the correct spectrum of markers. It appears likely that a more directly engineered approach may be required in the future in order to achieve pure populations. Nevertheless, it is clear that differentiation of stem cells is a route that many investigators will continue to pursue and one that holds great promise for possible replacement therapy.

Genomic approaches to AHC function

With the exception of some useful but small scale Expressed Sequence Tag (EST) projects (e.g. Resendes et al., 2001) the major genomic contribution to this field has been through microarray-based gene expression profiling. These present a considerable technical challenge because the inner ear is very small, necessitating either large-scale tissue procurement or extremely robust RNA amplification methods. It also contains a wide diversity of cell types, which complicates the expression analysis. As one means to partially circumvent these problems, Rivolta et al., (2002) conducted an analysis of gene expression in a conditionally immortal mouse cochlear cell line. Likewise, Chen and Corey (2002a) used postnatal mouse cochlear samples to analyze major gene expression changes and as the starting point for an inner ear gene expression database (Chen and Corey, 2002b). Both of these studies constitute important base line profiles of inner ear gene expression. Our group has investigated gene expression in pure populations of SE from the chicken inner ear (Hawkins et al., 2003). The chicken utricle SE is in a constant cycle of apoptosis and regeneration, whereas the cochlear SE is quiescent (if the hair cells are not damaged). We initially compared gene expression between these two SEs and identified >100 gene that showed significant differences. Of these, ~80 were TF genes identified using a cross-species TF microarray that we developed (Messina et al., 2004). We have now

extended these observations to a large-scale study of TF gene expression changes that occur in chicken cochlear and utricle SEs as they regenerate in response to different forms of damage. These have been compared to data derived from damaged mouse SE to identify similarities and differences. These time courses of gene expression have allowed us to identify known pathways of gene expression, as well as a core group of TF genes that are expressed in all chicken regenerative time courses (this thesis, Chapter 4). In addition to these profiling studies we have also conducted RNA interference studies to knockdown, phenotypically characterize and expression profile the effects of specific TF genes in chicken SE. This work is also described in this thesis.

Future Directions

It is likely that “solving” the developmental and regenerative gene “wiring diagram” for auditory hair cells will require connecting the currently known parts of the puzzle and discovering as yet unknown components. Hopefully, this will not occur one gene at a time. It seems likely that the elegant model systems that have been so painstakingly constructed and studied to date (and in particular, the ever increasing number of mouse mutants and knockouts), will prove amenable to more large scale technologies, such as microarray analysis, high throughput RNAi knockdowns, proteomics methods, and the application of new genomics approaches such as chromatin IP to define downstream targets of TFs. These technologies should provide the types of insights that will better inform current efforts towards gene and/or stem cell therapies for AHC damage.

Regeneration

In 1987 and 1988 several papers were published that made avian hair cells of the cochlea and utricle the premier model for studying hair cell regeneration, as it was discovered that regeneration occurred in avians. Almost by accident, researchers wanting to determine the affects of acoustic trauma (Cotanche 1987), and gentamicin toxicity (Cruz et al., 1987), on the stereociliary bundles of hair cells of the cochlea found that after allowing recovery from treatment, there were signs of new hair cells present. Next, Ryals and Rubel (1988) treated hatchling chicks for 10 days with gentamicin, a known ototoxic antibiotic. The cochleae were compared to time matched controls at 11, 18, 25, and 32 days. They noticed an apparent increase in hair cells in treated cochleae from 25 to 32 days compared to that of 18 days by light microscopy. Cotanche exposed chicks to 120 decibels of pure tone for 48 hours and then allowed chicks to recover for 0, 24, 48 hours and 6 and 10 days. Evidence of recovery was seen at 24 hours and they were almost fully recovered by the 10th day. The following year these groups would provide definitive evidence for hair cell regeneration in the avian ear with the incorporation of tritiated thymidine, which is incorporated into replicating DNA (Corwin and Cotanche, 1988; and Ryals and Rubel, 1988). Both groups speculated that either supporting cells or an as yet unidentified stem cell population gives rise to new hair cells. A vast amount of literature exists that show that newly regenerated hair cells become innervated and are therefore functional. That literature will not be covered here, but an excellent review exists from JW Smolders (1999). Another seminal paper was published in 1988, when Jorgensen and Mathiesen (1988) showed that the hair cells of the avian vestibular organs are continuously turned over, while those in the cochlea remain quiescent. Until these various observations were made, it was assumed that avians suffered permanent damage to their hair cells as in mammals. These studies

later led to additional investigation in the mammalian inner ear, which provided evidence for limited regenerative ability in the vestibular organs of mammals. Forge et al. (1993) and Warchol et al. (1993) both showed that the guinea pig utricle had formed immature hair cell bundles four weeks after treatment with the ototoxic antibiotic gentamicin. Warchol et al. (1993) also demonstrated regeneration in cultured human utricles, however in all cases, the amount of regeneration present was not enough to compensate for the damage that had occurred. It is therefore generally accepted that mammals cannot regenerate hair cells as the cochlea will not regenerate, and the utricle regeneration is so limited it would not repair any level of damage that might be sustained.

The two studies just mentioned also lent evidence to two different models of hair cell regeneration. The first model is derived from the work by Warchol et al. (1993) where they showed that the 5-bromo-2-deoxyuridine (BrdU) and tritiated thymidine labeled nuclei of proliferating cells lay in the basal edge of the sensory epithelia where supporting cells reside. Weeks later these cells appeared to migrate to the luminal layer containing hair cells and some had immature stereocilia, indicating that supporting cells underwent mitosis. The second model draws from the work by Forge et al. (1993) where they found a larger number of immature stereocilia than dividing supporting cells by SEM during recovery. This evidence suggests a model of transdifferentiation of supporting cells. Since then, it has been determined that when hair cells suffer only enough damage to destroy stereocilia but not to kill the hair cell, the cells are able to re-grow stereocilia (Zheng et al., 1999). The tip links of stereocilia, connecting the stereocilia to one another, are also able to regenerate if mild damage is sustained that does not destroy the stereocilia completely (Zhao et al., 1996). The stereocilia regeneration may explain why Forge et al. saw more immature stereocilia than dividing supporting cells. The debate still

continues between the first two models for how supporting cells give rise to new hair cells. It is possible that a combination of both occurs. The supporting cell may divide into two supporting cells instead of a supporting cell and a hair cell, and this second supporting cell may then differentiate into a hair cell. The reverse could also be imagined. Once a supporting cell has trans-differentiated to replace a damaged hair cell, additional supporting cells might divide to replace the now lost supporting cell that was once present, but it is known that developmentally these two cell types share a common progenitor. Cell lineage tracing experiments using replication-defective viral vectors delivered in the chicken hearing organ in the last few rounds of cellular proliferation, between E5 and E8, demonstrated that individual clones do give rise to both supporting cells and hair cells (Fekete et al., 1998). This provides support that a stem cell population does exist in the chicken inner ear.

The avian vestibular sensory epithelia are primarily used for regeneration studies due to ease of access. The vestibular sensory epithelia is comprised of three cells types: supporting cells, plus Type I and Type II hair cells (Figure 1-2). The hair cells are defined by morphology and innervation. Type I hair cells have a slight hour glass shape and the nerve forms a calyx around much of the cell, while Type II hair cells are columnar and innervated at the base of the cell body (Jorgensen and Christensen, 1989). In the epithelial layer the hair cells are located in between the supporting cells, but the cell body does not stretch the entire length of the supporting cell. Hair cells cover about two-thirds the length of the supporting cells, with the layer having an almost level upper edge. The supporting cell nuclei are located in the lower one-third of the cell, as are those of the hair cells. Therefore, the cell layer can be seen in three sections: the bottom third contains the supporting cell nuclei, the middle third contains supporting cell bodies and hair cell nuclei, the top third contains the apical end of each cell type and stereocilia of hair cells

projecting out. Labeling cells with tritiated thymidine identified supporting cell nuclei in the lower one-third of this layer (Tsue et al., 1994). Additional studies using the same labeling method during recovery after treatment with ototoxic antibiotics, found the same result. The labeled cells appear to migrate to the mid-level before dividing. The lower layer never loses the number of labeled supporting cells indicating that one of the cells migrates back and the other goes on to form a hair cell (Weisleder et al. 1995). Weisleder et al. also demonstrated by cell type counts that an abundance of new Type II hair cells proceed that of Type I hair cells, but over time this reverses as the number of Type II cells decrease and Type I cells increase. This suggests that supporting cells give rise to Type II hair cells that then transform into Type I hair cells. This evidence supported earlier work using BrdU incorporation in the avian vestibule, to show that only Type II hair cells were labeled and not Type I hair cells (Roberson et al., 1992).

Early evidence that supporting cells give rise to newly regenerated hair cells came from work done in the lateral lines of salamanders (Balak et al., 1990). The hair cells in this sensory system were destroyed using two independent methods. First, hair cells were killed using phototoxic methods of soaking the salamanders in a solution containing DASPEI, a fluorescent compound taken up by hair cells, and then exciting the chromophore by exposure to UV light. The excitation led to the killing of all hair cells present in the areas of the lateral line looked at. The only cells that could then be detected in the sensory epithelia of the lateral line were that of supporting cells. Following 6 days of recovery, newly formed hair cells began to appear. In the second approach, a laser microbeam was focused onto each individual hair cell for ablation of the cell, leaving the underlying supporting cell intact. Again, 5 days later hair cells had started to regenerate. This provided additional evidence that supporting cells are the progenitors for regenerated hair cells. A more thorough examination of the induction of hair cell proliferation in

the damaged cochlear epithelia revealed that the first cells to show evidence of DNA replication were indeed supporting cells (Warchol and Corwin, 1996). Here, hair cells were ablated with a laser microbeam in cochlea organ cultures and were immediately placed in medium containing either tritiated thymidine or BrdU to mark DNA replication. Following the laser ablation, hair cells died within 5 minutes. This allowed the authors to make an assessment of the amount of time taken for cells to re-enter the cell cycle, moving from arrest at G(o) to S-phase, as organ cultures remained in medium containing the labeled DNA precursor for 4 hrs, 8 hrs, 16 hrs, and 24 hrs. At 16 hours the signs of DNA replication were first seen in the underlying supporting cells indicating that the supporting cells had re-entered the cell cycle. However, this leaves several questions. When does this process truly begin? When are the signals received to start the process? How long before the transcriptional machinery is in place to activate the genes necessary for re-entering the cell cycle? It is likely that all of this takes place in the supporting cell hours before or within minutes of the hair cells dying off. Another significant aspect of this study is that supporting cells as far away as 200 μ m from the lesion site were labeled. This observation suggested that mitogenic factors may be present and responsible for signaling to these distant supporting cells.

Mitogenic Factors

Many studies suggest that mitogenic factors are responsible for the differentiation of supporting cells to hair cells. Many growth factors including FGF, EGF, IGF-1, insulin, TGF α , and BDNF have been used to induce proliferation in both mammals and avians inner ears. Yamashita and Oesterle (1995) reported the use of epidermal growth factor (EGF) and transforming growth factor alpha (TGF α) in the mouse utricle sensory epithelium to induce cell

proliferation. Proliferation was noted by tritiated thymidine incorporation, which occurred in the supporting cell layer. There was a synergistic effect when used in combination with insulin, but in all these cases the number of cells proliferating, while significant, is still very minimal. The presence of proliferating cells increased from less than one per utricle to 5.8 ± 1.0 (EGF + insulin) and 10.1 ± 1.4 (TGF α + insulin) per utricle. They also reported that bFGF and aFGF have no effect on cell proliferation. This does provide some evidence that hair cell proliferation can be induced in the mammalian inner ear using a specific combination of growth factors. However, the total number of cells induced to proliferate was small and this illustrates that the inhibitory mechanism in mammalian cells has not been completely over-ridden. Later, these results would be validated in the rat utricle, where bFGF (FGF-2) demonstrated the greatest effect on proliferation and that effect was additive with either IGF-1 or TGF α (Zheng et al., 1997). These authors also tested FGFs 4-7, and EGF, which all gave similar results. As further evidence for mitogenic factors playing a role in hair cell proliferation, several growth factors and growth factor receptors were identified in the avian cochlea under normal and noise-damaged conditions using RT-PCR and immunofluorescence (Lee and Cotanche, 1996). Transcripts were identified for EGF, fibroblast growth factor receptor (FGFR), insulin-like growth factor receptor (IGFR), insulin receptor (IR), retinoic acid receptor beta (RAR β), retinoic acid receptor gamma (RXRG), and bFGF. Immunofluorescence could not identify IGFR, while EGFR was localized to the stereocilia, bFGF was localized to the nuclei of supporting cells, and RAR β was localized to the perinuclear region of hair cells. These distributions did not change in the damaged cochleae. However, the localization of FGFR did change after damage. The protein was initially found in the stereocilia, but after damage, was expressed in the apical region of supporting cells. This, the authors claims may provide evidence for the role of FGF signaling during regeneration, as well

as retinoic acid, due to its perinuclear location. Moreover, FGFR3 has been shown to be expressed in the developing and regenerating sensory epithelia of the avian cochlea (Bermingham-McDonogh et al., 2001). Expression increased during regeneration and returned to normal levels following recovery.

The cyclic AMP (cAMP) pathway is a pathway that upon activation has been shown to have a dramatic effect on proliferation in the avian sensory epithelia. A transcript representing a component of this pathway, phosphodiesterase, was identified during regeneration (Navaratnam et al., 1996). The function of phosphodiesterase is to break down the second messenger cAMP. This led the authors to test the effects of a cAMP analog, 8-bromo-cAMP (8BcAMP), and forskolin, an activator of adenylyl cyclase. The average cochlea epithelia showed 1-3 proliferating cells per specified area (considered quiescent), whereas treatment with 8BcAMP led to an increase in cell proliferation of about 50 cells, and forskolin to approximately 180 cells. After damage the cochlea typically showed an increase to 50 proliferating cells. It is interesting to note that activating the pathway at the initial step has a greater effect than activation a few steps into the pathway. Additionally, it was shown that inhibitors of protein kinase A (PKA), reduced proliferation in the sensory epithelia, both in the presence of forskolin, reduced by 70-80%, and after damage with gentamycin, reduced 60-70%. Forskolin and cAMP are capable of inducing proliferating cells in neonatal rat utricles (Montcouquiol and Corwin, 2001a). In this system forskolin and bromo-cAMP had equivalent effects on proliferation, each increasing the number of proliferative cells by 11 to 12 fold. Recall that in the chick, forskolin had a more dramatic effect. In order to see an increase in proliferation, exposure to these compounds was limited to 15 minutes for forskolin and 1 hour for bromo-cAMP, since an initial prolonged exposure had no effect on inducing cells to enter S-phase. The authors also demonstrated a proliferative effect for

the mitogen glial growth factor 2 (rhGGF2), and this effect was synergistic with the addition of forskolin. To confirm the role of cAMP, PKA inhibitors were utilized and showed a reduction in the forskolin effect by 50 %. Additionally, membrane recycling inhibitors were used to test the hypothesis that cAMP induced S-phase entry can increase growth factor receptors. Again, there was a 50% reduction in proliferation after stimulation, indicating that receptor turnover or increased presence is important for S-phase entry. In the same system these authors used a series of activators and inhibitors to try to identify other signaling factors (Montcouquiol and Corwin, 2001b). Activation by rhGGF2 was inhibited by rapamycin, implicating a potential role for the mammalian target of rapamycin (mTOR). There was some evidence that inhibiting protein kinase C had an effect on rhGGF2-induced stimulation, but this appeared to be highly specific to the inhibitor tested (1 in 3 showed significant results), and its concentration, whereas, inhibition of phosphatidylinositol 3-kinase completely abolished the rhGGF2-induced proliferation.

Conclusion

These studies provide some evidence that induction of hair cell proliferation in the inner ear may be possible, even in the mammalian ear where hair cell regeneration is virtually non-existent. Unfortunately, while proliferation can be induced in a few hair cells, proliferation is not maintained at a level that can compensate for hair cell death that one might actually sustain, but this provided insights into some pathways that may be important for additional targeting. In all likelihood a more complete understanding of how regeneration is initiated and how hair cells proceed from damage through recovery will be necessary to activate hair cell regeneration in mammals. A more global picture of important pathways would allow multiple avenues for

targeting cells for regeneration. In this thesis, a subset of the transcriptome is assessed by microarray gene expression studies identifying transcription factors that are differentially expressed between the utricle and cochlea sensory epithelia, and during utricle hair cell regeneration following damage using two independent methods. Additionally, a library subtraction between the utricle and cochlea sensory epithelia was carried out to identify utricle genes, as it is in a constant state of hair cell turnover compared to the quiescent cochlea. These studies provide a vast amount of data on genes expressed during hair cell regeneration, as well as important clues as to which pathways are important for this process.

CHAPTER TWO

UTRICLE-COCHLEA MICROARRAY COMPARISONS

Introduction

In addition to the avian inner ear's robust regenerative capabilities, it also displays a unique pattern of sensory cell loss and turnover. Hair cells in the avian cochlea have long life spans and are not normally replaced unless they are lost by injury. As a result, the normal (undamaged) cochlea in mature birds contains very few proliferative cells (Oesterle and Rubel, 1993). In contrast, hair cells in the vestibular organs have a relatively short life span (estimated at 2-6 weeks [Kil et al., 1997; Stone et al., 1998; Goodyear et al., 1999; Wilkins et al., 1999]) and then undergo spontaneous apoptosis. Those cells are then quickly replaced by new sensory cells which are produced by ongoing proliferation of epithelial supporting cells (Kil et al., 1997; Stone et al., 1998; Wilkins et al., 1999; Jorgensen and Mathiesen 1988; Roberson et al., 1992). Thus, the avian vestibular organs, but not the cochlea, are in a constant state of ongoing sensory regeneration.

In the present study, two molecular technologies were combined to investigate differences in gene expression between constantly-regenerating chick utricle and the mitotically quiescent cochlea. The first was a micro-cDNA method that enabled us to construct representative cDNA libraries and microarray targets from the small number of cells in each sensory epithelium. The second was a set of custom microarrays. One contained probes for a collection of known inner ear-specific genes. The other contained probes for the vast majority of human transcription factors. Many of our significant findings were validated by quantitative PCR (qPCR) and in some cases by *in situ* detection methods.

Results

Feasibility and Design

This was an effort to characterize differences in gene expression between chick cochlear sensory epithelia that are normally quiescent and utricle epithelia that are in a constant process of apoptosis and regeneration. However, only a limited set of chicken (*Gallus gallus*) cDNAs and ESTs are available in public sequence databases. I therefore investigated the feasibility of using microarrays of human cDNAs to interrogate comprehensive sets of genes across species. To assess the feasibility of this approach with chicken versus human genes one of the few available chicken EST databases (<http://www.tigr.org/tdb/tgi/gggi/>) was examined by a bioinformatic researcher in our group, Cindy Helms. A set of 500 randomly chosen ESTs from this collection were compared by BLASTN to the unique set of human gene-oriented clusters from Unigene (Hs.seq.uniq). Of the 500 queried ESTs, 10% did not exhibit significant homology with human sequence. Further analysis of these ESTs suggested that they were derived from chicken 3' untranslated region sequences. The percent identities for the remaining 90% of this set of chicken ESTs ranged from 52% to 100% with a mean of 69%. These findings prompted our group to build microarrays that comprised only human coding regions and to hybridize them under stringencies appropriate for a 69% overall nucleotide homology (see Chapter 7 -Materials and Methods). Two custom microarrays were designed and built and are discussed in detail below:

Inner ear microarray

The first cDNA microarray constructed for the current study contained cDNA probes to 426 genes that have been shown to affect hearing or to be expressed in the inner ear (a complete

list is available at <http://hg.wustl.edu>). These human cDNA probes were prepared with PCR primers that would amplify several hundred base pairs of a unique segment of coding region. These arrays also contained probes for a number of control tags (see Materials and Methods).

Preparation of target

Comparative expression profiles of the chick cochlea and utricle were generated from the pseudostratified sensory epithelia. This is comprised entirely of sensory hair cells and supporting cells from the proliferative utricle and quiescent cochlea cells (see Materials and Methods). By implementing a micro-cDNA amplification scheme we were able to generate enough labeled targets from these small samples for multiple microarray hybridizations.

Targets were synthesized from an entire cDNA library or from primary cDNAs. In all cases we used multiple samples for our analyses to avoid any biases that might be introduced by genotypic variation or by sample preparations. All of the experimental hybridizations involved comparisons of multiple independent utricular or cochlear samples. In addition to these comparative hybridizations we conducted multiple self-to-self hybridizations (e.g. one utricle sample versus another) to test for sample variation and spurious dye effects. Encouragingly, these self-to-self hybridizations yielded no significant differences. For the comparative studies we conducted at least 8 separate hybridizations. At least three of these were experiments where the fluorescent dye was switched to compensate for any effect of dye intensity. To assess statistically significant differences in gene expression, the mixed model method recently described by Wolfinger et al., (2001) was applied.

Table 2-1 shows a summary of the top 20 most significant gene expression changes detected between chick cochlea and utricle epithelia when the Inner Ear Array was interrogated.

In the table the samples are ranked according to *P*-values. Only samples with a fold change of 1.26 or greater are shown (see below for more on this). The two artificial control tags that were introduced into cochlea and utricle targets at different concentrations were detected with significant *P*-values, validating the quantitative changes we observed.

One might argue that fold-change could be misleading for cross-species hybridizations. However, if we used a *P*-value of less than 1×10^{-4} as a cut off, then the number of genes showing differences in expression was 50 corresponding to 12% of those monitored. We therefore conclude in this case that our use of fold change as a cut off value is the more conservative approach.

Gene	Average Fold change on arrays *	<i>P</i> -value	Average Fold change by qPCR *	Validation by <i>In Situ</i> Hybridization
BMP4	-4.18	1×10^{-7}	-4.55	YES
SMAD2	3.32	1×10^{-7}	3.20	
SPARC	1.26	1×10^{-7}	2.25	
ENO1	1.76	1×10^{-7}	1.76	
GATA3	-1.94	1×10^{-7}	-5.15	YES
GSN	-2.03	1×10^{-7}	-211.3	YES
APP	1.72	1×10^{-7}	2.40	
KIT	2.66	1×10^{-7}	5.68	YES
MMP14	1.80	1×10^{-7}		
TWSG1	1.65	1×10^{-7}		
DLC1	-1.79	1×10^{-7}		
BMP2A	-1.69	1×10^{-7}		
MEF2C	1.40	1×10^{-7}		
PAX4	1.22	1×10^{-7}		
GJA3	-1.30	1×10^{-7}		
SDC4	-1.28	1×10^{-7}		
cMYC	-1.85	1×10^{-7}		
HBGF8/PTN	1.33	1×10^{-7}		
DLX3	1.45	1×10^{-7}		
RORA3	1.21	1×10^{-7}		

Table 2-1. Genes from the inner ear array. These show the most significant changes in expression ranked by *P*-values. (***Table 2-1 footnote**): Fold changes are displayed as levels in the utricle relative to the cochlea. Thus, a minus sign before the fold change indicates downregulation in the utricle relative to the cochlea. The results of qPCR assays (using primers designed to chick cDNA sequences) and in-situ hybridizations (see Figures 2-1 and 2-2) are shown. *P*-values for all these differences (obtained as described in methods) were highly significant.

Quantitative-PCR (qPCR)

Quantitative-PCR (Wittwer et al., 1997) was used as one independent method to validate the microarray-based observations. These results are also shown in Table 2-1. All of the qPCR assays agree with the trends observed from the microarrays and we were able to validate apparent microarray fold changes as low as 1.26-fold (see SPARC in Table 2-1). This array fold change is the average of 8 hybridizations ranging from a 1.10 to 1.55 fold increase). However, the exact fold changes in the qPCR did not always agree with the microarray observations. This is again illustrated by SPARC in Table 2-1 which had an average qPCR fold change of 2.25. This is not surprising given that microarrays of human cDNAs were used to detect changes in chick gene expression. It is expected that some compression of dynamic range will occur in cross-species hybridizations. By contrast, the qPCR primers were designed from chick cDNA sequences. It is therefore likely to be a better reflection of the expression level in each sample.

In situ hybridization and immunohistochemistry

In addition to the qPCR validation steps we also conducted a limited number of RNA *in situ* hybridizations with oligonucleotide probes to BMP4, GATA3, GELSOLIN and c-KIT. Figure 2-1 shows the differential expression of these genes in sensory epithelia of the cochlea and utricle. Consistent with previous observations (Oh et al., 1996) and our microarray and qPCR findings, expression of BMP-4 was observed only in the cochlea (Figure 2-1A) providing an internal validation of our observations. GATA3 was expressed in both organs, but was present throughout the sensory epithelium of the cochlea and restricted to the striolar region of the utricle (Figure 2-1B). Gelsolin was only detectable in the cochlea and was localized to a

region near the superior edge of the sensory epithelium (Figure 2-1C). Finally, expression of c-KIT was observed in the utricle. Notably, mutation of c-KIT in mice leads to dominant white spotting and ear abnormalities (Geissler et al., 1988), and is also mutated in one human deafness pedigree (Spritz and Beighton, 1998).

In other experiments, immunocytochemical techniques were used to examine the distribution of GATA3 protein in the cochlea and utricle (Figure 2-2). Consistent with the *in situ* results (above), GATA3-labeled cell nuclei were observed throughout the sensory region of the cochlea. In the utricle, however, GATA3 was present in only a 6-8 cell-wide region in the center of the striola. This region corresponds to the zone of specialized Type II hair cells that is located in the center of the striola in the avian utricle (Jorgensen, 1989). The orientation of hair cell stereocilia undergoes an abrupt 180° shift at this region, and it is tempting to speculate that GATA3 may play a role in defining the polarity of this interesting group of cells (Kido et al., 1993). This gene has already been implicated in inner ear development (Lawoko-Kerali et al., 2002; Rivolta and Holley, 1998).

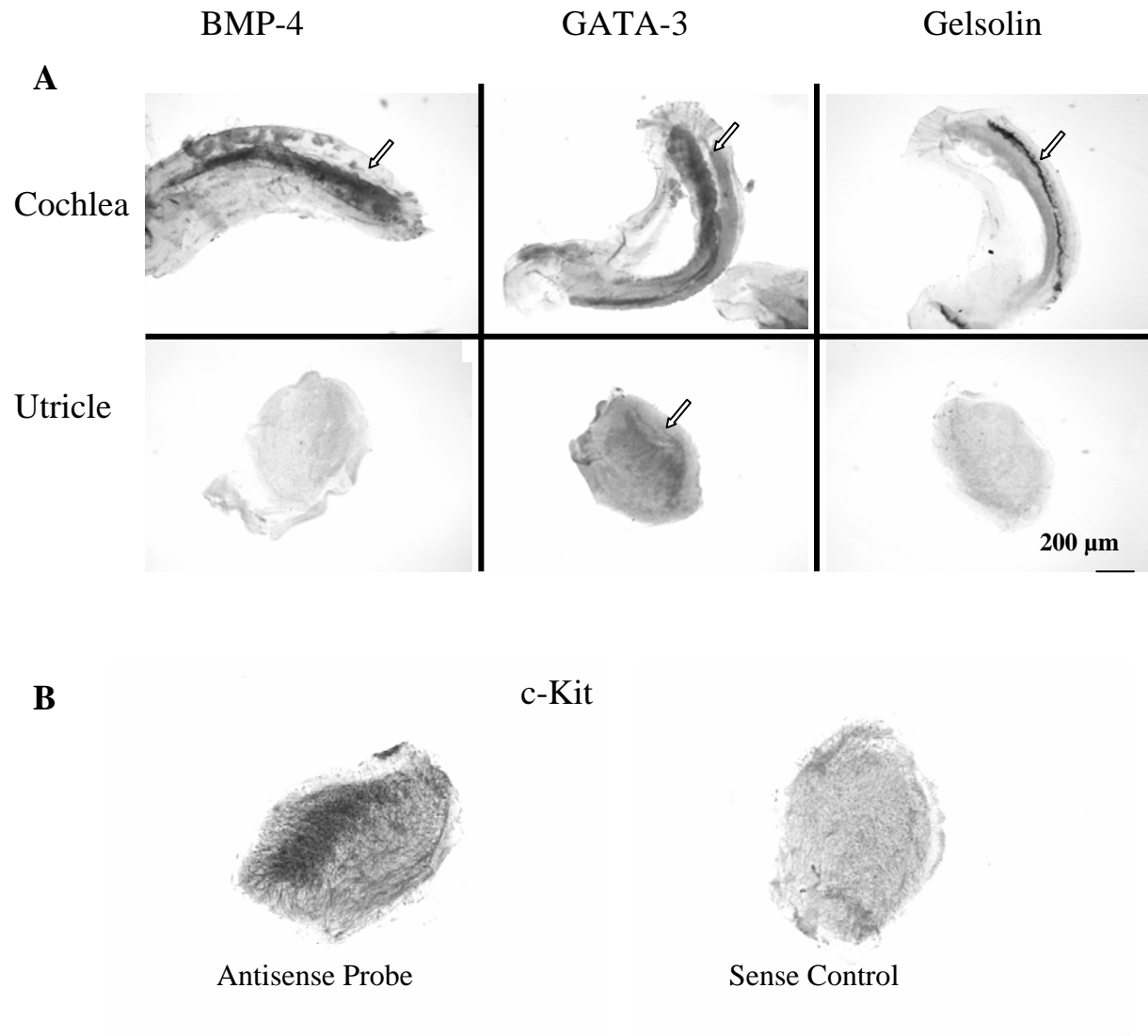


Figure 2-1. BMP4, GATA3, GELSOLIN, and KIT RNA *in situ* hybridizations. *In situ* hybridizations confirm the differential expression of four genes from our microarray data. **A** shows RNA *in situs* with antisense probes to BMP4, GATA3 and GELSOLIN on whole mount chick cochleae and utricles. Arrows indicate the areas of highest expression. (Sense probes are not shown but were uniformly negative). **B** shows sense and antisense RNA *in situ* hybridizations of a c-KIT probe in the chick utricle.

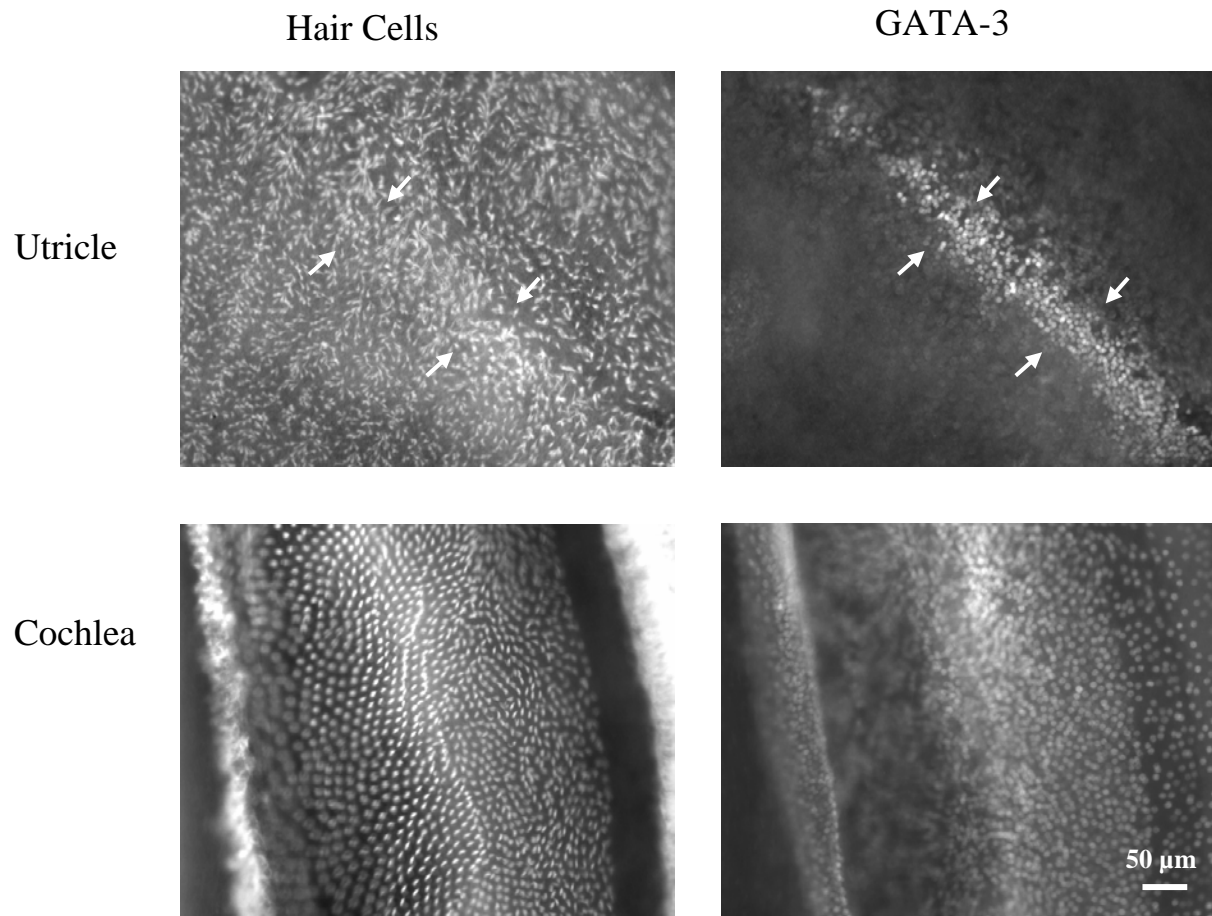


Figure 2-2. Immunohistochemical staining with a GATA3 antibody. The top two panels show GATA3 immunoreactivity in utricle hair cells and its localization to the nuclei of a strip of cells (the striola) in the utricle. The lower two panels show a more diffuse GATA3 staining in the cochlea.

The transcription factor microarray

The second microarray was targeted at interrogating the majority of transcription factor genes. The rationale in choosing transcription factors for this second line of investigation was that changes in these potent control molecules might reveal important switches in the genetic programs (apoptosis, quiescence or regeneration) that occur in the two sensory epithelia. We also reasoned that changes in transcription factor mRNAs might be less likely to be derived from non-specific variation. The design of this array is described elsewhere (Chapter 7 and Messina et al., 2004). The version of the TF array used in the current study consisted of probes for 1422 TFs plus a few transcriptional co-activators. This array also contained numerous 50-mer control probes (see Materials and Methods- Chapter 7).

Interrogation with the TF array revealed a large number of differences in expression profiles in the chick utricle and cochlea. The top 78 changes ranked according to *P*-value are shown in Table 2-2. This is a somewhat arbitrary cutoff, but as is noted below, I independently validated a gene at position 74 on this list and therefore took that approximate *P*-value as a cutoff value. Array fold changes were averaged across 6 hybridizations with duplicate spots and 2 dye switch experiments. It should be noted that the *P*-values in this data set are higher because the Bonferroni correction (a multiple comparison correction of the data) depends on the number of spots on the array and is expected to be somewhat conservative as it does not account for potential correlations and unknown relationships among the genes on the array. Since our TF array measures changes in ~1500 genes, this results in more modest *P* -values. For example, the changes in GATA3 and SMAD2 that were observed with the Inner Ear Array had *P*-values of less than 1×10^{-7} , while on the TF array these changes have *P*-values of 3.5×10^{-4} . It should also be noted that the detectable fold-differences are different between the two arrays,

presumably reflecting differences in degrees of homology between the chick cDNAs and the arrayed probes. However, while the values may differ slightly, the data are completely consistent in the trends they reflect between the two array types. Table 2-3 shows the top 50 TF changes in the utricle and cochlea ranked by microarray fold change rather than by *P*-values.

I again employed qPCR to independently validate this dataset and chose a range of fold-changes to check. The lowest of these was *TBX2*, which had a fold change of 1.72. This change was associated with a highly significant *P*-value of 1.60×10^{-5} . As shown in Table 2-2, the qPCR assays confirmed that this relatively low fold change reflected a real change in expression between the two epithelia. Interestingly, the trends shown by genes such as *EYA3* which had a fold change of 1.83, but a much less significant *P*-value of 9.24×10^{-3} (placing it at 74th on the rank order of *P*-values) were also confirmed in multiple qPCR experiments.

I also used this dataset to obtain an estimate of how many TFs are on or off in each sensory epithelia. Again, the cut off is somewhat arbitrary, but the internal controls in our experiments allowed us to set a sensitivity of detection threshold to guide our estimates. Based upon those calculations we estimate that approximately 600 TFs (out of 1422 assayed) are on in both epithelia (Table 2-4). I estimate that approximately 40 TFs in each organ epithelia are on in one and below the threshold of detection (presumably off) in the other (Table 2-5).

Table 2-2. The 78 most significant changes in TF gene expression ranked by *P*-values.

Gene	Array Fold Change	<i>P</i> -value	qPCR Fold Change
CBF2	-1.52	1.00x10 ⁻⁷	
BRD4	-1.50	1.00x10 ⁻⁷	
FOXF1	-3.68	1.00x10 ⁻⁷	
KIAA0329	2.41	1.00x10 ⁻⁷	
PRDM7	-4.31	1.00x10 ⁻⁷	
CRIP2	2.40	1.00x10 ⁻⁶	3.10
ATF5	1.65	1.00x10 ⁻⁶	
KIAA1528	2.01	2.00x10 ⁻⁶	
CBFA2T1	-1.66	2.00x10 ⁻⁶	
TRIP15	-2.83	3.00x10 ⁻⁶	
NFYB	-3.97	5.00x10 ⁻⁶	
SNAPC3	1.62	6.00x10 ⁻⁶	
RING1	2.36	6.00x10 ⁻⁶	
LOC51637	3.31	6.00x10 ⁻⁶	2.50
NR2F2	-5.18	7.00x10 ⁻⁶	
TNRC15	-2.47	8.00x10 ⁻⁵	
ETV1	4.74	1.10x10 ⁻⁵	
NKX2B	-2.21	1.50x10 ⁻⁵	
TBX2	1.72	1.60x10 ⁻⁵	1.40
TFDP1	-1.56	1.90x10 ⁻⁵	
FOXE1	1.93	2.10x10 ⁻⁵	
SREBF2	1.72	3.20x10 ⁻⁵	
LOC51131	-1.84	3.30x10 ⁻⁵	
NFE2L1	3.03	3.40x10 ⁻⁵	
NR2F1	-4.22	3.60x10 ⁻⁵	
IRF7	2.49	3.70x10 ⁻⁵	
E2F1	1.58	5.40x10 ⁻⁵	
ZNF76	4.50	6.10x10 ⁻⁵	
STRBP	-3.85	8.10x10 ⁻⁵	
M96	1.91	1.19x10 ⁻⁴	
IPEX	3.12	1.20x10 ⁻⁴	
IK	1.74	1.25x10 ⁻⁴	
ZNF43	1.78	1.37x10 ⁻⁴	
HMG20B	2.94	1.43x10 ⁻⁴	3.20
MAFG	3.70	1.44x10 ⁻⁴	1.70
TBP	1.30	1.45x10 ⁻⁴	
DBP	5.84	1.66x10 ⁻⁴	2.10
KIAA0194	2.17	2.29x10 ⁻⁴	
ACADVL	1.59	3.03x10 ⁻⁴	
FXC1	1.90	3.26x10 ⁻⁴	
GATA3	-2.95	3.47x10 ⁻⁴	-5.15
LMO1	3.11	3.53x10 ⁻⁴	
NFKBIL1	2.57	3.55x10 ⁻⁴	
DRIL1	1.73	4.08x10 ⁻⁴	
KLF4	1.41	4.37x10 ⁻⁴	
TFAP4	1.56	4.97x10 ⁻⁴	
CCT4	1.58	5.38x10 ⁻⁴	
ZNF183	2.28	6.07x10 ⁻⁴	
R32184-3	1.68	7.58x10 ⁻⁴	
ENO1	2.50	7.83x10 ⁻⁴	1.76
NFKBIE	-1.63	8.99x10 ⁻⁴	
FLJ20551	2.94	9.31x10 ⁻⁴	

LOC51042	-1.41	9.79x10 ⁻⁴	
DOCK3	1.72	1.12x10 ⁻³	
CYLD	1.66	1.35x10 ⁻³	
FLJ10142	2.65	1.41x10 ⁻³	
PLAG1	-1.31	1.56x10 ⁻³	
ICBP90	1.56	1.63x10 ⁻³	
ARNTL	-2.17	1.95x10 ⁻³	-2.40
TONDU	1.47	2.31x10 ⁻³	
ZNF288	1.85	2.81x10 ⁻³	
E2F2	1.56	3.06x10 ⁻³	
HOXC6	1.55	3.25x10 ⁻³	
SMARCB1	2.01	3.46x10 ⁻³	
COPEB	2.31	3.61x10 ⁻³	
FLJ22865	-1.09	3.81x10 ⁻³	
NR1D2	-1.08	4.33x10 ⁻³	
HOXC4	-1.07	4.96x10 ⁻³	
MNT	1.50	5.39x10 ⁻³	
HES2	1.19	5.65x10 ⁻³	
ZNF38	1.32	6.24x10 ⁻³	
HDAC2	1.51	6.59x10 ⁻³	
SIX4	1.52	8.10x10 ⁻³	
EYA3	1.83	9.24x10 ⁻³	1.20
CSRP2	-1.35	9.39x10 ⁻³	
IRF2	1.50	9.60x10 ⁻³	
CREBBP	1.67	9.62x10 ⁻³	
CALM2	-1.10	9.96x10 ⁻³	

(Table 2-2 footnote) Fold changes are displayed as levels in the utricle relative to the cochlea. Thus, a minus sign before the fold change indicates downregulation in the utricle relative to the cochlea. qPCR assays (using primers designed to chick cDNA sequences) were performed on various TFs and results are shown in the right hand column. Genbank accession numbers of these TFs can be found at <http://hg.wustl.edu/lovetts/projects/nohr/TFarray.html> .

Table 2-3. The 50 highest changes in TF gene expression ranked by microarray fold changes.

Cochlea Sensory Epithelia		Utricle Sensory Epithelia	
Gene ID	Fold change	Gene ID	Fold change
NR2F2	-5.18	DBP	5.84
PRDM7	-4.31	ETV1	4.74
NR2F1	-4.22	ZNF76	4.50
NFYB	-3.97	MAFG	3.70
STRBP	-3.85	LOC51637	3.31
FOXF1	-3.68	IPEX	3.12
GATA3	-2.95	LMO1	3.11
TRIP15	-2.83	NFE2L1	3.03
TNRC15	-2.47	HMG20B	2.94
NKX2B	-2.21	FLJ20551	2.94
ARNTL	-2.17	FLJ10142	2.65
HSHPX5	-2.12	FOXB1	2.62
LOC51131	-1.84	NFKBIL1	2.57
FLJ12628	-1.69	ENO1	2.50
GLI	-1.67	LOC51058	2.50
CBFA2T1	-1.66	IRF7	2.49
NFKBIE	-1.63	KIAA0329	2.41
SIAH1	-1.60	CRIP2	2.40
CRSP7	-1.59	RING1	2.36
EVX1	-1.57	COPEB	2.31
TFDP1	-1.56	ZNF183	2.28
CBF2	-1.52	LOC51652	2.23
BRD4	-1.50	KIAA0194	2.17
KIAA0164	-1.50	TTF2	2.15
HOXB2	-1.47	BRF2	2.02
ASH1	-1.46	SMARCB1	2.01
LOC51042	-1.41	PPARBP	2.01
MNDA	-1.40	KIAA1528	2.01
CSRP2	-1.35	EGR2	1.97
GSH2	-1.33	LDOC1	1.96
HTLF	-1.33	FOXE1	1.93
SMARCA3	-1.33	MADH2	1.93
PLAG1	-1.31	M96	1.91
ZNF151	-1.31	FXC1	1.90
IRF6	-1.31	ZNF288	1.85
PPARA	-1.31	EYA3	1.83
GATA2	-1.26	ZNF43	1.78
NR4A3	-1.26	SNAPC1	1.78
APC	-1.23	RNF4	1.77
KIAA1190	-1.22	GPA33	1.74
MLLT3	-1.22	HRIHFB2122	1.74
CSTF1	-1.20	IK	1.74
POU4F2	-1.19	DRIL1	1.73
NAP1L1	-1.19	TBX2	1.72
TCF7	-1.18	MAFF	1.73
C1orf2	-1.17	ARIX	1.73
IRF1	-1.16	SREBF2	1.72
CSRP3	-1.16	DOCK3	1.72
AF093680	-1.16	MGC2508	1.71
KIAA0026	-1.15	DLX1	1.71

(Table 2-3 footnote) Fold changes are displayed as average levels in the utricle relative to the cochlea.

Table 2-4. TFs on in both the cochlea and utricle SE.

AF5Q31	ETV2	HMGIC	M6A	PAX9	TAF2B
ARC	ETV5	HMG1Y	M96	PBX4	TAF2C1
ARIX	EVX1	HMX1	MAD4	PCMT1	TAF2H
ARNT	EWSR1	HNF3B	MADH2	PDEF	TAF2N
ARNT2	EZH1	HOX11	MADH3	PFKL	TAL2
ATBF1	FARSL	HOX11L	MADH4	PHAP1	TBCA
ATF3	FASTK	HOXA1	MADH7	PIG7	TBL1
ATF4	FGD1	HOXA3	MAFF	PITX2	TBP
ATF5	FHL1	HOXA4	MAFG	PKM2	TBX10
ATF6	FHL2	HOXA5	MAPK8IP1	PLAB	TBX15
ATOH1	FHX	HOXA7	MAX	PLAG1	TBX2
BAPX1	FKHL18	HOXB2	MBLL	PLCB3	TBX21
BARHL1	FLJ10142	HOXB3	MC1R	PLTP	TBX6
BAZ2B	FLJ10211	HOXB6	MCM7	PME-1	TCEAL1
BCL11A	FLJ10251	HOXB9	MDS1	POU2AF1	TCF3
BCL11B	FLJ10697	HOXC11	MECP2	POU2F1	TCF7
BCL6	FLJ10759	HOXC13	MEF2B	POU4F1	TCF7L2
BMP4	FLJ11040	HOXC6	MEF2C	POU5F1	TCFL1
BRD3	FLJ11186	HOXD1	MEF2D	PP3501	TCFL4
BRD4	FLJ12457	HOXD11	MEFV	PPARA	TCIRG1
BRF2	FLJ12517	HOXD9	MEIS3	PPARBP	TCOF1
BS69	FLJ12606	HPRP4P	METTL1	PPARD	TEL2
BTF3L2	FLJ12628	HPRP8BP	MGC10772	PPARG	TFAP2A
C11orf9	FLJ12644	HRIHFB2122	MGC11349	PPIA	TFAP4
C5orf7	FLJ12827	HRIHFB2436	MGC12942	PRDM10	TFDP1
CBF2	FLJ13222	HSAJ2425	MGC16733	PRDM15	TFEB
CBFA2T1	FLJ13659	HSHPX5	MGC2508	PRDM16	TGFB1
CBX1	FLJ14549	HSPC018	MGC3136	PRDM2	TGFB3
CBX4	FLJ14967	HSPC189	MHC2TA	PRDM6	THBS3
CBX5	FLJ20150	HSPX153	MITF	PRDM7	THRA
CCT4	FLJ20244	ICBP90	MLLT10	PREB	THRB
CDK7	FLJ20321	ID1	MLLT4	PRG2	TIEG
CDO	FLJ20551	ID3	MLLT7	PRKCSH	TIMELESS
CDX1	FLJ20557	ID4	MNT	PRKWNK4	TITF1
CDX2	FLJ20595	ILF1	MRIP-1	PROC	TNRC12
CEBPB	FLJ20772	ILF2	MSX2	PTTG1IP	TNRC15
CEBPG	FLJ21603	IPEX	MT2A	PURA	TNRC18
CERD4	FLJ22301	IPF1	MTF1	QDPR	TNRC6
CHD3	FLJ22865	IRF2	MTX1	R28830_2	TNRC9
CHST3	FLJ23309	IRF6	MYBL2	R32184_3	TONDU
CIAO1	FMR2	IRF7	MYC	RAI15	TRC8
CITED1	FOG2	IRLB	MYCL1	RALGDS	TRIM
CITED2	FOS	IRX4	MYCN	RARA	TRIP15
CL469780	FOSB	IRX5	MYD88	RARG	TRIP6
CLK2	FOSL1	ITGA3	MYF5	RBPSUHL	TSA1902
CNOT3	FOSL2	ITM3	MYH11	RELB	TST
COPEB	FOXB1	JUN	MYOD1	REQ	TTF2
CORO1A	FOXC2	JUNB	MYOG	RFP	TZFP
CREB1	FOXO1	KCNN2	MYT2	RFX2	UBB
CRIP1	FOXO2	KIAA0014	NCOR2	RFXANK	UBTF
CRIP2	FOXF1	KIAA0040	NEUD4	RGC32	USP14

CRSP7	FOXF2	KIAA0130	NEUROD1	RING1	UTF1
CRSP9	FOXG1A	KIAA0173	NEUROG1	RISC	VENTX2
CSDA	FOXH1	KIAA0194	NEUROG2	RNF24	WASF2
CSEN	FOXJ1	KIAA0211	NFATC1	RNF4	WBSCR14
CSRP1	FOXL2	KIAA0293	NFATC2	RORC	WHSC1
CSRP2	FOXO3A	KIAA0301	NFE2L1	RRBP1	XBP1
CUTL1	FOXP1	KIAA0306	NFE2L2	RREB1	YAF2
CYLD	FRG1	KIAA0329	NFIC	RXRA	ZFP91
CYP51	FTL	KIAA0414	NFKB2	SAFB	ZFP92
DAXX	FUS	KIAA0444	NFKBIA	SALL1	ZFPL1
DBP	FXC1	KIAA0478	NFKBIE	SALL3	ZIC1
DCTN2	FYCO1	KIAA0943	NFKBIL1	SATB1	ZIC4
DEAF1	GATA2	KIAA1037	NFRKB	SBB103	ZIC5
DFKZP434E026	GATA3	KIAA1050	NFX1	SDCCAG33	ZID
DKFZP434E2216	GATA4	KIAA1190	NFYC	SETDB1	ZNF142
DKFZP434P1750	GBA	KIAA1388	NKX2B	SH3BP2	ZNF147
DKFZp547H236	GBX1	KIAA1431	NKX2C	SHOX	ZNF155
DLX1	GBX2	KIAA1528	NKX6A	SIAH1	ZNF157
DLX3	GCMA	KIAA1610	NMP200	SIM2	ZNF161
DLX4	GCN5L1	KIAA1668	NONO	SIX1	ZNF162
DMRT1	GCN5L2	LBX1	NPAS1	SIX2	ZNF169
DRAP1	GFI1B	LDB1	NPTXR	SIX4	ZNF174
DRIL1	GIOT-2	LDOC1	NR0B1	SLB	ZNF179
DSCAM	GLI2	LEF1	NR1D1	SLC26A3	ZNF185
DSIP1	GLI3	LHX5	NR1D2	SMARCA3	ZNF187
DUX2	GLIS2	LHX6	NR1H3	SMARCA4	ZNF200
DUX4	GPRC5C	LMO1	NR1I3	SMARCE1	ZNF205
DXYS155E	GSH2	LMO4	NR2C1	SMCX	ZNF21
E2F1	GTF2A2	LMO6	NR2E3	SNAPC3	ZNF212
E2F2	GTF2H2	LOC51036	NR2F1	SOX14	ZNF213
E4F1	H-L(3)MBT	LOC51042	NR2F2	SOX30	ZNF22
EBF	H1F3	LOC51058	NR2F6	SP2	ZNF239
EED	H2AFY	LOC51131	NR4A2	SPI1	ZNF261
EGR1	HAND2	LOC51270	NR6A1	SPIB	ZNF268
EHF	HCNGP	LOC51580	NRIP1	SREBF1	ZNF274
EIF3S1	HDAC2	LOC51637	NUP153	SREBF2	ZNF275
EIF3S9	HDAC4	LOC51652	OAZ	SRF	ZNF288
ELAVL2	HES2	LOC55893	ONECUT2	SSX1	ZNF297
ELF3	HES7	LOC56270	OVOL1	SSX2	ZNF32
ELF4	HEY2	LOC57209	P1P373C6	SSX3	ZNF38
EMX1	HEYL	LOC58502	P2RX5	SSX4	ZNF6
ENO1	HHEX	LOC91120	P38IP	SSX5	ZNF75A
EP300	HKR1	LRP5	PAF65B	STAT1	ZNF76
EPAS1	HKR3	LW-1	PAFAH1B1	STAT3	ZNF79
ERCC3	HLA-B	LYL1	PAX4	STAT6	ZNF9
ERP70	HLX1	LZLP	PAX5	STOML1	ZNF93
ESR1	HLXB9	LZTR1	PAX6	SUPT4H1	ZXDA
ETV1	HMG20B	LZTS1	PAX7	SURB7	ZXDA/B

(Table 2-4 continued)

Table 2-5. TFs uniquely on in the cochlea or utricle SE.

Cochlea TFs	Utricle TFs
ARNTL	BLZF1
ASH1	BTEB1
ATF1	CART1
C1orf2	CHD4
CIR	CREBBP
EN1	CTCF
ERF	EGR2
ESR2	ELK3
ESRRA	EN2
GLI	EYA3
HNF3A	FBXO3
IRX7	FLJ22252
LHX4	GTF2H4
MLLT3	HIF1A
NCOR1	HOXA6
NFE2L3	HOXB7
NFYB	HOXD8
NR0B2	HSSOX6
NR1H2	H_GS165L15
NR4A3	IRF5
POU3F2	KIAA0237
PRDM12	KIAA0304
PRDM5	KIAA0602
PRDM9	KIAA1542
PRP17	LMO2
RFX4	LOC51173
RUNX1	MAF
SETBP1	MGC15716
STRBP	NAB2
TCFL5	NFIL3
TIEG2	NSEP1
TNRC10	PAX3
ZFP	POU4F3
ZIM2	SIX6
ZNF12	SNAI1
ZNF141	SNAPC1
ZNF151	SOX11
ZNF207	USF1
ZNF286	ZFY
ZNF33A	ZNF-kaiso
	ZNF183
	ZNF273
	ZNF43

Conclusion

This study had three distinct objectives. The first was the development of new molecular markers to investigate the development and regeneration of the cochlea and utricle epithelia. It is interesting to note that among the changes we observed, several were in genes previously shown to play important roles in inner ear development. These include GATA3 and TBX2 (Lakow-Kerali et al., 2002; van Esch et al., 2000; Karis et al., 2001; Gibson-Brown et al., 1998). I also observed changes in additional inner ear transcription factors such as MATH1 and BRN3C, which showed 1.17 and 1.52-fold changes respectively. However, these genes did not meet the criteria for inclusion in Table 2-2 (ranked by *P*-values) or in Table 2-3 (ranked by fold change). It is likely that these slight observed changes in gene expression reflect the expression of these genes in the hair cells of both sensory epithelia (Bermingham et al., 1999; Erkman et al., 1996). I expect that many of the other genes that were identified in this study will prove useful as markers of inner ear development. Of particular interest are transcription factors such as LOC51637 and HMG20B, about which little is known, but which are both upregulated in the sensory epithelium of the utricle. Another novel TF is the cysteine-rich protein CRIP2/CRP2. It is widely expressed and localized to actin filaments, leading to its implication in assembly and organization of the cytoskeletal components (Louis et al., 1997; Bonnin et al., 2002), but its precise function is unknown. Tables 2-1 and 2-2 contain many additional interesting genes that should prove useful as markers and as clues to inner ear genetic pathways in the future. The set of 78 transcription factors in Table 2-2 should also provide potential markers for the study of the mature cochlea and utricle and for the molecular embryology of these structures. They may also point to pathways, activators or downstream genes that might make interesting targets for future disruption.

The second aim in performing this study was to identify candidate deafness disease loci. A similar strategy has recently proved useful in the search for retinal degeneration loci (Blackshaw et al., 2001). The identification of several known “deafness” loci within our dataset (e.g. GATA3, KIT, and PAX3), suggests that further investigation of these genes as candidate disease loci might be productive. Figure 2-3 shows human chromosome ideograms with the mapped locations of as yet uncloned deafness loci and the localizations of 20 TFs from the list superimposed upon them. While some of these are likely to be coincidental colocalizations, these genes provide readily testable candidates for the various disease loci shown in Figure 2-3.

The final aim was to identify the signaling pathways that are responsible for sensory regeneration in the avian ear by analyzing changes in gene expression between the cochlea and the utricle. This is a complex problem and is further complicated by the dynamic nature of the processes that are occurring in the utricle sensory epithelia. At any given moment some utricular hair cells are undergoing apoptosis, and some supporting cells are quiescent while other are proliferating. Despite these complications it is possible to identify certain signaling pathways within our data set. For example, several stress response genes exhibit differential expression. This includes enolase 1 (ENO1) that is elevated in the utricle sensory epithelia. It acts as both a

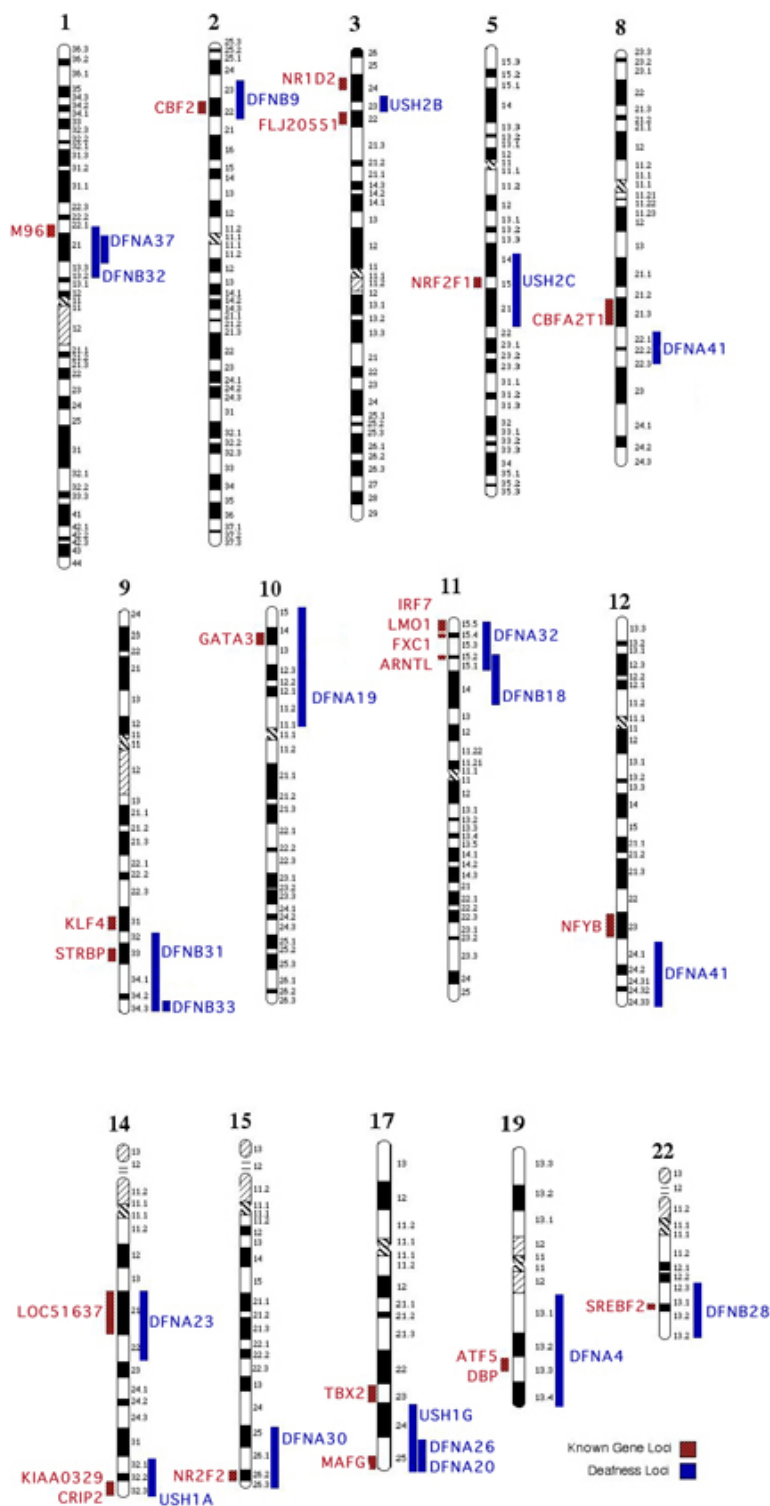


Figure 2-3. Differentially expressed TFs as candidate deafness loci. A set of human ideograms are shown with the bars at the right indicating the localization of various as yet uncloned deafness loci. At the left of each ideogram are shown the genomic locations of various TF genes that show differential expression in cochlea/utricle epithelia from our microarray analyses.

transcription factor and a glycolytic enzyme (Feo et al., 2000) and is involved in multiple events from hypoxia stress response and tumor progression (Jiang et al., 1997), to a structural function in the lens (Wistow et al., 1988). Its expression in the utricle has not been previously described. Another group of stress response genes are MAFs, (Suzuki et al., 2001; Dhakshinamoorthy and Jaiswal, 2000; Moran et al., 2002). These form homo- and heterodimers and act as both transcriptional activators and repressors (Kataoka et al., 1995; Motohashi et al., 2000; Kataoka et al., 2001), but have not previously been shown to be expressed in the inner ear. Our data suggest that MAFG is upregulated in the utricle.

One particularly intriguing result of the present study is the differing expression pattern of the zinc finger transcription factor GATA3 in the cochlea and utricle. Results of both *in situ* hybridization and immunohistochemical labeling indicate that GATA3 is expressed throughout the sensory epithelium of the cochlea, but is limited to the striolar region of the utricle (Figures 2-1 and 2-2). Prior studies have indicated that GATA3 plays several distinct roles in vertebrate development, including the differentiation of T-lymphocytes and selected populations of neural crest-derived and CNS neurons (Parient and McGhee et al., 2002). GATA3 also appears to be involved in the patterning of the developing ear and in pathfinding of the auditory neurons. During the embryonic development of the mammalian ear GATA3 is expressed in selected regions of the otocyst as well as in developing cochlea and in the striolar region of the utricle (Lawoko-Kerali et al, 2002; Rivolta and Holley, 1998; Karis et al., 2001). GATA3 is also expressed in a cell line derived from the mammalian organ of Corti, and is associated with genes that are implicated in neuronal guidance (Rivolta et al., 2002). The expression of GATA3 in the mammalian ear appears to be limited to embryonic development and GATA3 expression is downregulated following hair cell differentiation (Rivolta and Holley, 1998). It is also deleted in

DiGeorge Syndrome and hypoparathyroidism, sensorineural deafness, and renal dysplasia syndrome (HDR) (MIM#131320-GATA3). Data from the present study indicate that GATA3 expression is maintained in the mature avian ear. The observation that GATA3 is expressed in the striolar region of the mature utricle is of particular interest, since the striola defines a narrow boundary where hair cell phenotype, orientation and innervation undergo abrupt changes (e.g., Jorgensen, 1989). Since the mature avian utricle is constantly producing new hair cells, it is likely that the developmental cue(s) that specify the striola remain expressed throughout life. The present results, along with more recent observations (Warchol and Hu, 2003) suggest that GATA3 may serve as a ‘marker’ for the position of the striola during sensory regeneration in the utricle.

In the current study the tyrosine kinase receptor c-KIT was transcriptionally upregulated in the utricular sensory epithelia. Mutations in c-KIT cause piebaldism, a skin pigmentation defect, but mutations in the mouse c-kit gene cause ear abnormalities (Geissler, 1988) and a mutation at R796G in the intracellular kinase domain leads to deafness in one human pedigree (Spritz and Beighton, 1998). Several other genes that have been implicated in human deafness and pigmentation disorders are also upregulated in the avian utricle. These include PAX3 (implicated in Waardenburg Syndrome, [WS]) and TBX2, a known downstream target of MITF (Hone and Smith, 2001; Carreira et al., 2000 also implicated in WS) and regulator of Tyrosinase Related Protein 1 (Galibert et al., 1999). TBX2 has previously been shown to be expressed in the chick otic vesicle from stages 11-27 (Gibson-Brown, et al., 1998) and slight overexpression of this gene has been shown to repress the cell cycle checkpoint gene Cdkn2 and lead to cell immortalization (Jacobs et al., 2000; Sinclair et al., 2002). Interestingly, both melanogenesis and sensory hair cell proliferation can be stimulated by the addition of forskolin which initiates cyclic

AMP (cAMP) synthesis (Navaratnam et al., 1996; Montcouquiol and Corwin, 2001a; Busca and Ballotti, 2000). Both processes are also stimulated by insulin, insulin growth factor, and by beta-catenin (Kuntz and Oesterle, 1998; Warchol, 2002; Tachibana, 2000; Yamashita and Oesterle, 1995). The inner ear contains melanocyte populations (Cable and Steel, 1991), but these were not present in the sensory epithelia used in this study. It is tempting to speculate that the cKIT pathway plays a role in utricle hair cell proliferation independent of its known role in melanocyte differentiation. Despite these few tantalizing clues, most of the changes we have observed do not fall into discernible pathways or networks at this time. It is clear that synchronized regenerating hair cell populations will be important in determining which of these changes are important in the turnover and regeneration of sensory hair cells. Chapter 4 of this thesis addresses this precise point.

Our publication of this work (Hawkins et al., 2003) constituted the first report of the successful use of human microarrays to interrogate chick gene expression. This was also the first time that gene expression changes in such a large number of transcription factor genes have been simultaneously measured. By monitoring over 1800 genes, I identified approximately 100 significant differences in gene expression between the proliferative chick utricle epithelium and the quiescent sensory epithelium of the chick cochlea. By conducting multiple hybridizations, incorporating numerous controls, and using statistical analysis tools we were able to derive a robust set of observations. The changes in gene expression that were observed in this study should provide a diverse set of new reagents for investigating the molecular embryology of the inner ear as well as insights into the genetic pathways of hair cell turnover and regeneration.

CHAPTER THREE

UTRICLE-COCHLEA LIBRARY SUBTRACTION

Introduction

The chicken, *Gallus gallus*, has long served as a primary model organism in embryology, developmental biology, and inner ear hair cell regeneration. Even with its longstanding role in these fields of study, few ESTs are available compared to other organisms such as human, mouse, *Drosophila*, and zebrafish (Based on nucleotides sequenced, NCBI Genbank Per-organism statistics, <ftp://ftp.ncbi.nih.gov/genbank/gbrel.txt>). In this chapter I describe the construction of four cDNA libraries from the inner ear to be used as tools for identifying additional chick ESTs, with a primary interest in inner ear hair cell regeneration. These libraries consist of genes expressed in the sensory epithelia of the utricle and cochlea and represent the transcriptome of supporting cells and hair cells. While the cochlear and utricle hair cells serve different functions, hearing and balance respectively, they are developmentally and structurally similar. I have made use of these similarities in order to understand the gene expression differences between the utricle and cochlea sensory epithelia. I derived two subtracted utricle sensory epithelial (SE) libraries to identify genes involved in hair cell turnover. The cochlea library, containing quiescent hair cells, was used as the driver population of cDNAs against the utricle library of target molecules. The resulting subtracted library should be useful as a source of genes involved in regeneration and apoptotic events in the utricle. To evaluate its quality a total of 1152 clones were sequenced from the primary subtraction and a further 1152 clones were sequenced from a reiterative subtraction library.

Utricle and cochlear sensory epithelia cDNA libraries were constructed for use in a library subtraction scheme. Each of these was derived from pure inner ear sensory epithelia populations. Due to the small number of cells available, four organs were pooled and a micro-cDNA amplification scheme was used (Chapter 7 - Materials and Methods: Figure 7-1, 7-2;

Hawkins et al., 2003; Korshunova et al., in preparation). This methodology incorporates modifications to the SMART (or Super SMART) PCR cDNA Synthesis system (BD/Clontech) and uses a limited number of PCR cycles. Two primary modifications have been implemented. The first requires isolating the mRNA using oligo-dT paramagnetic beads and constructing the first strand cDNA attached to the beads. This allows one to return to the bead-captured cDNA for additional cycle amplification off the beads. The second modification is to add (CAU)₄/(CUA)₄ linkers for ligation-independent cloning into the pAMP1 vector. These linkers are added via PCR, bringing the total cycles for amplification to fifteen. This allows for the creation of libraries before subtraction. For subtractions the tester library (utricle) is converted to ssDNA using M13 Helper phage, and the driver population (cochlea) is PCR amplified in the presence of biotinylated dUTP. After hybridization, the common sequences are selectively isolated using streptavidin-coated paramagnetic beads. The remaining single-stranded tester is converted to double strands using PCR and transformed into bacteria to construct the subtracted library. There are no additional cloning steps to create the subtracted library, as is the case in using the PCR Select method by Clontech. Using these methods, the primary subtracted utricle library was created, and 1152 clones were DNA sequenced. This was followed by a reiterative subtraction to identify additional utricle genes and ESTs. Several of the primary subtraction clones were abundant and accounted for multiple clones. The 1152 primary clones were used as the driver, and the entire primary subtraction library as the tester in the reiterative subtraction to reduce redundancy and increase novel gene or EST discovery.

Results

Subtraction Scheme

To enrich for utricule genes we developed a subtraction methodology that makes use of previously constructed libraries (Figure 3-1). The tester library was converted to ssDNA by infection with M13 Helper phage. The single-stranded population was first checked for double-stranded contamination before proceeding. Double-stranded DNA was removed by DNasing the sample after infection, but before ssDNA isolation from the phage capsids (Simmons and Lovett, 1999). Plasmid DNA was isolated from the driver population and linearized to insure that this population would not result in transformants in the final step of creating the subtracted library. Once the driver library was linearized, the inserts are amplified using nested primers from the original micro-cDNA amplification to create excess driver DNA to drive the hybridization. Biotinylated dUTP was incorporated into the driver amplicons during this step. I also incorporated additional reactions with P³²-dCTP labeling to determine that adequate biotin incorporation/binding efficiency occurred to the streptavidin-coated beads. This was greater than 90%. The tester, excess biotinylated driver, and blocking oligos; oligo-dT, 3' and 5' nested primers, were combined and hybridized to a Cot of 30. Blocking oligos were necessary due to the common primer/linker sequences in each clone from the micro-cDNA amplification method. After hybridization the mixture was combined with streptavidin-coated paramagnetic beads. This allowed for the removal of the driver and tester:driver hybridized clones from the supernatant with a magnetic separator. The supernatant contained the enriched tester population, which was then "repaired" (converted to double strands using PCR), and transformed into host cells to construct the subtracted library. Before this step, the subtracted tester genes were boiled off the beads and inserts were amplified from the enriched tester and subtracted tester.

Amplicons were electrophoresed, blotted, and probed for the relative depletion of an abundant gene *GAPDH*. This gene was evaluated for overall subtraction in the enriched population. The subtracted library was then used in a reiterative subtraction to further enrich for tester genes.

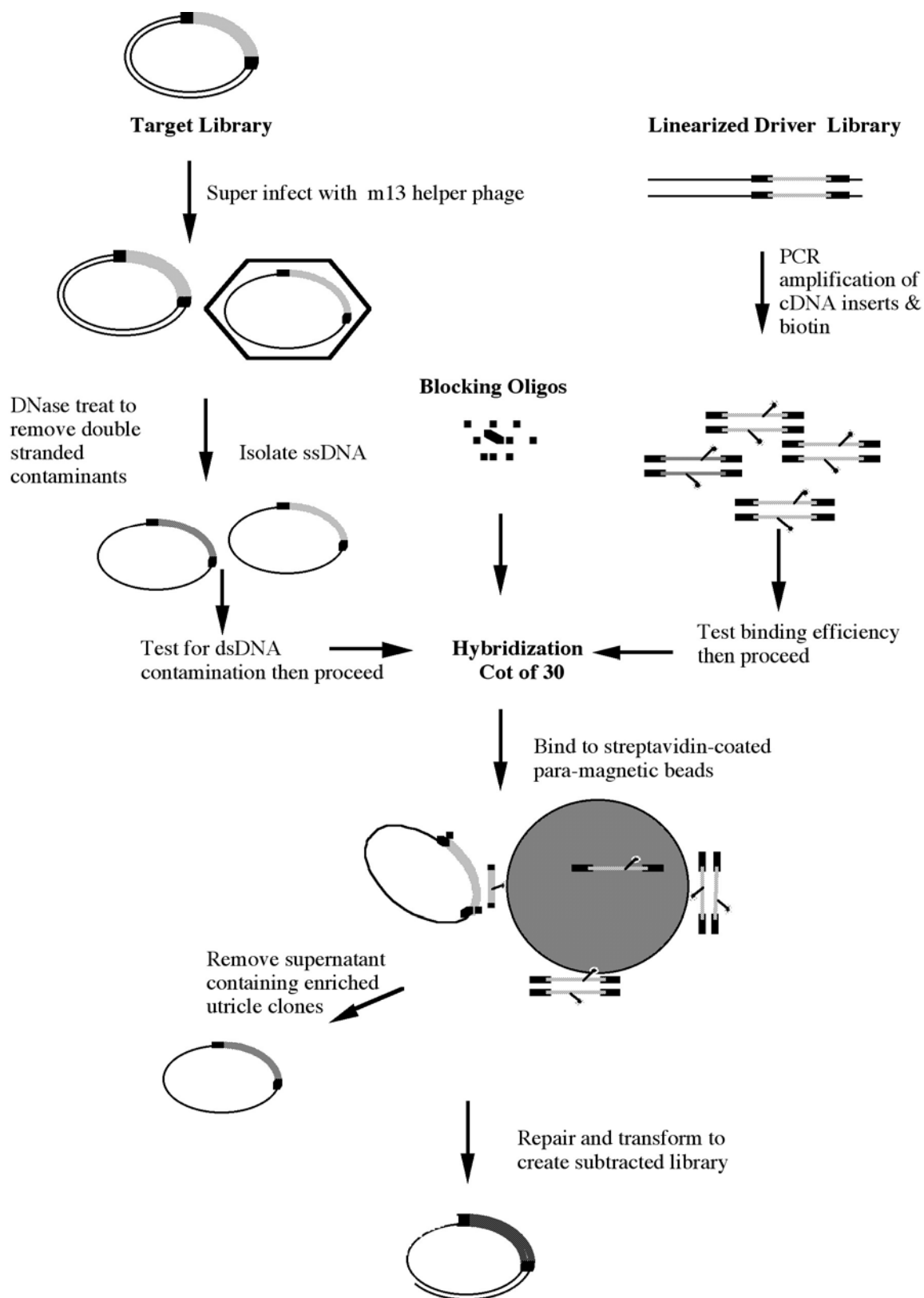


Figure 3-1. Library Subtraction Flow Diagram.

Primary Subtraction

The hair cells and supporting cells of the avian utricle and cochlea are structurally and developmentally very similar. Both will regenerate in response to damage, a process that does not occur in mammals. The hair cells of the cochlea remain quiescent under normal conditions, and the utricular hair cells are in a constant state of renewal. I used the quiescent cochlear SE as the driver against a proliferative utricle SE to identify genes involved in the processes necessary for renewal. Before constructing the actual subtracted library for the next round, the tester population (after subtraction) and the driver-bound tester were analyzed for depletion by amplifying inserts from each using vector-specific primers. The driver was amplified using a nested primer pair and did not contain the vector-specific priming site. Each portion of the tester population was screened for distribution of the abundant cDNA corresponding to chick *GAPDH* (see Materials and Methods and Figure 3-2). The PCR blots demonstrated a significant depletion of *GAPDH*, and the subtracted utricle library was then constructed. The two starting libraries and the primary subtraction library were subsequently screened again by colony lift hybridization with a *GAPDH* probe to quantitate the depletion of this abundant gene (Table 3-1). Starting with approximately equal number of clones, *GAPDH* was reduced 2.5 fold. From the primary subtraction library, 1152 clones were DNA sequenced. These produced 1002 good reads with ample sequence for BLASTing against various databases for clone identification.

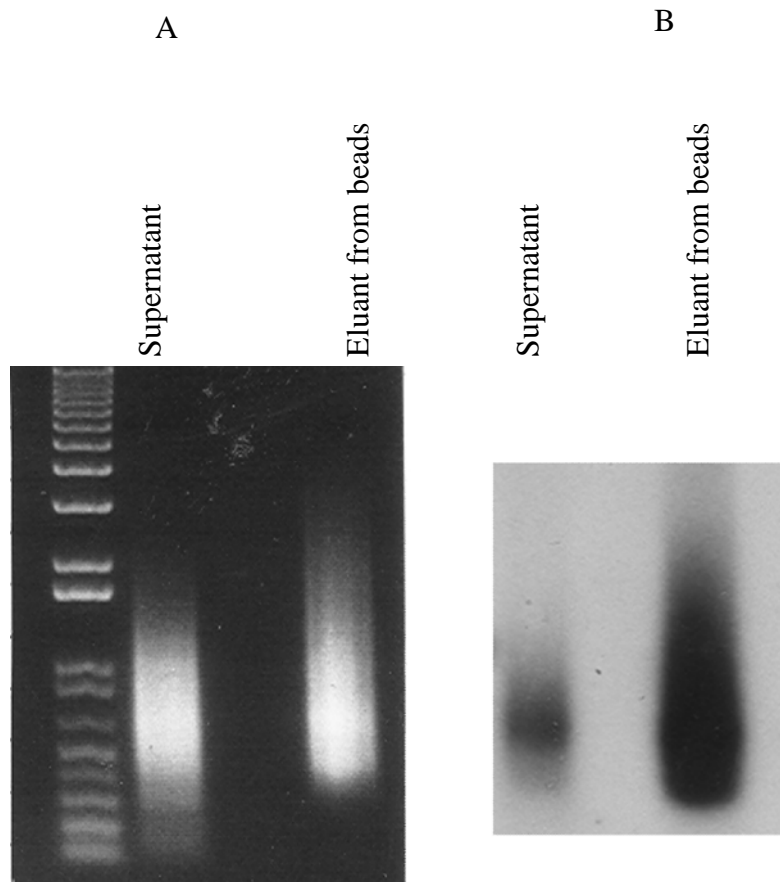


Figure 3-2. *GAPDH* Distribution. After binding the subtraction to the beads the supernatant was removed containing the enriched tester. The beads were then boiled to remove the subtracted-away tester. Each of these served as templates to amplify inserts by PCR. (A) Equal amounts of amplicons were electrophoresed on a 1% agarose gel and blotted. The two populations were screened for the presence of *GAPDH*, an abundant transcript in the driver and target. B shows *GAPDH* was subtracted away and greatly reduced in the supernatant (putative subtraction)

Table 3-1. *GAPDH* Distribution.

Library	<i>GAPDH</i> Colonies per 50,000 cfu
Cochlea Sensory Epithelia (driver)	100
Utricle Sensory Epithelia (tester)	75
Primary Subtraction (Utricle)	30

GAPDH was not screened in the Reiterative Library because it was not present in the driver collection of clones.

Reiterative Subtraction

In order to increase the discovery rate for novel ESTs within the subtraction and to consequently reduce sequencing costs, the original 1152 sequenced clones from the primary subtraction were employed as a driver against the primary subtraction. The rationale here was that these probably represented higher abundance genes in the primary subtraction. We reasoned that using these clones in the reiterative round as the driver, should reduce their presence in the reiterative library and increase the presence of lower abundant genes. An additional 1152 clones from the reiterative subtraction library were sent to the Washington University Genome Sequencing Center for DNA sequencing. Clones from all four libraries, two starting and primary plus reiterative subtractions, were screened for enrichment. The libraries were screened by colony hybridization for various genes that were identified from the reiterative subtraction's initial sequencing runs, all

three genes tested showed enrichment from the starting utricle library to the final reiterative subtraction library (Table 3-2). This result demonstrated how abundant genes can be depleted in a reiterative format so that additional genes or ESTs can be more rapidly identified by sequencing the same number of clones.

Table 3-2. Reiterative Subtraction Enrichment. Occurrence of genes per 5,000 cfu.

Library	<i>Myak-S</i>	<i>Annexin V</i>	<i>EGR1</i>
Cochlea SE	0	0	0
Utricle SE	0	1	4
Primary Subtraction	0	2	4
Reiterative Subtraction	2	16	11

Sequence Analysis

In order to analyze the sequenced clones from the primary and reiterative subtraction, they were BLASTed against various databases to assess whether they were clear orthologs or paralogs of known genes. To determine how many known chicken genes and ESTs were sequenced, the clones were BLASTed against the TIGR *Gallus gallus* index, BBSRC chicken finished cDNAs (University of Delaware), and NCBI

chicken ESTs. As many chicken genes have yet to be fully annotated, the clones were also BLASTed against the Human Unigene Build #175 to identify, where possible, the human orthologs. All sequencing information can be found at http://hg.wustl.edu/lovett/Gg_utr/ as it is too large to be represented in an Appendix.

Following removal of poor sequence reads and removal of concatemeric clones, 1002 clones comprised the primary subtraction library sequence analysis. Clones with overlapping sequence identity from each library were grouped into contigs. Four hundred eighty-seven clones were distributed across 108 contigs, and the remaining 515 were singlets (meaning they did not align with another clone sequenced in that round). The sequence returned from the reiterative library subtraction yielded fewer clones with good sequence reads; 708 in total. Of these clones, 555 grouped into 127 contigs, and the remaining 153 were singlets (all contigs can be viewed at http://hg.wustl.edu/lovett/Gg_utr/). As mentioned above, these clones were BLASTed against four databases to determine if the clone or contig was either novel or previously annotated. The criteria for chicken databases sequence searches was 90% sequence identity across a minimum of 80 bp with a probability cutoff of $1e-07$. For human database sequence searches the criteria were 70% identity within 80 bp and a cutoff of $1e-05$. Venn diagrams were compiled to show how each database provided information about the clones (Figure 3-3). The numbers in Figure 3-3 represent singlets and contigs. Thus, several clones that hit a gene or an anonymous contig were considered one entity in the Venn diagram (Figure 3-3). Only one clone from the primary library was uniquely found in the Delaware database, and one clone from each library was uniquely found in the Human Unigene database, whereas the TIGR database provided the highest number

of hits specific to one database. However, the Human database was useful in this comparison since many chicken ESTs are only annotated as an "EST", whereas the human BLAST comparisons provided a orthologous gene name (all annotations are available at http://hg.wustl.edu/lovet/Gg_utr/). The majority of information was derived from sequence hits in the *Gallus gallus* databases from TIGR and NCBI.

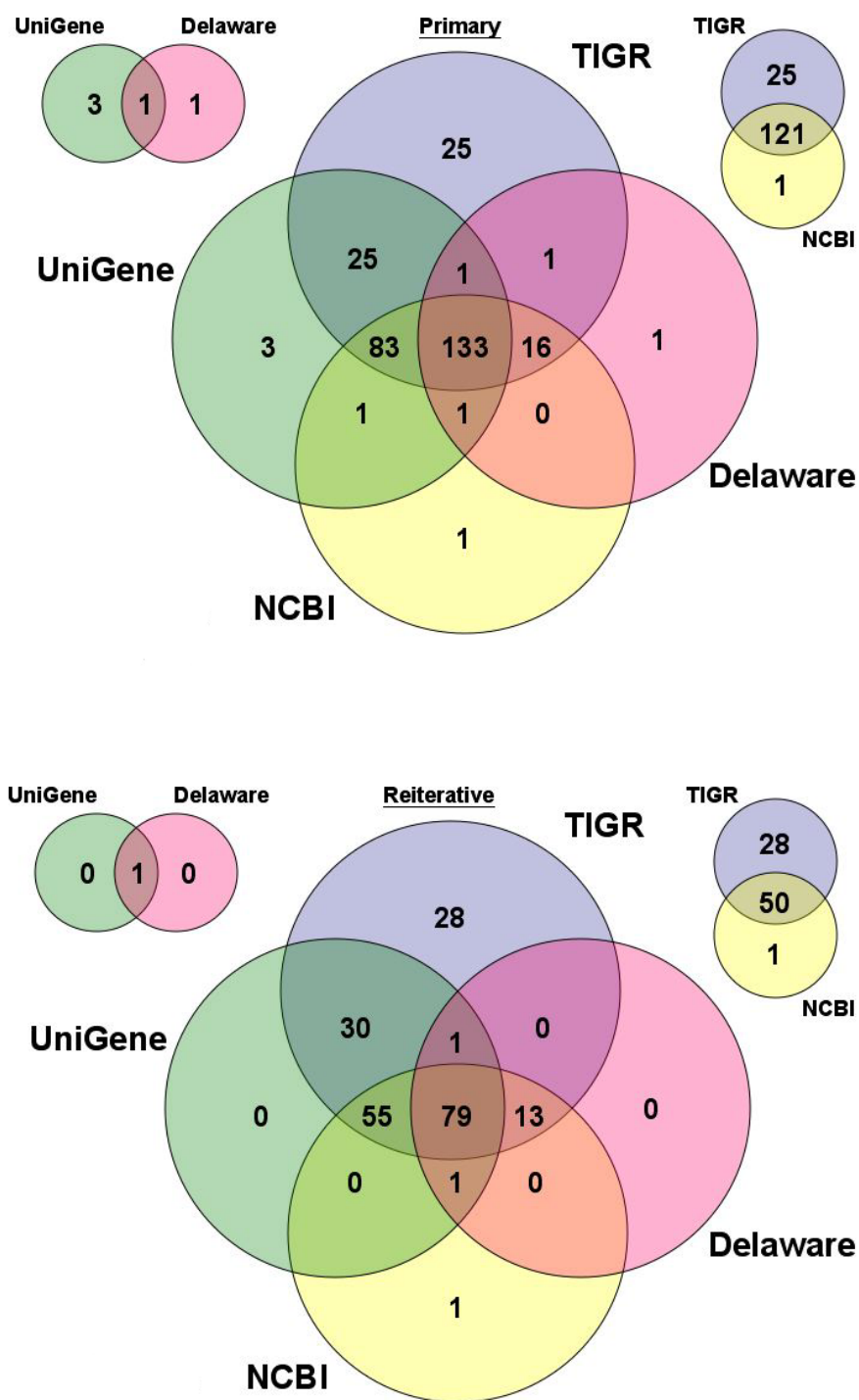
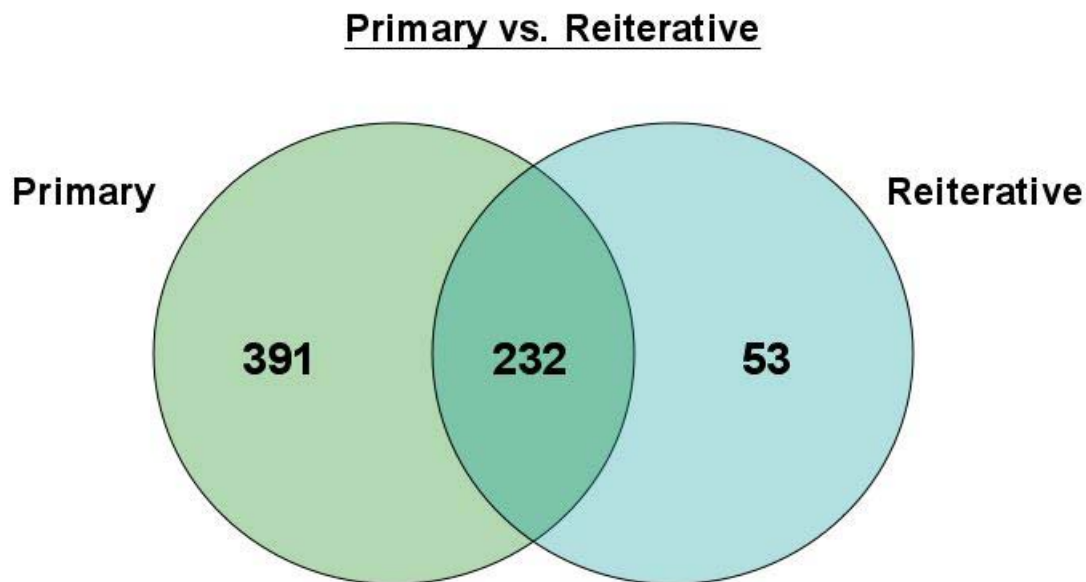


Figure 3-3. Database Venn Diagrams. The majority of genes and ESTs identified were found in the TIGR and NCBI databases. In a four-way comparison some commonalities cannot be shown and are therefore to each side of the main diagram. For example, it does not illustrate the clones found uniquely in Unigene and Delaware, but not found in NCBI or TIGR.

Genes that did not have a significant hit in these four databases were considered novel chicken ESTs. From the primary library there were 210 versus 22 in the reiterative round. Additionally, a comparison of the two libraries by BLASTing the reiterative against the primary reveals that more clones are unique to the primary subtraction (Figure 3-4).

Figure 3-4. Comparison of libraries for uniqueness. A greater number of clones are unique to



The reiterative library was blasted against the primary library to determine overlap the primary library as opposed to the reiterative.

The majority of clones in the reiterative round were previously sequence in the primary subtraction. This is possibly due to the library subtractions being driven to too large of a Cot value. For instance, recall that the primary round contains 515 singlets, whereas the reiterative has 153 singlets. A large number of clones that were represented by a single

clone, 360 to be exact, were completely removed in the reiterative round. However, the reiterative round does provide evidence that it was useful in enriching for clones specific to the utricle. The best example of utricle-specific enrichment is shown in Table 3-2. The three genes screened by colony hybridization against all four libraries not only show enrichment, but were absent from the cochlea library at the level screened. In fact, the *MYAK-S* is only present in the reiterative library. Had this round not been carried out, this gene would not be identified nor would the other 52 clones unique to this round (see Figure 3-4).

Conclusion

Subtraction Efficiency

In order to expedite the identification of novel genes and ESTs from the inner ear of the avian *Gallus gallus*, I employed a novel subtraction scheme. I used this in a reiterative manner to greatly reduce abundant genes such as *GAPDH* from the resulting library. The most abundant gene sequenced in the primary subtraction was ribosomal protein S3a present in 68 out of the 1002 clones with good sequence reads (6.8% of reads). This was reduced to 23 clones out of the 708 clones with good sequence reads in the reiterative subtraction (3.2% of reads). Another abundant cDNA, cytochrome c oxidase subunit I, was reduced from 20 copies to just 3 in the reiterative library (reduced from 2 to 0.4% of reads).

In addition this method demonstrates how several genes are enriched in a reiterative subtracted library as compared to the starting library. Reiterative contigs 114

and 118 increase from one copy to 7 and 8 copies, respectively (http://hg.wustl.edu/lovett/Gg_utr/). More importantly, screening the cochlear, utricle, primary and reiterative libraries for the presence of clones identified from the reiterative sequence reads, revealed that these gene were not present in the cochlear library, and were enriched by utilizing the reiterative round of subtraction. However, the utricle-specific enrichment achieved by multiple subtraction rounds, also lead to a decrease in newly identified clones in the second round. In future studies, this can likely be overcome by decreasing the Cot value to which the subtraction was driven.

"Interesting" genes present in the subtracted library

The reiterative subtraction was carried out on the sensory epithelia of two inner ear hair cell populations. Our primary interest in building this resource was to identify genes that play a role in the turnover of utricle hair cells. A full list of genes identified in the primary and reiterative subtraction can be found on our website (http://hg.wustl.edu/lovett/Gg_utr/). Among these is P311, which has previously been shown to play a role in neuronal regeneration (Fujitani et al., 2004) as well as increase proliferation and upregulate key signaling factors such as fibroblast growth factor 2 and platelet derived growth factor (PDGF), and PDGF receptors (Pan et al., 2002). Another identified gene that plays a role in neuronal growth and survival is homeodomain interacting protein kinase 2 (HIPK2) by interacting with Brn3a (Wiggins et al., 2004). Previously, it has been shown that *HIPK2* is expressed in retinal, muscle, and neural tissues (Pierantoni et al., 2002), and now utricle SE cells can be added to this list. In

addition to these two genes playing a role in neuronal growth and regeneration, their expression in the utricle SE may indicate a similar role in these cells.

As hair cells are regenerated, it is important that proper alignment and patterning be maintained. Within the utricle, an area known as the striola delineates where the orientation of the stereocilia change by 180°. This change in orientation is likely to due planar cell polarity (PCP), a process in the inner ear that, so far, has only been studied in cochlear hair cells due to several deaf mouse mutants harboring mutations in PCP genes (Montcouquiol et al., 2003; Curtin et al., 2003). While the authors made no mention of a utricle phenotype, these mice, and possibly other deaf mice, may have a vestibular phenotype, as deaf mice have a tendency to circle round and round, leading to names such as *deaf circler*, *waltzer*, and *whirler* (see Chapter 1). The *Spalt1* gene, identified in the reiterative library, has been shown to play a role in cell fate determination, pattern formation, and is controlled by FGF and Wnt signaling (a known PCP signaling cascade - see Chapter 1) in other tissues (Farrell et al., 2000). There are two orthologs of *Spalt1* in *Drosophila*, *spalt major* and *spalt-related*. These two genes are essential for establishing polarity in the R3 cell of the ommatidia (fly eye), and upregulating *Delta* which signals Notch in the R4 cell to establish that cell's fate (Domingos et al., 2004). It is unclear if *Spalt1* is playing a role in patterning as directly related to PCP and the striola, or if the signaling pathway in the fly eye defines hair cell versus supporting cell fates (see Notch signaling in Chapter 1) in the utricle, but the utricle SE provides an attractive model for testing such functions.

In order to regenerate hair cells, supporting cells have to re-enter the cell cycle. Several genes that have previously been shown to be involved in this process were

sequenced including, cyclinA, p21, an EST similar to CDC27, and KCIP-1, a 14-3-3 family member. The family of 14-3-3 genes relate mitogenic signals to the cell cycle through the roles of Rafs and CDCs (Aoki et al., 2000). I identified another gene from this family, 14-3-3 tau/theta that interacts with p27^{kip} after p27^{kip} phosphorylation by Akt (Fujita et al., 2002). p27^{kip} is a cell cycle kinase inhibitor that establishes when cell in the developing sensory epithelia of the cochlea stop proliferating and start differentiating into hair cells (see Chapter 1). Another rather more basic cell cycle gene found in the library is Nek-9, which is involved in interphase progression (Tan et al., 2004), and could likely be found in any cell that is replicating. Nevertheless, this validates the goal to identify genes involved cellular proliferation/regeneration.

In addition, several structural proteins were also expressed. These genes include *Microtubule-associated protein 1*, *Harmonin b3*, *Annexin V*, *Actin-like protein 2*, *Filamin*, *beta-tectorin*, *Troponin I*, and *Tubulin gamma complex associated protein 3*. The structural elements comprising the hair cell bundles both in the vestibular organs and the cochlea are essential for their function. Many of the deafness genes identified to date have affected these types of genes (for a complete list of human deafness genes and uncloned loci see the Hereditary Hearing Loss Homepage: <http://webhost.ua.ac.be/hhh/>). Interestingly, *beta-tectorin*, which brings to mind the tectoral membrane overlying cochlear hair cells, is also expressed in the utricle both in the otoconia membrane and in the sensory epithelia in the mouse inner ear (Rau et al., 1999). In the utricle SE, RNA *in situ* analysis revealed that the expression is localized to the striola and is continually expressed, at least until post-natal day 150 (P150), whereas beta-tectorin expression in the cochlear supporting cells subsides around P1 (Rau et al., 1999). If this temporal

expression is true for the chicken utricle and cochlea, it would indicate that *beta-tectorin* expression is utricle specific, exemplifying utricle gene enrichment in the library.

I have used a novel subtraction method that utilized libraries constructed from approximately 50,000 sensory epithelial cells from the chicken utricle and cochlea. These two libraries, along with the subsequent subtraction libraries are the first ever constructed from the chicken sensory epithelia. The starting libraries are comprised of 1×10^6 primary transformants, while the subtracted libraries are comprised of 10^5 primary transformants. All libraries have been made publicly available by deposition with ATCC (www.atcc.org). These libraries contain known inner ear genes such as *beta-tectorin* (Rau et al., 1999) and *Harmonin b3* (*USH1C*-Chapter 1; Boeda et al., 2002), as well as genes involved in the underlying processes necessary for hair cell regeneration. Additionally, from the 1,710 good sequence reads, over 200 novel chicken ESTs were identified making this a valuable resource additional chicken EST discovery and adding on to the expanding list of annotated chicken genes.

CHAPTER FOUR

UTRICLE SENSORY EPITHELIA TIME COURES OF REGENERATION

Introduction

Hair cells (HCs) of the inner ear are the mechano-electrical receptors that transmit sound sensation in the cochlea and detect head movement and acceleration in the vestibular organs. These cells are essential for hearing and balance, and damage leads to permanent deficits. However, avians possess the ability to regenerate these cells (Corwin and Cotanche, 1988; Ryals and Rubel, 1988). The underlying or surrounding supporting cells (SCs) in both the cochlea and utricle (vestibular organ) give rise to new hair cells after damage and death of HCs (Warchol and Corwin, 1996). The mammalian utricle has a limited ability to regenerate (Warchol et al., 1993; Forge et al., 1993), but not robust enough to compensate for substantial damage. Therefore, understanding avian regeneration should provide great insights into how the inhibition of this process in the mammalian inner ear can be bypassed. Several attempts have been made to induce HC regeneration by exposure to mitogenic factors, with limited success (Yamashita and Oesterle, 1995; Lee and Cotanche, 1996). Additionally, genes involved in this process in avians have traditionally been identified on an individual basis (Delta1-Stone and Rubel, 1999; FGFR3-Birmingham-McDonogh et al., 2001; Prox1-Stone et al., 2004). Previously, I employed microarray technologies to interrogate avian utricular regeneration genes by comparison to the quiescent cochlea (Hawkins et al., 2003). In this chapter, I describe expression profiles of the utricle sensory epithelia (SE), hair cells and supporting cells, following time courses of recovery after damage by either laser ablation or ototoxic drug exposure. I was able to identify treatment-, as well as time point-specific transcription genes. I will also describe commonalities that were identified between the utricle and cochlea SE subjected to the same treatments and time courses (work that was done at the same time by another individual in the Lovett lab).

Results

In this study I used an oligonucleotide arrays comprised of 50mers that interrogate human transcription factor genes, to assess the expression of the orthologous chicken genes during HC regeneration. We, as well as others, have shown that cross-species hybridizations can be used on array platforms with a large degree of success (Hawkins et al., 2003 and Renn et al., 2004). I monitored regeneration in the chicken utricle after damage by two separate agents, in each case profiling only the sensory epithelia, which contains HCs and SCs. First, HCs were ablated by a laser microbeam to instantly kill the cells. After laser ablation the sensory epithelia was allowed to recover over a three hour time course with sampling at the following times: 30 minutes (min), 1 hour (hr), 2 hrs, and 3 hrs. Each time point was matched with a control. In the second set of time courses, organ cultures were treated with the ototoxic antibiotic neomycin for 24 hrs. The drug containing media was then replaced with fresh media and the cultures were allowed to recover for the following times: 0hr (immediately following 24 hr neomycin treatment), 24 hrs, and 48hrs. Again, each time point has a time matched control for profiling. Previous studies have shown that supporting cells are already dividing and differentiating within this time frame (Stone and Cotanche, 1994). Due to the instant death of cells following laser ablation these cells were sampled at early time points. In the case of the neomycin, a majority of HCs are killed in the initial 24 hours of drug exposure, necessitating a longer recovery and therefore, were sampled at later and broader time points, nearing full recovery by the 48 hr time point (personal communication -Dr. Mark Warchol; Kil et al., 1997).

Array analysis

Each time course consisted of pools from 4-5 damaged utricle SE cultures. Each time course and set of array hybridizations was also replicated with additional biological samples, including controls. Treatment time points and time matched controls were hybridized a minimum of four times, two and two dye switch experiments. The study comprised a minimum of 56 hybridizations. The array data was put through series of biostatistical steps to achieve the best output for fold changes in expression with associated statistical confidence limits. First, the array data was normalized by LOWESS, a locally weighted linear regression model, to compensate for dye effects (Quackenbush 2002). Second, data from multiple hybridizations for a time point was hierarchically clustered along with a dataset from an additional time point to identify the hybridizations that were most similar for that specific time point. Clusters typically included samples labeled with both dyes (a treatment clustered with the dye switch experiments, indicating minimal dye bias), and contained hybridizations from both biological samples (data not shown). In addition to including both biological samples in the cluster, t-tests were performed between samples to ensure similarity. Data was filtered in an additional step to remove spots/genes below an arbitrary threshold for background intensity. The threshold was determined by the spot intensity of controls that should not show expression, and by how these spots fell in the overall distribution of intensity values. Approximately 10-20% of all TFs were removed at this step. Gene expression fold changes were determined for genes following a trend in 80% of the clustered hybridizations (e.g. if a cluster contained 10 hybridizations, gene A would need to have a similar fold change in 8 out of 10 of those hybridizations to pass the filter). This was applied to every gene in the data set. The average fold change of each gene was calculated from the clustered experiments fitting this trend. A P-value was calculated using a

one-sample t-test. In general the vast majority of TFs showed small expression fold changes. This may be due to either of two main reasons. The compression of the dynamic range in gene expression due to cross-species hybridizations, and TFs themselves may only change slightly in their expression levels in order to have a dramatic effect on the gene expression of their targets (Bolouri and Davidson, 1993). Therefore, I set a fairly low fold expression change threshold of 1.2 fold for this data set. However, many of these "small" changes have highly significant P-values (e.g. DEAF1 at 0hr, 1.32 fold change, P-value = 0.002). As a means of validation, qPCR assays (conducted with chicken-specific primers) showed close agreement with arrays over 14 microarray data points in this study. An additional 14 data points were validated by Dr. Stavros Bashiardes in the Lovett lab, who profiled similar time courses on the chicken cochlea SE using the same TF microarray. His work (similar in size and scope to my utricle study) is only briefly discussed below in a comparison of utricle and cochlea regeneration.

Venn Diagrams: Genes that are "on"

In addition to using the normalized intensity values to calculate fold changes, intensity values were used to determine which TFs were "on" at each of the time points. Based on control spots that should not hybridize, a background intensity level was set to determine which TFs were above the threshold in the damaged samples. Venn diagrams (Figure 4-1) were used to illustrate the number of genes that are on in each time course, and how these genes may be specific to, or in common with, another time point. A large number of TFs are always expressed in each time course regardless of the time point (center of the Venn diagram), but the number of genes commonly on in each treatment did differ significantly. The neomycin damage time course showed 367 TFs being always expressed (Figure 4-1A; Appendix Table A4-1), while the

laser damage time course revealed the expression of 535 commonly expressed TFs (Figure 4-1B; Appendix Table A4-2). By comparing the two groups of genes that are always on in each treatment, 256 are in common between the two types of damage, comprising a core group of TF genes (data not shown). These genes are expressed in the damaged utricle sensory epithelia regardless of the type of damage and regardless of the time of recovery following damage. Determining whether a gene was on in each treatment was based solely on expression levels in the damaged time points. Whether a gene was expressed in the control as well was not considered. Therefore, comparing this core group of 256 genes to a core group of control utricle genes would distinguish which genes are always on in the utricle and which are always on but only after damage.

The difference in the number of genes expressed during the laser treatment as compared to the neomycin treatment is likely to signify an early response to damage and initiation of repair. Similarly, the neomycin 0 hr time point shows the largest number of genes expressed in that time course with a total of 786 genes. Additionally, genes that are unique to each time point are represented in the non-overlapping areas of each diagram (Appendix Tables A4-1 and A4-2). These are not expressed at any other time during that time course. The use of Venn diagrams provides a useful visual means for correlating expression data between multiple time points or samples.

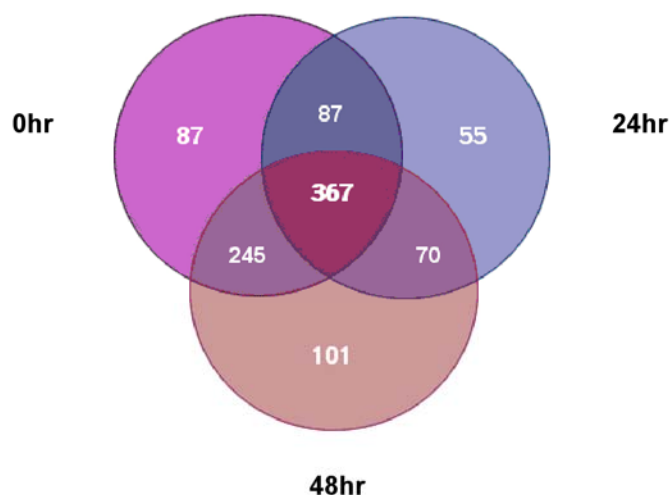
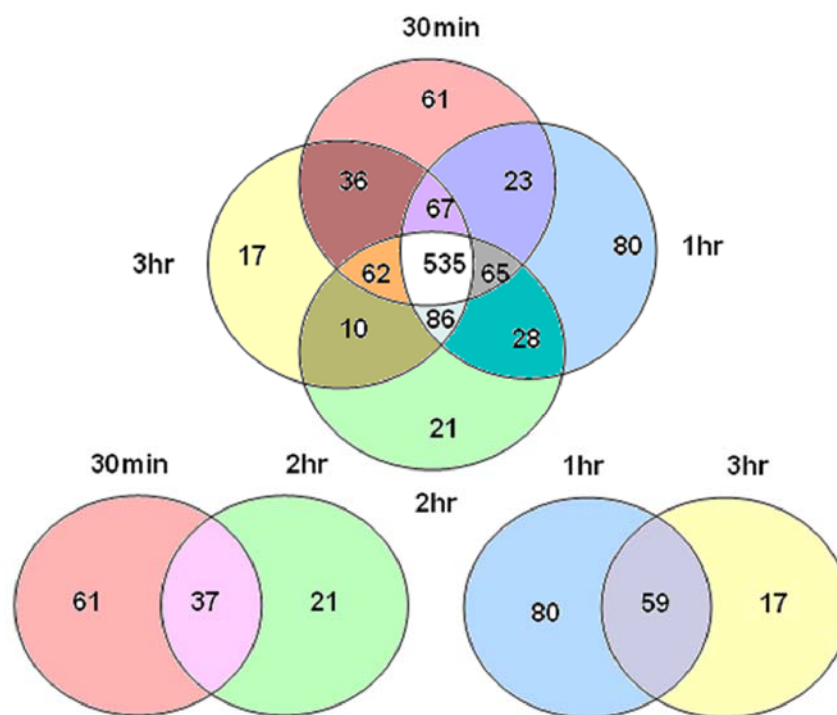
A. Neomycin**B. Laser**

Figure 4-1. Venn Diagrams illustrating the number of genes "on" at each time point. **A.** Neomycin Venn diagram shows genes on at each recovery time point following neomycin damage. **B.** Laser Venn diagram shows genes shared and unique between laser recovery time points. Two time point commonalities (30mins-2hr ; 1hr-3hr) cannot be displayed in the primary Laser Venn diagram and are therefore shown below it. Gene names are listed in Appendix Tables A4-1 and A4-2.

Neomycin Time Course

The utricle SE were cultured in the presence of neomycin for 24 hrs to kill the majority of HCs. At the end of this 24 hr period, time points were profiled after 0 hrs, 24 hrs, and 48 hrs of recovery in fresh media. Due to the small amount of cells available 3-5 cultures were pooled to comprise 30,000-50,000 cells, and the micro-cDNA amplification method was implemented before profiling. Again, since number of cells was limiting, each time point was set up as a different experiment (meaning, that it is not possible to remove a select number of cells for one time point and allow the remaining cells to continue to recover until the next time point). For this reason, each time point has its own time matched control. Comparison of controls across time points (e.g. 0 hr control versus 48 hr control), did show some variability, implying some expression differences due to length of time in culture. This again underscores the need for having separate controls for each time point.

At the 0 hr time point, the sensory epithelia is comprised primarily of SCs, as the majority of HCs have been killed by the ototoxic antibiotic, and by 48 hrs the HCs are close to full recovery. After expression profiling the neomycin time course, 195 TFs made it through the data analysis filters for the three time points (Appendix Table A4-3). All of these genes were differentially expressed in at least one of the time points. Across this time course of differentially expressed genes, the highest expression activity was evident at 48 hrs. There are 69 genes upregulated at 48 hrs, compared to 41 at 0 hr and 22 at 24 hrs.

In order to verify the microarray changes, several data points that showed differential expression were validated by quantitative PCR (qPCR). A total of 14 data points were shown to be in complete agreement with, or similar to, the microarray data (Table 4-1). Additionally, three genes were tested by qPCR at all three time points to not only validate fold changes but the

trend of genes expression during regeneration (Figure 4-2). The genes validated were *KIAA0173*, a novel TF; *CTNNB1*, which is prevalent during SE proliferation (Warchol 2002); and *TRIP15*, a component of the COP9 signalsome (Yang et al., 2002), which can inhibit G1-S transition through interactions with p27, an important regulator of cellular proliferation during auditory HC development (Chen and Segil, 1999). The array fold changes and qPCR fold changes were plotted together and show striking similarities. However, one data point for *TRIP15*, at 24 hrs, is slightly different, as the array data is virtually 1 and the qPCR shows upregulation. The correlation of qPCR results to microarray changes validates the cross-species hybridizations, array fold changes, and expression trends. Again, 14 additional data points were verified from the cochlea time course (additional work conducted by others in the Lovett lab) corroborating the validity of the profiling system and the analytical steps taken.

	Array	P-value	qPCR
NEO 0			
CEBPG	-0.4525	0.0395	-1.4739
CTNNB1	-0.2195	0.0923	-0.5778
KIAA0173	0.3925	0.0090	0.7655
BRD1	-0.5733	0.0059	-0.0291
TRIP15	-0.2823	0.0125	-0.6781
NEO 24			
CTNNB1	-0.1677	0.1007	-0.3219
KIAA0173	-0.1010	0.7074	-0.0291
TRIP15	-0.0347	0.5894	0.4854
NEO 48			
BCL11A	0.4154	0.0260	1.1506
CTNNB1	1.3530	0.0354	1.1827
KIAA0173	0.3658	0.1105	0.6781
CUTL1	0.4661	0.0056	0.3785
CYLD	-0.3515	0.0083	-0.0589
TRIP15	0.4103	0.1410	0.3785

Table 4-1. Microarray validation by qPCR.
Fold changes are log2 values.

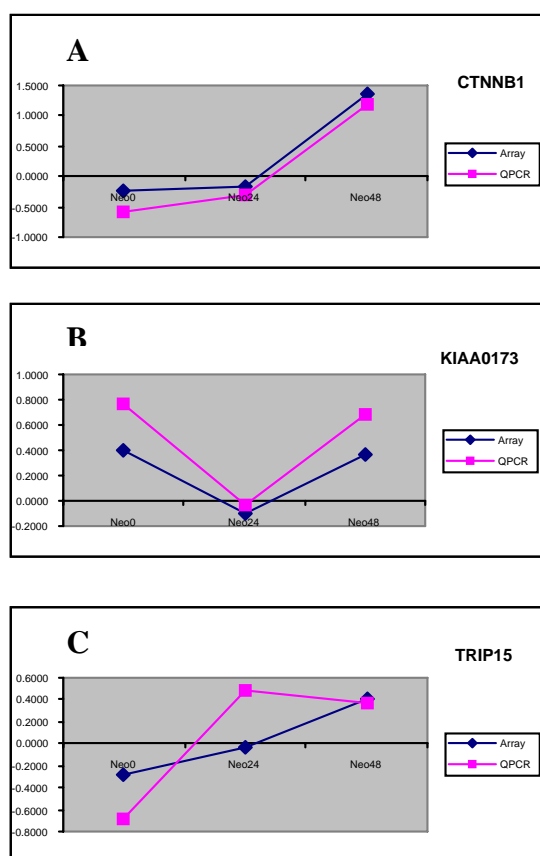


Figure 4-2. Array-qPCR comparisons for beta-catenin (A), KIAA0173 (B), and TRIP15 (C). Fold changes are plotted in log base 2 values from neomycin 0hr-24hr-48hr for microarray values (blue) and qPCR (pink).

Laser Time Course

The advantage of killing hair cells via laser ablation is that there is essentially instantaneous cell death and loss of the hair cell, which in turn signals to the supporting cells to start regenerating. Previous work by our collaborator, Dr. M. Warchol, showed that by 16 hours following laser ablation, BrdU labeling signified that supporting cells had re-entered the cell cycle (Warchol and Corwin, 1996). To understand what is starting this process one must look much earlier. I profiled laser damaged SE compared to time matched controls at 30 mins, 1 hr, 2

hrs, and 3 hrs after laser lesions. Once again, these experiments were set up individually to obtain enough cells for profiling. Assessment of all four time points indicates a total of 261 TFs as differentially expressed (Appendix Table A4-4). Unlike the neomycin time course, which showed more upregulation at the beginning and ending time points, the laser data follows an upward trend of increased gene expression. The number of genes upregulated at each time point is as follows; 36, 56, 68, and 92. These early time points are likely identifying genes that immediately respond to damage and the initiation of moving back into the cell cycle in order to regenerate new hair cells. The TFs that are expressed early may be key to activating hair cell regeneration in mammals by inducing supporting cell division. While artificially activating TFs will likely prove difficult, several TFs expressed in this time course may prove more accessible. Some of these TFs are steroid/hormone activated receptor TFs or their interacting co-activators. These include androgen receptor (AR), RAR-related orphan receptor gamma (RORC), thyroid hormone receptor interacting protein 15 (TRIP15), and a host of nuclear receptors; NR1H3, NR1I3, NR2E3, NCOA1. These TFs may make more feasible targets for activating hair cell regeneration with known drugs or other chemical compounds.

Pathways

Gene profiling leads to gaining large amounts of data that may be difficult to extract meaning from. For time courses, one way to view the data is to see how the pattern of gene expression changes with time or treatment. Grouping genes into similar expression patterns is particularly interesting in identifying underlying reasons for this co-segregation. The more complex this pattern becomes, i.e. the more time points, the less likely it is that genes are showing co-variance due to chance. Co-segregation could imply regulation by a common

transcription factor, or genes common to a particular genetic or signaling pathway. Networking the various interactions between transcription factors involved in regeneration will help describe how the SE progresses from damage to full recovery. This will have important implications for 'jumpstarting' this process in the mammalian inner ear. Self-organizing maps (SOM) were constructed combining each time course, laser and neomycin, to determine how differentially expressed transcription factors co-segregate across such a complex time course (Figure 4-3). Since all the expression values for a gene may not have passed the filter at every time point, values were filled in, in order to create the SOMs. Changes in gene expression at non-represented time points were discerned using a "trend following cutoff" below that of the typical 80% threshold, and this value was then filled in to construct the patterns of gene expression across all seven time points. While some patterns show how genes are both up and downregulated across the entire time course, centroids 9-12 in Figure 4-3 illustrate how many of these genes peak at a single time point and are relatively unchanged at other time points (genes in each centroid are listed in Appendix Table A4-5). Determining if these peaks of expression are critical for regenerative progression might prove beneficial in establishing a transcription network and the triggering of downstream gene expression (See Chapter 5 on RNAi).

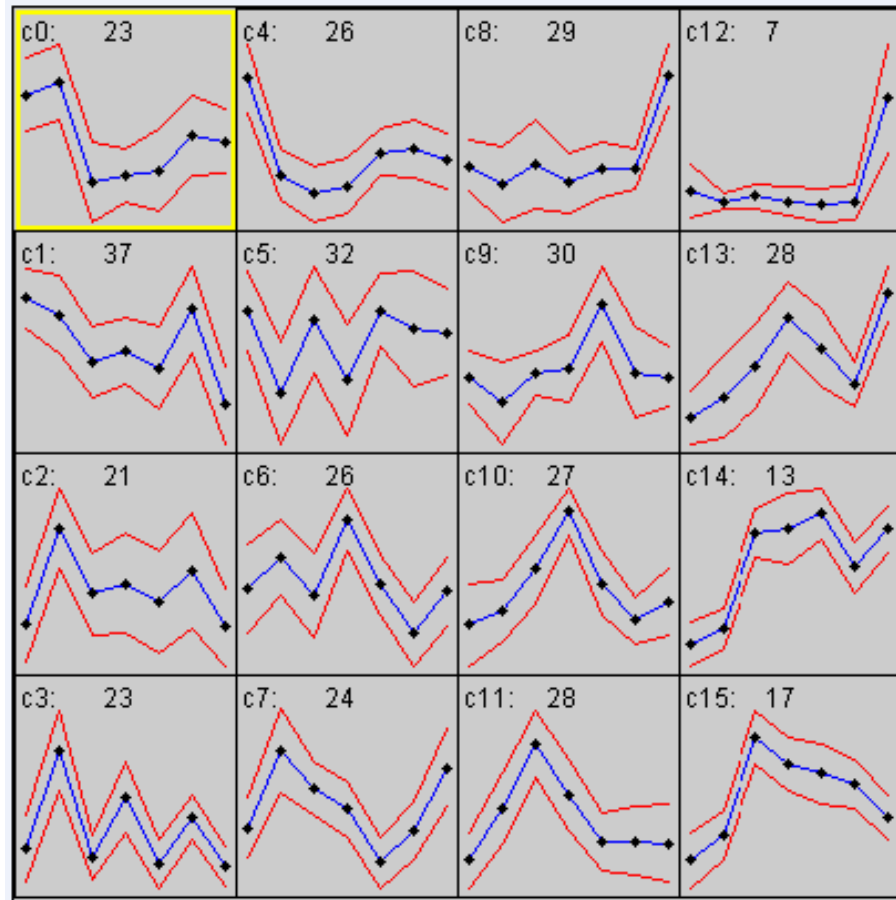


Figure 4-3. Self-Organizing Maps (SOMs). Gene expression patterns were clustered into SOMs following the laser then neomycin time course. The x-axis reflects the seven time points (treatment vs. control): laser(30 mins, 1 hr, 2 hrs, 3 hrs); neomycin(0 hr, 24 hrs, 48 hrs). Each frame/cluster is designated a centroid, see yellow highlighted box. The upper-left corner notes centroid number (e.g. c0). The center number indicates the number of genes that are in that cluster. Time points are indicated by each node along the center blue line (the average ratio change). The red lines indicate the minimum and maximum values.

As another means of parsing genes into particular pathways, genes were searched against several databases for gene interactions, pathway placement, and cellular process. Several of the TFs differentially expressed in this study have a direct link to the cell cycle, cell proliferation, or apoptosis, events necessary for hair cell regeneration to occur. A number of TFs identified in this study are directly associated with cell cycle regulation or proliferation (Table 4-2). For instance, BRD7 has been shown to inhibit G1-S progression (Zhou et al., 2004). The TF, CUTL1, is another gene that plays a role in cell cycle progression via p27 (Ledford et al., 2002). Expression of these various genes should provide insights into how the avian inner ear differs from that of mammals with regards to regeneration. Another important aspect of hair cell survival in mammals is to prevent the death of these cells altogether. Therefore a more complete understanding of hair cell apoptosis will be necessary to prevent it. Insight into that process may be provided here as several of the TFs differentially expressed during avian hair cell regeneration play a role in apoptosis (Table 4-3). While most of the genes in Table 4-3 work by activating apoptosis, some like PLAB and RORC have been shown to have inhibitory effects on cell death in other systems (Subramaniam et al., 2003; Kurebayashi et al., 2000).

Table 4-2. Cell Cycle - Proliferation affiliated TFs.

Cell Cycle - Proliferation	Annotation/Pathway Affiliation	Reference
BRD7	Inhibits G1-S progression through ras/MEK/ERK & Rb/E2F pathways.	Zhou et al., 2004
BCL11B	Negative regulation of cell proliferation	Wakabayashi et al., 2003
CUTL1	Plays a role in cell cycle progression via p27.	Ledford et al., 2002
H1F3	Chromatin remodeling.	Marzluff et al., 2002
CDK7	Member of TFIIF complex. Cell cycle progression.	Serizawa et al., 1995; Akoulitchiev et al., 1998
DEAF1	Inhibitor of cell cycle entry.	Manne et al., 2001
DMTF1	cyclinD binding myb-like TF1.	Hirai and Sherr 1996
ID1	Overexpression increases proliferation by inactivating p16Ink4a/Rb pathway. Upstream regulation of NFkB to activate proliferation.	Lee et al., 2003a Ling et al., 2003
MCM7	cell cycle; DNA replication	Fujita et al., 1996
MYBL2	Phosphorylated by cyclinA/CDK2 during S-phase.	Saville et al., 1998
MYC	Cell proliferation, cell cycle progression.	Patel et al., 2004 (Review)
MYCBP	Interacts with c-MYC.	Taira et al., 1998
OCT11 (POU2F3)	Suppresses cellular replication and apoptosis.	Enomoto et al., 2004
PURA	Development coupled cell proliferation.	Khalili et al., 2003
RGC32	Regulation of cyclin dependent protein kinase activation.	Badea et al., 1998
SMARCA2	Negative regulation of cell proliferation	Reyes et al., 1998
TRIP15	Member of COP9 complex regulating p27	Yang et al., 2002

Table 4-3. Apoptosis affiliated TFs

Apoptosis	Annotation/Pathway Affiliation	Reference
FOXO3A	Targets TRAIL(TNF apoptosis inducing ligand). Downstream target of Akt promoting apoptosis via FLIP downregulation.	Modur et al., 2002 Skurk et al., 2004
HIF1A	Hypoxic cell death	Lee et al., 2004
HNF3B (FOXA2)	Leads to significant growth reduction, proliferation arrest, and apoptosis.	Halmos et al., 2004
HOXA5	Can induce apoptosis through Caspase 2 & 8	Chen et al., 2004
MYC	Induces apoptosis in polycystic kidney disease	Couillard et al., 2002
OCT11 (POU2F3)	Suppresses cellular replication and apoptosis.	Enomoto et al., 2004
PLAB (GDF15)	Inhibits apoptosis by through Akt and inhibiting ERK.	Subramaniam et al., 2003
RORC	Negative regulator of apoptosis.	Kurebayashi et al., 2000

During development of the mammalian inner ear key signaling or genetic cascades have been identified. These include Notch (see Chapter 1), Pax-Six-Eya-Dach (see Chapter 1), FGFs (Maroon et al., 2002; Wright and Mansour, 2003), and possibly Shh (Riccomagno et al., 2002; Liu et al., 2002). However, little is known about pathways that are responsible for hair cell regeneration in the avian. *DELTAI* has been shown to be upregulated during this process (Stone and Rubel 1999), implicating a role for Notch signaling, but until now we have had no global viewpoint of this process. For the first time, in this study, hair cell regeneration was assessed on a large-scale multigenic platform, and signatures of well established signaling and genetic cascades were detectable during this process. One of the signaling pathways with the most elements identified during regeneration in both the utricle and cochlea was that of transforming growth factor beta (TGF β). Several transcription factors and co-activators in this pathway are differentially expressed. These include immediate targets of TGF β like *FOXP3 (IPEX)* (Fantini et al., 2004), and *ETV1*, which attenuates TGF β signaling by activating *SMAD7* (Dowdy et al., 2003), another gene that is also differentially expressed. In addition to *SMAD7* other SMADs are present during regeneration (Table 4-4). This data suggests that as hair cells regenerate, a prominent aspect of the signaling taking place is being coordinated through the TGF β pathway. Recall from Chapter 1, that treatment of the mammalian epithelia with TGF α had little effect in stimulating proliferation. However, adenovirus-mediated overexpression of TGF β in combination with glial derived neurotrophic factor provides protection against ototoxic damage in the guinea pig cochlea (Kawamoto et al., 2003b). A number of activator and inhibitor experiments can now be undertaken to work out the more exact interconnections of these genes in the regeneration process.

Table 4-4. List of genes differentially expressed during regeneration linked to TGF β signaling.

TGFβ Signaling	Annotation/Pathway Affiliation	Reference
DLX3	Activated by BMP2 through SMAD1 and SMAD4.	Park and Morasso 2002
ELF3	Mediates expression of TGF β RII.	Lee et al., 2003b
ETV1	Attenuation of TGF β signaling by activating SMAD7.	Dowdy et al., 2003
FOXH1	Interacts with SMAD2 to bind activin response elements	Zhou et al., 1998
FOXP3 (IPEX)	Activated by TGF β .	Fantini et al., 2004
ID1	Stimulated by BMP2 through BMPR-A1 & SMAD1 and SMAD4. Overexpression increases proliferation by inactivating p16Ink4a/Rb pathway. Upstream regulation of NF κ B to activate proliferation.	Katagiri et al., 2003 Lee et al., 2003a Ling et al., 2003
SMAD2	Phosphorylation by activin II kinase or TGF β receptor leads to interaction with SMAD4. cJUN associates with SKI to suppress SMAD2 transcriptional activity.	Marcias-Silva et al., 1996 Pessah et al., 2002
SMAD4	Necessary for DACH suppression of TGF β signaling. Interacts with SMAD3 to activate BAMBI. Interacts with DLX1 and blocks signaling from activin A.	Wu et al., 2003 Sekiya et al., 2004 Chiba et al., 2003
SMAD7	Suppresses TGF β signaling. Repressed by SKI.	Ferrigno et al., 2002 Denissova and Liu, 2004
TCF8	Interacts with SIP1, CtBP, & EF1 to suppress TGF β /BMP signaling	Postigo 2003
TGFBR3	betaglycan receptor. LIKELY NONTF	
TIEG2	TGF β Inducible Early Growth response 2; Activated by TGF β signaling.	Ellenrieder et al., 2004
TITF1 (NKX2.1)	Interacts with SMAD3.	Li et al., 2002b

Another developmentally important pathway represented during regeneration is Pax-Eya-Six-Dach signaling (Table 4-5). *Pax8* is the earliest marker for otic cell fate (Pfeffer et al., 1998) and it can directly activate the expression of another TF, *HHEX* (Puppini et al., 2004), a gene identified in the expression analysis. Loss of *Pax2*, another early marker of otic development (Torres et al., 1996; Hutson et al., 1999), leads to significant cell death in the developing cochlea in a region where *Pax2* expression overlaps proliferative cells (Burton et al., 2004). During the regeneration time course *PAX2* is upregulated at the neomycin 0 hr time point in the utricle. Recall that at this time point the SE had been treated with the ototoxic antibiotic for 24 hours, killing the majority of hair cells. The remaining cells are the surrounding supporting cells, which divide and differentiate into new hair cells. This suggests that *PAX2* might be an early marker for the advancement of supporting cells to hair cells via the proliferative process. Chapter 5 describes how this gene and others are necessary for supporting and hair cell proliferation. Interestingly, this gene does not appear to be differentially expressed in the cochlea. This raises the question of whether another PAX gene is playing a similar role in that organ or if the initial step in this pathway is somehow bypassed in the cochlea. *EYA* and *SIX* genes are known to be downstream signals of PAX in a multitude of systems (Kawakami et al., 2000, Review). This appears to hold true during regeneration as *EYA3* (utricle) and *EYA1* (cochlea) show altered gene expression. Continuing through this signaling cascade several *SIX* genes and *DACH* are altered during regeneration as well. Interestingly, *DACH* was recently shown to interact with *SIX6* to repress the expression of various cell cycle inhibitors, including p27 (Li et al., 2002c). p27 is expressed in the sensory primordia of the cochlea at a critical period when cellular proliferation halts and hair cell differentiation begins (Chen and Segil 1999). *DACH* also interacts with *SMAD4* to repress TGF β signaling (Wu et al., 2003), identifying a direct connection between

these two signaling cascades. In addition to PAX genes signaling to SIX genes, *PROX1*, ortholog of the *Drosophila* gene *Prospero*, can activate *SIX3* (Lengler and Graw 2001). The expression of *PROX1* has been shown to be altered during hair cell regeneration but only in the cochlea, not in the utricle (Stone et al., 2004). In agreement with this, I did not observe *PROX1* gene expression as being altered in the utricle time courses. However, this gene is upregulated in the cochlea at 1 hour post-laser ablation (data not shown, Dr. Bashiardes-personal communication).

The utricle regeneration time courses identified differential expression in all elements of the PAX-EYA-SIX-DACH pathway during regeneration, indicating that not only is it important for development of the inner ear but probably for hair cell regeneration as well. Our lab has recently finished profiling inner ear development in the mouse at half-day stages starting at embryonic day 9 through to day 15. It will be interesting to determine if and when all aspects of this pathway are shut off in mammals. It would also be of interest if this cascade failed to reactivate in a damaged mouse ear, since it does not regenerate its hair cells. It would also be interesting to determine if a constitutively active PAX gene would lead to additional hair cells in the mouse inner ear.

Table 4-5. List of genes differentially expressed during regeneration that are linked to the PAX-EYA-SIX-DACH cascade

PAX-EYA-SIX-DACH	Annotation/Pathway Affiliation	Reference
PAX1	Interacts with Pax9 to activate Bapx1. Interacts with Hox genes to regulate epithelial cell death and proliferation in the thymus.	Rodrigo et al., 2003 Su et al., 2001
PAX2*	Early otic marker. Role in proliferation during development of the inner ear.	Torres et al., 1996 Burton et al., 2004
SIX3	Can be regulated by the following: PAX6, PROX1, and/or MSX2.	Lengler and Graw 2001
SIX4		
SIX6	Interacts with DACH to suppress cdk inhibitors, including p27.	Li et al., 2002c
EYA3	Phosphatase activity switches SIX1-DACH function from express to activation.	Li et al., 2003c
DACH	Interacts with SIX6. Interacts with SMAD4 to inhibit TGF β signaling.	Li et al., 2002c Wu et al., 2003
BAPX1(NKX3.2)	Activated by PAX1 and PAX9.	Rodrigo et al., 2003
HHEX	Regulated by PAX8.	Puppin et al., 2004
TITF1 (NXX2.1)	Interacts with PAX8. Interacts with SMAD3.	Di Palma et al., 2003 Li et al., 2002b

*PAX2 originally did not make it through the filtering steps of the data analysis. See Chapter 5 for more explanation.

Commonalities

Interestingly, there are more alterations in TF gene expression in the laser time course than the neomycin time course. This may be due to the immediate sampling in the laser time course as opposed to the broad and fewer time points in the neomycin time course. However, there are some commonalities between these two time courses. I was able to identify 65 TFs that were differentially expressed after laser and neomycin damage. These genes are not differentially expressed at a specific time point, but are instead changing at a minimum of one time point in each regenerative time course. The remaining genes may be clues to early versus late time point changes, or how the cells respond to a particular type of damage, making them treatment specific.

In addition to the utricle time courses presented here, a Post-Doctoral Fellow in the lab, Dr. Stavros Bashiardes, expression profiled the same time courses in the regenerating cochlear sensory epithelia. The cochlear SE were treated in the same manner, therefore, we wanted to make comparisons between hair cell regeneration in the avian utricle and that of the avian cochlea. We have found 107 genes that are differentially expressed in both organs following neomycin damage (Table 4-6). Additionally, there are 89 genes common after laser ablation (Table 4-7). The genes are not always time point matched, and in some cases show opposite changes in gene expression. Nevertheless, it gives us an idea of a core set of genes involved in regeneration following a particular type of damage to hair cells. The last comparison was to ask which genes always changed regardless of damage or tissue type (utricle or cochlea). Table 4-8 shows a list of 20 genes that fit these criteria. This small set of genes may define a subset essential for regeneration, or at the other end of the spectrum, these genes may serve very general functions in cell division, cell cycle, DNA replication, or just hair cell maintenance. The latter

scenario would probably contain genes that are non-essential for hair cell regeneration specifically. In the next chapter I will discuss the importance of some of these genes in regeneration following RNA interference (RNAi).

Both the utricle and the cochlea can regenerate hair cells, but the utricle will do so on an ongoing basis while the quiescent cochlea only regenerates upon damage (Jorgensen and Mathiesen, 1988). This process does not occur in the mammalian inner ear. Therefore, it will be important to understand the cell cycle regulation that persists in the avian inner ear, as new hair cells are regenerated. As to better understand what may be the underlying differences between the utricle and cochlea, 65 TFs were also found to be unique to utricle SE during regeneration (Appendix Table A4-6 and A4-7), and these should also provide many candidates for pathway analysis in the utricle of birds and mammals.

Table 4-6. Genes differentially expressed in the utricle and cochlea SE following neomycin damage.

Utricle - Cochlea Neomycin Commonalities

AF5Q31	EBF	HHEX	ISGF3G	NHLH2	TBX15
ARIX	EOMES	HIF1A	JUNB	NR1H3	TBX21
ATF2	ERCC6	HIRA	KIAA0130	NR5A2	TCF8
BCL11A	ESR1	H-L(3)MBT	KIAA0173	POU4F1	TITF1
BCL11B	EZH1	HNF3A	KIAA1041	POU4F3	TNRC5
BRD1	EZH2	HOXA13	LOC51058	PPARGC1	TRIP15
C21orf18	FHL1	HOXB7	LOC57209	PROP1	WHSC1
CBX4	FHL2	HOXB9	LOC58500	PTTG1IP	ZF5128
CEBPB	FLJ20321	HOXD12	MAPK8IP1	PURA	ZNF10
CHD3	FLJ20595	HOXD8	MGC2508	RBL2	ZNF174
CITED1	FOG2	HRIHFB2436	MLLT2	RNF10	ZNF271
CREG	FOXF2	HSAJ2425	MORF	RNF14	ZNF6
CRSP6	GCN5L1	HSF2BP	MTA1L1	SIX3	ZNF7
CSDA	GIOT-2	HSPC018	MYBL2	SOX14	ZNF76
CTNNB1	GTF2A1	HSPX153	MYCBP	SUPT4H1	ZNF79
CUTL1	GTF2E1	ILF1	NEUROD6	TAF-172	ZNF90
DEAF1	GTF2F1	IPEX	NFE2L1	TAF1C	ZNF93
DLX6	GTF3C4	IRF2	NFIB	TAF2H	

Table 4-7. Genes differentially expressed in the utricle and cochlea SE following laser treatment.

Utricle - Cochlea Laser Commonalities

AF5Q31	FLJ12517	HOXA6	LOC57209	PAF65A	TNRC9
BACH2	FLJ12606	HOXD8	M96	PBX1	TRIP15
BCL11A	FLJ13222	HS747E2A	MADH5	PER2	VAX2
BLZF1	FLJ20321	HSAJ2425	MADH7	PRDM13	VENTX2
CRSP6	FOG2	IPEX	MAFF	RFP	XPB1
DDIT3	FOXB1	JUNB	MAPK8IP1	RGC32	ZIC4
DKFZP434P1750	FOXE1	KIAA0014	MEF2B	SIAH1	ZID
DKFZp547H236	FOXH1	KIAA0173	MEIS3	SNAPC4	ZNF165
DKFZp762K2015	GCN5L1	KIAA0395	MHC2TA	SRY	ZNF174
DSIPI	GLI2	KIAA0414	MORF	TBX5	ZNF230
E4F1	GLI3	KIAA1528	MYT2	TCF21	ZNF239
ELK4	HES7	KLF5	NMI	TCFL1	ZNF273
ESR1	HLX1	KLHL4	NR1H3	TIEG2	ZNF75A
ETV1	HMGIIY	LDB2	NR1I3	TITF1	ZNF93
FLJ11186	HNF3B	LOC51270	OCT11	TNRC6	

Table 4-8. Genes differentially expressed in the cochlea and utricle SE and both laser and neomycin treatments.

Utricle - Cochlea Neomycin and Laser Commonalities

AF5Q31	FLJ20321	HSAJ2425	LOC57209	TITF1
BCL11A	FOG2	IPEX	MAPK8IP1	TRIP15
CRSP6	GCN5L1	JUNB	MORF	ZNF174
ESR1	HOXD8	KIAA0173	NR1H3	ZNF93

Conclusion

In the current study I identified 391 transcription factors that are differentially expressed in the utricle sensory epithelia during regeneration. These cells were damaged using two different methods: laser ablation and an ototoxic antibiotic, neomycin. Time points were profiled during recovery and regeneration to determine which genes are involved in this process, as compared to time matched controls. From the neomycin time course 195 TFs were differentially expressed as a few hair cells remaining at 0 hours of the time course are near full recovery at 48 hours after removal from damage. Looking at very early time points following instant hair cell death due to laser ablation, 261 TFs were differentially expressed through 3 hours of recovery. In comparing these two time courses, there are 65 TFs in common (Appendix Table A4-8) The remaining are either time point- or treatment-specific.

Finally, I was able to illustrate an interconnection for many of the TFs, in cases where they fell into particular known pathways. As one might expect, several TFs identified are involved in cell cycle regulation or proliferation. This process is essential for the supporting

cells to divide and give rise to newly formed hair cells. Before these cells begin to divide, damaged cells must first die off. In regards to this, many TFs that play a role in apoptosis were differentially expressed during the time courses. To place additional TFs into putative signaling cascades they were searched against three databases: Gene Ontology (GO) (www.geneontology.org), KEGG (www.genome.jp/kegg/), and NCBI GENE (www.ncbi.nlm.nih.gov/entrez/query.fcgi?db=gene). GO was primarily used to search for cellular process, while KEGG provides information on several established pathways or cascades. Additional information was found by searching each TF in the NCBI GENE database, which provides a summary of published (PubMed) articles. These searches identified several important signaling pathways that included TGF β signaling and the Pax-Eya-Six-Dach cascade. Finding relationships between genes that show co-regulation in the SOMs I built may shed additional light on interactions between these genes and genetic pathways that are involved in hair cell regeneration. Many of the early genes may serve as upstream regulators for those that are expressed later in regeneration. This potential is illustrated by targeting genes using siRNA and assessing downstream effects on both proliferation and TF gene expression. In Chapter 5, I describe how I used that exact approach to identify possible downstream targets and some putative regulatory motifs.

The two methods for damaging the sensory epithelia proved quite complementary. Laser ablation leads to instant death of the cells allowing for samples to be profiled at very early times following damage. However, it is difficult to damage a large number of cells by this method. Treating the cells with neomycin on the other hand kills the majority of hair cells after a 24 hour treatment. However in this method, death of the hair cells is not really synchronized. Therefore, there are likely to be some small sub-populations of cells at various stages of apoptosis, and the

initiation of regeneration will be slightly varied. It is also quite likely that drug treatment affects the kinetics of supporting cell recovery, division, and differentiation. For these reasons a broad distribution of regeneration was chosen, with the 0 hr time point consisting primarily of supporting cells.

This study constitutes the first time hair cell regeneration has been studied on a large scale. A vast number of microarray hybridizations were used to assess what turned out to be small changes in transcription factor gene expression. However, due to the large number of experiments significant P-values were obtained, and as will be demonstrated in the next chapter, a relatively small decrease in a transcription factor can have a dramatic effect on cellular proliferation. This, along with the qPCR, provides adequate validation for these small changes being important. Also, it should be noted that some of the small apparent changes were due to the use of cross-species hybridizations, which lead to a compression of the dynamic range. It is rare by this method to see a spot image that shows maximum expression. Spot intensity is typically at the medium to lower end of the scale when our human-based oligos are used for chicken gene expression.

Another point to consider when looking through the microarray data deals with the P-values themselves. Great lengths were taken to insure the best statistical analysis of this data set. P-values help to qualify the expression fold changes as being significant. However, keep in mind that microarray data can be very noisy. So even if a gene is upregulated in every hybridization, if those numbers vary by much, this creates a large standard deviation and will result in a bad P-value. Thus, the data analysis is a quite conservative synthesis and may be excluding some genes that change, but have some variability across biological replicates. Additionally, I decided to implement an 80% trend cutoff, as explained earlier, to be sure that

genes were truly changing. This may have been a slightly high threshold, as you will see in the next chapter explaining more on the fold change of *PAX2*, but my primary concern here was to be conservative in the data analysis.

CHAPTER FIVE

FUNCTIONAL GENOMICS: siRNA, INHIBITORS, & NETWORK PROFILING

Introduction

RNA interference is mediated by a duplex of 21-23 nucleotide (nt) long RNA, termed short interfering RNA (siRNA) (Elbashir et al., 2001a; Elbashir et al., 2001b). Longer double stranded RNA is cleaved into short sequences by an RNase III family member Dicer (Bernstein et al., 2001). Introduction of siRNAs into cells leads to suppression of transcript expression (Elbashir et al., 2001b) by targeting the selected gene to the RISC complex for cleavage. It is now possible to generate "diced" dsRNA in vitro (see Chapter 7 - Materials and Methods) for an economical and efficient way to generate siRNA, as opposed to purchasing synthesized 23nt RNA oligos. RNAi is a useful tool for studying the effects of decreased gene expression without making a true knockout, and should accelerate the study of gene function. By taking a functional genomics approach of combining RNAi with microarray expression studies, gene expression changes can be monitored not only for the targeted gene, but for genes downstream in a pathway or signaling cascade that are affected by the loss of the targeted gene. This should provide a powerful method for pathway dissection.

Here I describe the identification of several key genes necessary for cellular proliferation and regeneration in the avian inner ear. The genes were identified in an extensive study utilizing microarrays containing transcription factor genes and damaged sensory epithelia. Several genes identified in the previous study (See Chapter 4) were targeted with siRNAs to specifically reduce the expression level of the gene. This was followed by two sets of experiments. First, I expression profiled sensory epithelia cells following RNAi. This had two purposes: (1) it allowed me to determine if the targeted gene was indeed downregulated. (2) I also wanted to identify potential downstream targets of the transcription factor that was targeted by RNAi. Second, parallel RNAi cultures were monitored for proliferation in the sensory epithelial cells

following by monitoring 5-bromo-2-deoxyuridine (BrdU) incorporation. A decrease in BrdU labeling would indicate a decrease in cell proliferation, showing that the targeted gene was necessary for hair cell proliferation. Utilizing this functional genomics approach, I assessed how genes might fit into a genetic cascade. The putative pathway was expanded by looking at the intersection of expression profiles from genes targeted by RNAi or drug inhibition. Further evidence of genes falling into a pathways was provided by identifying putative regulatory elements, and conserved motifs in downstream genes that appeared to be co-regulated or linked in a pathway of interactions.

Results

Proliferation

Beta-catenin siRNA

In collaboration with Dr. Mark Warchol, RNAi experiments were conducted on utricle sensory epithelia cells, hair cells and supporting cells, cultured on glass coverslips. In the initial series of experiments, damage by laser microbeam ablation was used to create a wound in the sensory epithelia. This leads to an increase in cellular proliferation as detected by the incorporation of 5-bromo-2-deoxyuridine (BrdU) at the site of the lesion (Figure 5-1). As BrdU incorporation is monitored farther from the lesion site, there are fewer cells labeled. To test the feasibility of RNAi in these cells, they were transfected with dsRNA that had been cleaved into 23mers using the Dicer enzyme (see Chapter 7 - Materials and Methods) following laser ablation. The first gene targeted in this manner was the transcription factor *Beta-catenin*

(*CTNNB1*), which is differentially expressed during regeneration (Appendix Table A4-3) and part of the Wnt signaling pathway. The *CTNNB1* siRNA did show a significant decrease in protein levels detected via immunofluorescence at the lesion site when stained 24 hours after damage. *CTNNB1* was not reduced in the control experiment, which used a 'diced' dsRNA to target the green fluorescent protein gene (GFP) (not expressed in these cells) (Figure 5-2B & D). Here the expression of *CTNNB1* was uniform across the section. Note that the wound had fully healed 24 hours after laser damage. This experiment shows for the first time in chicken sensory epithelial cells that gene and protein expression levels can be reduced using RNAi, and that the gene of interest was targeted using a diced dsRNA. It was important in this first experiment to test a transcription factor that had a chicken antibody available in order to illustrate that RNAi works in this cell system. As many TFs do not have antibodies available, the effectiveness of RNAi on other genes was assessed at the transcript level using the microarray as a readout of efficient knockdown. Additional experiments determined whether β -catenin had an effect on proliferation as determined by BrdU incorporation. Twenty-four hours after laser damage and transfection, β -catenin RNAi showed the same number of BrdU labeled cells as the GFP control. The proliferative index scale, which is the percentage of labeled nuclei in a given area, showed β -catenin at 14 ± 2 % and GFP was 11 ± 2 %, indicating no effect on proliferation by this WNT signaling transcription factor (Figure 5-3).

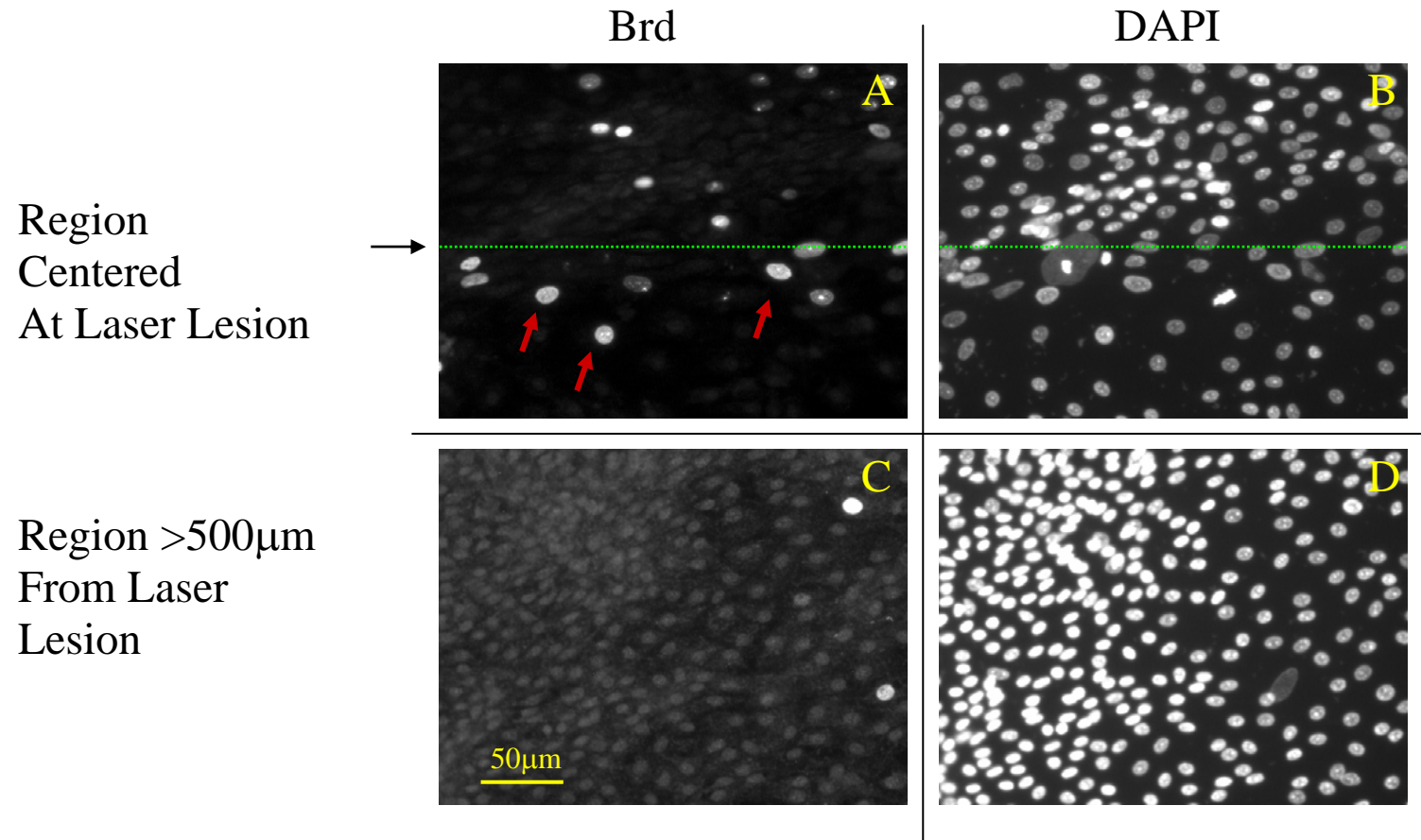


Figure 5-1. Increased Proliferation after laser damage. Specimens received a 4 hour pulse of BrdU 20 hours after damage by laser microbeam. Panels A and B show the utricle sensory epithelium at the site of laser damage as indicated by the green line and black arrow to the left of panel A. Panels C and D show the sensory epithelium ~500μm from the site of damage. Panels A and C show BrdU incorporation, which is more prominent near the laser lesion (see red arrows in panel A). DAPI staining in panels B and D show fewer nuclei are present at the site of damage (B) where more cells are dividing (A) than further from the lesion (D). (Image courtesy of M. Warchol)

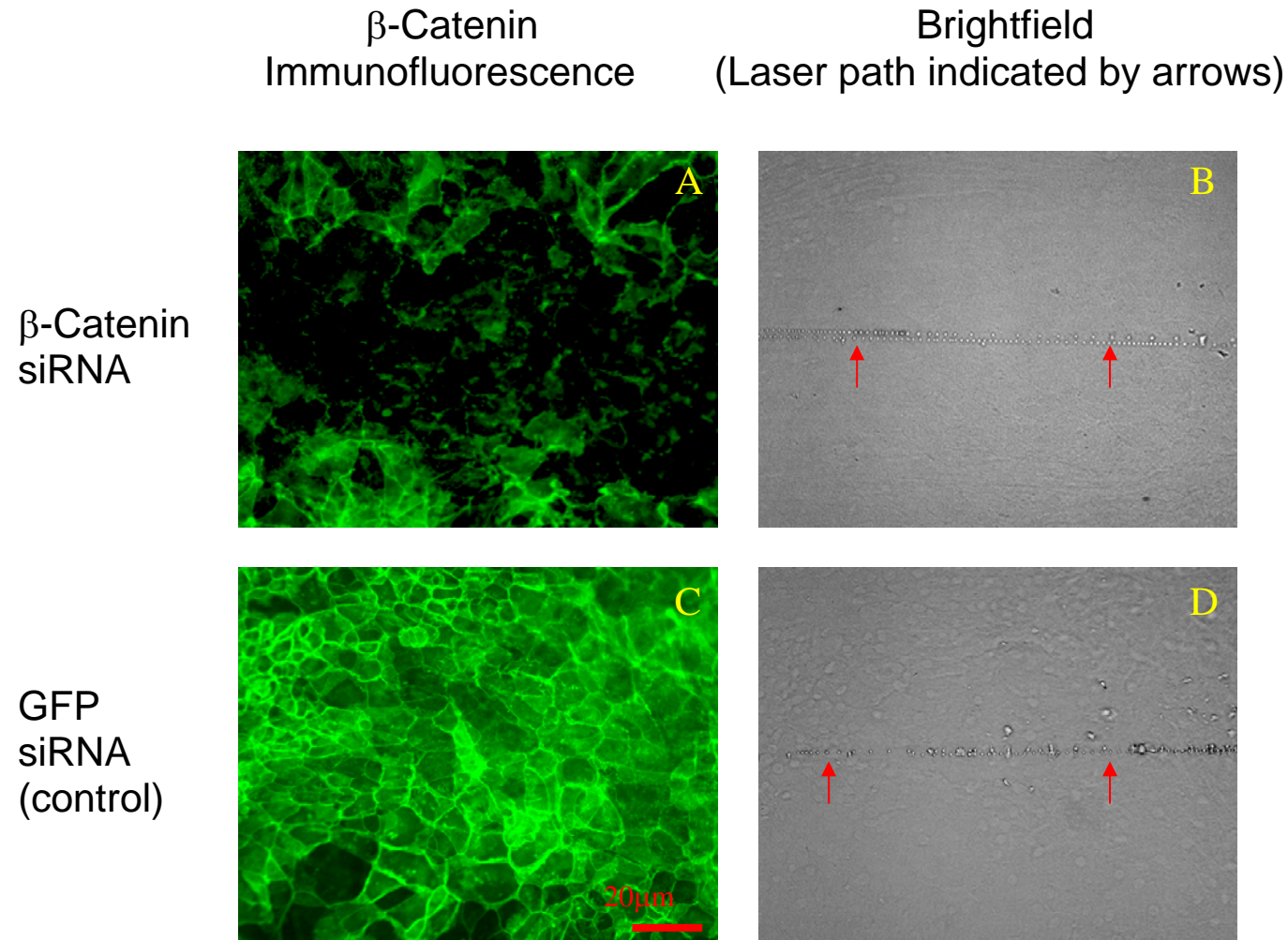


Figure 5-2. Beta-Catenin RNAi. Panel A shows CTNNB1 protein levels at the laser lesion site 24 hours after damage. Panel B shows the lesion path (red arrows). Panel C shows the control GFP siRNA had no effect on CTNNB1 levels. Panel D shows the lesion path for the control. (Image courtesy of M. Warchol)

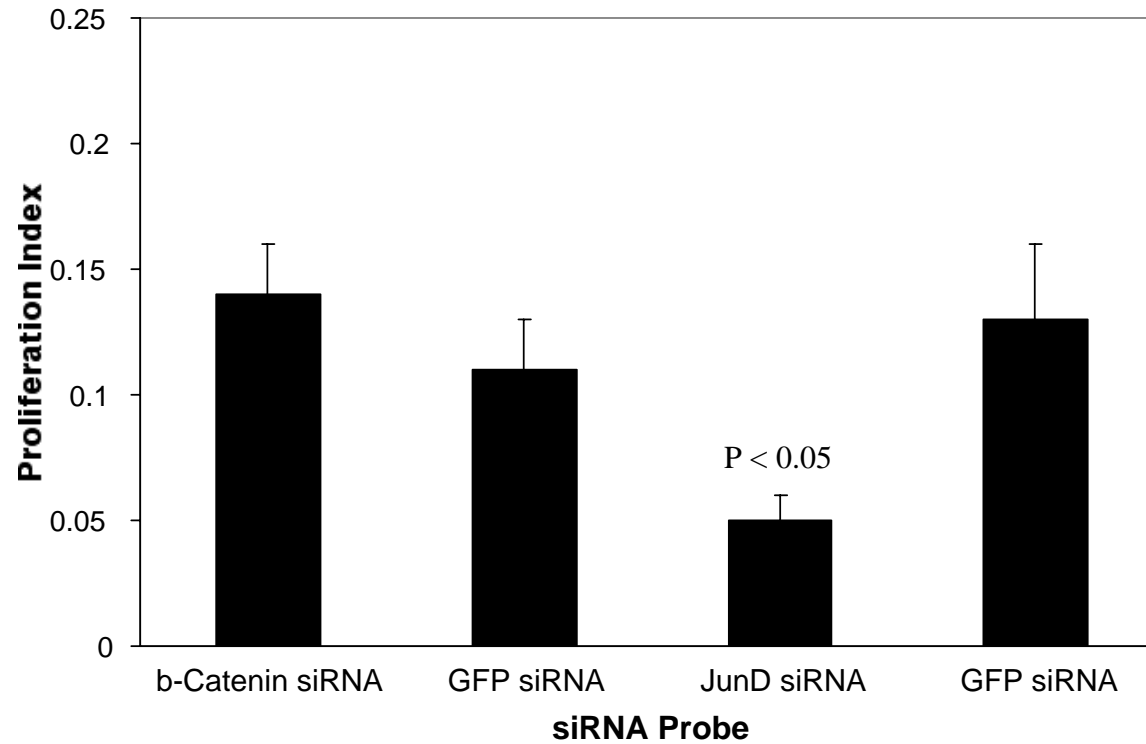


Figure 5-3. Inhibition of proliferation after laser ablation and RNAi. Following laser ablation and transfection with siRNAs in the utricle sensory epithelium, proliferation was assessed by BrdU incorporation. BrdU labeled nuclei are expressed as a percentage of total nuclei in a given area. Reduction in proliferation was seen after targeting *JUND*. *CTNNB1* was comparable to its control.

JUND siRNA

One gene that is differentially expressed in all four time courses, utricle-cochlea-neomycin-laser, is *JUNB*, a member of the JUN family of TFs. Jun proteins, including JUNB, are known members of the activating protein 1 (AP-1) complex. This complex is induced by a host of signaling molecules including growth factors, hormones, and neurotransmitters, as well as physical and chemical stress (for review see Shaulian and Karin, 2002). This complex is important for regulation of the cell cycle proliferation and differentiation. For instance, c-JUN is required to alleviate the inhibition of p53 on cell cycle entry (Shaulian et al., 2000). Additionally, AP-1 can both activate and inhibit Cyclin D1 depending on which JUN and FOS dimers are present (Shaulian and Karin, 2002).

Because *JUNB* was differentially expressed in at least one point in all regenerative time courses, this made it an excellent candidate to target by RNAi. However, attempting to target chicken *JUNB* by RNAi has proved a difficult task. Initially, a region of sequence from the human *JUNB* gene that aligns with the array oligo was BLASTed against chicken ESTs in the TIGR *Gallus gallus* database. A chicken EST with greater than 70% sequence identity was identified. Unfortunately additional BLAST would show this EST was instead chicken *JUND*, and no chicken *JUNB* transcript is currently annotated in TIGR, NCBI, or the University of Delaware chicken EST databases. A search for JUN loci in the chicken genome using the UCSC browser reveals only one locus on chromosome 19. All other sequenced vertebrates checked (human, mouse, zebrafish, and fugu) have separate loci for all versions of JUN (*c-JUN*, *JUNB*, and *JUND*). Our lab is now working with the Washington University Genome Sequencing Center in an attempt to identify a chicken *JUNB* locus.

In the version of the array used in the previous study, *JUND* was not represented so expression changes were not obtained. *JUND* expression changes across the neomycin time course were checked by qPCR with oligos designed on the chicken *JUND* sequence. Results showed that *JUND* was differentially expressed across the neomycin utricle time course (0-24-48hrs) by 2.8, 3.5, and 1.4 fold increases respectively. To assess the role of *JUND* in hair cell regeneration, the transcript was targeted with siRNAs generated by 'dicing' a double-stranded RNA product. Since this region has some sequence identity to the human *JUNB* transcript, I cannot be completely sure that it is not targeting *JUNB*, a possible scenario. However, since *JUNB* often acts as a repressor, by forming a homodimer, and *JUND* typically acts as an activator of proliferation, the phenotype (monitoring cell proliferation) of decreasing the expression of both genes would reflect the *JUND* knock down phenotype. The *JUND* siRNA was transfected in utricle SE cultures following laser ablation and allowed to recover for 24 hours. The *JUND* siRNA significantly reduced cellular proliferation by 61.5% as monitored by BrdU incorporation (Figure 5-3). Control siRNA transfections directed at GFP had no effect on proliferation. The GFP control showed a total of $13 \pm 3\%$ of nuclei are labeled, while the *JUND* RNAi sample showed an average of $5 \pm 1\%$ ($P < 0.05$) labeled nuclei.

96-well RNAi

In order to test the effects of RNAi on transcription factors in a more efficient manner, dissociated cells from the utricle sensory epithelia were cultured in a 96-well format and cellular proliferation was assessed by BrdU labeling before the cultures reached confluency. This assay was tested by the afore mentioned RNAi to *JUND* and behaved similarly to a laser-induced proliferation assay. The following differentially expressed transcription factors were targeted by

RNAi in this format and compared to a GFP siRNA cell culture. *PAX2*, *CEBPG*, *BCL11A*, and *TRIP15* genes were selected for very particular reasons. Both *BCL11A* and *TRIP15* are differentially expressed in at least one time point in each time courses in both organs (i.e. laser and neomycin utricle and laser and neomycin cochlear samples). *CEBPG* showed an interesting expression pattern in relationship to the utricle neomycin time course. At 0 hrs when the majority of hair cells are dead or dying yet all supporting cells are still intact and will regenerate to give rise to new hair cells, *CEBPG* is downregulated compared to the normal SE cells. Later *CEBPG* becomes upregulated during regeneration. Finally, *PAX2*, as described earlier, is an important otic marker and its expression overlaps regions of proliferation during inner ear development. However, following a complete analysis, *PAX2* does not appear in the laser or neomycin data sets. *PAX2* was "filtered out" from the 0 hr time point, where it is likely differentially expressed because it did not meet the "trend cutoff" filter of 80%. This constraint meant that the gene must show the same trend of expression in 80% of hierarchical clustered hybridizations. The 0 hr time point contained ten hybridizations that clustered well, *PAX2* was upregulated in 7/10 (1.22 fold) and therefore did not meet the 80% criteria. Since *PAX2* is upregulated in 70% of these hybridizations, and plays an important role in mouse otic development, it was targeted by RNAi.

Of these four transcription factors that were targeted by RNAi, only *PAX2* and *CEBPG* showed a reduction in proliferation (Figure 5-4). Each of these reduced proliferation as measured by BrdU labeling by nearly 50 percent: *PAX2*: $6 \pm 1\%$ ($P < 0.02$); *CEBPG*: $7 \pm 1\%$ ($P < 0.05$); GFP: $13 \pm 3\%$ BrdU labeled nuclei. In addition, immunofluorescent detection of the *PAX2* protein after RNAi shows about a 50% decrease in expression as compared to the control (Figure 5-5). As this is the only example that correlates protein expression reduction and

proliferation reduction, it can only be assumed to be coincidence that they are both around 50%. Considering that RNAi is not a true knockout, it would be interesting to know if reducing gene expression even further would entirely halt proliferation.

Here it is shown that PAX2 and CEBPG are necessary for wild-type levels of proliferation for sensory epithelia cells in the avian utricle. It also establishes a more efficient way of screening additional genes by RNAi. In the previous examples the sensory epithelia was cultured and damaged before assaying a phenotype. Since the assay is determining if cells continue to proliferate, this is now done by measuring cell proliferation while the cells are in culture. Currently, approximately 10,000 cells are placed into wells of a 96-well plate, and 5 transfected wells are pooled for profiling. Based on the technology that is currently used, I believe this could be reduced to at least three wells, allowing for more genes to be screened on the limited cells from the sensory epithelia. Eventually this might possibly be reduced to a single well.

JNK Inhibition

Our collaborator Dr. Mark Warchol has shown that Jun Kinase (JNK) activity is evident at the site of laser lesions in the utricle sensory epithelia as indicated by the presence of phosphorylated c-JUN (Figure 5-6A). Use of a JNK inhibitor, SP600125, leads to a failure for the wound to close illustrating that functional JNK signaling is essential for wound healing and hair cell regeneration in this assay (Figure 5-6B) whereas the control, DMSO, regenerates the sensory epithelia to heal the wound. The addition of other pathway inhibitors have yet to produce the same effect as JNK (Figure 5-6, erbB-2, and IGF(data not shown)). Unknowingly at the time, we have shown that inhibition of downstream targets of JNK have a similar phenotype.

It is also now known that the PAX2 protein is activated by phosphorylation through Jun Kinase (JNK) signaling (Cai et al., 2002). CEBPG has been described previously to interact with FOS to activate the IL-4 gene (Davydov et al., 1995). This system may be another instance where CEBPG is interacting with FOS or other members of the AP-1 complex to regulate proliferation. It remains to be determined what the interacting partners of CEBPG in hair cells or supporting cells are, but reduced expression of this gene has a dramatic effect on proliferation. As shown below, very strong supporting evidence places this gene downstream of JNK signaling as well.

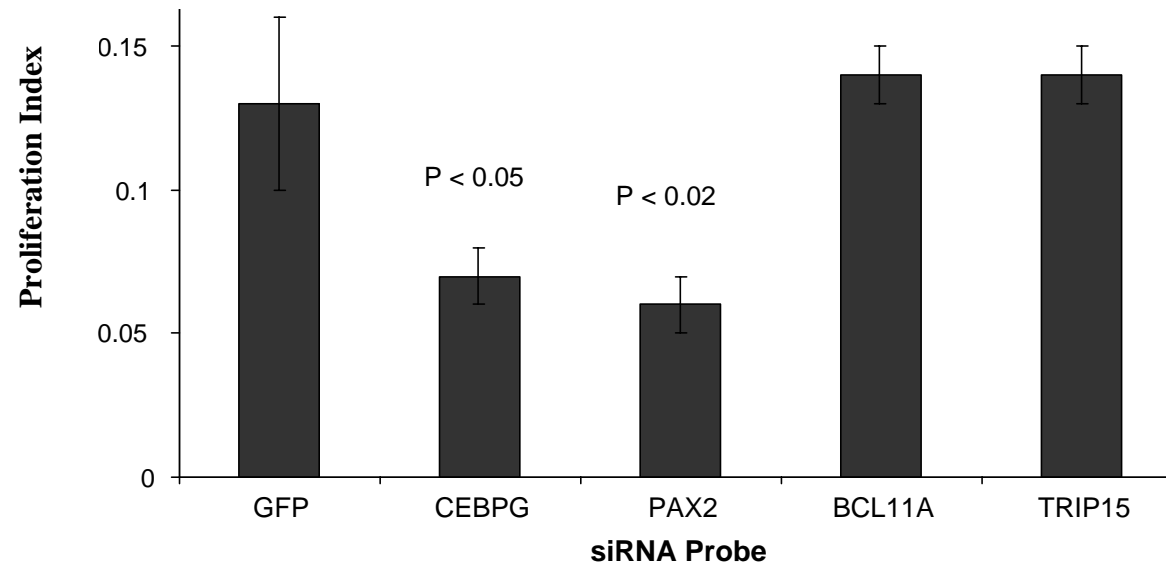


Figure 5-4. Proliferation index for TFs - 96-well format. *CEBPG* and *PAX2* show a 50% reduction in proliferation as compared to the GFP control. Other genes tested were comparable to the control.

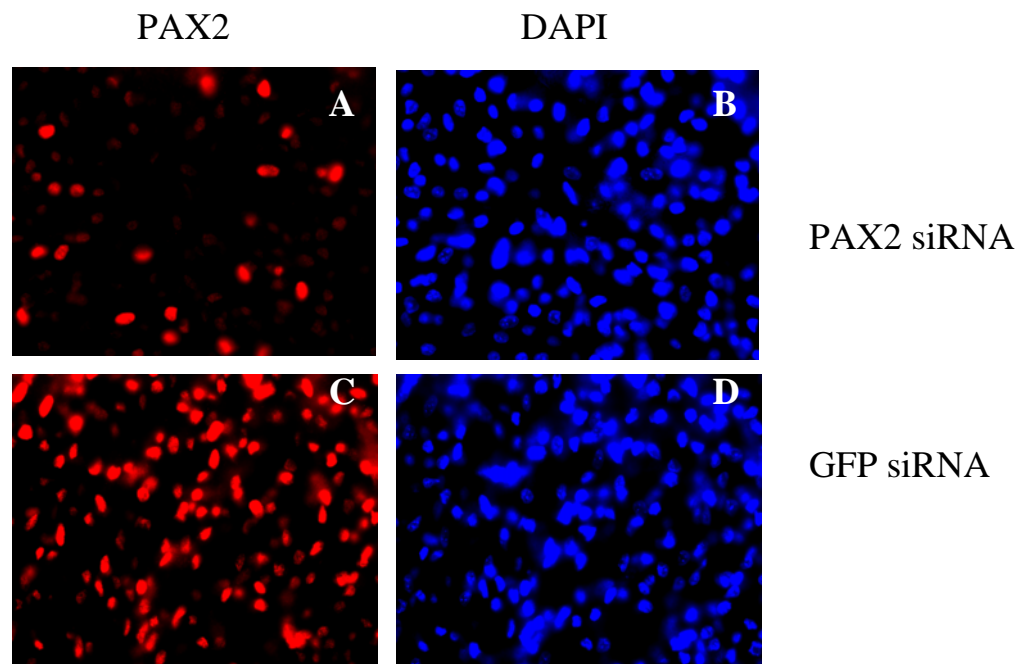
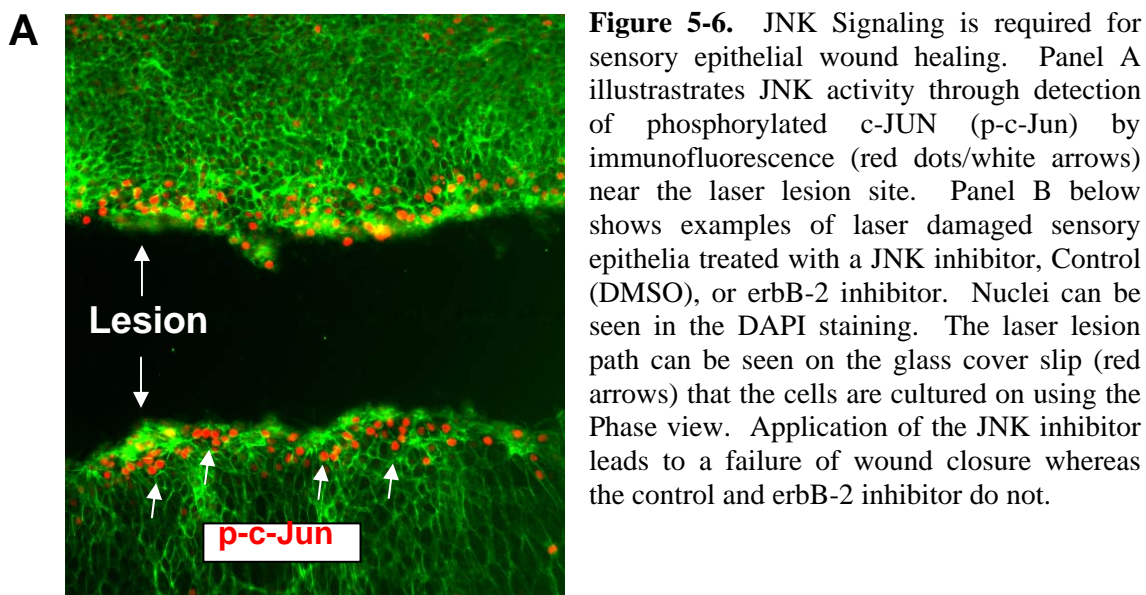
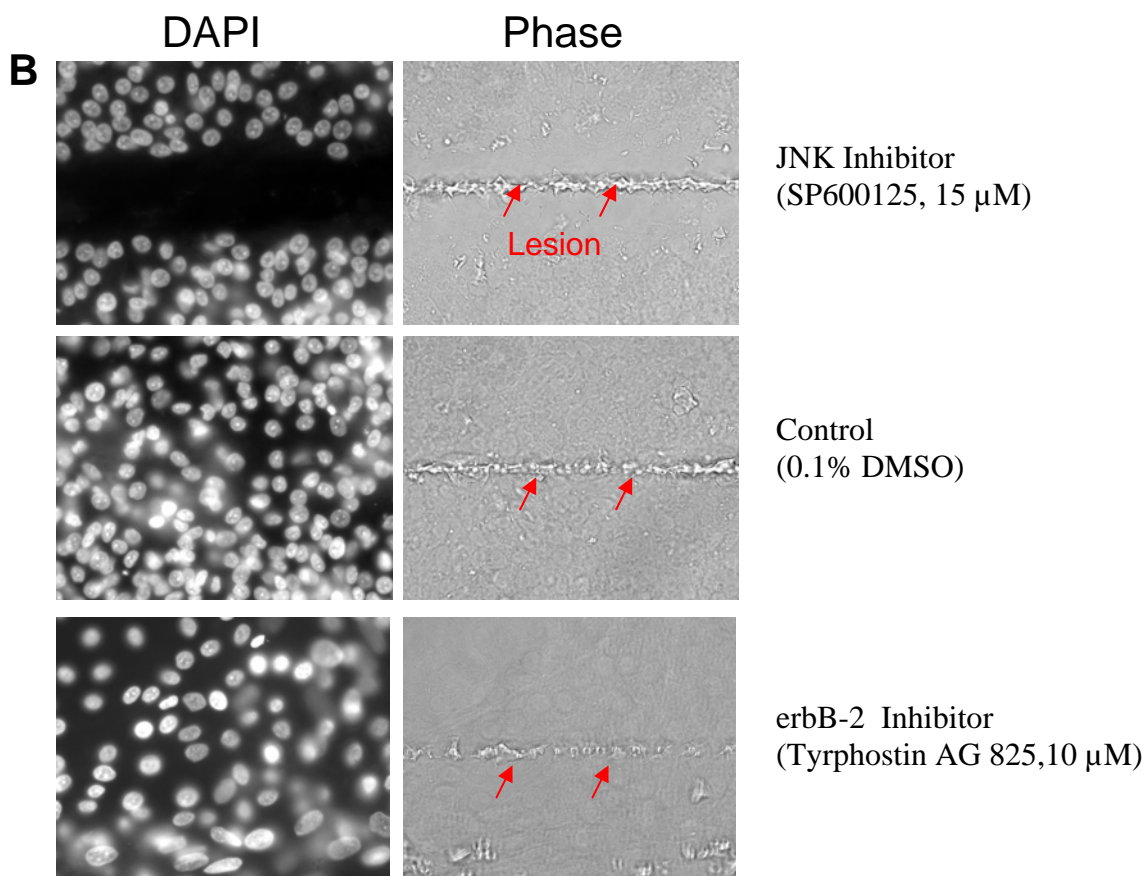


Figure 5-5. PAX2 immunohistochemistry following RNAi in 96-well primary cultures. Sensory epithelial cells were cultured in 96-well format and transfected with siRNAs for Pax2 (A&B) or GFP(C&D). Panels B and D show DAPI staining of nuclei. Panel A shows a reduction in PAX2 protein expression detected by immunofluorescence as compared to the GFP control in panel C (PAX2 positive cells: PAX2 siRNA: $28 \pm 7.0\%$; GFP siRNA: $63 \pm 8.3\%$ SEM). (Image courtesy of M. Warchol)



(Image courtesy of M. Warchol)



Expression Profiles

RNAi is a powerful tool for unlocking the role a gene plays in its cellular system, while gene expression profiles can provide a snapshot of that system's transcriptome. Combining these two techniques potentiates genetic networking by identifying putative downstream targets in a pathway. Taking a functional genomics approach to understanding pathway parsing, I have profiled JUND and CEBPG RNAi experiments, and sensory epithelia treated with a JNK inhibitor to determine which transcription factors are downregulated as potential downstream targets. Each of these profiles shows a number of TFs downregulated after inhibitory treatment (Appendix Tables A5-1 CEBPG, A5-2 JUND, A5-3 JNK). I also compared the list of RNAi downregulated genes to those differentially expressed in the time course profiles. By plotting some of the genes in common between an RNAi treatment and the regeneration time course, expression profiles can be identified that share similar patterns across the time course and in the RNAi treatment. A common expression pattern or similar pattern that is out of phase by one time point, is useful in determining if one gene is potentially downstream of another gene. The example in Figure 5-7 illustrates these points showing several TFs that have a similar expression profile to *CEBPG* during regeneration and are all downregulated following CEBPG RNAi. One could infer that some of these genes may be regulated by CEBPG, which would help explain the co-variation across the time course. For example *CEBPG* and *IPEX* have the exact same profile pattern with only the peaks and valleys differing in height. *CEBPG* and *LRP5* only differ at the 24 hour time point, with *LRP5* on a downward trend from 0 to 48 hours and *CEBPG* peaking at 24 hrs.

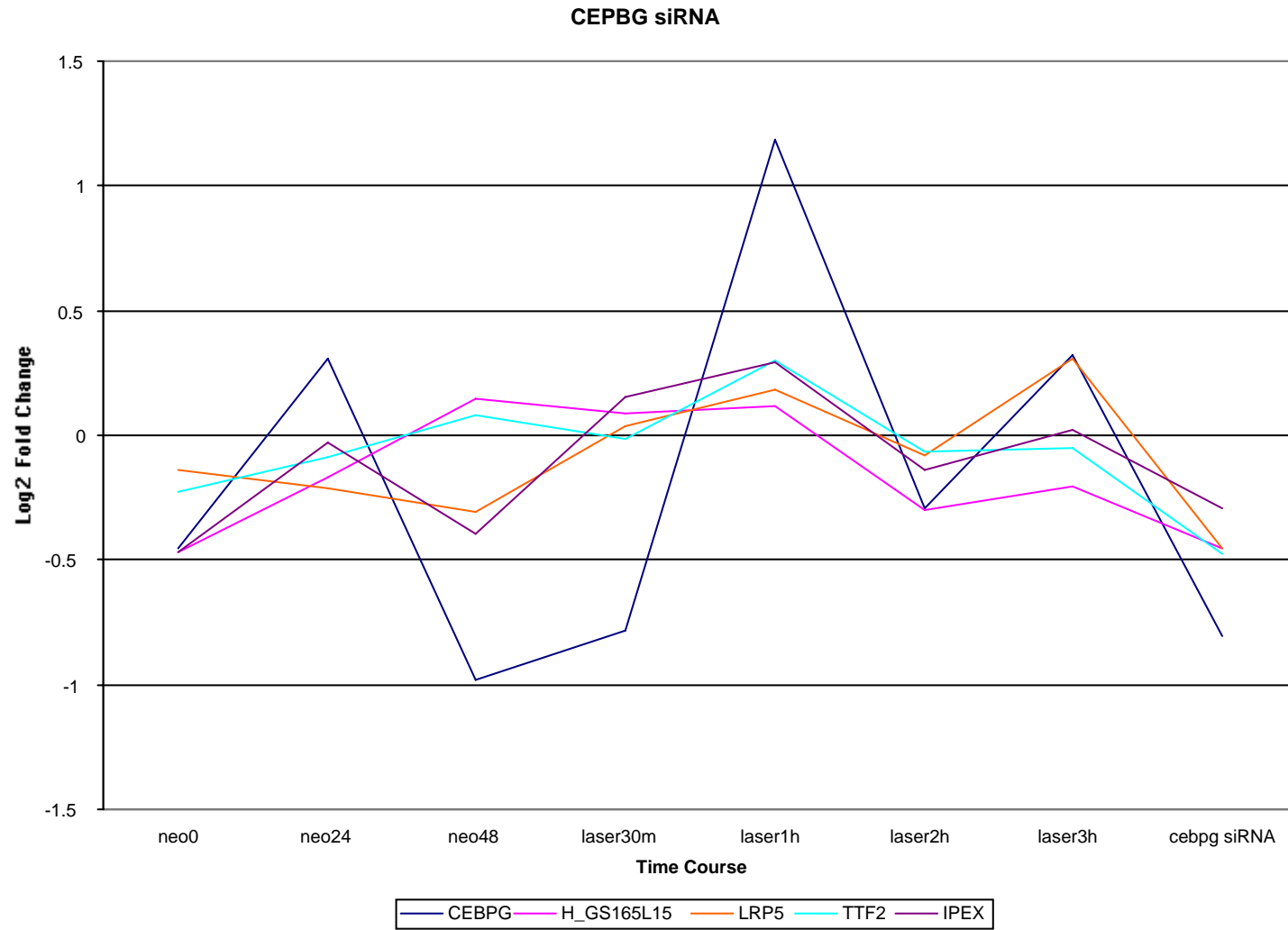


Figure 5-7. Genes co-varying with *CEBPG* during regeneration and CEBPG RNAi.

Genes showing co-variance are strong candidates for being either co-regulated, or, at the limits of resolution of the time courses, they may be downstream targets. Identifying intersections of multiple treatments increases the likelihood that the genes falling at these intersections are downstream of those initially targeted. It seemed likely that the JNK inhibition profile would have commonalities with the JUND RNAi profile. However, it was unexpected to find CEBPG downregulated following JNK inhibition and later in the JUND RNAi experiment. This would suggest that these genes fall into a single signaling cascade, placing JUND downstream of JNK, and CEBPG downstream of both. Continuing to make comparisons between each treatment identified multiple transcription factors that were commonly downregulated (Figure 5-8, Appendix Table 5-1).

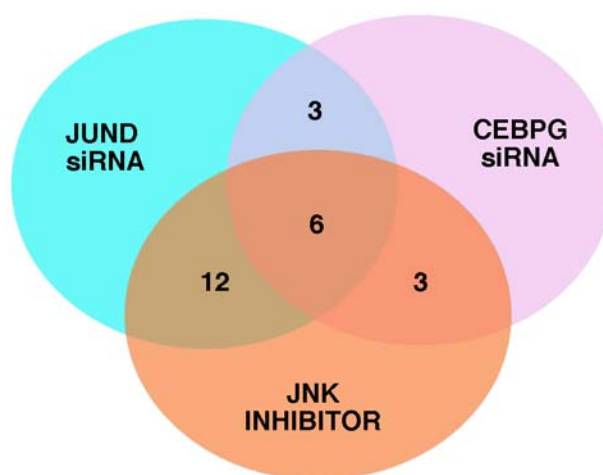


Figure 5-8. Venn diagram illustrating genes downregulated in multiple inhibitory treatments. Only genes common to more than one treatment are shown. All differentially expressed genes can be found in the Appendix.

Table 5-1. CEBPG siRNA, JUND siRNA, and JNK Inhibitor downregulated commonalities.

Gene ID	Gene Annotation
CEBPG siRNA - JUND siRNA	
NR6A1	nuclear receptor subfamily 6, group A, member 1
TTF2	transcription termination factor
ZNF76	zinc finger protein 76
CEBPG siRNA - JNK Inhibitor	
KIAA0161	KIAA0161 gene product
PROC	protein C (inactivator of coagulation factors Va and VIIIa)
TNRC9	trinucleotide repeat containing 9
JUND siRNA - JNK Inhibitor	
BRD1	bromodomain-containing 1
DAZAP1	DAZ associated protein 1
FHL1	four and a half LIM domains 1
GBX2	gastrulation brain homeobox 2
JUNB *	Jun B proto-oncogene
MYT2	myelin transcription factor 2
NEUROD6	neurogenic differentiation 6
PAX1	paired box gene 1
PRDM16	PR domain containing 16
PREB	prolactin regulatory element binding
SRY	sex determining region Y
TAF2H	TATA box binding protein (TBP)-associated factor, RNA polymerase II, H
CEBPG siRNA - JUND siRNA - JNK Inhibitor	
CEBPG	CCAAT/enhancer binding protein (C/EBP), gamma
IRX7	iroquois homeobox protein 7
LRP5 *	low density lipoprotein receptor-related protein 5
RARA	retinoic acid receptor, alpha
TAF-172 *	TBP-associated factor 172
ZNF44	zinc finger protein 44 (KOX 7)

* JUNB (in the JUND siRNA), LRP5 (JUND siRNA), and TAF-172 (CEBPG siRNA) were just below the fold cutoff, but were added back in for comparisons here. See Appendix for exact fold changes in each RNAi treatment.

As Figure 5-8 illustrates, most commonalities are between JNK inhibition and JUND RNAi. Interestingly, even though CEBPG appears to be downstream of both JNK and JUND, there are three genes in common to the JUND and CEBPG RNAi treatment but not JNK inhibition. It may be possible that the signaling effect was lost on these three genes, or they simply did not make it through the filtering process in the JNK experiment. There are another three genes common to the JNK and CEBPG treatments. This may represent a scenario where some genes require JNK activity to phosphorylate a different regulator that may in turn heterodimerize with CEBPG to activate the transcription of these three genes, somehow bypassing the need for JUND. This is, of course, speculative but can be tested.

The best evidence for constructing a signaling cascade lay in the overlap between all three inhibitory treatments. As mentioned earlier, *CEBPG* is downregulated in all three instances. Additionally, five other genes fall into this same category; *IRX7*, *LRP5*, *RARA*, *TAF-172*, and *ZNF44*. These five genes can be placed downstream of the afore mentioned genes. This illustrates how a functional genomics approach can be used to construct putative pathways of genes, as is diagrammed in Figure 5-9. However, the correlations are not definitive. Inhibition of JNK signaling, *JUND*, and *CEBPG*, all reduced proliferation in the utricle sensory epithelia. It would be expected that if the genes are in the same signaling/genetic cascade they would have similar phenotypes when inhibited. To further test this, I am currently designing siRNAs for *LRP5* and *IRX7* (*IRX4* in chicken) to determine if they have a similar phenotype.

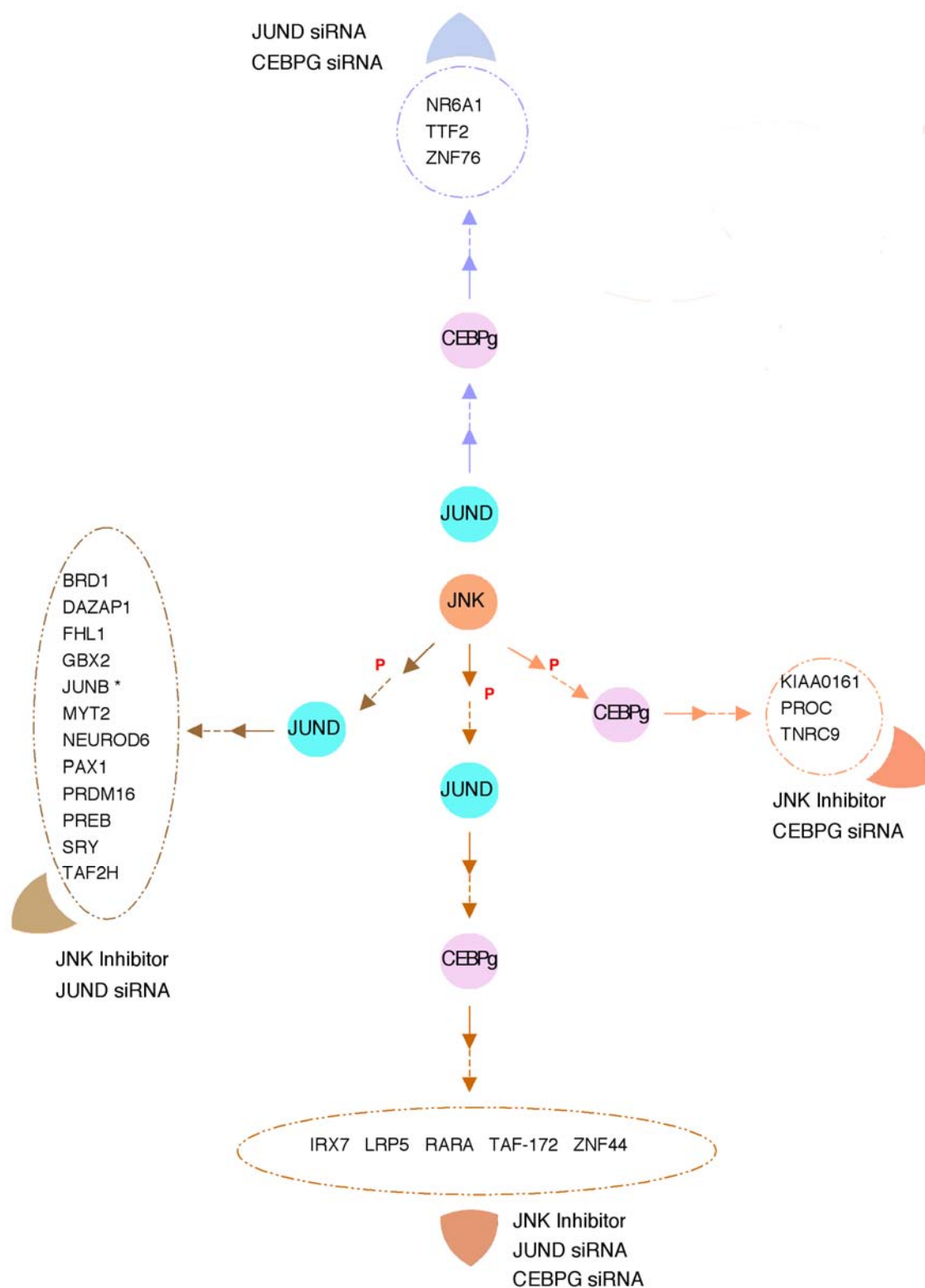


Figure 5-9. Signaling/Genetic network of genes downstream of JNK, JUND, and CEBPG. Dashed arrows imply that multiple signaling steps may be involved. **P** = phosphorylation. Color segments refer to parts of the Venn diagrams in Figure 5-8.

With the sequencing of many genomes, chicken now included, much is being made of comparative genomics to identify conserved elements across species. The focus of some of this effort has been identifying putative regulatory elements. With the help of a computational biology student, Steven Woolley, I tried to identify conserved motifs for genes downstream in the inhibitory treatments. The first 5000bp upstream of each gene's start site was used to search for motifs. Genes downstream of *CEBPG*, as indicated by RNAi knockdown, were initially searched. One such downstream gene *IRX7* contained a motif approximately 2000bp upstream that was entirely conserved across six species; human, mouse, rat, chicken, chimp, and dog. The most interesting aspect of this motif is that it contains a CAAT box, which is what one might expect to find for direct targets of CEBPG - CAAT element binding protein gamma (Figure 5-10), although maybe not that far upstream.



Figure 5-10. *IRX7* conserved motif. An 11 base motif entirely conserved in *IRX7* across 6 species; chicken, chimp, dog, human, mouse, and rat.

A second motif was also found in *IRX7* closer to the start site. This motif was not as highly conserved across the same species, but it was found in another gene potentially

downstream of *CEBPG*, *LRP5*. Figure 5-11 shows the weight of each nucleotide across a 19 base span conserved across the same six species. The motif is located ~80 nt upstream of *LRP5* and ~2kb upstream of *IRX7*.



Figure 5-11. IRX7 and LRP5 conserved motif. The putative regulatory element is found upstream of both genes and conserved across chicken, chimp, dog, human, mouse and rat. The height of the base represents how conserved it is across various species.

These conserved motifs add another layer of inferential evidence to the identification of a pathway emerging from the functional genomic data presented here. If the second motif is indeed a conserved regulatory element, it might mean that *IRX7* and *LRP5* are regulated by the same transcription factor(s). It will be interesting to see what effect knocking down these two genes have on hair cell proliferation, and on the expression of other TFs. The identification of motifs also opens the door for future experiments to test if these elements can drive expression and if they are direct targets of CEBPG.

Additionally, I have begun profiling various other genes targeted by RNAi, small molecule inhibitors, or activators. These include *PAX2*, *ID1*, a Smoothened inhibitor, and forskolin, a cAMP activator. Most of these are in the initial stages (i.e. only one biological sample). The same approach will be taken with these treatments to parse out pathways of gene

interactions. One TF worth expanding upon here is *ID1*. This gene shows very little change in regenerative gene expression until the neomycin 48hr time point (Figure 4-3:SOMs, Chapter 4). At this time point the gene is increased in expression indicating it is upregulated some time after 24 hrs as the cells are nearing recovery at 48hrs. In other cells this gene has been shown to be involved in cell cycle regulation through two pathways. Overexpression of *ID1* increases proliferation by inactivating p16Ink4a/Rb pathway (Lee et al., 2003a), and plays a role in upstream regulation of NF-kappa B to activate proliferation (Ling et al., 2003). This makes *ID1* an excellent target for RNAi to not only assess its role in hair cell proliferation, but to identify downstream TFs as well. Initial RNAi experiments for the purpose of profiling demonstrated that the expression level of *ID1* was reduced 1.4 fold, a fold change typical for this platform. Several TFs were also downregulated after ID1 siRNA targeting (Table 5-2).

Table 5-2. Genes downregulated following laser ablation and ID1 RNAi

GENE ID	GENE NAME
ATBF1	AT-binding transcription factor 1
ATRX	alpha thalassemia/mental retardation syndrome X-linked
GFI1	growth factor independent 1
HMG20B	high-mobility group 20B
HNF3B	forkhead box A2
ID1	inhibitor of DNA binding 1
NR2F2	nuclear receptor subfamily 2, group F, member 2
SIX2	sine oculis homeobox homolog 2 (Drosophila)
TFAP2A	transcription factor AP-2 alpha
UBP1	upstream binding protein 1 (LBP-1a)
ZFP103	zinc finger protein 103 homolog (mouse)

If two genes are very tightly regulated temporally, it would be expected that these genes might cluster in the same centroid of a SOM. This is the case for a gene downregulated following ID1 RNAi, *HNF3B* (Chapter 4, Figure 4-3: SOMs - centroid 12). This lends weight to a potential regulatory interaction for these two transcription factors. Another downregulated gene is of increasing interest to inner ear biologist. *GFII*, which is downregulated following ID1 RNAi, was recently shown to be downstream of another transcription factor, the deafness gene *Pou4f3* (*Brn3c*) by profiling inner ears from a *Pou4f3* mouse knockout (Hertzano et al., 2004). This is important to the field because as mentioned in Chapter 1, the *Pou4f3* knockout results in a failure of hair cell maturation (Xiang et al., 1997) the underlying reason for it being known as a deafness gene. Moreover, it has also been shown that *GFII* is required for hair cell differentiation as well (Wallis et al., 2003). *POU4F3* is not in the ID1 RNAi profile. Therefore, *ID1* is possibly downstream of *POU4F3* or acts on *GFII* through another mechanism. The proliferation assay for the ID1 RNAi is now ongoing with expectations being that it will also have a role in hair regeneration.

Conclusion

In this study, genes thought to be important for hair cell regeneration, as identified from the expression profiles, were targeted by siRNAs. I was able to show that RNAi works in this system by the downregulation of beta-catenin immunofluorescence, as well as by microarray readouts (e.g. CEBPG siRNA). In addition to the genes targeted by RNAi, the JNK signaling pathway was inhibited because the microarray data suggested that elements in this pathway may be at work during the early phases of regeneration (Table 5-3). The RNAi on *PAX2*, *JUND*, and

CEBPG reduced proliferation of hair cells by greater than 50%. Following laser ablation of the utricle sensory epithelia, inhibition of JNK signaling, using a JNK inhibitor molecule, stopped the epithelia from healing the wound and regenerating new hair cells. This provided functional validation of the genes identified in the previous study. This study illustrates for the first time that RNAi can work in primary sensory epithelia cultures and that targeting of genes can block hair cell regeneration.

In addition to identifying functionally important genes, these inhibitory experiments were profiled to identify putative downstream targets. By identifying additional downregulated genes, I was able to identify possible pathway members. Finding an intersection of genes from more than one treatment enhances the idea that particular genes fall downstream of another gene. Several commonalities were found in the profiles of JNK, JUND, and *CEBPG* inhibition. The most important of these is that the *CEBPG* gene is downregulated in all three treatments establishing a pathway of JNK to JUND to *CEBPG*. *CEBPG* is downregulated by only 1.75 fold, just under the standard two-fold threshold. However, knocking down this gene has a dramatic effect on sensory cell proliferation. Further evidence of a pathway evolving from the data, is demonstrated by another five genes being downregulated in all three treatments. One of these, the *IRX7* gene, contains a highly conserved CAAT box, which is a possible binding element for the CEBP family of TFs. Additionally, both *IRX7* and *LRP5*, which can be placed downstream in all treatments, share an additional conserved motif upstream of their respective start sites, implying they may share a common regulator. This approach illustrates how various genomic tools can be used to partition genes into putative pathways, which can then be specifically tested for interactions and epistatic relationships.

Table 5-3. JNK and AP1 (JUN-FOS-ATF) related genes.

JNK - AP-1 Genes	Annotation/Pathway Affiliation	Reference
ATF2	Activated by JNK.	Gupta et al., 1995
ATF7	Most similar to ATF4 of ATF/CREB family.	Peters et al., 2001
CEBPG	Interacts with c-FOS. Can form homo and heterodimers with CEBPs.	Davydov et al., 1995 Williams et al., 1991
CROC4	Activates c-FOS.	Jeffrey et al., 2000
ELK4	Activates c-FOS.	Mo et al., 1998
FOSB		
FOSL1		
JUN		
JUNB		

We have now moved our RNAi screening into a more high-throughput method. This should allow for the rapid testing of many more transcription factors identified in the regeneration profiles. We should also be able to make better use of the micro-cDNA amplification method to profile fewer cells from the 96-well RNAi cultures. This is beneficial since the amount of cells in the sensory epithelia is quite limiting. Therefore, reducing the number of cells profiled means increasing the number of genes that can be screened each time the sensory epithelia is harvested. With the soon to be released Affymetrix chicken chip, it will be possible to cast the net even wider to find genes downstream after RNAi knockdown. By continuing to connect the dots and networking more and more genes, this will provide a clearer picture of what genetic series of programs are necessary to regenerate an inner ear hair cell.

CHAPTER SIX

GENERAL CONCLUSIONS

The inner ear is a remarkable organ. A little more than 10,000 hair cells per ear are responsible for detecting a broad range of sound. The fact that avians (and other lower vertebrates like fish and amphibians) can regenerate hair cells of the cochlea and vestibular organs and mammals cannot, is astounding. Considering that one-third of people over the age 65 suffer from some form of hearing loss, primarily due to hair cell or nerve damage, possessing the ability to regenerate one's hair cells would be of great benefit. Therefore research in this area is of great biological as well as clinical interest.

In the previous chapters, I described the use of microarrays and library subtractions to identify genes expressed in the chicken utricle sensory epithelia (SE) during regeneration of its hair cells. The SE is comprised of supporting cells, which give rise to new hair cells, and the hair cells themselves. It was only recently that the sequence of the chicken genome became available (Wallis et al., 2004; Wong et al., 2004; Hillier et al., 2004), this meant that there was only a limited amount of sequence information on this species and no commercial gene chips were available. To compensate for this, our lab developed, *de novo*, a human transcription factor (TF) gene array that would interrogate this important class of genes across diverse species, including chicken. Hybridization conditions for the microarray were adjusted for an approximate 70% sequence identity between human and chicken.

In the first study I conducted, the SE of the chicken utricle was compared to that of the cochlea. The reasoning behind this study was that the utricle SE is constantly turning over its hair cells while the hair cells of the cochlea remain quiescent and that a comparison might yield insights into the turnover process. The hair cells in these two organs serve different purposes, but are structurally and developmentally very similar. Additionally, avian cochlear hair cells are capable of regeneration following damage. Therefore, the mechanism must typically be

inhibited in the cochlea as in mammals, or some signaling event is present in the utricle to maintain hair cell turn over. Using the TF array and a smaller array containing known inner genes and some signaling molecules, nearly 100 genes were identified as differentially expressed at a statistically significant level. It is important to note that very few cells are obtained from the inner ear. In order to profile 20,000-50,000 cells our lab also developed a linear micro-cDNA amplification protocol that has now been validated by several methods. The amplification method was used in the construction of libraries from these two samples. A utricle subtracted library was constructed to complement the microarray study. A subtraction methodology was developed to utilize the micro-cDNA amplified libraries. The subtraction was carried out using the cochlea SE as the driver population. This allowed for the identification of novel chick ESTs and genes expressed in the utricle in addition to those discovered in the microarray study.

Having established the first use of cross-species microarrays, additional profiling experiments were designed based on the above systems. The utricle SE was damaged using two independent methods, laser microbeam ablation and exposure to ototoxic drugs. Expression profiles created from these two treatments revealed some key signaling cascades are present during regeneration. Several genes were identified that fell into the TGF β signaling pathway implicating the importance of this pathway for regeneration. Also, a very important pathway expressed during otic development was played out entirely during regeneration. This was the PAX-EYA-SIX-DACH pathway. Each aspect of this pathway was expressed as well as other interacting transcription factors, but as in normal inner ear development, it is still unclear if these genes fall immediately downstream of one another as the nomenclature would suggest. These epistatic relationships remain to be elucidated.

Following damage to the hair cells it might be expected that apoptotic pathways would be induced and indeed that was the case here. I was able to identify several genes that play a role in apoptosis. In many ways these genes are just as important as those involved in proliferation. As the mammalian inner ear is incapable of regenerating hair cells, it would be beneficial to prevent them from actually dying. Just as neomycin was used to kill hair cells here, all aminoglycoside antibiotics are toxic to hair cells, as are chemotherapeutics such as cisplatin. Being able to inhibit apoptosis would therefore be beneficial to those who have to take these drugs.

Because hair cell regeneration implicitly involves cell proliferation, I looked for transcription factors that were involved in cell cycle regulation or proliferation in general. Induction and proper control of supporting cell division will be essential for a hair cell replacement therapy. Remarkable strides have been made utilizing a *Math1* expressing adenovirus as a gene therapy in deafened guinea pigs (Kawamoto et al., 2003a; Izumikawa et al., 2004). While these animals form new hair cells that show some functionality the morphology of these new hair cells indicates that a supporting cell has partially differentiated into a hair cell and no cell division has taken place. This leads to cellular deficit and may have an effect on how the organ of corti as a whole moves in response to the sound waves. Therefore, while this is an exciting step in the right direction more information is need to drive the supporting cells to divide before differentiating into a new hair cell.

The use of microarrays has provided a large number of genes that are likely to be important for hair cell regeneration, and the use of RNAi has proved the functional importance of several of those genes and the pathways they are a part of. Inhibition of JNK signaling established that this signaling pathway is essential for hair cell proliferation. The targeting of three genes, *PAX2*, *JUND*, and *CEBPG* with siRNAs illustrated the proliferative importance of

these genes as well. By profiling the cells following RNAi, a pathway began to emerge from the data showing an intersection of genes that were always downregulated. This allows for the positioning of genes downstream of those that were targeted. Profiling of RNAi treated cells has proved a powerful tool for pathway parsing, and networking many transcription factors.

Most of the experiments discussed in this thesis were research "firsts" for the field of hair cell biology. We have provided the first use, to my knowledge, of cross-species microarray hybridizations; the first use of expression profiling on SE cells to compare the cochlea to the utricle; the first expression profiles of regenerating hair cells; and the first use of RNAi in chicken SE cells (possibly even the first use of RNAi in chicken primary cell cultures). I feel this is a significant contribution to the field of study I have been involved in over the past several years.

CHAPTER SEVEN

MATERIALS AND METHODS

Sensory Epithelia Isolation

Our group was fortunate enough to have collaborated with Dr. Mark Warchol (Department of Otolaryngology, Washington University School of Medicine), who is an expert in isolating inner ear samples and especially the sensory epithelia. Dr. Warchol provided all samples for the microarray studies using the following methods. White Leghorn chicks (10-21 days post-hatch) were euthanized by CO₂ asphyxiation and decapitated. Cochleae and utricles were quickly removed and placed in chilled Medium 199 with Hanks salts (Invitrogen). The tegmentum vasculosum and lagena were removed from each cochlea and the otolithic membrane and associated otoconia were removed from the utricles. Sheets of isolated sensory epithelia were then obtained from these specimens following published methods (Warchol 2002; Warchol 1995). Briefly, sensory organs were incubated for 60 minutes in 500µg/ml thermolysin (Sigma, dissolved in Medium 199 with Earles salts) at 37°C. Specimens were then returned to chilled Medium 199 with Hanks salts, and a fine needle was used to remove individual sensory epithelia from their native basement membranes and connective tissue. Sensory epithelia from individual cochleae or utricles were then pooled together in 100µl Medium 199 (8-10 samples in each experiment).

Antibiotic treatment

Isolated sensory epithelia from 4-5 utricles were pooled together in 100µl Medium 199. Neomycin sulfate (Pharma-Tek, Huntington, NY) was prepared as a 100mM stock solution in sterile water and added directly to the culture wells at a final concentration of 1mM. Sensory epithelia were cultured in presence of neomycin for 24hrs and allowed to recover by transferring to fresh media in the absence of neomycin. Samples were harvested at 0hr, 24hr and 48hr

recovery. Time point matched control sensory epithelia were cultured following the same protocol with the absence of neomycin.

Laser microbeam ablations

Hair cell lesions in the cultured utricle sensory epithelia were created by laser microsurgery as previously described (Warchol and Corwin, 1996). Sensory epithelia were allowed to recover by remaining in culture and samples were removed at 30min, 1hr, 2hr and 3hr for analysis.

Total RNA Isolation

Approximately 50,000 sensory epithelial cells from either the utricle or cochlea were suspended in Trizol (Invitrogen) and total RNA was isolated as per the manufacturer's protocol. To the Trizol, 1/5th volume of chloroform was added. The tube is shaken by hand for 15 seconds and then incubated at room temperature for 2-3 mins. Samples were centrifuged at 12.3K rpms (12,000 x g) for 15 mins in a bench-top centrifuge. For those paranoid about the RNA, this can be done at 4°C. The RNA remains in the upper aqueous layer (~60% of original Trizol volume), which is then removed and placed in a new tube. To precipitate the total RNA, add isopropanol at a volume equal to 1/2 of original Trizol volume. Invert tube several times to mix. Incubate at room temperature 10 mins. To aid in precipitation, a carrier can be used. I would typically add 0.5µl of 20mg/ml glycogen. Spin samples at 12.3K rpms for 15-20 mins at 4°C. Remove supernatant. Wash the pellet (not always visible with such a small amount of RNA) with 75% ethanol at a volume equal to the amount of Trizol used. Vortex and centrifuge at 9.8K rpms

(9,000 x g) for 10 mins at 4°C. Remove supernatant and allow pellet to air dry. Resuspend RNA in 3-10µl of RNase free water. This typically yields 300-500ng of total RNA.

mRNA Isolation, cDNA Synthesis, and Amplification

Polyadenylated RNAs were isolated using 10µl of oligo dT₂₅ streptavidin coated paramagnetic beads (Dynal) and these were introduced into a cDNA synthesis and PCR amplification. Total RNA was combined with an equal volume of binding buffer (20mM Tris-HCl, pH 7.5, 1.0M LiCl, 2mM EDTA), and heated at 72°C for 3 minutes. Place on ice for 5 minutes. Place beads in tube next to magnet and remove supernatant. Add RNA and buffer to beads, mix, and incubate at room temperature for 20 minutes. Beads were then washed 2X in 50µl wash buffer (10mM Tris-HCl pH 7.5, 0.15M LiCl, 1mM EDTA). In every step involving bead work, removing liquid requires the tube to be placed next to a magnetic tube holder in order to maintain the beads. An initial cDNA synthesis was conducted on the beads using Superscript II reverse transcriptase (RT) (Invitrogen) in a 10µl reaction at 42°C for 1 hour. Reaction: 4µl water, 1µl 5'SMART oligo (10µM), 1µl 5X first strand buffer (Invitrogen), 1µl 0.1M DTT(dithiothreitol), 1µl 10mM dNTPs, 1µl RT(200U/µl). The reaction is done in the presence of a modified 5' SMART linker (Endege et al., 1999; Korshunova et al., in preparation). The oligo sequence is

SM-NotI-3G: 5'-GCGGCCGCTAATACGACTCACTATAGGG-3'.

This system makes use of the fact that the RT will add three Cs to the end of the 1st strand cDNA. Therefore, the 5' oligo will anneal (note the three Gs) at the reaction temperature of 42°C. This now provides a template to extend the 1st strand cDNA, adding the complementary sequence to the 3' end of the cDNA. Because the RT is likely to add another set of Cs at the end

the linker sequence. The oligo contains a NotI site to remove linker concatemers. The beads with cDNA attached were washed two times with 50µl wash buffer as above, followed by two washes with 1X 50µl NotI digest buffer (50mM Tris-HCl, 10mM MgCl₂, 100mM NaCl, 1mM dithiothreitol). cDNAs were then digested with NotI to remove concatenated linkers. Digest reaction: 0.5µl NotI (10U/µl), 9.5µl 1X digest buffer incubated with beads for 10 minutes at 37°C. Beads/cDNA were washed twice with 50µl of water. The cDNA was subjected to 3 cycles of PCR amplification using the following two primers:

5'-SM-PCR primer: 5'-CATGCTAATACGACTCACTATAG-3', and

SM-CDS primer: 5'-AAGCAGTGGTAACAACGCAGAGTACTTTTTTTTTTTTTTTTVN-3'.

1st Round PCR: 5µl 10X Advantage Taq PCR Buffer (Clontech), 2µl dNTPs (2.5mM each), 1µl 5'-SM-PCR primer (10µM), 1µl SM-CDS primer (10µM), 1µl Advantage Taq (5U/µl, Clontech), 41µl water. Heat start Taq by initially denaturing at 95°C for 2 minutes. Cycle: 95°C - 10 seconds, 34°C - 15 seconds (anneal), 68°C - 6 minutes (extend). See Figure 7-1 below

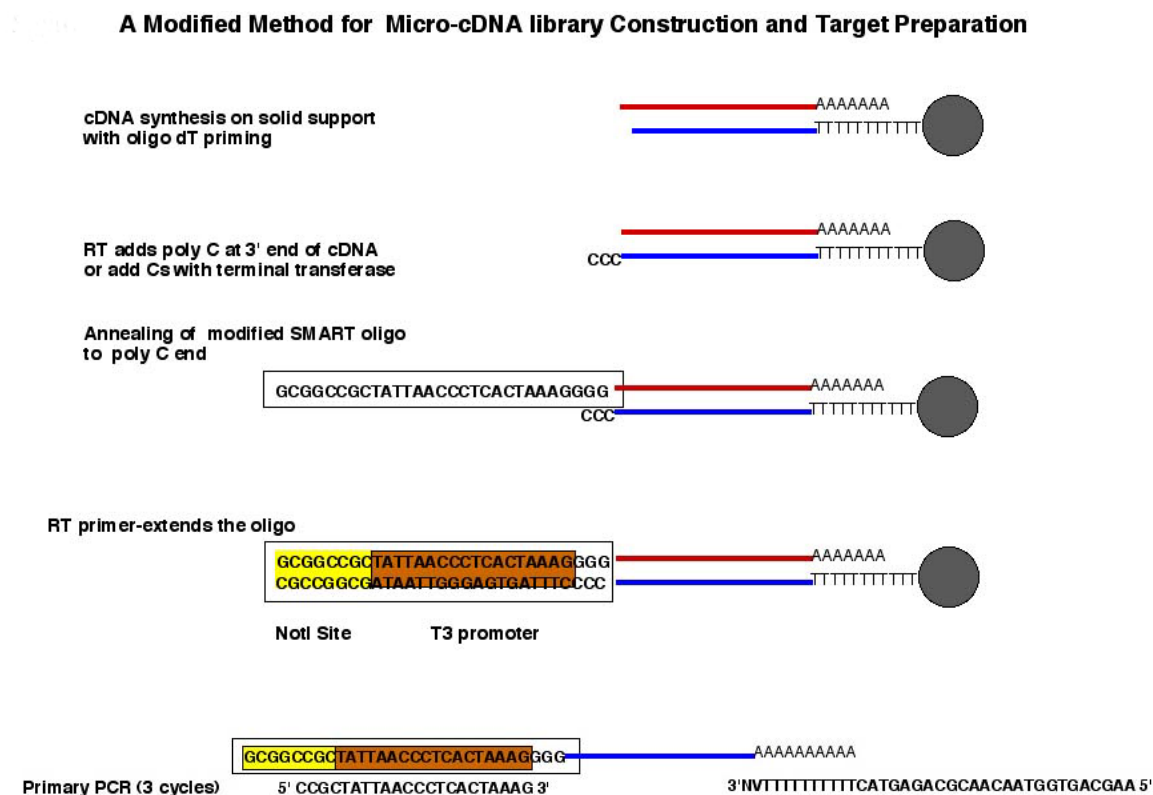


Figure 7-1. micro-cDNA Amplification Part I. mRNA is captured on oligo-dT beads. This allows for first strand cDNA to remain attached to the beads. Linker concatemer is digested following second strand synthesis and cDNA is ready for 1st round of amplification.

Beads were then magnetically captured and the amplified cDNA in the supernatant was removed. The entire cDNA supernatant was then amplified in twice the original reaction volume for an additional 7 cycles with the following primers (Treat the entire primary reaction(50μl) as the template in a 100μl reaction, but the new reaction mix is based on 50μl, since 50% is already made up in the original reaction).

5'-SM-PCR primer: 5'-CATGCTAATACGACTCACTATAG-3', and

3'-SM-PCR primer: 5'-AGTGGTAACAACGCAGAGTAC-3'.

2nd Round PCR conditions were as above, except increasing the 3'-SM-PCR primer volume and Taq volume to 2µl. Adjust the water volume accordingly. Cycle as above, except increasing the annealing temperature to 60°C. Amplified cDNA was desalted on a Sephadex G50 minicolumn, and one-third of the reaction was used in a tertiary PCR to add linkers for UDG cloning into the pAMP1 vector (Invitrogen). The 3rd Round PCR: 33µl cDNA, 5µl 10X Buffer, 2µl dNTPs, 2µl 5'-CAU primer (10µM), 2µl 3'-CUA primer, 1µl Taq, 5µl water. Cycle as in 2nd Round for 5 cycles. The primer sequences are

5'-CAU primer: 5'-CAUCAUCAUGCTAATACGACTCACTATAG-3', and

3'-CUA primer: 5'-CUACUACUACUAGTGGTAACAACCAGAGTAC-3'.

The tertiary PCR is only necessary for creating libraries, as was done for the utricle and cochlea sensory epithelia samples. Otherwise, the second round can be increased to 12 cycles to fully amplify the cDNA. The 5'-SM-PCR primer contains a T7 promoter, allowing for uncloned cDNA to be used in In Vitro Transcription (IVT) Reactions. All time point comparisons were done utilizing this method. In each case the total number of PCR cycles is 15. This keeps the amplification in a linear range. See figure 7-2 below.

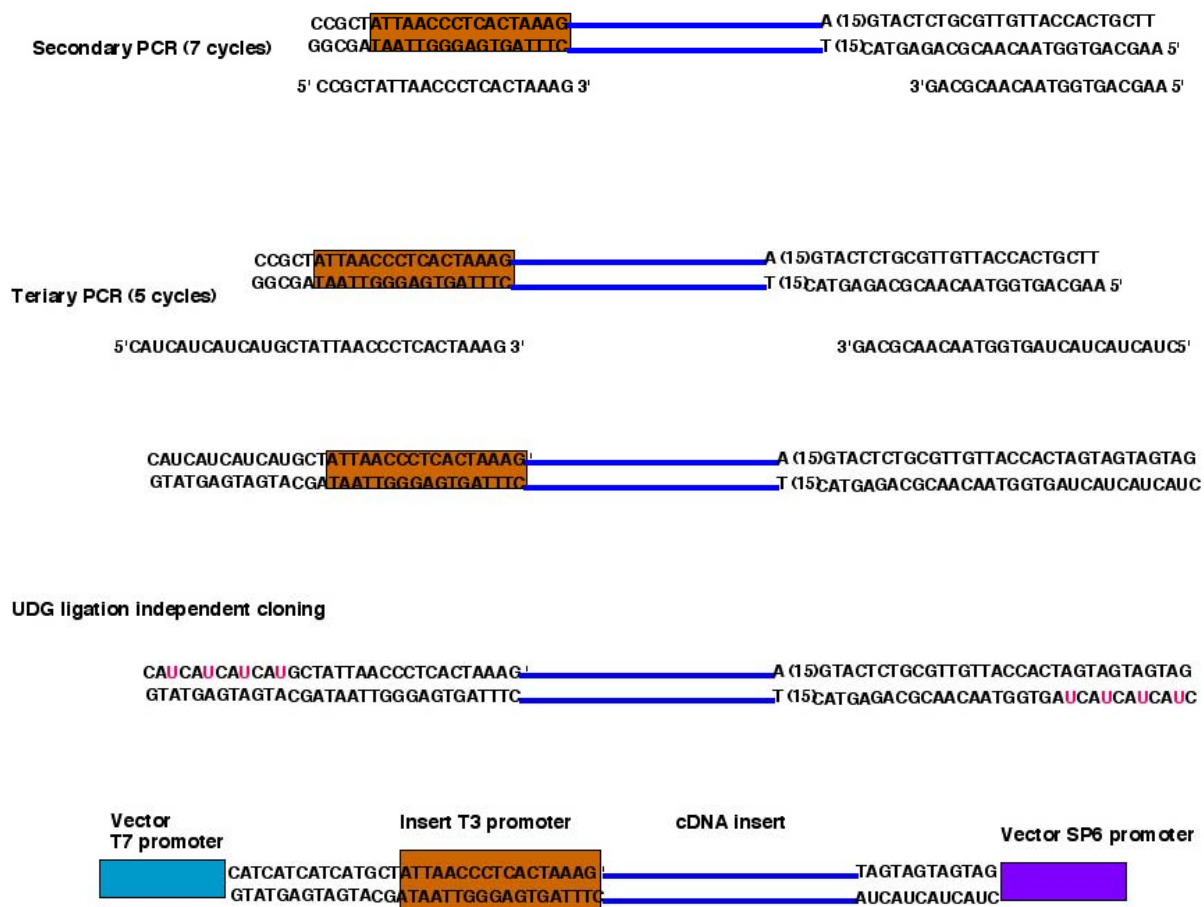


Figure 7-2. Micro cDNA amplification Part II. cDNA is put through a second round of amplification using additional primers for 7 cycles. This can be increased to 12 if using immediately in an IVT reaction. Otherwise, a tertiary round is used to add CAU/CUA ligation independent cloning linkers.

Micro-cDNA Library Construction

The pAMP1 vector (Invitrogen) contains overhangs of (CAT)₄ and (CTA)₄ for directional cloning (Figure 7-2). This also allows for ligase-independent cloning. The uracils in the cDNA linkers are removed by uracil DNA glycosylase (UDG), leaving overhangs complementary to the vector overhangs. The overhangs are annealed and ready for transformation. The nicks are repaired in the cell during replication. To remove small fragments, concatemers, and primer dimers, which clone more rapidly, the cDNA is first cleaned over a size separating column. SizeSep 400 Spun Columns (Amersham Pharmacia) retain DNA fragments smaller than 400bps. First the column is drained, then equilibrated with 2ml of a buffer suitable for the next step, here, 1X annealing buffer for pAMP1 [20mM Tris-HCl (pH 8.4), 50mM KCl, 1.5mM MgCl₂]. This is repeated two more times. Each time resuspend the gel by inverting the column several times. On the last wash, stop the elution just as the liquid enters the top of the gel. Spin the column in a 15ml tube at 400 x g for 2 minutes. Place the column in a clean tube and slowly add the cDNA. Spin again for 2 minutes, DNA larger than 400bp will be in the effluent. 10-50ng of cDNA in a volume of 2μl are used in the pAMP1 cloning/annealing reaction: 2μl cDNA(10-50ng), 2μl pAMP1 vector DNA(25ng/μl), 1μl UDG, 15μl 1X annealing buffer. Mix and incubate for 30 minutes at 37°C. The Greater than 10⁶ primary transformants were constructed by chemical transformation of UltraMax DH5α-FT competent cells (Invitrogen). Typically 2μl were transformed, and 20-30 transformation were needed to construct a library at 10⁶. Cells are thawed on ice and 100μl are mixed with annealing reaction by gently flicking tube. Incubate on ice for 30 minutes. Cells are heat-shocked in a 42°C water bath for 45 seconds and placed on ice for 2 minutes. Add 0.9ml of S.O.C. Medium, and shake at 225 rpm, 37°C for 1 hour. Plate 10μl on a LB/Amp agar plate (100μg/ml ampicillin) to determine titer. Spin cell down into a pellet (2

minutes at 3000 rpm). Remove 800µl medium. Plate the remaining broth on a 150mm LB/Amp plate (~50,000 colonies). Grow plates upside down in a 37°C incubator overnight. Add 2-3 ml of LB/Amp medium (100µg/ml ampicillin) to each plate and scrape off cells, placing in a cryo-safe tube. Add enough glycerol for a final concentration of 25-30% to freeze cells. Snap freeze each tube in a dry ice-ethanol bath.

In Vitro Transcription (RNA run-offs)

RNA templates were generated from purified plasmid DNAs (Sambrook and Russell, 2001; Qiagen Qiaprep Spin Miniprep Kit) for the utricle and cochlea libraries. Pooled purified plasmids were linearized by digestion with NotI and gel purified. 1µg of linearized (library) plasmid DNAs was added to an Ambion T7 Megascript reaction and *in vitro* run-off transcripts were generated as per the manufacturer's instructions. For run-off production from uncloned samples the PCR products after Sephadex G-50 desalting (above) were ethanol precipitated, resuspended in nuclease-free water, and directly added to an Ambion T7 Megascript reaction. 20µl reaction: 8µl DNA(300ng-1.0µg), 2µl each 75mM ATP, GTP, CTP, and UTP, 2µl 10X reaction buffer, 2µl T7 Enzyme Mix. Place at 37° overnight. To remove DNA template add 1µl DNase I (2U/µl) and incubate at 37°C for 30 minutes. Run-off RNAs were LiCl precipitated by adding 30µl LiCl Solution [7.5M LiCl, 50mM EDTA] and 30µl nuclease-free water. Mix thoroughly and chill at -20°C for 1hr. Centrifuge for 15 minutes at maximum speed in a benchtop microfuge. Remove supernatant and wash pellet with 75% ethanol. Resuspended in nuclease-free water at a concentration of 0.5-1.0µg/µl. The overall yield, typically 50-100µg, and quality of run-off products were assessed by gel electrophoresis.

Target Labeling

Run-off RNAs were used as templates in an oligo dT₁₂₋₁₅ primed cDNA synthesis reaction that included amino-allyl dUTP (Sigma, 0.2mM). Combine 2µg RNA and 2µg Oligo-dT, incubating at 70°C for 10 minutes. Chill on ice for 10 minutes. Add 3µl 10X Stratascript RT buffer (Stratagene), 0.6µl 50X aa-dNTPs [mix 10µl each 100mM dATP, dCTP, dGTP, 6µl 100mM dTTP, 4µl 100mM amino allyl-dUTP (Sigma)], 3µl 0.1M DTT, 3µl Stratascript RT (50U/µl), water to a final volume of 30µl. Incubate at 42°C for 2 hours. RNA was hydrolyzed by adding NaOH and EDTA at a final concentration of 100mM and 10mM, respectively, and heating at 65°C for 10 minutes. The reaction was cleaned and concentrated by washing and spinning in a Microcon-30 tube 3 times. At this stage the cDNA was coupled to either Cy3 or Cy5 mono-ester dyes (Amersham Pharmacia) in the presence of coupling buffer [final concentration of 50mM sodium bicarbonate]. The cy3 and cy5 dye labeled samples can be purified separately or combined using Qiaquick PCR Purification column. This will remove uncoupled dyes and salts. Labeled cDNA can elute in less than the recommended volume. If necessary, the sample can be concentrated using a Microcon-30 column or precipitated.

Microarray Hybridizations

Labeled cDNA is resuspended in 20µl hybridization buffer (30% formamide, 6X SSPE, 5X Denhardt's, 0.5% SDS, 10% Dextran Sulfate). cDNA Microarray slides were hybridized at 42°C for 12 hours. TF oligonucleotide slides were hybridized at 37°C for 12 hours. Slides were washed 5 minutes each in 0.2X SSC followed by 0.05X SSC and dried. Slides were scanned using a GMS 418 scanner at gains ranging from 25-35 scanner units. Microarray targets included spiked control RNAs. Each of these three controls consisted of a few hundred base

pairs of specific *C. elegans* cDNA sequence with a polyA tract inserted at its 3' end. The short sequence was directionally cloned adjacent to a T7 promoter. A T7 polymerase RNA run-off from each cloned *Ce* tag produced a short polyadenylated RNA that does not share significant sequence homology with any human, mouse or chick sequences (by BLAST search). These RNAs were then seeded into the two targets (at different concentrations) prior to cDNA synthesis. These controls are listed at <http://hg.wustl.edu/lovett/projects/nohr/intlctrl.html>.

Microarray Slide Processing and Printing

Slides for printing were pre-treated by washing for 2 hours in a 10% (w/v) NaOH, 57% (v/v) ethanol solution. Slides were then rinsed four times in water. They were coated in a solution of 10% poly-L-lysine, 10% PBS for 1 hour at room temperature, rinsed in water and dried by spinning in floor centrifuge at 1000 rpm for 5 minutes. Slides are baked at 45°C for 10 minutes. PCR amplicons and oligonucleotides were resuspended in printing buffer (50% DMSO, 1.5M Betaine for PCR products, and 6%DMSO, 1.5M Betaine for oligonucleotides). Microarrays were printed on a GMS 417 arrayer. After printing, slides were baked at 80°C for 2 hours, then cross-linked at 65mJ before use.

Design of Custom cDNA and Oligonucleotide Microarrays

Our lab designed and built two microarrays for this study. Both of these are listed at <http://hg.wustl.edu/lovett/projects/nohr/hair-cell.html>. The Inner Ear cDNA array interrogated a collection of 426 genes that I selected that are known to either affect hearing or to be expressed in the inner ear. Many of these were derived from three web sites (<http://dnalab-www.uia.ac.be/dnalab/hhh/>, <http://www.ihr.mrc.ac.uk/hereditary/genetable/index.shtml> and

<http://hearing.bwh.harvard.edu/estinfo.HTM>). Primers for this array were designed using Primer3 (http://www-genome.wi.mit.edu/cgi-bin/primer/primer3_www.cgi) to generate amplicons 150-300bp in length. Each primer was designed to be 20-22bp in length with an average annealing temperature of 58°C with 50% GC content, and a GC clamp. Amplicons were generated from a pool of human libraries including HeLa cells, thymus, fetal brain, testis, and pancreas. PCR products were gel purified and ethanol precipitated. Following verification by DNA sequencing they were resuspended in printing buffer (50% DMSO, 1.5M Betaine) at a concentration of 300ng/μl. In all cases every gene or control was spotted in triplicate. The Ce tags mentioned above were also spotted onto this array. These artificial control tags were also introduced at various concentrations into the cochlea and utricle targets, and served as normalization factors and measures of detection sensitivity.

The TF array is listed at <http://hg.wustl.edu/lovett/projects/nohr/TFarray.html> and contains 50mer oligonucleotide probes to the majority of known human transcription factor genes, plus some anonymous ESTs that contain transcription factor motifs and a few transcriptional co-activators. The design of this array was the work of another graduate student in the lab, David Messina. As it is essential to this study, a brief description follows. The seed set for the array covered all orthologs of TFs in Flybase and TRANSFAC as well as TFs in REFSEQ. A complete list of the TFs that this array interrogates is available at <http://hg.wustl.edu/lovett/projects/nohr/TFarray.html>. The number of genes interrogated by this array was 1422. It should be noted that while this is a very large set, our informatics analysis indicates that it does not comprise the entire set of TFs encoded by the human genome (Messina et al., 2004). It is well known that many transcription factors contain highly related sequence motifs (for example zinc finger motifs). We therefore carried out a detailed analysis (Messina et

al., 2004) to derive a set of oligonucleotides from outside these shared motifs so that each transcription factor could be individually interrogated. In building these probes we were also particularly careful to avoid picking 3' untranslated regions (UTRs) as the specific probes, since this would render them useless for monitoring gene expression in different species (e.g. interrogating the chick samples in this study). For a discussion of the degree of sequence conservation on average between human and chick see below. All of the 50mers were T_m-matched. All were precipitated and resuspended at a concentration of 60μM in 6% DMSO and 1.5M Betaine. The TF array also contained within it individual 50mers to interrogate each Ce control tag. All TF probes were spotted in duplicate on each printed slide.

Quantitative PCR

Total RNA was extracted from the sensory epithelia as described above. Approximately 50ng of total RNA was used to generate cDNA using a Qiagen Sensiscript cDNA Synthesis Kit. The resulting cDNA (approximately 0.72 ng) was diluted to 50μl and 2μl were used in each Q-PCR reaction. PCRs were set up using Applied Biosystem's SYBR Green PCR Master Mix in 25μl reactions. Primers were designed using the ABI Primer Express software. Melting curves and PCRs were run on an ABI 7700 machine and results analyzed using ABI Sequence Detector software for the utricle-cochlear comparisons. Damaged time point samples were assessed using the Stratagene MXP3000 machine and analytical software. To identify chick orthologs and design chick primers for each tested gene I BLASTed the corresponding human gene against the TIGR *Gallus gallus* EST database (<http://tigrblast.tigr.org/tgi/>).

In situ Hybridizations and Immunocytochemistry

I generated PCR amplicons with primers designed to amplify chick sequences. A second round of amplifications was used to add T7 and T3 promoter sequences to the 5' and 3' ends respectively. PCR products were gel purified and an aliquot was DNA sequenced to verify the identity of the product. Amplicons of 200-300 bp were used as templates to generate DIG-labeled *in vitro* transcripts (Ambion Maxi-script kit). Sense (T7) and anti-sense (T3) probes were separately generated from the respective promoters. Cochleae and utricles were harvested from chicks (10-21 days post-hatch) and processed for whole mount *in situ* hybridization following a published protocol (Henrique et al., 1995) by our collaborator Dr Mark Warchol. Labeled specimens were mounted in glycerol/PBS (9:1) and viewed with conventional brightfield microscopy (Nikon Eclipse 2000). Images were obtained using a monochrome CCD camera (Q-Imaging).

Other specimens were processed for immunohistochemical labeling of GATA3. Cochleae and utricles were fixed in chilled 4% paraformaldehyde (in PBS) for 20 minutes. Nonspecific antibody binding was blocked by incubation for 2 hours in 2% NHS, 1% BSA, and 0.2% Triton X-100 (in PBS). Specimens were then incubated overnight in anti-GATA3 (Santa Cruz Biotechnology, mouse IgG), diluted 1:200 in PBS, with 2% NHS and 0.2% Triton X-100. Following thorough rinsing in PBS, specimens were incubated in biotinylated anti-mouse IgG (Vector) followed by streptavidin-conjugated Alexa 594 (Molecular Probes). Specimens were counter-stained with Alexa 488-labeled phalloidin (Molecular Probes) and bisbenzamide (Sigma) and were viewed with epifluorescence microscopy (Nikon Eclipse 2000). Similar steps were taken for beta-catenin and PAX2 immunohistochemical labeling.

Data Analysis

Microarray images were analyzed with the BioDiscovery ImaGene and GeneSite-Lite programs. The Cy3 and Cy5 images were computationally overlaid, aligned and gridded. The intensity of each spot was measured by laser scanning (as described above). The Imagen program uses the signal mean ratio of the \log_{10} intensity values to determine fold expression changes. These values (over at least four different experiments and with at least two dye labeling switches) were then analyzed as described by Wolfinger et al., 2001, in collaboration with Dr. Nancy Saccone (Division of Human Genetics, Washington University School of Medicine). This method uses two steps, a normalization step and a model fitting step, to obtain statistically significance levels that take into account experimental variability. SAS (SAS Institute, Cary, NC) code from Wolfinger et al (<http://statgen.ncsu.edu/ggibson/Manual.htm>) was adapted to our data. In the normalization step, we included fixed effects for tissue, dye, and spot repetition (the last to account for the triple or double-spotting of each probe onto the slide) as well as interaction terms; random effects were included to model variability among the experiments and the 4 pins of the arrayer, and interactions between random and fixed effects. The subsequent t-tests were corrected using a Bonferroni correction for the number of genes on the array.

Over the course of my thesis work the ways of analyzing microarray data advanced and the regenerative time point data was analyzed using other software and statistical methods. The majority of the statistical analysis was done by a biostatistician in the lab, Veena Bhonagiri. Data analysis and hierarchical clustering were performed using TIGR TMEV2.2 and TIGR MIDAS2.17 (TIGR, www.tigr.org). Gene clustering for self-organizing maps (SOMs) was performed using GeneCluster 2.0 (MIT, www.broad.mit.edu). Each time course was replicated

with additional biological samples, including controls. Treatment time points and time matched controls were hybridized a minimum of four times, two and two dye switch experiments. The study is comprised of a minimum of 56 hybridizations. The array data was put through series of biostatistic steps to achieve the best output for fold changes in expression with confidence limits. First, the array data was normalized by LOWESS, a locally weighted linear regression model, to compensate for dye effects by removing such artifacts from the data in a log2 ratio format (Quackenbush 2002). The LOWESS method detects systematic deviations in a ratio-intensity plot (R-I) plot and corrects them by carrying out the local weighted linear regression as a function of the log10 product of each channel intensity value ($\log_{10}(I(A) \cdot (B))$) and subtracting the calculated best fit average log2 ratio ($\log_2(I(B)/I(A))$) from the experimentally observed ratio for each data point. I=intensity, B=channel value, A= channel value. The two channel values come from the Cy3 and Cy5 scans. Figure 7-3 illustrates a dye bias and how LOWESS corrects for such a bias.

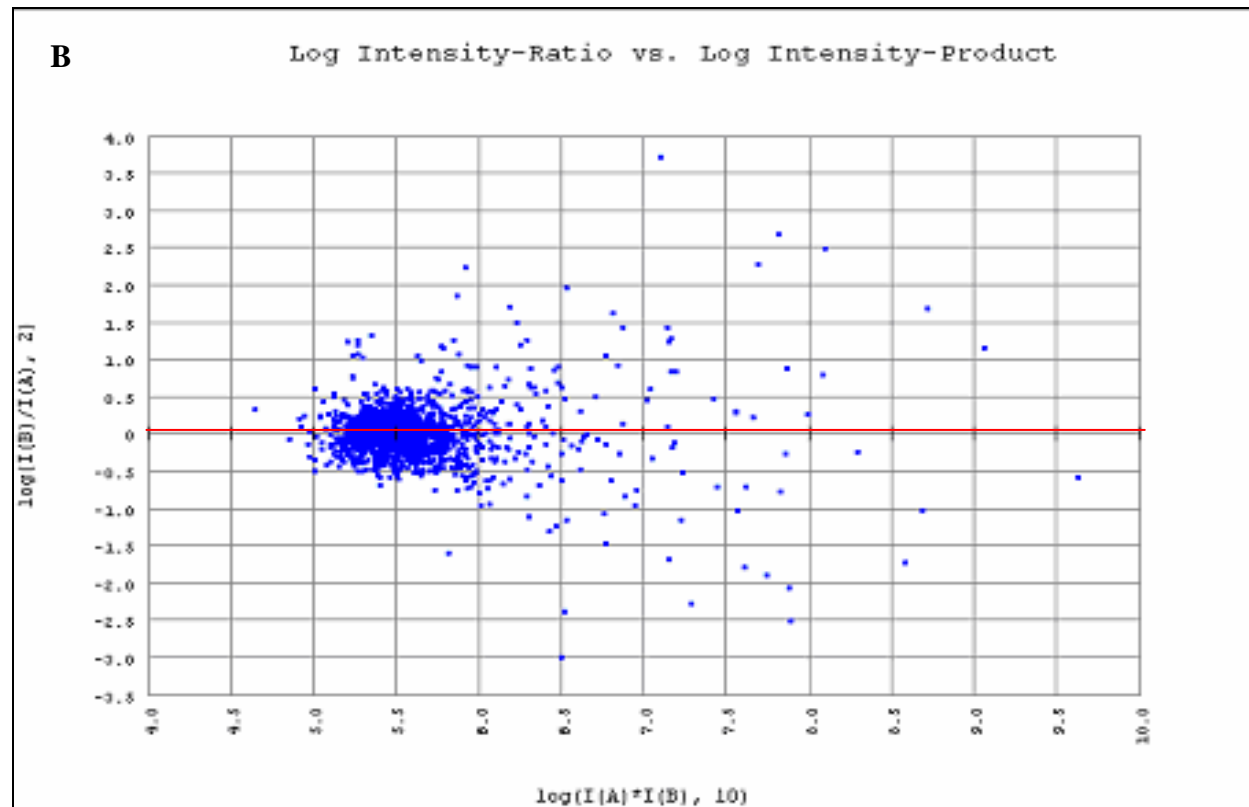
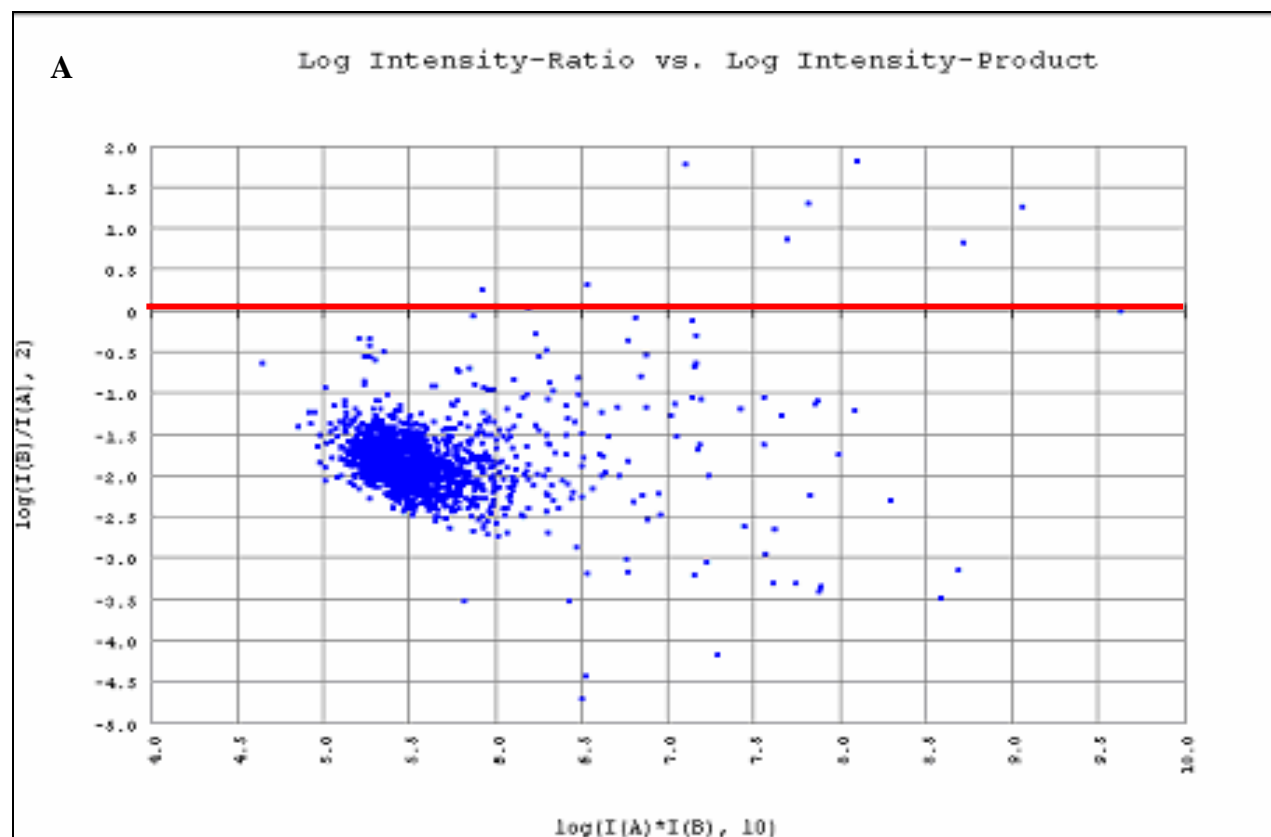


Figure 7-3. R-I plots (ratio-intensity) showing the effect of LOWESS Normalization. Log₂ (IB/IA) ratio (channel B /channel A intensity ratio) is plotted on Y-axis and log₁₀ (IB*IA) on X-axis. It displays log₂ (IB/IA) ratio for each element on the array as a function of the log₁₀ (IB/IA) product intensities and can reveal systematic intensity dependent effects in the measured log₂ (ratio) values. **A.** Intensity ratios before LOWESS normalization, illustrating a dye bias towards channel A and appear as upregulated (dye-specific artifact). **B.** Intensity ratios after data adjustments. The above dye specific artifact is corrected.

Next, a method within the MIDAS software was utilized to adjust for position effects on the arrays termed standard deviation regularization (SD-reg). The array once printed appears in 4 distinct panels. Occasionally there might be variation from one panel to the next. SD-reg was carried out to adjust for any variation in the measured log₂ ratios. The channel A and channel B intensity pair for each spot is scaled so that the spot sets within each panel have the same standard deviation as other panels. As spots within each block are printed by the same print-tip, Sd-reg allowed us to minimize the system bias caused by different print-tips. Following this step, data was filter to remove spots/genes below an arbitrary threshold for background intensity. The threshold was determined by the spot intensity of controls that should not show expression, and by how these spots fell in the overall distribution of intensity values. Approximately 10-20% of all TFs were removed at this step.

Data from the multiple hybridizations for a time point are hierarchically clustered along with a set from an additional time point to identify the most similar hybridizations. Clusters typically included samples labeled with both dyes, and contained hybridizations from both biological samples. t-tests were performed between samples to ensure similarity. Genes within a data set that are dissimilar are filtered from the gene list and samples are re-clustered (Figure 7-4). Genes expression fold changes were determined for genes following a trend in 80% of the clustered hybridizations. This is applied to every gene in the data set. Average fold changes of each gene were calculated from the clustered experiments fitting this trend. A P-value was calculated using a one-sample t-test. In order to create the self-organizing map not all genes

passed the filter in both time courses, therefore changes in gene expression were discerned using a cutoff below that of 80% for genes not present in both and filled in to construct the patterns of gene expression across all seven timepoints. .

Figure 7-4. Hierarchical Cluster of data from neomycin 24 vs control and neomycin 48 versus control. **A** demonstrates how before removal of bad hybridizations and filtering inconsistent spots leads to various clusters that are not grouped based on the same time point. **B** Re-re-clustering following filtering.

Subtraction Materials and Methods

Target Preparation

Inoculate 2 mls LB-Amp (50 µg/ml) from frozen glycerol stock to an OD₆₀₀=0.3-0.4 and incubate at 37°C with shaking at 250 rpm for 1.5 hours. Add 75 µl of M13K07 (GibcoBRL) at a titer of 1×10^{11} pfu/ml and continue incubation at 37°C with shaking at 275 rpm for 1 hour. Add Kanamycin to a final concentration of 75 µg/ml and continue to incubate at 37°C with shaking for an additional 2-3 hrs. To isolate ssDNA, spin culture in 2 ml microfuge tube for 15 minutes at 5000 rpm in a microfuge. Transfer supernatant to a clean tube, add 4 µl DNase I, RNase-free (Roche) and incubate 45 minutes at 37°C (Simmons and Lovett, 1997). Continue isolation of ssDNA per Qiagen M13 kit. Check 5 µl on gel. Denature gel in 0.4M NaOH then neutralize in 0.5M Tris-HCl pH 7.5, 1.5M NaCl, 0.001M EDTA. Blot gel 12 hours in 20X SSC and check for dsDNA contamination with (-) strand oligo, 5'-CATGCTAATACGACTCACTATAC-3'. In a 10µl reaction kinase 1µl of 10µM oligo using 10U T4 Kinase (Invitrogen), 20µCi γ -P³² dATP and forward exchange buffer. Hybridize 12 hours at 38°C.

Driver Preparation

Plasmid DNA isolated from the library by miniprep was digested with SalI and gel purified to remove circular plasmid contamination. 100ng of linearized plasmid DNA was used in linear PCR. The driver population was amplified incorporating biotin-16-dUTP (Roche, 33µM) at a ratio of 1:1.5 with dTTP using the 3' blocking oligo (5'-AGTGGTAACAACGCAGAGTAC-3'). Several 30µl reactions were pooled to obtain ~6µg. Pool reactions were passed over a prepared G50 sephadex column for removal of unincorporated

biotin. Incorporation of biotin was monitored by checking for binding to streptavidin coated paramagnetic beads (Dyna) by simultaneously setting up a reaction with 10uCi P32 dCTP. Increase 30µl reaction volume to 100µl and clean up by spinning through a sephadex G50 column. Measure the counts per minute (cpms) generated by the reaction. Place 125µl Dynal beads in a microfuge tube and place against magnet for 2 minutes then remove supernatant. Wash the beads 3X by resuspending in 200µl of TEN100 binding buffer (10mM Tris pH7.5, 1mM EDTA, 100mM NaCl), capture beads with magnet and discard supernatant. Resuspend beads after final wash in 100µl TEN100. Add radioactive PCR and incubate at room temperature for 1hr. Remove supernatant from beads after binding and determine the cpms remaining in the supernatant for binding efficiency.

Subtraction Hybridization

Subtractions were hybridized to a Cot value of 30 using the following conditions: 100ng single stranded target DNA , 3µg driver, 10µg each of 3 blocking oligos
 3' blocking oligo: 5'-AGTGGTAACAACGCAGAGTAC-3',
 5' blocking oligo: 5'-CCCTATAGTGAGTCGTATTAGCATG-3' and oligo dT₁₅. Add 3.6µl 100% deionized formimide, bring volume to 10.8 µl with ddH₂O, and overlay with 20µl mineral oil. Denature at 95°C, lower to 45°C slowly in a stepwise manner. 1 cycle in PCR machine: 95°C for 3 min, 90°C - 30 sec, 85°C - 30 sec, 80°C - 30 sec, 75°C - 30 sec, 70°C - 30 sec, 65°C - 2 min, 60°C - 30 sec, 55°C - 30 sec, 50°C - 30 sec. At 45°C add 1.2µl 10X buffer (1.2M NaCl, 0.1M Tris [pH 8.0], 50 mM EDTA; Bonaldo et al., 1996, method 4) under mineral oil and incubate at 45°C for 26 hours.

Target isolation after hybridization

After incubation is complete, remove 12 μ l reaction from under mineral oil, and bring volume to 100 μ l. Pass through a sephadex-G50 column. Divide hybridization reaction between three 125 μ l aliquots of beads. Wash beads as above and add an equal volume of binding buffer as reaction volume. Bind for 1 hour with periodic mixing and capture beads with magnet then remove and save supernatant (containing the unbound ssDNA). Radioactive labeled controls indicated that this is adequate for greater than 95% binding. Wash beads two times with 200 μ l of TEN1000 (10mM Tris pH7.5, 1mM EDTA, 1.0M NaCl),. Add 100 μ l ddH₂O to pooled washed bound bead mixture and boil at 100°C for 5 minutes to elute bound target population. Quick chill on ice. Put beads against magnet and remove eluant.

Set up PCR reactions from both the supernatant and the eluant, using M13 forward and reverse primers, which anneal to the vector only. This insures that only target library inserts are amplified. Concentrate the supernatant by reducing the volume in a speedvac to about 10 μ l and repair. Prepare a southern blot of equal amounts of PCR product from both the supernatant and eluant. Blots were probed for the presence of abundantly expressed genes like GAPDH.

Partial Repair of ssDNA for Transformation

Single stranded DNA from the subtraction is repaired by PCR in a total volume of 30 μ l. Five units of Advantage Taq(Clonetech) is used with a final concentration of 0.33 μ M for the 3' blocking oligo. Mix and incubate 2 min @ 85°C, 1 min @ 72°C, 1 min 30 sec @ 68°C, 1 min 30 sec @ 52°C, 45 min @ 68°C. Transform 3-5 μ l and plate onto large LB Amp plates, to check titer, or for making glycerol stock do several transformations and plate all. For initial analysis of

normalization, do plate lifts (2 copies each) and hybridize with probes that delete the levels of both low and highly abundant cloned genes to gauge the success of subtraction.

Reiterative Subtraction

Using the same methodology, 1152 (twelve 96well plates) clones were picked from the 1°Subtraction, and plasmid DNA was isolated for sequencing by the Washington University Genome Sequencing Center. This same 1152 clones were pooled (10µl each, followed by plasmid isolation as above) and used as the driver in a reiterative subtraction. The target was ssDNA isolated from the 1°Subtraction library.

Sequence Analysis

Sequence for the library clones were BLASTed against the following four databases to determine the number of novel ESTs identified and to determine proper annotation for those previously available.

- 1) Human Unigene Build #175 (54,560 unique sequences; source: <ftp://ftp.ncbi.nlm.nih.gov/repository/UniGene/>);
- 2) BBSRC chicken finished cDNAs (July 2004, 19,626 sequences; source: <http://www.chickest.udel.edu/>);
- 3) NCBI chicken ESTs (492,640 G. gallus sequences extracted from NCBI's Oct. 2004 file est_other.gz source: <ftp://ftp.ncbi.nlm.nih.gov/blast/db/FASTA/>);
- 4) TIGR GgGI (G. gallus gene index), release 7 (May 2004, 118,873 sequences; source: <http://www.tigr.org/tdb/tgi/>);

Sequences from the two constructed libraries also were BLASTed against each other following Phrap analysis to determine library overlap, additional subtraction, and enrichment.

Phrap was performed to group clones having overlapping sequence identity into contigs. For the purpose of library comparisons, clones that fell into a contig were considered a single entity, explaining lower numbers showed in the comparison diagrams of Chapter 3.

siRNA Generation

siRNAs were generated by generating PCR amplicons of 200-300 bp from chicken cDNA. Amplicons were re-amplified to add RNA polymerase promoters to the 5' and 3' ends. Reactions were cleaned up using Qiagen PCR Clean up kits (Qiagen). aRNA and cRNA were synthesized by IVT using MaxiScript Kit (Ambion). The complementary RNA strands were annealed by heating at 75°C for 5 minutes and cooling to room temperature at the bench for 1.5 hours. Annealing was assessed by size distribution on a 2% agarose gel. Annealed products were converted to siRNAs by cutting with the Dicer enzyme utilizing the Dicer siRNA Generation Kit (Gene Therapy Systems) per manufacturer's protocol. Following clean-up over the sizing column to remove un-diced products, the dsRNA is checked on a 3% agarose gel to ensure the proper size of 22-23 bp.

APPENDIX

Table A4-1. Neomycin Venn Diagram Gene List.

O HR EXPRESSION - 87 GENES				
AIB3	GCN5L2	MYF6	STAT6	ZNF145
ATF3	GLI3	NFKBIE	TAF2A	ZNF151
CBX6	HIVEP1	NKX2B	TAF2E	ZNF162
CEZANNE	HMX1	NR2F2	TAF2F	ZNF193
CHD4	HOXC9	NR4A2	TAF2J	ZNF197
CNOT8	HYPH	POU1F1	TAF2K	ZNF202
CSRP3	IRF4	PPARA	TBX19	ZNF262
DACH	ISL1	RBPSUHL	TBX22	ZNF274
DMRT1	KIAA0130	RERE	TCF12	ZNF278
DR1	KIAA0426	RFX4	TEAD2	ZNF32
DRAP1	LEF1	RFXANK	TEF	ZNF38
DSIP1	LOC56270	RUNX1	TGIF	ZNF41
EYA4	LZTR1	RXRA	TIEG	ZNF8
FLJ13590	MAFF	SAFB	TIMELESS	ZNF81
FLJ20557	MDS032	SALF	TP53	ZNF84
FLJ20729	MLLT1	SNAPC1	TRIP4	
FLJ22332	MNDA	SOX13	WHN	
FOXC1	MYCL1	STAT5A	ZNF134	
24 HR EXPRESSION - 55 GENES				
AF093680	DLX5	GLI	MEF2A	SIX3
AHR	DLX6	GTF2E1	MEIS1	SLUG
ALY	E2F4	HDAC1	MID1	SSRP1
ATF5	E2F6	HNF4G	MYT1	TBX20
BHLHB2	EGR2	HOX11L	NFKB1	TRIM28
BMI1	EMX2	HRV	NHLH2	ZFP26
CL469780	EP300	IRF5	PPARD	ZNF208
COPEB	FOSL2	KIAA0222	RB1	ZNF220
CREM	FOXF2	KIAA0293	RELA	ZNF232
CSEN	GATA3	LDB1	RORB	ZNF35
DLX2	GFI1	MADH9	RXRG	ZNF7
48 HR EXPRESSION - 101 GENES				
ATOH1	FLJ20321	KIAA1388	PBX3	ZIC1
BAZ2B	FOG2	LOC51637	PEGASUS	ZNF125
BC002881	FOXI1	LOC55885	PLRG1	ZNF132
BRF2	FOXO1A	M96	PMF1	ZNF161
BRPF1	GATA2	MADH3	POU5F1	ZNF173
C5orf7	GCN5L1	MAZ	PRDM8	ZNF175
CDX2	GSH2	MDS1	RFX2	ZNF185
CRIP1	HDAC4	MED6	RNF14	ZNF221
CTNNB1	HKR3	MILD1	SAP18	ZNF258
DBP	HLF	MLLT7	SDCCAG33	ZNF259
DKFZp547H236	HOXA3	MYOG	SMARCA3	ZNF26
DLX4	HOXD11	NAB1	SNW1	ZNF261
DRPLA	HOXD9	NFIX	TAF2B	ZNF264
DUX4	HR	NFRKB	TAL2	ZNF265
ELK4	HRIHFB2436	NMI	TCF3	ZNF268
ESR2	HSPC189	NR1D1	TFE3	ZNF286
ETV2	ICBP90	NR2E3	THRA	ZNF83
EYA2	ID4	NR3C2	TITF1	

EZH2	IRF7	NR5A2	TRIP11
FLJ125	IRX5	ONECUT1	TRPS1
FLJ12827	KIAA0952	OVOL1	ZFP289

O HR - 24 HR CO-EXPRESSION - 87 GENES

ALX3	ELK1	HSF2	NCOR2	SOX10
ARC	ERG	ICSBP1	NEUROD1	SOX5
ARNT	ETV6	ID2	NFATC2	SRF
ATF1	FKHL18	IGHMBP2	NFATC4	SURB7
ATF7	FLJ11186	ILF1	NPAS1	TBPL1
BARX1	FLJ12457	JUN	NPAS2	TBX10
BATF	FLJ12525	KLF12	ONECUT2	ZFP93
BAZ2A	GATA1	KLF5	OTX2	ZNF142
CART1	GTF2F2	KRML	PAX5	ZNF146
CBFA2T1	GTF2H3	LMO4	PAX8	ZNF16
CEBPE	HIRA	LOC57862	PCAR	ZNF234
CHD2	HOXA10	MAD	PGR	ZNF256
CREBBP	HOXA2	MAF	POU2F1	ZNF45
CROC4	HOXA7	MGC12942	PRDM1	ZNF46
CRX	HOXC8	MNAT1	PRDM11	ZNF80
DDIT3	HOXD10	MSX2	R32184_3	
EGR1	HOXD4	MYT1L	RFP2	
ELF1	HRIHFB2122	NCOA2	SHOX	

O HR - 48 HR CO-EXPRESSION - 245 GENES

ARIX	GTF2F1	LOC92283	PRDM9	TIEG2
ARNT2	GTF2H1	LW-1	RARA	TMF1
ATF4	GTF3C5	LYL1	RARG	TNRC3
AWP1	HCF2	LZTS1	RBBP9	TNRC6
BANP	HDAC2	M6A	RBL2	TRIP15
BAPX1	HEY2	MADH4	RELB	UTF1
BRD7	HEYL	MADH5	REST	VAX2
C1orf2	HKR2	MADH7	RGC32	VXS1
CBFA2T3	HNF3B	MEF2B	RLF	ZFH1B
CBX3	HNF3G	MEF2C	RNF13	ZFP
CLOCK	HOXA13	MEF2D	RNF2	ZFP91
CNOT3	HOXA6	MGC16733	RNF3	ZFP95
CRSP7	HOXB13	MGC2508	RNF8	ZIC4
DFKZP434E026	HOXB3	MHC2TA	RORA	ZNF123
DKFZP434B195	HOXD1	MITF	RREB1	ZNF131
DKFZP434N043	HOXD13	MLL	SALL3	ZNF135
DKFZP564F1422	HOXD3	MLLT10	SBB103	ZNF137
DUX2	HSA275986	MTA1	SCML2	ZNF14
E4F1	HSAJ2425	MYBL1	SETDB1	ZNF141
EHF	HSF2BP	MYCN	SHOX2	ZNF15L1
ELF5	HSPC018	MYF5	SIM1	ZNF165
EMX1	HSPX153	NCOA3	SIX6	ZNF177
EN1	KIAA0040	NEUD4	SMARCA1	ZNF179
EPAS1	KIAA0071	NEUROD6	SMARCC1	ZNF18
ERCC2	KIAA0156	NEUROG1	SNAPC3	ZNF184
ERF	KIAA0164	NFATC1	SNAPC4	ZNF192
ESR1	KIAA0244	NFE2L2	SNAPC5	ZNF20
ESRRA	KIAA0306	NFIB	SOX3	ZNF200
ETV5	KIAA0469	NFKBIL1	SOX30	ZNF207
FHL2	KIAA0535	NFYA	SP2	ZNF21
FLJ10469	KIAA0943	NR1H2	SP3	ZNF214

FLJ10697	KIAA0972	NR6A1	SRF	ZNF217
FLJ11191	KIAA0998	NSEP1	STAT1	ZNF22
FLJ12606	KIAA1528	NYCM	STAT2	ZNF229
FLJ13222	KLF4	OAZ	STAT3	ZNF230
FLJ13659	KLF7	p100	TAF1B	ZNF267
FLJ20039	KLHL4	P1P373C6	TAL1	ZNF271
FLJ20595	LDB2	PAF65B	TBR1	ZNF275
FMR2	LDOC1	PAX6	TCF7L2	ZNF277
FOXC2	LHX6	PER3	TCFL4	ZNF281
FOXE2	LMO2	PFDN5	TEAD1	ZNF288
FOXP1	LMO6	PHTF1	TEL2	ZNF29
GABPB1	LMO7	PIASX-BETA	TFAP2A	ZNF294
GAS41	LOC51045	PMX1	TFAP2B	ZNF6
GBX2	LOC51087	PPARG	TFAP2C	ZNF75A
GCMB	LOC51131	PRDM12	TFDP1	ZNF9
GIOT-3	LOC51132	PRDM16	TFEB	ZNF90
GLI2	LOC51290	PRDM4	TGFB1I1	ZNF93
GTF2A2	LOC65243	PRDM5	THR3	ZXDA

24 HR - 48 HR CO-EXPRESSION - 70 GENES

ARNTL	EYA3	HSSOX6	NFKBIL2	TBX2
BARHL1	FLJ10734	HTLF	NFX1	YAF2
BHLHB3	FLJ14549	H_GS165L15	NR4A1	ZFP92
BRD3	FLJ20531	ID1	NRIP1	ZFPL1
BRPF3	FLJ21603	ILF3	PBX2	ZFX
BTF3L2	FLJ22252	IRF3	PIG7	ZNF-kaiso
CBX5	FLJ23309	KIAA0161	RING1	ZNF169
CE1	FOS	KIAA1041	SCAND2	ZNF19
CHD3	FOXJ1	KIAA1542	SIAH1	ZNF211
CRSP3	GLP	KLF3	SIX2	ZNF213
CXorf6	HLXB9	LHX2	SSX5	ZNF216
DLX3	HOXA9	LMO1	SUPT6H	ZNF236
EDR1	HOXB1	MYCBP	TAF2C2	ZNF254
ELF2	HOXC6	NFKBIA	TBX18	ZNF273

0 HR - 24 HR - 48 HR CO-EXPRESSION - 367 GENES

ADNP	FLJ12644	IRX7	NFYB	TAF-172
AF020591	FLJ14967	JMJ	NFYC	TAF2C1
AF5Q31	FLJ20244	JUNB	NKX3A	TAF2H
AR	FLJ20392	KIAA0014	NR1H3	TAF2S
ASH1	FLJ22301	KIAA0026	NR1I2	TAF3B2
ASH2L	FOSB	KIAA0173	NR1I3	TBP
ATBF1	FOSL1	KIAA0237	NR2E1	TBX15
ATRX	FOXB1	KIAA0326	NRF	TBX21
BACH2	FOXE1	KIAA0352	NRL	TBX5
BAZ1B	FOXH1	KIAA0395	OCT11	TBX6
BCL11A	FOXL2	KIAA0414	P38IP	TCF-3
BCL11B	FOXM1	KIAA0478	PAF65A	TCF19
BLZF1	FOXO3A	KIAA0602	PAX1	TCF21
BRD1	GABPA	KIAA0669	PAX2	TCF4
BRD2	GATA4	KIAA0798	PBX1	TCF8
BRD4	GATA6	KIAA1190	PBX4	TCFL1
BRDT	GBX1	KIAA1321	PDEF	TCFL5
BS69	GCMA	KIAA1431	PER2	TEAD3
BTF3	GF11B	LAF4	PHAP1	TFCP2
BTF3L1	GIOT-2	LBP-9	PITX2	TFDP2

C11orf9	GLIS2	LBX1	PKNOX2	TFEC
C21orf18	GTF2A1	LHX5	PLAGL2	THG-1
CBX4	GTF2B	LIM	PMX2B	TNRC12
CCT4	GTF2E2	LMX1B	POU2AF1	TNRC18
CDK7	GTF2H2	LOC51036	POU3F2	TNRC4
CDK8	GTF2H4	LOC51042	POU4F1	TNRC5
CDX1	GTF3A	LOC51043	POU4F2	TNRC9
CE4	GTF3C1	LOC51058	POU6F1	TONDU
CEBPB	GTF3C3	LOC51088	PP3501	TRIM15
CEBPG	GTF3C4	LOC51186	PPARBP	TRIM22
CIAO1	H-L(3)MBT	LOC51193	PRDM10	TRIP6
CITED1	HAND2	LOC51270	PRDM13	TZFP
CITED2	HBOA	LOC51652	PRDM2	UBTF
CNOT4	HCNGP	LOC55893	PRDM7	USF1
CORO1A	HES2	LOC57167	PREB	VENTX2
CREB1	HES7	LOC57209	PROP1	WHSC1
CREB3	HESX1	LOC58500	PSMC5	XBP1
CREBL2	HEY1	LOC91120	PTTG1IP	ZFP36
CRIP2	HHEX	LOC91614	PURA	ZFR
CRSP9	HIF1A	LZLP	RAI15	ZFY
CSDA	HIS1	MAD4	RBBP5	ZHX1
CSRP1	HIVEP2	MADH1	REL	ZIC2
CSRP2	HKR1	MADH2	REQ	ZIC3
CUTL1	HLX1	MADH6	RFP	ZIC5
DEAF1	HMG2	MAFG	RFX3	ZID
DKFZP434B0335	HMG20B	MAPK8IP1	RNF4	ZIM2
DKFZP434P1750	HMGIC	MAX	RORC	ZNF10
DKFZp762K2015	HMGIIY	MBLL	SALL1	ZNF133
DKFZp762M136	HMX2	MECP2	SALL2	ZNF138
DLX1	HNF3A	MEIS2	SAP30	ZNF147
DXYS155E	HNF4A	MEIS3	SATB1	ZNF174
E2F2	HOX11	MEOX2	SETBP1	ZNF187
EBF	HOXA11	MGC11349	SIAH2	ZNF195
EED	HOXA4	MGC15716	SIM2	ZNF205
EGR4	HOXA5	MLL2	SIX4	ZNF212
ELF3	HOXB2	MLLT2	SLB	ZNF226
ELK3	HOXB5	MLLT6	SMARCA2	ZNF23
EN2	HOXB6	MNT	SMARCA4	ZNF239
EOMES	HOXB7	MORF	SMARCE1	ZNF297
EPLIN	HOXB8	MSC	SMCX	ZNF304
ERCC3	HOXB9	MTA1L1	SNAI1	ZNF306
ESRRB	HOXC13	MTF1	SOX11	ZNF31
ESRRG	HOXC4	MYBL2	SOX2	ZNF361
ETV3	HOXC5	MYC	SOX4	ZNF37A
ETV4	HOXD12	MYCL2	SPI1	ZNF43
EZH1	HOXD8	MYT2	SREBF1	ZNF44
FALZ	HS747E2A	NCOA1	SSX1	ZNF74
FHL1	HSF1	NEUROG2	SSX2	ZNF76
FLJ10142	ID3	NFE2L1	SSX3	ZNF79
FLJ10251	ILF2	NFIA	SSX4	ZNF92
FLJ10298	IPEX	NFIC	SUPT4H1	ZXDA/B
FLJ10759	IPF1	NFIL3	T	
FLJ10891	IRF2	NFKB2	TADA2L	
FLJ12517	IRX4	NFKBIB	TADA3L	

Table A4-2. Laser Venn Diagram Gene List.

30 MIN EXPRESSION - 61 GENES				
AF093680	ID2	RFX5	UBP1	ZNF225
ARNTL	ILF3	RNF10	VDR	ZNF234
ATF2	ISGF3G	SIM1	YY1	ZNF256
ATF6	KLF15	SP1	ZFP289	ZNF259
BNC	LOC51173	SPIB	ZNF124	ZNF263
BTF3	MAFK	STAT4	ZNF136	ZNF265
CBX8	MEIS1	TAF2D	ZNF157	ZNF266
CSRP3	MYB	TAF2G	ZNF160	ZNF272
DMRT2	NFE2	TEAD4	ZNF180	ZNF33A
DRIL1	NRF1	TFAP4	ZNF189	
ETS1	PAX4	TIF1	ZNF195	
ETS2	PML	TP73	ZNF202	
FOXD1	RARB	TRAP150	ZNF215	

1 HR EXPRESSION - 80 GENES				
AF020591	FLJ22252	MAZ	PRDM9	TCF12
ARNT	GABPB1	MNDA	RBL2	TMF1
AWP1	GTF2F2	MSX2	REST	TRIM28
BANP	HKR2	MYF5	RFX2	TRIP4
BARX1	HNF4A	NCOA2	RUNX1	VSX1
CBFA2T3	HOXA11	NFATC4	RXRA	ZFP95
CBX6	HOXA2	NFE2L1	RXRG	ZNF135
CE1	HOXC10	NFIX	SALF	ZNF137
CREB3	HOXD10	NR3C1	SOX10	ZNF143
CREG	HOXD3	NR4A2	SOX5	ZNF145
CRX	IRF4	NR6A1	STAT3	ZNF184
DATF1	IRF6	NYCM	STAT5A	ZNF19
DMTF1	KIAA0194	PAX2	STAT6	ZNF192
E2F6	LBX1	PLAGL1	TAF2F	ZNF22
ELF1	LOC51132	POU2F1	TBX19	ZNF229
EYA2	LOC56930	PPARA	TBX22	ZNF264

2 HR EXPRESSION - 21 GENES				
CHES1	HLF	POU3F4	ZNF193	ZNFN1A1
CRSP8	HSAJ2425	RLF	ZNF216	
FACTP140	LOC51087	TAF1C	ZNF287	
FIP2	MGC10772	ZFP103	ZNF295	
FLJ20531	NFATC1	ZNF133	ZNF85	

3 HR EXPRESSION - 17 GENES				
BACH1	E2F3	LHX1	PER1	ZNF84
BAZ1A	ELF2	NCOA4	ZNF219	
BTEB1	HNF3G	NFAT5	ZNF232	
DLX6	IRF1	NFATC3	ZNF30	

30 MIN - 1 HR CO-EXPRESSION - 23 GENES				
ASH1	FLJ20729	PER3	SMARCA1	ZFP26
CBFA2T1	ISL1	PIAS3	TADA2L	ZNF278
CBX1	KIAA0462	PRDM1	TCF7	ZNF35
CSEN	LEF1	RNF22	ZF5128	
DR1	NFKBIE	SHOX	ZFP106	

1 HR - 2 HR CO-EXPRESSION - 28 GENES				
C11orf9	FKHL18	HSU90653	R32184_3	TRIP11
CART1	FLJ10688	ICSBP1	RORA	ZNF177
COPS5	FLJ12457	NKX2B	SIAH1	ZNF200
CUTL1	FLJ22332	NR2F6	SNAPC1	ZNF7
EN1	FOXB1	PAX6	SNW1	
EPLIN	HSGT1	PPARGC1	SOX14	
2 HR - 3 HR CO-EXPRESSION - 10 GENES				
GFI1	GTF3C2	KIAA0211	MLL	REQ
GIOT-3	HOXC12	KIAA1388	NR4A3	ZNF91
30 MIN - 3 HR CO-EXPRESSION - 36 GENES				
ATF1	FHX	PGR	TEL2	ZNF26
ATF3	IRF3	PIASX-BETA	THG-1	ZNF8
CEZANNE	KIAA1041	PRDM8	TIF1GAMMA	ZNF81
CTCF	KLF13	SP4	USF2	ZNFN1A3
DKFZP564F1422	MEOX2	SREBF2	ZNF123	
E2F4	MID1	TAF2I	ZNF132	
E2F5	MLLT3	TAF2K	ZNF144	
EZH2	NR3C2	TBX18	ZNF258	
30 MIN - 2 HR CO-EXPRESSION - 37 GENES				
ARC	GATA2	PAX3	TAF1A	ZNF213
BRPF1	HMX1	PKNOX1	TBX20	ZNF25
CDR2	KIAA0014	POU2F2	TBX4	ZNF261
EGR2	KIAA0961	PRDM14	TCF2	ZNF73
ELF4	KIAA1442	RBPSUHL	TCF8	ZNF83
ETV2	LOC56270	RFP2	ZNF-U69274	
EYA1	NFKB1	SLUG	ZNF138	
FLJ10211	NR0B1	SUPT5H	ZNF147	
1 HR - 3 HR CO-EXPRESSION - 59 GENES				
AIB3	GCN5L2	HOXC5	MYBL1	RUNX2
ATOH1	GTF2H1	HOXC8	NFIA	SIM2
ERCC2	GTF3C1	IGHMBP2	NFKBIA	SRF
ERG	HESX1	KIAA0535	NPAS2	TCF19
ESRRG	HIRA	KLF12	NR5A2	TIEG
EYA3	HMG20B	LMO7	NSEP1	WT1
FLI1	HOX11	LOC51045	PAX8	ZFR
FLJ125	HOXA9	LYL1	PBX1	ZNF151
FOXM1	HOXB1	MAF	PHTF1	ZNF16
FOXO1A	HOXB2	MEF2A	PPARBP	ZNF286
GABPA	HOXB7	MLLT1	PROX1	ZNF29
GATA6	HOXB8	MXI1	RFX4	
30 MIN - 1 HR - 2 HR CO-EXPRESSION - 65 GENES				
AHR	GAS41	KIAA1668	RNF24	TRPS1
BHLHB2	GASC1	LOC57862	RRN3	YAF2
CDX2	GCN5L1	M6A	SAP18	ZFX
CIR	GRLF1	MED6	SNAPC5	ZIC1
CRIP1	GSH2	MEFV	SOX3	ZNF11B
CRSP6	GTF2I	MLLT7	SRA1	ZNF169
DFKZP434E026	HLX1	NAB1	SUPT3H	ZNF208
DLX4	HOXC11	NR0B2	TAF2A	ZNF221

DSIP1	HOXC13	PFDN5	TAF2C2	ZNF254
ELF5	HOXC9	PLRG1	TAF2J	ZNF288
ELK4	HSF4	PMF1	TAL1	ZNF306
EOMES	IPF1	PPARG	THRA	ZNF9
FUBP1	IRF5	RBBP9	TRIP13	ZNF92

1 HR - 2 HR - 3 HR CO-EXPRESSION - 86 GENES

ATF5	FLJ20557	KLF4	p100	TEAD1
BRD2	FOXF2	LHX4	PEGASUS	TEF
BRD3	FOXI1	LHX5	POU4F2	TFCP2
BRPF3	GATA4	LMO2	PRDM12	TGFB111
BS69	GLI2	LMO6	PRDM15	ZFP
C1orf2	GTF2H2	MDS1	PRDM4	ZHX1
CREBBP	GTF2H4	MEIS3	PRDM7	ZIC5
CREBL1	GTF3C4	MGC11349	REL	ZNF-kaiso
DKFZp762M136	HCF2	MILD1	SETDB1	ZNF14
DLX2	HNF4G	MTA1	SIX1	ZNF141
DUX2	HOXA1	MYBBP1A	SIX2	ZNF207
EBF	HOXA10	MYOG	SNAPC3	ZNF267
EGR1	HOXA7	MYT1L	SRCAP	ZNF268
EGR3	HRIHFB2436	NEUROD1	SSX1	ZNF37A
ELK3	HRV	NEUROD6	TAF2E	
EPAS1	HSSOX6	NPAS1	TBX1	
ERF	KIAA0478	NR1H2	TBX3	
ESRRA	KIAA0943	NR2F1	TCFL4	

30 MIN - 2 HR - 3 HR CO-EXPRESSION 62 GENES

ABT1	DBP	HNF3B	NFE2L2	SMARCB1
ATBF1	DKFZP434B195	HOXB9	NFE2L3	SOX11
BRF2	ESR2	HSPC189	NFIL3	SUPT6H
BTF3L2	FLJ12517	HYPH	NFKBIB	T
CBX5	FLJ12525	H_GS165L15	PAX1	TCF7L2
CDX1	FLJ13222	KIAA0304	PBX2	TEAD2
CE3	FLJ20039	LHX2	PBX3	ZNF173
CEBPE	FLJ23309	LHX9	POU6F1	ZNF297
CHD2	GATA1	LOC51186	PROP1	ZNF45
CLOCK	GTF2E1	LOC51637	RARG	ZNF76
COPEB	HBOA	MADH3	RELA	
CREM	HEY1	NCOA3	SIX3	
DACH	HIVEP1	NCOR1	SLB	

30 MIN - 1 HR - 3 HR CO-EXPRESSION - 67 GENES

BARHL1	FLJ20392	KRML	NRL	TFAP2C
BRD7	FOSL2	LHX6	ONECUT2	TIMELESS
BRDT	GTF2B	LMO4	PMX1	USF1
CE4	GTF2H3	LOC51042	POU1F1	ZFH1B
CRSP3	GTF3C5	LOC51290	POU3F2	ZIC3
CSDA	HHEX	LOC91614	R28830_2	ZNF20
CXorf6	HOXD12	MAD	RFXANK	ZNF23
DDIT3	HOXD4	MGC12942	RNF2	ZNF262
DLX1	IRX7	MYT1	SCAND2	ZNF275
EDR1	KIAA0132	NFATC2	SMARCC2	ZNF304
ESRRB	KIAA0222	NFYA	SREBF1	ZNF74
ETV3	KIAA0469	NFYB	SSRP1	
FALZ	KIAA0798	NR1D1	TBX10	

FLJ10734	KLF3	NR2C1	TCF4	
30 MIN - 1 HR - 2 HR - 3 HR CO-EXPRESSION - 535 GENES				
ADNP	FOS	KIAA0414	NR1I2	TAF1B
AF5Q31	FOSB	KIAA0602	NR1I3	TAF2B
ALY	FOSL1	KIAA0669	NR2E1	TAF2C1
AR	FOXC1	KIAA0700	NR2E3	TAF2H
ARIX	FOXC2	KIAA0952	NR2F2	TAF2N
ARNT2	FOXE1	KIAA0972	NR4A1	TAF2S
ASH2L	FOXE2	KIAA0998	NR5A1	TAF3B2
ATF4	FOXH1	KIAA1190	NRF	TAL2
ATF7	FOXJ1	KIAA1321	NRIP1	TBP
ATRX	FOXL2	KIAA1431	OAZ	TBPL1
BACH2	FOXO3A	KIAA1528	OCT11	TBR1
BAPX1	FOXP1	KIAA1542	OG2x	TBX15
BAZ1B	GATA3	KLF5	OVOL1	TBX2
BAZ2A	GBX1	KLHL4	P1P373C6	TBX21
BAZ2B	GBX2	LAF4	P38IP	TBX5
BC002881	GCMA	LBP-9	PAF65A	TBX6
BCL11A	GCMB	LDB1	PAF65B	TCEAL1
BCL11B	GFI1B	LDB2	PAX5	TCF-3
BHLHB3	GIOT-2	LDOC1	PAX7	TCF21
BLZF1	GLI3	LIM	PBX4	TCF3
BRD1	GLIS2	LMO1	PC4	TCFL1
BRD4	GLP	LMX1B	PCAR	TCFL5
BTF3L1	GTF2A1	LOC51036	PDEF	TEAD3
C21orf18	GTF2A2	LOC51043	PER2	TFAP2A
C5orf7	GTF2E2	LOC51058	PHAP1	TFDP1
CBX3	GTF2F1	LOC51088	PIG7	TFDP2
CBX4	GTF3A	LOC51131	PILB	TFE3
CCT4	GTF3C3	LOC51193	PITX2	TFEB
CDK7	H-L(3)MBT	LOC51270	PKNOX2	TFEC
CDK8	HAND2	LOC51652	PLAG1	TGIF
CEBPB	HCNGP	LOC55885	PLAGL2	THRB
CEBPG	HDAC1	LOC55893	PMX2B	TIEG2
CERD4	HDAC2	LOC57167	POU2AF1	TITF1
CHD3	HDAC4	LOC57209	POU4F1	TNRC12
CIAO1	HES2	LOC58500	POU5F1	TNRC18
CITED1	HES7	LOC65243	PP3501	TNRC3
CITED2	HEY2	LOC91120	PPARD	TNRC4
CL469780	HEYL	LOC92283	PRDM10	TNRC5
CNOT3	HIF1A	LW-1	PRDM11	TNRC6
CNOT4	HIS1	LZLP	PRDM13	TNRC9
CORO1A	HIVEP2	LZTR1	PRDM16	TONDU
CREB1	HKR1	LZTS1	PRDM2	TP53
CREBL2	HKR3	M96	PRDM5	TRIM15
CRIP2	HLXB9	MAD4	PRDM6	TRIM22
CROC4	HMG2	MADH1	PREB	TRIP15
CRSP7	HMGIC	MADH2	PSMC5	TRIP6
CRSP9	HMG1Y	MADH4	PTTG1IP	TSC22
CSRP1	HMX2	MADH5	PURA	TZFP
CSRP2	HNF3A	MADH6	RAI15	UBTF
CTNNB1	HOX11L	MADH7	RARA	UTF1
DEAF1	HOXA13	MADH9	RBBP5	VENTX2
DKFZP434B0335	HOXA3	MAFF	RBL1	WHSC1
DKFZP434N043	HOXA4	MAFG	RELB	XPB1

DKFZP434P1750	HOXA5	MAPK8IP1	RERE	ZFP36
DKFZp547H236	HOXA6	MAX	RFP	ZFP91
DKFZp762K2015	HOXB13	MBLL	RFX3	ZFP92
DLX3	HOXB3	MDS032	RGC32	ZFP93
DRAP1	HOXB5	MECP2	RING1	ZFPL1
DRPLA	HOXB6	MEF2B	RNF13	ZFY
DUX4	HOXC4	MEF2C	RNF14	ZIC2
DXYS155E	HOXC6	MEF2D	RNF3	ZIC4
E2F2	HOXD1	MEIS2	RNF4	ZID
E4F1	HOXD11	MGC15716	RNF8	ZIM2
EED	HOXD13	MGC16733	RORB	ZNF10
EGR4	HOXD8	MGC2508	RORC	ZNF131
EHF	HOXD9	MHC2TA	RREB1	ZNF134
ELF3	HR	MITF	SAFB	ZNF142
ELK1	HRIHFB2122	MLL2	SALL1	ZNF146
EMX1	HS747E2A	MLLT10	SALL2	ZNF155
EMX2	HSA275986	MLLT2	SALL3	ZNF15L1
EN2	HSF1	MLLT4	SAP30	ZNF161
EP300	HSF2BP	MLLT6	SATB1	ZNF162
ERCC3	HSHPX5	MNAT1	SBB103	ZNF174
ERCC6	HSPC018	MNT	SCML2	ZNF179
ESR1	HSPX153	MORF	SDCCAG33	ZNF183
ETV1	HSU79252	MSC	SETBP1	ZNF185
ETV4	HTLF	MTA1L1	SHARP	ZNF187
ETV5	ICBP90	MTF1	SHOX2	ZNF205
ETV6	ID1	MYBL2	SIAH2	ZNF21
EVX1	ID3	MYC	SIX4	ZNF211
EYA4	ID4	MYCBP	SIX6	ZNF212
EZH1	ILF1	MYCL1	SMARCA2	ZNF220
FHL1	ILF2	MYCL2	SMARCA3	ZNF230
FHL2	IPEX	MYCN	SMARCA4	ZNF236
FLJ10142	IRF2	MYF6	SMARCC1	ZNF239
FLJ10251	IRF7	MYOD1	SMARCE1	ZNF271
FLJ10298	IRLB	MYT2	SMCX	ZNF273
FLJ10469	IRX4	NCOA1	SNAI1	ZNF274
FLJ10697	IRX5	NCOR2	SNAPC4	ZNF277
FLJ10759	JMJ	NEUD4	SOX13	ZNF281
FLJ10891	JUN	NEUROD4	SOX2	ZNF294
FLJ11186	JUNB	NEUROG1	SOX30	ZNF31
FLJ11191	KIAA0026	NEUROG2	SOX4	ZNF32
FLJ12606	KIAA0040	NFIB	SP2	ZNF361
FLJ12644	KIAA0071	NFIC	SP3	ZNF38
FLJ12827	KIAA0130	NFKB2	SPI1	ZNF41
FLJ13590	KIAA0156	NFKBIL1	SRY	ZNF43
FLJ13659	KIAA0161	NFKBIL2	SSX2	ZNF44
FLJ14549	KIAA0164	NFRKB	SSX3	ZNF46
FLJ14967	KIAA0173	NFX1	SSX4	ZNF6
FLJ20244	KIAA0237	NFYC	SSX5	ZNF75A
FLJ20321	KIAA0244	NHLH2	STAT1	ZNF79
FLJ20595	KIAA0293	NKX3A	STAT2	ZNF80
FLJ21603	KIAA0306	NKX6A	SUPT4H1	ZNF90
FLJ22301	KIAA0326	NMI	SURB7	ZNF93
FMR2	KIAA0352	NR1D2	TADA3L	ZXDA
FOG2	KIAA0395	NR1H3	TAF-172	ZXDA/B

Table A4-3. Utricle Neomycin Genes (195).

Gene ID	0 hr		24 hr		48 hr		Notes/Description
	Fold change	P-value	Fold Change	P-value	Fold Change	P-value	
AF5Q31	1.113	0.475	0.662	0.211	1.071	0.702	ALL1 fused gene from 5q31
ARIX	0.745	0.14	1.039	0.568	0.939	0.513	aristaless homeobox
ASH2L	0.99	0.89	0.781	0.006	1.028	0.548	ash2 (absent, small, or homeotic, Drosophila, homolog)-like
ATF2	0.804	0.021	1.013	0.886	0.754	0.39	activating transcription factor 2
BCL11A	1.327	0.127	1.051	0.577	1.334	0.026	B-cell CLL/lymphoma 11A (zinc finger protein)
BCL11B	0.842	0.146	0.919	0.262	0.785	0.001	B-cell CLL/lymphoma 11B (zinc finger protein)
BRD1	0.635	0.006	0.94	0.646	0.603	0.002	bromodomain-containing 1
C21orf18	0.538	0.029	0.954	0.779	0.603	0.003	chromosome 21 open reading frame 18
CBX3	1.21	0.046	1.017	0.772	0.951	0.532	chromobox homolog 3 (Drosophila HP1 gamma)
CBX4	0.588	0.037	1.192	0.074	0.823	0.511	chromobox homolog 4 (Drosophila Pc class)
CDK7	1.022	0.816	0.871	0.216	0.829	0.036	cyclin-dependent kinase 7 (homolog of Xenopus MO15 cdk-activating kinase)
CEBPB	1.062	0.443	0.788	0.453	0.878	0.9	CCAAT/enhancer binding protein (C/EBP), beta
CEBPG	0.646	0.04	1.236	0.43	0.506	0.008	CCAAT/enhancer binding protein (C/EBP), gamma
CHD3	1.057	0.451	1.059	0.26	1.39	0.123	chromodomain helicase DNA binding protein 3
CITED1	1.521	0.036	0.689	0.182	0.985	0.885	Cbp/p300-interacting transactivator, with Glu/Asp-rich carboxy-terminal domain, 1
CREBL1	0.994	0.902	1.072	0.088	1.322	0.032	cAMP responsive element binding protein-like 1
CREG	0.95	0.424	1.124	0.159	0.807	0.045	cellular repressor of E1A-stimulated genes
CRIP2	1.005	0.873	1.047	0.494	0.63	0.134	cysteine-rich protein 2
CROC4	0.907	0.062	0.689	0.05	0.972	0.857	transcriptional activator of the c-fos promoter
CRSP6	0.694	0.013	1.062	0.705	0.989	0.949	cofactor required for Sp1 transcriptional activation, subunit 6 (77kD)
CRX	1.17	0.057	1.199	0.038	1.048	0.268	cone-rod homeobox
CSDA	1.056	0.484	0.973	0.747	1.321	0.008	cold shock domain protein A
CSRP2	1.006	0.939	0.914	0.393	0.778	0.049	cysteine and glycine-rich protein 2
CTNNB1	0.789	0.092	0.89	0.101	3.097	0.035	catenin (cadherin-associated protein), beta 1 (88kD)
CUTL1	0.857	0.012	1.097	0.14	1.381	0.006	cut (Drosophila)-like 1 (CCAAT displacement protein)
DEAF1	1.321	0.002	1.275	0.24	1.003	0.97	deformed epidermal autoregulatory factor 1 (Drosophila)
DKFZP434B0335	0.69	0.112	0.905	0.256	0.807	0.001	DKFZP434B0335 protein
DLX4	1.027	0.7	1.132	0.373	0.82	0.138	distal-less homeobox 4
DLX6	0.784	0.016	0.85	0.087	0.991	0.953	distal-less homeobox 6
DUX2	1.254	0.01	1.198	0.086	1.136	0.041	double homeobox 2

E2F2	0.927	0.627	1.203	0.006	0.558	0.087	E2F transcription factor 2
E2F5	0.778	0.015	0.949	0.446	1.07	0.45	E2F transcription factor 5, p130-binding
EBF	0.789	0.009	1.08	0.413	1.16	0.184	early B-cell factor
EOMES	0.979	0.81	0.992	0.877	1.209	0	eomesodermin (<i>Xenopus laevis</i>) homolog
ERCC6	0.928	0.253	0.964	0.54	1.203	0.007	excision repair cross-complementing rodent repair deficiency, complementation group 6
ESR1	0.962	0.681	0.787	0.597	1.647	0.163	estrogen receptor 1
ETV5	0.952	0.441	0.829	0.028	1.017	0.876	ets variant gene 5 (ets-related molecule)
EYA3	1.031	0.668	0.728	0.075	0.936	0.375	eyes absent (<i>Drosophila</i>) homolog 3
EZH1	0.708	0.127	1.011	0.898	0.749	0.102	enhancer of zeste homolog 1
EZH2	1.076	0.383	0.883	0.917	1.234	0.005	enhancer of zeste homolog 2
FHL1	0.709	0.062	1.042	0.512	0.743	0	four and a half LIM domains 1
FHL2	0.889	0.029	1.037	0.606	0.802	0.255	four and a half LIM domains 2
FLJ10251	1.225	0.002	1.229	0.135	1.057	0.29	hypothetical protein FLJ10251
FLJ10891	1.25	0.005	1.174	0.22	1.025	0.356	hypothetical protein FLJ10891
FLJ12827	1.219	0.018	1.01	0.811	1.143	0.33	hypothetical protein FLJ12827
FLJ13590	1.248	0.006	1.023	0.458	1.207	0.029	hypothetical protein FLJ13590
FLJ20321	0.999	0.983	1.034	0.386	1.288	0.083	hypothetical protein
FLJ20595	1.346	0.01	0.917	0.252	0.91	0.055	hypothetical protein FLJ20595
FLJ22252	1.05	0.154	1.031	0.732	0.824	0.168	likely ortholog of mouse SRY-box containing gene 17
FOG2	0.974	0.736	0.808	0.113	0.76	0.001	friend of GATA2
FOXF2	1.021	0.731	1.201	0.055	1.07	0.4	forkhead box F2
GCN5L1	0.93	0.301	1.164	0.172	1.355	0.161	GCN5 (general control of amino-acid synthesis, yeast, homolog)-like 1
GIOT-2	0.977	0.813	0.689	0.047	0.702	0.036	GIOT-2 for gonadotropin inducible transcription repressor-2
GLI2	0.857	0.067	1.065	0.387	1.343	0.194	GLI-Kruppel family member GLI2
GTF2A1	1.431	0.013	1.171	0.101	1.321	0.041	general transcription factor IIA, 1 (37kD and 19kD subunits)
GTF2E1	1.063	0.399	0.92	0.044	1.22	0.007	general transcription factor IIE, polypeptide 1 (alpha subunit, 56kD)
GTF2F1	0.785	0.001	0.939	0.237	1.18	0.068	general transcription factor IIF, polypeptide 1 (74kD subunit)
GTF2H1	0.936	0.161	1.023	0.763	1.283	0.013	general transcription factor IIH, polypeptide 1 (62kD subunit)
GTF2H3	1.049	0.505	1.017	0.697	1.2	0.006	general transcription factor IIH, polypeptide 3 (34kD subunit)
GTF3C4	1.286	0.022	0.876	0.829	1.106	0.165	general transcription factor IIIC, polypeptide 4 (90kD)
H-L(3)MBT	1.474	0.002	1.041	0.739	0.968	0.717	lethal (3) malignant brain tumor l(3)mbt protein (<i>Drosophila</i>) homolog
HEY1	0.786	0.033	0.922	0.517	1.02	0.837	hairy/enhancer-of-split related with YRPW motif 1
HHEX	1.123	0.031	1.023	0.665	1.452	0.046	hematopoietically expressed homeobox
HIF1A	0.816	0.081	0.703	0.048	1.071	0.616	hypoxia-inducible factor 1, alpha subunit (basic helix-loop-helix transcription factor)
HIRA	1.095	0.328	0.948	0.194	1.22	0.029	HIR (histone cell cycle regulation defective, <i>S. cerevisiae</i>) homolog A

HIVEP1	1.013	0.866	1.038	0.672	1.243	0.041	human immunodeficiency virus type I enhancer-binding protein 1
HMGIIY	0.899	0.187	0.75	0.255	0.946	0.354	high-mobility group (nonhistone chromosomal) protein isoforms I and Y
HNF3A	1.01	0.787	1.262	0	0.801	0.039	hepatocyte nuclear factor 3, alpha
HNF3B	0.859	0.162	0.912	0.217	1.948	0.055	hepatocyte nuclear factor 3, beta
HOXA13	0.67	0.008	0.947	0.502	0.934	0.437	homeo box A13
HOXB7	1.135	0.07	0.976	0.724	1.277	0.018	homeo box B7
HOXB9	1.285	0.356	0.995	0.974	0.797	0.299	homeobox B9
HOXD12	1.066	0.385	1.127	0.011	1.367	0.047	homeo box D12
HOXD8	1.39	0.035	1.226	0.147	1.339	0.312	homeobox D8
HRIHFB2436	0.971	0.679	1.056	0.594	0.778	0.101	endocrine regulator
HSAJ2425	1.288	0.043	0.978	0.788	1.282	0.127	p65 protein
HSF1	0.937	0.614	0.904	0.61	0.58	0.015	heat shock transcription factor 1
HSF2BP	0.892	0.272	0.749	0.075	0.729	0.044	heat shock transcription factor 2 binding protein
HSPC018	1.11	0.134	0.969	0.404	1.2	0.014	HSPC018 protein
HSPX153	1.174	0.012	1.04	0.417	1.385	0.063	HPX-153 homeobox
ILF1	0.645	0.018	0.944	0.475	1.06	0.089	interleukin enhancer binding factor 1
ILF2	1.013	0.79	0.726	0.063	0.921	0.304	interleukin enhancer binding factor 2
IPEX	0.724	0.014	0.981	0.714	0.711	0.061	immune dysregulation, polyendocrinopathy, enteropathy, X-linked
IRF2	0.681	0.029	1.188	0.117	0.829	0.058	interferon regulatory factor 2
IRF3	0.981	0.735	1.015	0.731	1.316	0.123	interferon regulatory factor 3
ISGF3G	0.799	0.008	1.051	0.382	1.054	0.316	interferon-stimulated transcription factor 3, gamma (48kD)
JUN	0.829	0.336	0.993	0.971	0.957	0.698	v-jun avian sarcoma virus 17 oncogene homolog
JUNB	0.849	0.21	1.36	0.661	0.751	0.074	Jun B proto-oncogene
KIAA0014	1.037	0.616	1.297	0.454	1.89	0.061	KIAA0014 gene product
KIAA0130	1.35	0.003	1.109	0.392	0.943	0.687	KIAA0130 gene product
KIAA0173	1.365	0.009	0.932	0.707	1.289	0.11	KIAA0173 gene product
KIAA0395	0.983	0.785	0.871	0.049	1.29	0.044	KIAA0395 protein
KIAA1041	0.665	0.016	0.837	0.148	0.934	0.624	KIAA1041 protein
KIAA1528	1.187	0.033	1.028	0.408	1.353	0.002	KIAA1528 protein
LHX4	1.257	0.025	1.024	0.665	0.964	0.091	LIM homeobox protein 4
LOC51058	1.268	0.089	1.031	0.853	1.497	0.052	hypothetical protein
LOC51131	1.201	0.036	1.009	0.855	1.21	0.097	putative zinc finger protein NY-REN-34 antigen
LOC57209	1.631	0.019	1.157	0.28	1.29	0.014	Kruppel-type zinc finger protein
LOC58500	0.887	0.245	0.969	0.722	1.301	0.275	zinc finger protein (clone 647)
LZLP	1.157	0.023	0.954	0.421	1.324	0.012	leucine zipper-like protein
MADH2	1.03	0.678	1.102	0.191	1.32	0.034	MAD (mothers against decapentaplegic, Drosophila) homolog 2

MADH7	0.909	0.34	1.228	0.765	0.823	0.14	MAD (mothers against decapentaplegic, Drosophila) homolog 7
MAPK8IP1	1.228	0.054	0.642	0.008	0.889	0.231	mitogen-activated protein kinase 8 interacting protein 1
MEIS2	1.16	0.059	1.202	0.187	1.114	0.026	homeobox protein MEIS2
MGC2508	0.985	0.836	1.055	0.516	1.216	0.273	hypothetical protein MGC2508
MID1	0.812	0.161	1.027	0.677	0.976	0.79	midline 1 (Opitz/BBB syndrome), zinc finger X and Y
MLLT2	1.027	0.491	1.018	0.805	1.313	0.096	myeloid/lymphoid or mixed-lineage leukemia (trithorax (Drosophila) homolog); translocated to 2
MLLT6	1.144	0.118	0.749	0.046	0.917	0.231	myeloid/lymphoid or mixed-lineage leukemia (trithorax (Drosophila) homolog); translocated to 6
MNT	0.875	0.162	0.969	0.793	1.235	0.187	MAX binding protein
MORF	0.805	0.108	0.792	0.132	0.74	0.038	histone acetyltransferase
MTA1L1	0.937	0.478	1.013	0.856	0.81	0.023	metastasis-associated 1-like 1
MTF1	1.016	0.872	1.028	0.811	0.766	0.003	metal-regulatory transcription factor 1
MYBL2	0.785	0.014	0.936	0.152	1.009	0.958	v-myb avian myeloblastosis viral oncogene homolog-like 2
MYCBP	0.941	0.34	0.931	0.553	1.364	0.006	c-myc binding protein
MYCL2	1.245	0.019	1.032	0.844	1.073	0.359	v-myc avian myelocytomatosis viral oncogene homolog 2
MYT1	0.916	0.203	1.098	0.217	0.822	0.013	myelin transcription factor 1
NEUROD6	0.84	0.142	1.07	0.349	0.792	0	neurogenic differentiation 6
NFE2L1	0.813	0.005	1.085	0.372	1.065	0.672	nuclear factor (erythroid-derived 2)-like 1
NFIB	0.801	0.021	1.08	0.465	1.01	0.623	nuclear factor I/B
NFKBIA	0.991	0.799	1.008	0.818	0.819	0.119	nuclear factor of kappa light polypeptide gene enhancer in B-cells inhibitor, alpha
NHLH2	0.873	0.047	0.776	0.124	1.036	0.797	nescient helix loop helix 2
NR1H2	1.018	0.756	0.976	0.776	1.479	0.128	nuclear receptor subfamily 1, group H, member 2
NR1H3	0.945	0.626	0.739	0.205	0.734	0.025	nuclear receptor subfamily 1, group H, member 3
NR5A2	0.992	0.896	0.985	0.376	0.778	0.162	nuclear receptor subfamily 5, group A, member 2
NRF	1.281	0.005	0.929	0.698	1.054	0.507	transcription factor NRF
NRL	1.116	0.137	1.012	0.52	1.281	0.082	neural retina leucine zipper
PBX4	0.886	0.226	1.088	0.236	0.729	0.003	pre-B-cell leukemia transcription factor 4
PDEF	1.292	0.016	1.003	0.962	1.097	0.027	prostate epithelium-specific Ets transcription factor
PILB	1.39	0.002	1.12	0.088	1.164	0.032	pilin-like transcription factor
PKNX2	1.056	0.228	1.084	0.289	1.262	0.216	PBX/knotted 1 homeobox 2
PLAG1	1.132	0.014	1.224	0.024	1.035	0.335	pleiomorphic adenoma gene 1
PMF1	1.031	0.465	0.81	0.019	0.953	0.585	polyamine-modulated factor 1
POU4F1	0.937	0.378	1.037	0.507	1.285	0.051	POU domain, class 4, transcription factor 1
POU4F3	0.936	0.202	0.894	0.602	1.211	0.03	POU domain, class 4, transcription factor 3
PPARBP	0.823	0.04	1.079	0.278	1.043	0.719	peroxisome proliferator activated receptor binding protein

PPARGC1	0.978	0.816	1.056	0.301	1.73	0.014	peroxisome proliferative activated receptor, gamma, coactivator 1
PROP1	1.199	0.009	0.939	0.376	0.948	0.439	prophet of Pit1, paired-like homeodomain transcription factor
PSMC5	0.82	0.013	0.822	0.02	1.221	0.03	proteasome (prosome, macropain) 26S subunit, ATPase, 5
PTTG1IP	1.135	0.083	1.018	0.463	1.532	0.098	pituitary tumor-transforming 1 interacting protein
PURA	0.746	0.016	1.395	0.01	0.897	0.169	purine-rich element binding protein A
RBL2	0.859	0.121	1.231	0.023	0.803	0.319	retinoblastoma-like 2 (p130)
RERE	1.266	0	1.114	0.26	1.184	0.105	arginine-glutamic acid dipeptide (RE) repeats
RFX3	0.803	0.007	1.03	0.616	0.699	0.002	regulatory factor X, 3 (influences HLA class II expression)
RNF10	0.987	0.857	0.996	0.975	0.787	0.015	ring finger protein 10
RNF14	0.916	0.172	0.961	0.729	2.058	0.025	ring finger protein 14
RNF15	0.934	0.323	1.104	0.31	0.81	0.015	ring finger protein 15
SAP30	1.203	0.03	0.843	0.268	0.985	0.703	sin3-associated polypeptide, 30kD
SCAND2	0.936	0.191	1.122	0.179	0.757	0.06	SCAN domain-containing 2
SIX3	0.753	0.003	0.934	0.401	0.95	0.547	sine oculis homeobox (Drosophila) homolog 3
SIX6	1.263	0.01	1.006	0.881	1.015	0.783	sine oculis homeobox (Drosophila) homolog 6
SMARCA4	1.013	0.825	0.988	0.806	1.347	0.124	selective LIM binding factor
SMARCB1	0.825	0.036	1.01	0.789	0.814	0.183	SWI/SNF related, matrix associated, actin dependent regulator of chromatin, subfamily a, member 4
SOX14	0.826	0.031	0.833	0.085	1.185	0.067	SWI/SNF related, matrix associated, actin dependent regulator of chromatin, subfamily b, member 1
SREBF1	0.825	0.079	1.045	0.479	0.834	0.014	SRY (sex determining region Y)-box 14
SSX4	1.106	0.075	1.085	0.381	1.417	0.022	sterol regulatory element binding transcription factor 1
STAT3	0.802	0.034	1.254	0.121	0.885	0.009	signal transducer and activator of transcription 3 (acute-phase response factor)
SUPT4H1	0.828	0.197	1.189	0.055	0.799	0.12	suppressor of Ty (S.cerevisiae) 4 homolog
TAF-172	0.871	0.314	1.048	0.712	0.784	0.007	TBP-associated factor 172
TAF1B	0.744	0.026	1.013	0.921	0.948	0.568	TATA box binding protein (TBP)-associated factor, RNA polymerase I, B, 63kD
TAF1C	0.991	0.918	1.062	0.466	0.829	0.015	TATA box binding protein (TBP)-associated factor, RNA polymerase I, C, 110kD
TAF2B	0.782	0.125	0.919	0.02	1.212	0.168	TATA box binding protein (TBP)-associated factor, RNA polymerase II, B, 150kD
TAF2H	0.802	0.097	1.062	0.611	0.659	0.019	TATA box binding protein (TBP)-associated factor, RNA polymerase II, H, 30kD
TAF2I	0.796	0.025	1.024	0.702	0.871	0.062	TATA box binding protein (TBP)-associated factor, RNA polymerase II, I, 28kD
TAF2K	0.81	0.007	1.007	0.946	0.955	0.656	TATA box binding protein (TBP)-associated factor, RNA polymerase II, K
TBX15	1.423	0.008	1.277	0.106	1.199	0.029	T-box 15
TBX21	0.907	0.247	1.048	0.371	1.232	0.277	T-box 21
TCF21	0.702	0.016	1.042	0.46	0.83	0.003	transcription factor 21
TCF8	0.943	0.296	0.734	0.091	0.754	0.005	transcription factor 8 (represses interleukin 2 expression)

TGFB11	1.013	0.794	0.83	0.042	0.927	0.466	transforming growth factor beta 1 induced transcript 1
TITF1	0.984	0.867	0.815	0.028	1.129	0.416	TG-interacting factor (TALE family homeobox)
TNRC12	0.991	0.802	0.699	0.014	0.96	0.538	trinucleotide repeat containing 12
TNRC5	0.876	0.466	1.432	0.161	0.668	0.137	trinucleotide repeat containing 5
TRIP15	0.799	0.013	0.976	0.589	1.41	0.141	thyroid receptor interacting protein 15
UBTF	1.129	0.072	1.293	0.1	1.079	0.274	upstream binding transcription factor, RNA polymerase I
WHSC1	1.248	0.065	1.054	0.41	1.221	0.049	Wolf-Hirschhorn syndrome candidate 1
XBP1	0.824	0.236	0.888	0.165	1.076	0.388	X-box binding protein 1
ZF5128	1.004	0.968	1.054	0.406	1.238	0.021	zinc finger protein
ZFP91	0.922	0.377	1.043	0.384	0.805	0.467	zinc finger protein homologous to Zfp91 in mouse
ZNF10	1.626	0.01	1.297	0.259	0.997	0.951	zinc finger protein 10 (KOX 1)
ZNF174	1.357	0.104	0.907	0.385	1.503	0.022	zinc finger protein 174
ZNF20	1.239	0.013	0.952	0.399	1.131	0.009	zinc finger protein 20
ZNF212	1.312	0.008	1.08	0.175	0.857	0.38	zinc finger protein 212
ZNF239	0.993	0.907	0.881	0.092	1.295	0.058	zinc finger protein 239
ZNF271	1.158	0.014	1.061	0.192	0.918	0.287	zinc finger protein 271
ZNF274	0.797	0.372	0.818	0.045	0.849	0.048	zinc finger protein 274
ZNF281	1.314	0.006	1.092	0.081	1.014	0.628	zinc finger protein 281
ZNF286	1.058	0.28	1.16	0.119	1.495	0.026	zinc finger protein 286
ZNF288	0.795	0.026	0.889	0.154	1.197	0.031	zinc finger protein 288
ZNF6	1.034	0.73	0.985	0.825	1.326	0.271	zinc finger protein 6
ZNF7	0.823	0.02	0.902	0.18	1.198	0.369	zinc finger protein 7 (KOX 4, clone HF.16)
ZNF76	0.913	0.206	0.813	0.022	1.07	0.467	zinc finger protein 76 (expressed in testis)
ZNF79	1.359	0.035	1.06	0.321	1.549	0.003	zinc finger protein 79 (pT7)
ZNF90	1.451	0.034	1.127	0.039	1.157	0.21	zinc finger protein 90 (HTF9)
ZNF93	1.31	0.029	1.199	0.041	1.346	0.002	zinc finger protein 93 (HTF34)
ZXDA/B	0.94	0.276	0.988	0.818	1.226	0.235	zinc finger, X-linked, duplicated B

Table A4-4. Utricle Laser Genes (261).

Gene ID	30min		1hr		2hr		3hr		Notes/Description
	Fold change	P-value	Fold Change	P-value	Fold Change	P-value	Fold Change	P-value	
ABT1	0.795	0.428	1.025	0.304	0.89	0.152	1.076	0.102	TATA-binding protein-binding protein
AF5Q31	0.847	0.425	1.378	0.47	0.752	0.954	0.753	0.008	ALL1 fused gene from 5q31
ALY	0.795	0.743	1.013	0.619	1.067	0.973	1.086	0.501	transcriptional coactivator
AR	1.153	0.618	1.24	0.362	0.73	0.365	0.782	0.091	androgen receptor (dihydrotestosterone receptor)
ATBF1	1.096	0.201	0.647	0.066	1.594	0.662	0.768	0.774	AT-binding transcription factor 1
ATF7	1.248	0.576	1.121	0.85	1.103	0.756	1.023	0.718	activating transcription factor 7
BACH2	0.684	0.9	1.409	0.861	0.662	0.811	1.422	0.116	BTB and CNC homology 1, basic leucine zipper transcription factor 2
BAPX1	1.056	0.596	1.363	0.963	0.734	0.722	0.742	0.096	bagpipe homeobox (Drosophila) homolog 1
BAZ1B	1.122	0.267	1.086	0.472	0.82	0.594	1.081	0.191	bromodomain adjacent to zinc finger domain, 1B
BCL11A	0.879	0.959	0.801	0.166	1.251	0.382	1.371	0.005	B-cell CLL/lymphoma 11A (zinc finger protein)
BLZF1	0.777	0.056	1.003	0.038	0.923	0.172	1.215	0.004	basic leucine zipper nuclear factor 1 (JEM-1)
BRD1	0.829	0.846	1.462	0.715	0.665	0.791	0.802	0.079	bromodomain-containing 1
BRD2	0.954	0.124	0.87	0.06	1.06	0.533	1.223	0.982	bromodomain-containing 2
BRD4	0.67	0.208	0.697	0.244	1.271	0.785	1.101	0.004	bromodomain-containing 4
BRD7	0.807	0.556	1.071	0.733	1.401	0.196	1.067	0.051	bromodomain-containing 7
BS69	0.919	0.358	1.152	0.928	0.976	0.217	0.825	0.532	adenovirus 5 E1A binding protein
CCT4	1.082	0.062	1.167	0.024	1.045	0.55	1.243	0.27	chaperonin containing TCP1, subunit 4 (delta)
CDK7	1.142	0.015	0.807	0.94	0.949	0.336	0.778	0.876	cyclin-dependent kinase 7 (homolog of Xenopus MO15 cdk-activating kinase)
CEBPE	0.929	0.495	0.918	0.744	0.966	0.546	0.742	0.327	CCAAT/enhancer binding protein (C/EBP), epsilon
CEBPG	0.481	0.09	2.27	0.076	0.817	0.209	1.351	0.054	CCAAT/enhancer binding protein (C/EBP), gamma
CIAO1	1.156	0.502	1.056	0.297	0.998	0.944	1.234	0.174	WD40 protein Ciao1
CREM	1.049	0.856	0.994	0.43	0.805	0.102	1.222	0.103	cAMP responsive element modulator
CRSP6	0.78	0.16	1.104	0.555	1.22	0.416	1.112	0.061	cofactor required for Sp1 transcriptional activation, subunit 6 (77kD)
CRSP7	0.962	0.765	1.101	0.559	0.791	0.501	1.078	0.076	cofactor required for Sp1 transcriptional activation, subunit 7 (70kD)
CSRP2	0.798	0.255	1.078	0.548	0.835	0.307	0.851	0.027	cysteine and glycine-rich protein 2
DACH	1.032	0.092	1.096	0.358	0.766	0.789	0.967	0.016	dachshund (Drosophila) homolog
DDIT3	0.898	0.222	0.995	0.953	0.925	0.177	0.827	0.385	DNA-damage-inducible transcript 3
DEAF1	1.073	0.267	1.132	0.015	1.23	0.769	1.276	0.617	deformed epidermal autoregulatory factor 1 (Drosophila)
DKFZP434P1750	0.869	0.008	0.991	0.682	1.135	0.911	1.301	0.162	DKFZP434P1750 protein
DKFZp547H236	1.238	0.767	1.289	0.734	1.01	0.254	0.895	0.032	MEIS3 homolog

DKFZp762K2015	0.899	0.567	1.104	0.962	1.046	0.069	1.221	0.803	hypothetical protein DKFZp762K2015
DKFZp762M136	1.124	0.348	1.016	0.667	1.081	0.728	1.337	0.089	hypothetical protein DKFZp762M136
DLX3	0.698	0.467	1.051	0.947	0.907	0.909	0.849	0.033	distal-less homeobox 3
DRPLA	0.963	0.156	0.906	0.29	0.586	0.975	1.087	0.275	dentatorubral-pallidoluysian atrophy (atrophin-1)
DSIP1	1.051	0.068	1.305	0.936	0.887	0.294	0.914	0.217	delta sleep inducing peptide, immunoreactor
E4F1	0.946	0.014	1.009	0.101	1.346	0.227	1.297	0.421	E4F transcription factor 1
EED	1.327	0.837	0.839	0.724	0.796	0.665	0.904	0.771	embryonic ectoderm development
ELF3	1.291	0.007	1.045	0.314	0.825	0.595	1.059	0.16	E74-like factor 3 (ets domain transcription factor, epithelial-specific)
ELK4	1.04	0.034	0.769	0.603	0.978	0.025	1.154	0.031	E74-like factor 4 (ets domain transcription factor)
EN2	0.91	0.797	1.254	0.955	1.151	0.482	1.123	0.061	engrailed homolog 2
ESR1	0.984	0.095	0.929	0.504	1.261	0.813	1.019	0.001	estrogen receptor 1
ETV1	0.929	0.286	1.496	0.895	1.328	0.833	1.006	0.005	ets variant gene 1
FHL1	0.681	0.524	1.406	0.467	0.928	0.814	1.26	0.047	four and a half LIM domains 1
FLJ10142	1.066	0.016	1.356	0.625	0.958	0.904	1.233	0.061	hypothetical protein FLJ10142
FLJ10697	0.811	0.11	1.002	0.482	1.122	0.911	1.362	0	hypothetical protein FLJ10697
FLJ11186	0.9	0.136	0.713	0.294	1.491	0.345	1.193	0.007	hypothetical protein FLJ11186
FLJ12517	1.193	0.052	0.766	0.92	1.012	0.026	1.218	0.177	hypothetical protein FLJ12517
FLJ12606	0.96	0.249	0.939	0.187	1.054	0.128	1.2	0.219	hypothetical protein FLJ12606
FLJ13222	1.01	0.011	1	0.092	1.205	0.246	1.251	0.003	likely ortholog of mouse testis expressed gene 27
FLJ20321	0.971	0.244	1.1	0.546	1.226	0.114	1.041	0.085	hypothetical protein
FOG2	0.795	0.628	1.31	0.067	0.747	0.723	0.871	0.011	friend of GATA2
FOSB	1.032	0.613	1.143	0.67	0.789	0.972	1.112	0.863	FBJ murine osteosarcoma viral oncogene homolog B
FOSL1	1.006	0.477	1.182	0.59	0.897	0.161	1.245	0.095	FOS-like antigen 1
FOXB1	1.611	0.64	1.001	0.068	0.778	0.359	0.95	0.281	forkhead box B1
FOXE1	0.979	0.851	1.026	0.974	1.35	0.308	1.173	0.01	forkhead box E1 (thyroid transcription factor 2)
FOXH1	0.947	0.411	0.775	0.362	0.948	0.342	1.017	0.001	forkhead box H1
FOXO3A	1.593	0.415	1.054	0.783	0.932	0.359	0.747	0.978	forkhead box O3A
FOXP1	1.261	0.649	1.699	0.029	0.822	0.951	1.156	0.001	forkhead box P1
GCMA	1.082	0.831	1.024	0.056	1.249	0.52	1.115	0.187	glial cells missing (Drosophila) homolog a
GCN5L1	1.1	0.275	1.346	0.508	1.129	0.75	1.027	0.001	GCN5 (general control of amino-acid synthesis, yeast, homolog)-like 1
GIOT-2	1.205	0.765	1.117	0.213	0.738	0.114	1.204	0.051	GIOT-2 for gonadotropin inducible transcription repressor-2
GLI2	1.154	0.338	0.806	0.153	0.966	0.405	0.926	0.194	GLI-Kruppel family member GLI2
GLI3	0.813	0.081	0.97	0.368	1.138	0.249	1.125	0.232	GLI-Kruppel family member GLI3 (Greig cephalopolysyndactyly syndrome)
GLP	0.979	0.18	0.911	0.143	1.035	0.269	1.228	0.812	golgin-like protein

GSH2	1.218	0.689	1.086	0.51	1.032	0.304	0.966	0.071	genomic screened homeo box 2 (mouse) homolog
GTF2E2	0.714	0.342	1.212	0.437	0.806	0.26	0.884	0.704	general transcription factor IIE, polypeptide 2 (beta subunit, 34kD)
GTF2H2	1.103	0.396	0.948	0.404	0.823	0.237	1.017	0.233	general transcription factor IIH, polypeptide 2 (44kD subunit)
HCNGP	0.99	0.092	1.02	0.784	0.856	0.061	1.312	0.454	transcriptional regulator protein
HDAC2	1.181	0.793	1.009	0.142	0.83	0.274	0.922	0.001	histone deacetylase 2
HES7	0.899	0.012	1.439	0.752	1.056	0.681	1.215	0.001	hairy and enhancer of split 7 (Drosophila)
HEY2	0.922	0.839	0.988	0.192	1.218	0.003	1.122	0.951	hairy/enhancer-of-split related with YRPW motif 2
HLX1	1.316	0.038	1.032	0.853	0.925	0.567	0.943	0.014	H2.0 (Drosophila)-like homeo box 1
HLXB9	1.152	0.277	0.951	0.943	0.816	0.169	0.85	0.15	homeo box HB9
HMG1Y	1.076	0.331	0.883	0.227	1.272	0.077	0.855	0.976	high-mobility group (nonhistone chromosomal) protein isoforms I and Y
HMX1	1.393	0.295	0.828	0.898	1.081	0.717	0.938	0.972	homeo box (H6 family) 1
HMX2	1.202	0.098	0.917	0.242	0.97	0.128	1	0.408	homeo box (H6 family) 2
HNF3A	1.132	0.938	2.01	0.492	0.796	0.167	0.807	0.66	hepatocyte nuclear factor 3, alpha
HNF3B	1.036	0.124	1.19	0.453	0.978	0.03	1.203	0.002	hepatocyte nuclear factor 3, beta
HOX11L	0.88	0.472	1.085	0.278	1.377	0.924	1.161	0.3	homeo box 11-like 1
HOXA13	1.076	0.19	1.314	0.06	0.741	0.707	1.196	0.14	homeo box A13
HOXA5	1.164	0.398	0.679	0	1.258	0.382	1.014	0.002	homeo box A5
HOXA6	0.999	0.142	0.849	0.324	1.201	0.445	0.783	0.059	homeobox A6
HOXA7	1.243	0.565	0.83	0.099	0.812	0.703	0.871	0.149	homeobox A7
HOXB13	1.22	0.425	1.079	0.905	0.96	0.755	0.992	0.202	homeo box B13
HOXC5	1.295	0.592	0.928	0.973	0.78	0.333	0.82	0.53	homeo box C5
HOXC6	0.856	0.238	1.195	0.598	1.659	0.704	1.061	0.425	homeo box C6
HOXD8	0.847	0.251	0.988	0.744	1.392	0.372	1.21	0.002	homeobox D8
HRIHFB2122	1.057	0.145	1.226	0.065	1.174	0.801	0.888	0.316	putative nuclear protein
HS747E2A	0.922	0.19	0.642	0.124	1.115	0.472	0.803	0.088	hypothetical protein
HSAJ2425	0.978	0.372	0.921	0.689	1.202	0.231	1.139	0	p65 protein
HSF1	1.103	0.779	1.187	0.094	0.94	0.323	0.784	0.02	heat shock transcription factor 1
H_GS165L1 5	1.061	0.317	1.115	0.115	0.813	0.992	0.868	0.084	cAMP response element-binding protein
ID1	1.399	0.137	0.852	0.766	0.98	0.903	0.758	0.214	inhibitor of DNA binding 1, dominant negative helix-loop-helix protein
ILF1	0.763	0.886	1.356	0.164	0.997	0.527	1.125	0.086	interleukin enhancer binding factor 1
IPEX	1.112	0.87	1.287	0.302	0.827	0.3	0.947	0.015	immune dysregulation, polyendocrinopathy, enteropathy, X-linked
IRF2	1.106	0.371	1.289	0.79	0.861	0.613	1.035	0.034	interferon regulatory factor 2
JUN	1.22	0.865	0.729	0.165	0.874	0.895	0.827	0.045	v-jun avian sarcoma virus 17 oncogene homolog
JUNB	0.997	0.962	1.446	0.295	0.98	0.223	1.654	0.019	Jun B proto-oncogene
KIAA0014	1.507	0.055	0.972	0.394	0.985	0.818	0.947	0.051	KIAA0014 gene product

KIAA0040	0.643	0.701	1.021	0.224	1.166	0.17	1.207	0.006	KIAA0040 gene product
KIAA0161	0.766	0.795	1.15	0.727	1.064	0.869	1.203	0.259	KIAA0161 gene product
KIAA0173	1.003	0.845	1.329	0.432	0.635	0.705	1.511	0	KIAA0173 gene product
KIAA0237	0.909	0.815	1.052	0.725	1.145	0.602	1.273	0.498	KIAA0237 gene product
KIAA0395	0.953	0.037	1.066	0.246	1.106	0.344	1.225	0.032	KIAA0395 protein
KIAA0414	0.886	0.267	1.002	0.002	1.202	0.178	1.241	0.011	KIAA0414 protein
KIAA0478	1.167	0.677	0.996	0.077	0.732	0.47	0.897	0.029	KIAA0478 protein
KIAA0669	1.042	0.962	1.179	0.812	0.907	0.134	1.23	0.008	KIAA0669 gene product
KIAA1528	0.868	0.27	1.038	0.044	1.145	0.487	1.378	0	KIAA1528 protein
KLF5	0.507	0.97	1.363	0.364	0.856	0.26	1.033	0.325	Kruppel-like factor 5
KLHL4	0.993	0.318	0.707	0.1	1.138	0.52	1.013	0.057	kelch (Drosophila)-like 4
LAF4	0.943	0.587	1.367	0.168	0.789	0.956	1.439	0.094	lymphoid nuclear protein related to AF4
LDB2	1.124	0.168	1.172	0.711	1.091	0.85	1.274	0.559	LIM domain binding 2
LDOC1	0.8	0.22	1.499	0.644	0.8	0.692	1.199	0.327	leucine zipper, down-regulated in cancer 1
LEF1	1.04	0.11	0.928	0.189	0.918	0.996	0.828	0.843	lymphoid enhancer factor 1
LIM	1.055	0.934	0.637	0.624	1.098	0.792	1.159	0.023	LIM protein (similar to rat protein kinase C-binding enigma)
LMX1B	1.316	0.357	0.923	0.117	1.068	0.485	1.068	0.23	LIM homeobox transcription factor 1, beta
LOC51036	0.976	0.059	0.819	0.007	1.431	0.296	1.067	0.026	retinoic acid receptor-beta associated open reading frame
LOC51058	1.059	0.071	0.774	0.48	0.932	0.542	1.22	0.399	hypothetical protein
LOC51088	1.043	0.287	1.064	0.014	1.073	0.56	1.2	0.363	lymphocyte activation-associated protein
LOC51131	0.811	0.242	1.013	0.012	1.178	0.991	1.302	0.001	putative zinc finger protein NY-REN-34 antigen
LOC51193	0.999	0.493	1.014	0.79	1.199	0.502	1.381	0.109	zinc finger protein ANC_2H01
LOC51270	0.992	0.366	0.911	0.056	1.094	0.951	0.811	0.563	E2F-like protein
LOC51290	0.943	0.407	1.11	0.24	1.11	0.467	1.207	0.224	CDA14
LOC51637	1.176	0.922	0.946	0.584	0.932	0.483	0.807	0.012	KRAB-zinc finger protein SZF1-1
LOC55893	0.909	0.586	1.026	0.004	1.083	0.671	1.209	0.108	papillomavirus regulatory factor PRF-1
LOC57167	0.877	0.419	0.748	0.294	1.096	0.335	1.18	0.276	similar to SALL1 (sal (Drosophila)-like
LOC57209	0.706	0.764	0.797	0.298	1.297	0.251	1.348	0.012	Kruppel-type zinc finger protein
LOC58500	0.865	0.004	1.09	0.13	1.386	0.437	1.228	0.177	zinc finger protein (clone 647)
LOC65243	0.845	0.187	0.858	0.007	1.206	0.304	1.093	0.04	hypothetical protein
LOC91120	1.288	0.714	1.019	0.374	0.808	0.338	1.181	0.006	similar to ZINC FINGER PROTEIN 85 (ZINC FINGER PROTEIN HPF4) (HTF1) (H. sapiens)
LOC92283	1.114	0.594	0.924	0.133	0.939	0.586	1.237	0.004	gonadotropin inducible transcription repressor-1 (GIOT-1)
M96	1.386	0.062	0.83	0.32	0.781	0.022	0.865	0.858	putative DNA binding protein
MADH4	0.933	0.253	1.062	0.313	1.151	0.147	1.405	0.084	MAD (mothers against decapentaplegic, Drosophila) homolog 4
MADH5	0.777	0.141	1.087	0.013	0.972	0.476	0.824	0.138	MAD (mothers against decapentaplegic, Drosophila) homolog 5

MADH7	1.542	0.334	1.431	0.127	0.661	0.861	0.961	0.241	MAD (mothers against decapentaplegic, Drosophila) homolog 7
MAFF	1.028	0.01	0.555	0.05	1.026	0.067	0.558	0.463	v-maf musculoaponeurotic fibrosarcoma (avian) oncogene family, protein F
MAPK8IP1	0.699	0.69	0.966	0.014	0.918	0.749	1.355	0.239	mitogen-activated protein kinase 8 interacting protein 1
MAX	1.258	0.336	1.156	0.636	0.705	0.685	1.025	0.283	MAX protein
MBLL	0.917	0.795	1.039	0.437	1.043	0.053	1.243	0.298	C3H-type zinc finger protein; similar to D. melanogaster muscleblind B protein
MDS1	1.075	0.956	0.979	0.178	0.818	0.443	0.89	0.225	myelodysplasia syndrome 1
MED6	0.989	0.56	0.984	0.56	1.308	0.879	1.045	0.365	RNA polymerase II transcriptional regulation mediator (Med6, S. cerevisiae, homolog of)
MEF2B	1.177	0	0.565	0.638	0.852	0.716	1.156	0.037	MADS box transcription enhancer factor 2, polypeptide B (myocyte enhancer factor 2B)
MEIS3	1.086	0.011	0.878	0.855	1.059	0.205	0.806	0.076	meis1-related protein 2 aka MRG2
MGC11349	1.044	0.883	0.803	0.831	0.989	0.617	0.978	0.153	hypothetical protein MGC11349
MGC2508	1.02	0.082	0.893	0.611	1.217	0.602	1.14	0.12	hypothetical protein MGC2508
MHC2TA	0.858	0.05	1.037	0.567	1.303	0.321	1.188	0.447	MHC class II transactivator
MLLT1	1.406	0.067	0.991	0.864	0.752	0.738	0.757	0.398	myeloid/lymphoid or mixed-lineage leukemia (trithorax (Drosophila) homolog); translocated to, 1
MLLT2	0.997	0.923	1.026	0.853	1.199	0.656	1.277	0.155	myeloid/lymphoid or mixed-lineage leukemia (trithorax (Drosophila) homolog); translocated to 2
MNDA	1.061	0.684	0.802	0.525	0.995	0.807	0.915	0.795	myeloid cell nuclear differentiation antigen
MORF	0.992	0.873	1.091	0.007	1.22	0.114	1.253	0.051	histone acetyltransferase
MSC	0.986	0.749	1.322	0.678	1.239	0.777	1.067	0.206	musculin (activated B-cell factor-1)
MTF1	1.06	0.54	1.08	0.043	0.997	0.028	0.828	0.432	metal-regulatory transcription factor 1
MYC	0.853	0.63	1.1	0.217	1.239	0.799	1.347	0.375	c-myc proto-oncogene
MYCBP	0.774	0.358	0.664	0.087	0.993	0.692	1.271	0.001	c-myc binding protein
MYT2	0.917	0.501	1.406	0.044	0.685	0.041	1.176	0.287	myelin transcription factor 2
NCOA1	0.928	0.239	1.035	0.053	1.174	0.849	1.254	0.084	nuclear receptor coactivator 1
NFYB	1.153	0.236	0.854	0.946	0.874	0.776	0.809	0.796	nuclear transcription factor Y, beta
NFYC	0.866	0.407	1.224	0.807	1.375	0.427	1.204	0.07	nuclear transcription factor Y, gamma
NKX3A	0.983	0.745	0.765	0.884	0.805	0.621	0.779	0.81	NK homeobox (Drosophila), family 3, A
NMI	0.843	0.558	1.066	0.224	1.212	0.325	1.203	0.55	N-myc (and STAT) interactor
NR1H3	0.745	0.935	1.327	0.041	1.373	0.24	0.843	0.009	nuclear receptor subfamily 1, group H, member 3
NR1I3	1.068	0.586	1.258	0.035	0.924	0.817	0.968	0.077	nuclear receptor subfamily 1, group I, member 3
NR2E1	1.087	0.298	0.724	0.396	0.955	0.906	1.024	0.415	nuclear receptor subfamily 2, group E, member 1
OCT11	0.945	0.175	1.153	0.905	0.772	0.281	1.066	0.089	POU transcription factor
PAF65A	0.933	0.027	1.393	0.882	0.734	0.394	1.196	0.965	PCAF associated factor 65 alpha
PAX1	0.821	0.978	0.956	0.792	0.922	0.184	0.934	0.452	paired box gene 1
PBX1	0.971	0.174	0.816	0.815	1.024	0.502	0.848	0.021	pre-B-cell leukemia transcription factor 1

PC4	0.993	0.055	1.335	0.253	1.407	0.461	1.164	0.269	activated RNA polymerase II transcription cofactor 4
PCAR	0.864	0.345	1.043	0.729	1.285	0.234	1.228	0.28	hypothetical protein I38022
PER2	1.042	0.546	0.965	0.036	0.965	0.308	0.813	0.069	period (Drosophila) homolog 2
PHAP1	0.956	0.365	0.878	0.301	1.196	0.382	1.335	0.009	putative human HLA class II associated protein I
POU2AF1	1.213	0.296	1.213	0.871	0.827	0.396	0.894	0.003	POU domain, class 2, associating factor 1
POU4F1	0.879	0.34	0.662	0.347	0.903	0.581	1.181	0.84	POU domain, class 4, transcription factor 1
POU4F2	0.767	0.76	0.823	0.693	0.871	0.442	0.693	0.027	POU domain, class 4, transcription factor 2
POU5F1	0.905	0.926	0.893	0.955	1.241	0.756	0.957	0.18	POU domain, class 5, transcription factor 1
PRDM13	1.133	0.002	1.061	0.41	0.803	0.514	0.812	0.006	PR domain containing 13
PRDM16	0.893	0.041	1.49	0.325	0.706	0.049	1.013	0.06	PR domain containing 16
PRDM2	1.275	0.521	0.777	0.461	0.897	0.129	0.934	0.237	PR domain containing 2, with ZNF domain
PREB	0.866	0.834	0.941	0.758	0.917	0.208	1.307	0.461	prolactin regulatory element binding
PSMC5	0.755	0.277	1.219	0.371	1.114	0.951	1.25	0.046	proteasome (prosome, macropain) 26S subunit, ATPase, 5
R28830_2	1.284	0.657	1.071	0.719	0.963	0.279	0.897	0.048	similar to ZNF197 (ZNF20)
R32184_3	0.881	0.097	0.981	0.496	1.244	0.161	1.16	0.047	hypothetical protein MGC4022
RBL2	0.964	0.203	0.829	0.382	0.883	0.173	0.824	0.998	retinoblastoma-like 2 (p130)
RFP	1.148	0.201	0.859	0.102	1.038	0.421	1.269	0.015	ret finger protein
RFX3	0.892	0.726	1.072	0.552	0.785	0.41	1.117	0.073	regulatory factor X, 3 (influences HLA class II expression)
RGC32	0.725	0.891	0.994	0.019	1.063	0.119	1.343	0.001	RGC32 protein
RING1	1.094	0.076	1.473	0.168	0.971	0.438	0.893	0.9	ring finger protein 1
RNF22	0.743	0.494	1.02	0.932	1.204	0.782	1.09	0.443	ring finger protein 22
RNF3	0.958	0.06	1.091	0.902	1.22	0.894	1.168	0.838	ring finger protein 3
RORC	0.644	0.371	1.363	0.342	0.681	0.616	1.219	0.097	RAR-related orphan receptor C
SBB103	1.197	0.478	1.244	0.638	0.867	0.495	0.978	0.251	hypothetical SBB103 protein
SETDB1	1.074	0.573	0.818	0.869	1.134	0.388	1.138	0.171	SET domain, bifurcated 1
SIAH1	0.986	0.073	0.904	0.641	1.215	0.129	0.97	0.572	seven in absentia (Drosophila) homolog 1
SIX4	1.21	0.99	1.133	0.167	1.09	0.277	1.109	0.027	sine oculis homeobox (Drosophila) homolog 4
SMARCA2	0.828	0.93	1.04	0.558	1.026	0.729	1.201	0.036	SWI/SNF related, matrix associated, actin dependent regulator of chromatin, subfamily a, member 2
SMARCE1	1.038	0.807	0.759	0.211	1.021	0.481	1.014	0.282	SWI/SNF related, matrix associated, actin dependent regulator of chromatin, subfamily e, member 1
SNAPC4	0.91	0.472	0.829	0.639	1.041	0.139	1.027	0.002	small nuclear RNA activating complex, polypeptide 4, 190kD
SOX2	1.478	0.716	0.796	0.879	1.048	0.373	0.891	0.019	SRY (sex determining region Y)-box 2
SRY	0.541	0.105	1.041	0.33	0.89	0.692	0.645	0.014	sex determining region Y
SSX4	0.813	0.44	1.02	0.736	1.082	0.489	1.327	0	synovial sarcoma, X breakpoint 4
STAT1	1.272	0.453	1.392	0.904	0.753	0.704	0.857	0.052	signal transducer and activator of transcription 1, 91kD
TAF2B	1.078	0.371	1.058	0.232	1.224	0.615	1.07	0.696	TATA box binding protein (TBP)-associated factor, RNA polymerase

									II, B, 150kD
TAF2C1	1.08	0.005	1.065	0.355	0.95	0.287	0.815	0.071	TATA box binding protein (TBP)-associated factor, RNA polymerase II, C1, 130kD
TAF2H	0.977	0.522	1.522	0.221	0.823	0.326	0.92	0.028	TATA box binding protein (TBP)-associated factor, RNA polymerase II, H, 30kD
TAL2	0.962	0.717	1.377	0.171	1.002	0.922	0.898	0.331	T-cell acute lymphocytic leukemia 2
TBX15	0.807	0.762	0.847	0.164	1.309	0.268	1.448	0.01	T-box 15
TBX2	1.082	0.673	1.202	0.699	1.1	0.55	0.963	0.453	T-box 2
TBX21	1.089	0.411	0.786	0.382	1.032	0.729	1.037	0.255	T-box 21
TBX5	0.758	0.757	0.974	0.055	1.217	0.367	1.192	0.017	Holt-Oram syndrome
TCF21	0.973	0.95	1.502	0.056	0.784	0.581	1.44	0.055	transcription factor 21
TCF8	1.237	0.041	0.937	0.882	0.885	0.682	0.826	0.352	transcription factor 8 (represses interleukin 2 expression)
TCFL1	0.831	0.124	0.874	0.023	0.939	0.475	1.293	0.41	transcription factor-like 1
TCFL4	1.35	0.182	0.947	0.333	0.766	0.15	0.889	0.812	represses Txn by recruiting Sin3A-HDAC complex; has bHLH and LeuZip domains
TCFL5	1.145	0.815	0.934	0.344	1.01	0.65	1.202	0.668	transcription factor-like 5 (basic helix-loop-helix)
TEF	1.102	0.042	0.903	0.44	0.962	0.386	0.828	0.663	thyrotrophic embryonic factor
TFE3	0.743	0.79	1.013	0.069	1.339	0.436	1.264	0.046	binds to Ig heavy-chain enhancer; has HLH domain
TFEB	1.01	0.951	1.058	0.035	1.199	0.696	1.226	0.463	transcription factor EB
TGFB111	0.78	0.703	1.232	0.92	0.935	0.461	1.124	0.149	transforming growth factor beta 1 induced transcript 1
TIEG2	1.322	0.704	1.247	0.366	1.011	0.083	0.914	0.085	TGFB inducible early growth response 2
TITF1	0.868	0.018	1.22	0.506	0.871	0.364	1.222	0.15	thyroid transcription factor 1
TNRC6	1.026	0.137	1.006	0.686	1.239	0.804	1.217	0.46	trinucleotide repeat containing 6
TNRC9	0.883	0.082	1.073	0.029	0.997	0.772	1.256	0.035	trinucleotide repeat containing 9
TONDU	0.9	0.621	1.036	0.54	1.087	0.911	1.25	0.579	TONDU
TRIP15	0.96	0.087	1.313	0.041	0.955	0.898	0.975	0.011	thyroid receptor interacting protein 15
VAX2	0.914	0.101	0.945	0.046	0.856	0.184	0.822	0.45	homeobox protein VAX2
VENTX2	1.11	0.782	1.299	0.007	0.807	0.181	0.907	0.244	haemopoietic progenitor homeobox
WHSC1	0.96	0.203	0.998	0.39	1.264	0.228	1.178	0.166	Wolf-Hirschhorn syndrome candidate 1
XBP1	0.828	0.227	1.461	0.513	1.026	0.39	0.976	0.008	X-box binding protein 1
ZFP36	0.895	0.13	1.048	0.866	1.067	0.175	1.271	0.764	zinc finger protein homologous to Zfp-36 in mouse
ZFY	0.773	0.847	0.83	0.644	1.38	0.976	1.613	0.042	zinc finger protein, Y-linked
ZHX1	0.84	0.307	0.976	0.985	1.295	0.139	1.278	0.035	zinc-fingers and homeoboxes 1
ZIC2	0.923	0.195	0.945	0.523	1.315	0.381	1.371	0.256	zic family member 2 (odd-paired Drosophila homolog, heterotaxy 1)
ZIC4	0.928	0.124	1.03	0.304	1.186	0.095	1.247	0.195	zinc family member 4 protein HZIC4
ZID	0.749	0.023	0.957	0.321	1.297	0.592	1.324	0.018	zinc finger protein with interaction domain
ZNF135	0.997	0.412	0.966	0.328	0.968	0.318	0.798	0.028	zinc finger protein 135

ZNF144	1.304	0.624	0.989	0.198	0.885	0.27	0.908	0.212	zinc finger protein 144 (Mel-18)
ZNF15L1	0.822	0.499	1.044	0.439	1.279	0.438	1.264	0.618	zinc finger protein 15-like 1 (KOX 8)
ZNF165	0.884	0.669	0.914	0.652	0.886	0.224	0.827	0.244	zinc finger protein 165
ZNF174	0.818	0.648	1.094	0.244	0.926	0.63	0.962	0.006	zinc finger protein 174
ZNF187	0.775	0.17	1.038	0.316	1.329	0.251	1.311	0.054	zinc finger protein 187
ZNF205	0.986	0.778	0.726	0.302	1.045	0.518	0.897	0.007	zinc finger protein 205
ZNF21	0.973	0.699	0.806	0.027	1.124	0.966	1.132	0.322	zinc finger protein
ZNF212	0.86	0.383	0.903	0.733	1.242	0.174	1.109	0.004	zinc finger protein 212
ZNF214	0.996	0.669	0.882	0.263	0.838	0.612	0.799	0.034	zinc finger protein 214
ZNF230	0.989	0.01	1	0.971	1.419	0.659	1.028	0.894	zinc finger protein 230
ZNF239	0.865	0.769	1.317	0.4	1.157	0.08	1.099	0.008	zinc finger protein (C2H2) homologous to mouse MOK-2
ZNF264	0.953	0.042	0.908	0.412	0.902	0.174	0.825	0.097	zinc finger protein 264
ZNF273	0.863	0.239	1.005	0.146	1.315	0.169	1.285	0.737	zinc finger protein 273 aka HZF9
ZNF29	1.144	0.226	0.956	0.017	0.792	0.522	0.801	0.232	zinc finger protein 29 aka KOX 26
ZNF295	1.162	0.262	1.015	0.7	1.035	0.871	0.826	0.237	zinc finger protein 295
ZNF32	0.896	0.575	0.892	0.627	1.328	0.256	1.195	0.552	zinc finger protein 32 (KOX 30)
ZNF38	0.97	0.169	1.623	0.715	1.072	0.828	0.945	0.733	zinc finger protein 38 (KOX 25)
ZNF41	0.771	0.24	0.992	0.885	1.187	0.938	1.132	0.025	zinc finger protein 41
ZNF44	0.891	0.583	1.089	0.586	1.222	0.729	1.152	0.084	zinc finger protein 44 (KOX 7)
ZNF46	0.919	0.268	0.985	0.915	1.337	0.735	0.993	0.747	zinc finger protein 46 (KUP)
ZNF75A	0.79	0.953	1.016	0.228	1.494	0.275	1.305	0	zinc finger protein 75a
ZNF79	0.643	0.627	0.895	0.798	1.47	0.522	1.436	0.557	zinc finger protein 79 (pT7)
ZNF80	1.258	0.554	1.169	0.486	0.909	0.627	0.958	0.492	zinc finger protein 80 (pT17)
ZNF90	0.906	0.016	0.989	0.291	1.116	0.745	1.211	0.246	zinc finger protein 90 (HTF9)
ZNF93	0.811	0.018	0.781	0.06	1.377	0.32	1.396	0.002	zinc finger protein 93 (HTF34)
ZXDA	0.922	0.002	0.965	0.03	0.934	0.86	0.824	0.013	zinc finger, X-linked, duplicated A

Table A4-5. Self Organizing Map Centroid Groups.

Centroid 0				
ATF7	HOXB13	NR1I3	SIX4	VENTX2
BAPX1	H_GS165L15	PURA	STAT1	ZNF295
DKFZp547H236	MADH7	RING1	TAF2C1	ZNF80
DSIP1	MAX	SBB103	TIEG2	
GSH2	MDS1	SIX3	UBTF	
Centroid 1				
AR	FHL2	MID1	RBL2	TAF1B
BAZ1B	FLJ22252	MTF1	RNF10	TAF2I
CBX4	HMX2	MYT1	RNF15	TAF2K
CREG	HRIHFB2436	NFKBIA	SCAND2	TCF8
CRIP2	HSF1	NR5A2	SMARCB1	ZFP91
DACH	IPEX	PBX4	SREBF1	
DLX4	KIAA0478	POU2AF1	STAT3	
E2F2	KIAA1041	PRDM13	SUPT4H1	
Centroid 2				
ABT1	DDIT3	GTF2E2	RFX3	ZXDA
AF5Q31	DKFZP434B0335	MADH5	SRY	
ALY	DLX3	NEUROD6	TAF-172	
ATF2	DLX6	OCT11	TNRC5	
CSRP2	FOG2	PAX1	ZNF274	
Centroid 3				
BACH2	FHL1	HOXA13	LDOC1	TAF2H
BRD1	FLJ10142	IRF2	MYT2	TCF21
C21orf18	FOXP1	JUNB	PAF65A	ZNF38
CEBPG	HES7	KLF5	PRDM16	
EZH1	HNF3A	LAF4	RORC	
Centroid 4				
CRX	GTF2H2	HOXC5	MLLT1	ZNF144
EED	HDAC2	JUN	MTA1L1	ZNF29
ELF3	HLX1	LMX1B	PRDM2	
FOXB1	HLXB9	LOC51637	R28830_2	
FOXF2	HMX1	LOC91120	SOX2	
FOXO3A	HOXA7	M96	TCFL4	
Centroid 5				
CDK7	HOXA5	MEIS3	PER2	ZNF165
CEBPB	HOXA6	MGC11349	SMARCE1	ZNF205
CEBPE	HS747E2A	MNDA	SNAPC4	ZNF214
CROC4	ISGF3G	NFYB	TAF1C	ZNF264
ELK4	LEF1	NKX3A	TEF	
FOXH1	LOC51270	NR2E1	VAX2	
HMGY	MAFF	PBX1	ZNF135	
Centroid 6				
ASH2L	ETV5	HSF2BP	NHLH2	TNRC9
BCL11B	EYA3	KIAA0161	PMF1	ZNF76
CREM	FOSB	KIAA0669	PREB	
CRSP7	FOSL1	LOC57167	TGFB111	
DKFZp762K2015	GIOT-2	MAPK8IP1	TITF1	
DRPLA	HCNGP	MLLT6	TNRC12	
Centroid 7				
ARIX	GCN5L1	MNT	SOX14	XBP1
CUTL1	GTF2F1	MYBL2	TAF2B	ZNF239

E2F5	HEY1	NFE2L1	TAL2	ZNF288
EN2	HIF1A	PPARBP	TBX2	ZNF7
ETV1	ILF1	PSMC5	TRIP15	
Centroid 8				
ATBF1	ERCC6	HHEX	NR1H2	TBX21
BS69	EZH2	HIRA	NRL	ZF5128
CREBL1	FLJ20321	HIVEP1	POU4F2	ZNF286
CSDA	GLI2	HOXD12	POU4F3	ZNF6
EBF	GTF2H1	IRF3	PTTG1IP	ZXDA/B
EOMES	GTF2H3	KLHL4	SMARCA4	
Centroid 9				
CBX3	FLJ12827	KIAA0130	NRF	SIX6
CITED1	FLJ13590	LHX4	PDEF	TCFL5
DUX2	FLJ20595	LIM	PILB	ZNF10
FLJ10251	GTF3C4	MEF2B	PLAG1	ZNF21
FLJ10891	H-L(3)MBT	MEIS2	PROP1	ZNF271
FLJ12517	HOXB9	MYCL2	SETDB1	ZNF281
Centroid 10				
BRD2	GLP	MADH4	RNF3	ZIC2
CCT4	KIAA0237	MBLL	SAP30	ZIC4
CIAO1	LDB2	NCOA1	SMARCA2	ZNF20
DKFZp762M136	LOC51088	PHAP1	TNRC6	
FLJ12606	LOC51290	RFP	TONDU	
FLJ13222	LOC92283	RGC32	ZFP36	
Centroid 11				
BRD7	HOXC6	MORF	NR1H3	SIAH1
CRSP6	HRIHFB2122	MSC	PC4	TFEB
E4F1	ILF2	MYC	PCAR	ZNF230
FOX E1	LOC58500	NFIB	POU5F1	ZNF44
GCMA	MED6	NFYC	R32184_3	
HOX11L	MHC2TA	NMI	RNF22	
Centroid 12				
CTNNB1	ESR1	HNF3B	ID1	KIAA0014
PPARGC1	RNF14			
Centroid 13				
BLZF1	HSAJ2425	LOC51058	MGC2508	SSX4
CHD3	HSPC018	LOC51131	MLLT2	TCFL1
DKFZP434P1750	HSPX153	LOC51193	MYCBP	ZNF174
GLI3	KIAA0173	LOC55893	PKNOX2	ZNF273
GTF2E1	KIAA0395	LZLP	POU4F1	
HOXB7	KIAA1528	MADH2	RERE	
Centroid 14				
BCL11A	GTF2A1	TBX15	ZFY	ZNF93
BRD4	HOXD8	TBX5	ZNF79	
FLJ10697	LOC57209	WHSC1	ZNF90	
Centroid 15				
DEAF1	KIAA0414	ZHX1	ZNF212	ZNF75A
FLJ11186	LOC51036	ZID	ZNF32	
HEY2	LOC65243	ZNF15L1	ZNF41	
KIAA0040	TFE3	ZNF187	ZNF46	

Table A4-6. Genes uniquely on in the utricle as compared to the cochlea.

ASH1	LOC56930	TAF1B	ZNF175	ZNF256
AWP1	MYBL1	TBX1	ZNF177	ZNF258
BARX1	MYT1	TBX22	ZNF18	ZNF263
DMRT1	NCOA2	TMF1	ZNF184	ZNF264
FLJ11191	NCOR1	WT1	ZNF192	ZNF267
FLJ21603	NSEP1	ZFP106	ZNF195	ZNF29
HOXC10	POU4F2	ZNF135	ZNF197	ZNF30
HR	RLF	ZNF14	ZNF202	ZNF73
HSF2	SALF	ZNF143	ZNF214	ZNF84
HSU79252	SP1	ZNF144	ZNF217	ZNF85
HYPH	SRY	ZNF165	ZNF219	

Table A4-7. Genes uniquely differentially expressed in the utricle as compared to the cochlea.

ABT1	GLP	LOC65243	PKNOX2	TBX2
ALY	GSH2	LOC92283	PMF1	TCFL4
AR	GTF2H1	LZLP	PRDM16	TFE3
ASH2L	HDAC2	MADH4	PSMC5	TFEB
BAZ1B	HEY1	MBLL	R28830_2	TGFB1I1
BRD2	HIVEP1	MEIS2	R32184_3	UBTF
BS69	HMX2	MGC11349	RBL2	ZFP36
CBX3	HOX11L	MID1	RERE	ZFP91
CCT4	HOXA5	MLLT1	RFP	ZHX1
CDK7	HSF1	MLLT2	RFX3	ZIC2
CEBPE	ID1	MLLT6	RNF15	ZNF15L1
CEBPG	IRF3	MNDA	RNF3	ZNF187
CREBL1	JUN	MNT	SAP30	ZNF20
CRIP2	KIAA0040	MTF1	SCAND2	ZNF21
CRSP7	KIAA0237	MYC	SIX6	ZNF212
CSRP2	KIAA0478	MYCL2	SMARCA2	ZNF264
DACH	KIAA0669	MYT1	SMARCA4	ZNF274
DLX4	LEF1	NCOA1	SMARCE1	ZNF281
EED	LHX4	NFKBIA	SREBF1	ZNF286
ETV5	LMX1B	NFYB	SRY	ZNF288
EYA3	LOC51036	NFYC	SSX4	ZNF29
FLJ10251	LOC51088	NR1H2	STAT1	ZNF32
FLJ10891	LOC51131	NR2E1	STAT3	ZNF41
FLJ13590	LOC51193	NRF	TAF2B	ZNF44
FLJ22252	LOC51290	NRL	TAF2H	ZNF90
FOSB	LOC51637	PBX4	TAF2I	ZXDA
GCMA	LOC55893	PDEF	TAF2K	

Table A4-8. Utricle Laser-Neomycin Differentially Expressed Commonalities.

AF5Q31	FOG2	ILF1	LOC57209	PSMC5	TITF1
BCL11A	GCN5L1	IPEX	LOC58500	RBL2	TRIP15
BRD1	GIOT-2	IRF2	MADH7	RFX3	WHSC1
CDK7	GLI2	JUN	MAPK8IP1	SSX4	XBP1
CEBPG	HMGY	JUNB	MGC2508	TAF2B	ZNF174
CRSP6	HNF3A	KIAA0014	MLLT2	TAF2H	ZNF212
CSRP2	HNF3B	KIAA0173	MORF	TBX15	ZNF239
DEAF1	HOXA13	KIAA0395	MTF1	TBX21	ZNF79
ESR1	HOXD8	KIAA1528	MYCBP	TCF21	ZNF90
FHL1	HSAJ2425	LOC51058	NR1H3	TCF8	ZNF93
FLJ20321	HSF1	LOC51131	POU4F1	TGFB11	

Table A5-1. CEBPG siRNA Profile.

Gene ID	Fold Change	P-value	Gene Annotation
ARIX	0.7915	0.0361	aristaless homeobox
ATF4	0.8319	0.0886	activating transcription factor 4 (tax-responsive enhancer element B67)
CEBPG	0.5712	0.0132	CCAAT/enhancer binding protein (C/EBP), gamma
EIF2B2	0.7404	0.0170	eukaryotic translation initiation factor 2B, subunit 2 (beta, 39kD)
GLIS2	0.8219	0.0717	Kruppel-like zinc finger protein GLIS2
GTF2F1	0.7483	0.1120	general transcription factor IIF, polypeptide 1 (74kD subunit)
HNF3A	0.8240	0.1070	forkhead box A1
H_GS165L15	0.7295	0.0612	cAMP response element-binding protein
IPEX	0.8163	0.1052	forkhead box P3
IRX5	0.8085	0.0623	iroquois homeobox protein 5
IRX7	0.7480	0.0060	iroquois homeobox protein 7
KIAA0478	0.7527	0.0573	KIAA0478 protein
LOC51173	0.7910	0.0912	zinc finger DNA binding protein Helios
LRP5	0.7291	0.0336	low density lipoprotein receptor-related protein 5
MAD	0.5253	0.1774	MAX dimerization protein
MYBL2	0.7359	0.0112	v-myb myeloblastosis viral oncogene homolog (avian)-like 2
NR2C1	0.6584	0.0522	nuclear receptor subfamily 2, group C, member 1
NR6A1	0.6933	0.0250	nuclear receptor subfamily 6, group A, member 1
POU1F1	0.8026	0.0726	POU domain, class 1, transcription factor 1 (Pit1, growth hormone factor 1)
RARA	0.6859	0.0697	retinoic acid receptor, alpha
RBL2	0.6103	0.1085	retinoblastoma-like 2 (p130)
RING1	0.7940	0.0481	ring finger protein 1
SIX3	0.7855	0.0834	sine oculis homeobox homolog 3 (Drosophila)
SIX4	0.8225	0.1665	sine oculis homeobox (Drosophila) homolog 4
SLB	0.7903	0.0395	selective LIM binding factor
SNAPC3	0.7764	0.2820	small nuclear RNA activating complex, polypeptide 3, 50kD
SOX11	0.8153	0.0008	SRY (sex determining region Y)-box 11
SPI1	0.5775	0.0730	transcription factor SP1
SREBF1	0.6661	0.0383	sterol regulatory element binding transcription factor 1
SUPT6H	0.8022	0.1184	suppressor of Ty (S.cerevisiae) 6 homolog
TNRC12	0.7357	0.0946	E1A binding protein p400
TNRC9	0.6856	0.0420	trinucleotide repeat containing 9
TAF-172 *	0.8499		TBP-associated factor 172
TRAP150	0.8053	0.1996	thyroid hormone receptor-associated protein, 150 kDa subunit
TTF2	0.7193	0.0338	transcription termination factor, RNA polymerase II
ZIC4	0.7802	0.0141	zinc family member 4 protein HZIC4
ZNF162	0.8297	0.0517	may be Txnal corepressor
ZNF179	0.8043	0.0076	zinc finger protein 179
ZNF44	0.7883	0.0722	zinc finger protein 44
ZNF76	0.7840	0.0512	zinc finger protein 76
BLZF1	1.3028	0.0841	basic leucine zipper nuclear factor 1 (JEM-1)
DACH	1.3611	0.2223	dachshund (Drosophila) homolog
EN1	1.3126	0.0126	engrailed homolog 1

FOXM1	1.2948	0.2320	forkhead box M1
HES7	1.3174	0.0311	hairy and enhancer of split 7 (Drosophila)
HMG20B	1.2551	0.0317	high-mobility group 20B
HNF3B	1.2321	0.1336	forkhead box A2
KIAA0395	1.2955	0.2303	triple homeobox 1
LHX5	1.3134	0.1584	LIM homeobox protein 5
LMO2	1.2172	0.0747	LIM domain only 2
LOC51036	1.3136	0.0701	retinoic acid receptor-beta associated open reading frame
LOC57209	1.2419	0.1375	Kruppel-type zinc finger protein
M96	1.1960	0.0392	likely ortholog of mouse metal response element binding transcription factor 2
MYOG	1.3484	0.0090	myogenin (myogenic factor 4)
NCOA3	1.2362	0.2010	nuclear receptor coactivator 3
NFKB2	1.2457	0.0116	nuclear factor of kappa light polypeptide gene enhancer in B-cells 2 (p49/p100)
NONO	1.3453	0.1314	non-POU-domain-containing, octamer-binding
NSEP1	1.2830	0.0397	nuclease sensitive element binding protein 1
PAF65B	1.2779	0.1911	PCAF associated factor 65 beta
PPARGC1	1.2911	0.0853	peroxisome proliferative activated receptor, gamma, coactivator 1
RBBP9	1.3310	0.0150	retinoblastoma-binding protein 9
RXRA	1.2805	0.0325	retinoid X receptor, alpha
SSX3	1.2372	0.0157	synovial sarcoma, X breakpoint 3
TAF3B2	1.2389	0.2172	TATA box binding protein (TBP)-associated factor, RNA polymerase III, GTF3B subunit 2
TBX5	1.2593	0.0006	T-box 5
TEAD4	1.2374	0.0597	TEA domain family member 2 aka TEF-4
TEF	1.2048	0.0443	thyrotrophic embryonic factor
VSX1	1.2712	0.0247	visual system homeobox 1 (zebrafish) homolog (CHX10-like)
ZF5128	1.2702	0.1343	zinc finger protein
ZNF125	1.3499	0.0958	zinc finger protein of the cerebellum 4
ZNF135	1.2790	0.1682	zinc finger protein 135
ZNF165	1.3580	0.0174	zinc finger protein 165
ZNF174	1.4409	0.2423	zinc finger protein 174
ZNF184	1.3202	0.0249	zinc finger protein 184
ZNF192	1.3415	0.0169	zinc finger protein 192
ZNF193	1.2539	0.2088	zinc finger protein 193
ZNF197	1.2539	0.0335	zinc finger protein 197
ZNF200	1.3557	0.0655	zinc finger protein 200
ZNF202	1.3670	0.0274	zinc finger protein 202
ZNF214	1.2305	0.1367	zinc finger protein 214
ZNF30	1.2315	0.0732	zinc finger protein 30
ZNF31	1.3065	0.0708	zinc finger protein 31
ZNF73	1.2935	0.1489	zinc finger protein 73

* Gene did not meet cutoff, but was added in for comparison to other experiments.

Table A5-2. JUND siRNA Profile.

Gene ID	Fold Change	P-value	Gene Annotation
ATBF1	0.4575	0.0053	AT-binding transcription factor 1
ATRX	0.7622	0.2861	alpha thalassemia/mental retardation syndrome X-linked (RAD54 (S. cerevisiae) homolog)
BARX2	0.7643	0.4449	barH-like homeobox 2
BRD1	0.7183	0.9748	bromodomain-containing 1
CEBPG	0.3657	0.0012	CCAAT/enhancer binding protein (C/EBP), gamma
CHES1	0.7712	0.5542	checkpoint suppressor 1
CITED1	0.4385	0.0010	Cbp/p300-interacting transactivator, with Glu/Asp-rich carboxy-terminal domain, 1
CRSP9	0.7489	0.2674	cofactor required for Sp1 transcriptional activation, subunit 9 (33kD)
CYLD	0.5830	0.0355	cylindromatosis (turban tumor syndrome)
DAZAP1	0.7915	0.4950	DAZ associated protein 1
DEAF1	0.5459	0.0220	deformed epidermal autoregulatory factor 1 (Drosophila)
DUX2	0.7955	0.3299	double homeobox 2
EEF1D	0.7988	0.1175	eukaryotic translation elongation factor 1 delta (guanine nucleotide exchange protein)
FHL1	0.7277	0.1012	four and a half LIM domains 1
FOG2	0.7597	0.0132	friend of GATA2
FOSL1	0.7518	0.0487	FOS-like antigen 1
FOXP1	0.6463	0.3117	forkhead box P1
GBX2	0.3745	0.0122	gastrulation brain homeobox 2
H-L(3)MBT	0.6307	0.0333	lethal (3) malignant brain tumor l(3)mbt protein (Drosophila) homolog
HEYL	0.5963	0.2701	hairly/enhancer-of-split related with YRPW motif-like
HMGIC	0.7300	0.4276	high-mobility group (nonhistone chromosomal) protein isoform I-C
HNF3B	0.7780	0.1490	hepatocyte nuclear factor 3, beta
HSF1	0.5101	0.0548	heat shock transcription factor 1
ID1	0.6764	0.2081	inhibitor of DNA binding 1, dominant negative helix-loop-helix protein
IRX7	0.6758	0.1379	iroquois homeobox protein 7
KLF5	0.4237	0.1082	Kruppel-like factor 5
LAF4	0.6001	0.0634	lymphoid nuclear protein related to AF4
LHX2	0.3492	0.0025	LIM homeobox protein 2
LHX6	0.7568	0.1684	LIM homeobox protein 6
MAX	0.6874	0.0260	MAX protein
MYT2	0.7920	0.1603	myelin transcription factor 2
NEUROD6	0.5204	0.0121	neurogenic differentiation 6
NFKBIB	0.6849	0.0199	nuclear factor of kappa light polypeptide gene enhancer in B-cells inhibitor, beta
NR1I3	0.6053	0.1784	nuclear receptor subfamily 1, group I, member 3
NR6A1	0.6680	0.0046	nuclear receptor subfamily 6, group A, member 1
NUP153	0.7640	0.4361	nucleoporin 153kD
PAX1	0.6718	0.1578	paired box gene 1
PMX1	0.6014	0.0339	paired mesoderm homeo box 1
POU3F4	0.7070	0.3254	POU domain, class 3, transcription factor 4
POU4F1	0.7192	0.0244	POU domain, class 4, transcription factor 1
PRDM16	0.7957	0.0842	PR domain containing 10
PREB	0.7940	0.0691	prolactin regulatory element binding

RARA	0.6751	0.1285	retinoic acid receptor, alpha
SRY	0.7350	0.0998	sex determining region Y
TAF-172	0.7725	0.0085	TBP-associated factor 172
TAF1A	0.6834	0.4775	TATA box binding protein (TBP)-associated factor, RNA polymerase I, A, 48kD
TAF2H	0.6043	0.0183	TATA box binding protein (TBP)-associated factor, RNA polymerase II, H, 30kD
TCEB1	0.4877	0.0262	transcription elongation factor B (SIII), polypeptide 1 (15kD, elongin C)
TIEG2	0.7801	0.0115	TGFB inducible early growth response 2
TNRC5	0.4793	0.0215	trinucleotide repeat containing 5
TRAF6	0.5237	0.0592	TNF receptor-associated factor 6
TRIP6	0.7948	0.1588	thyroid hormone receptor interactor 6
TTF2	0.7347	0.1041	transcription termination factor, RNA polymerase II
ZHX1	0.7947	0.1836	zinc-fingers and homeoboxes 1
ZNF-kaiso	0.7735	0.0211	Kaiso
ZNF10	0.5319	0.0526	zinc finger protein 10 (KOX 1)
ZNF142	0.7259	0.3533	zinc finger protein 142
ZNF147	0.7659	0.1999	zinc finger protein 147 (estrogen-responsive finger protein)
ZNF174	0.5833	0.1997	zinc finger protein 174
ZNF38	0.6230	0.1289	zinc finger protein 38 (KOX 25)
ZNF44	0.7525	0.0878	zinc finger protein 44 (KOX 7)
ZNF76	0.7029	0.1350	zinc finger protein 76 (expressed in testis)
ZNF80	0.6285	0.0026	zinc finger protein 80 (pT17)
ZXDA	0.7070	0.2344	zinc finger, X-linked, duplicated A
LRP5 *	0.8757		low density lipoprotein receptor-related protein 5
JUNB *	0.8762		Jun B proto-oncogene
AR	1.2249	0.8523	androgen receptor (dihydrotestosterone receptor)
ATF4	1.2084	0.3963	activating transcription factor 4 (tax-responsive enhancer element B67)
ATF6	1.3156	0.0720	activating transcription factor 6
ATF7	1.5153	0.0471	activating transcription factor 7
BRPF3	1.2605	0.2263	bromodomain and PHD finger containing, 3
BTF3	1.2316	0.0842	basic transcription factor 3
CBX5	1.3104	0.4096	chromobox homolog 5 (Drosophila HP1 alpha)
CDX1	1.2058	0.0455	caudal-type homeobox transcription factor 1
CDX2	1.1999	0.2211	caudal-type homeobox transcription factor 2
CNOT8	1.2408	0.3543	CCR4-NOT transcription complex, subunit 8
DATF1	1.2564	0.3671	death associated transcription factor 1
DED	1.4131	0.2302	apoptosis antagonizing transcription factor
DLX1	1.2244	0.4049	distal-less homeobox 1
E2F1	1.3011	0.1117	E2F transcription factor 2
ELAVL2	1.4587	0.0646	ELAV (embryonic lethal, abnormal vision, Drosophila)-like 2
ELF1	1.7686	0.2460	E74-like factor 1 (ets domain transcription factor)
EOMES	1.2186	0.0431	eomesodermin (Xenopus laevis) homolog
ESR1	1.9466	0.0176	estrogen receptor 1
EYA1	1.2418	0.1884	eyes absent (Drosophila) homolog 1
HEY2	1.3019	0.2317	hairly/enhancer-of-split related with YRPW motif 2
HIF1A	1.2358	0.1130	hypoxia-inducible factor 1, alpha subunit (basic helix-loop-helix transcription factor)
HMGIIY	1.2351	0.0231	high-mobility group (nonhistone chromosomal) protein isoforms I and Y

HOXA4	1.2563	0.0061	homeo box A4
HOXA7	1.2404	0.0537	homeobox A7
HOXB1	1.2236	0.2507	homeobox B1
HOXD1	1.3577	0.1326	homeobox D1
HS747E2 A	1.4021	0.0289	hypothetical protein
HSAJ2425	1.3370	0.0421	transcription factor (SMIF gene)
KLF12	1.2526	0.2774	Kruppel-like factor 12
KLHL2	1.2600	0.2141	kelch (Drosophila)-like 2 (Mayven)
LDB1	1.2022	0.0735	LIM domain binding 1
LOC55885	1.3721	0.3460	neuronal specific transcription factor DAT1
LOC57209	1.9500	0.1147	Kruppel-type zinc finger protein
LOC58500	1.2810	0.2118	zinc finger protein (clone 647)
LZLP	1.3476	0.2170	leucine zipper-like protein
M96	1.2671	0.2162	putative DNA binding protein
MCM4	1.2292	0.3427	minichromosome maintenance deficient (<i>S. cerevisiae</i>) 4
MEF2B	1.3661	0.1891	MADS box transcription enhancer factor 2, polypeptide B (myocyte enhancer factor 2B)
MEIS2	1.3113	0.0086	homeobox protein MEIS2
MEIS3	1.3228	0.5193	meis1-related protein 2 aka MRG2
MEOX2	1.2570	0.0409	mesenchyme homeo box 2 (growth arrest-specific homeo box)
MYC	1.2288	0.2712	c-myc proto-oncogene
NCOA4	1.2210	0.3048	nuclear receptor coactivator 4
NFIB	1.4932	0.0322	nuclear factor I/B
NFKB2	1.4313	0.5653	nuclear factor of kappa light polypeptide gene enhancer in B-cells 2 (p49/p100)
NFKBIL1	1.2218	0.2045	nuclear factor of kappa light polypeptide gene enhancer in B-cells inhibitor-like 1
NR0B1	1.2353	0.0359	nuclear receptor subfamily 0, group B, member 1
NR1H3	1.4195	0.2325	nuclear receptor subfamily 1, group H, member 3
OAZ	1.2250	0.3807	OLF-1/EBF associated zinc finger gene
P38IP	1.2896	0.0109	transcription factor (p38 interacting protein)
PAX7	1.5752	0.0012	paired box gene 7, isoform 1
PBX3	1.2613	0.0245	pre-B-cell leukemia transcription factor 3
PGR	1.2455	0.2634	progesterone receptor
PPARD	1.4877	0.4431	peroxisome proliferative activated receptor, delta
PPARG	1.4003	0.1290	peroxisome proliferative activated receptor, gamma
PRDM1	1.3058	0.0475	positive regulatory domain I-binding factor 1; B-lymphocyte-induced maturation protein 1
PRDM2	1.3122	0.0913	PR domain containing 2, with ZNF domain
PRDM5	1.2160	0.7242	PR domain containing 5
RAI15	1.2190	0.1764	retinoic acid induced 15
RFP	1.5088	0.0771	ret finger protein
RFP2	1.4018	0.0410	ret finger protein 2
RGC32	1.2117	0.1650	RGC32 protein
SOX11	1.2509	0.1151	SRY (sex determining region Y)-box 11
SOX30	1.3288	0.1811	SRY (sex determining region Y)-box 30
SPI1	1.2275	0.9081	transcription factor SP1
SSRP1	1.2929	0.1222	structure specific recognition protein 1
SSX1	1.3934	0.1147	synovial sarcoma, X breakpoint 1
SSX2	1.2270	0.1177	synovial sarcoma, X breakpoint 2
STAT4	1.2019	0.4628	signal transducer and activator of transcription 4
TBX1	1.2470	0.1538	T-box 1

TBX21	1.2838	0.1269	T-box 21
TCF-3	1.2808	0.1406	HMG-box transcription factor 3
TCF12	1.3313	0.1933	transcription factor 12 (HTF4, helix-loop-helix transcription factors 4)
THRB	1.2107	0.0692	thyroid hormone receptor, beta (avian erythroblastic leukemia viral (v-erb-a) oncogene homolog 2)
TP53	1.2295	0.2984	tumor protein p53 (Li-Fraumeni syndrome)
ZIC3	1.2354	0.2849	Zic family member 3 (odd-paired Drosophila homolog, heterotaxy 1)
ZIC4	1.3101	0.4863	zinc family member 4 protein HZIC4
ZNF12	1.3481	0.0316	zinc finger protein 12 (KOX 3)
ZNF155	1.2607	0.2749	zinc finger protein 155 (pHZ-96)
ZNF160	1.2147	0.2311	zinc finger protein 160
ZNF162	1.2007	0.3055	may be Txnal corepressor
ZNF173	1.2064	0.3475	zinc finger protein 173
ZNF211	1.3714	0.1206	zinc finger protein 211
ZNF212	1.2235	0.4702	zinc finger protein 212
ZNF228	1.2032	0.1923	zinc finger protein 228
ZNF268	1.3173	0.2024	zinc finger protein 268
ZNF274	1.4600	0.3337	may mediate Txnal repression
ZNF278	1.2959	0.1099	zinc finger protein 278
ZNF294	1.3270	0.1628	zinc finger protein 294
ZNF306	1.2081	0.1129	zinc finger protein zfp47
ZNF37A	1.2602	0.2783	zinc finger protein; Kruppel-related protein
ZNF41	1.2940	0.2009	zinc finger protein 41
ZNF73	1.2023	0.1432	zinc finger protein 186 (Kruppel type)
ZNF75A	1.5364	0.0176	zinc finger protein 75a
ZNF93	1.2807	0.1862	zinc finger protein 93 (HTF34)

* These genes did not meet the cut-off but are listed because (1) JUNB is a potential off target and (2) LRP5 shows a slight decrease and is important for comparison to other siRNA comparisons.

Table A5-3. JNK Inhibitor Profile.

Gene ID	Fold Change	P-value	Gene Annotation
ABT1	0.7274	0.1467	activator of basal transcription 1
ARIX	0.8305	0.0910	aristaless homeobox
ATOH1	0.7432	0.0015	atonal homolog 1
BARX1	0.7417	0.1342	BarH-like homeobox 1
BCL11A	0.6140	0.0448	B-cell CLL/lymphoma 11A (zinc finger protein)
BCL11B	0.7992	0.1446	B-cell CLL/lymphoma 11B (zinc finger protein)
BLZF1	0.4949	0.1070	basic leucine zipper nuclear factor 1 (JEM-1)
BRD1	0.7123		bromodomain-containing 1
BRD4	0.4015	0.0055	bromodomain-containing 4
C21orf18	0.7776	0.2664	chromosome 21 open reading frame 18
CART1	0.8087	0.2098	cartilage paired-class homeoprotein 1
CDX1	0.7407	0.0150	caudal-type homeobox transcription factor 1
CEBPG	0.7620	0.1459	CCAAT/enhancer binding protein (C/EBP), gamma
COPEB	0.5182	0.0002	core promoter element binding protein
CREBBP	0.7975	0.0494	CREB binding protein
CREBL1	0.8122	0.1330	cAMP responsive element binding protein-like 1
CSDA	0.6422	0.0106	cold shock domain protein A
CSRP1	0.8182	0.0194	cysteine and glycine-rich protein 1
DAZAP1	0.6986		DAZ associated protein 1
DLX2	0.6829	0.0005	distal-less homeobox 2
E2F1	0.8055	0.0744	E2F transcription factor 1
EGR1	0.7376	0.1000	early growth response 1
ELF1	0.6857	0.0751	E74-like factor 1 (ets domain transcription factor)
ELF3	0.6333	0.0081	E74-like factor 3 (ets domain TF, epithelial-specific)
ETV6	0.7446	0.0448	ets variant gene 6, TEL oncogene
FHL1	0.7206		four and a half LIM domains 1
FHL2	0.6807	0.0175	four and a half LIM domains 2
FLJ11186	0.3335	0.0031	chromosome 14 open reading frame 106
FLJ125	0.7232	0.1046	hypothetical protein
FLJ14549	0.6038	0.0243	hypothetical protein FLJ14549
FMR2	0.6889	0.0023	fragile X mental retardation 2
FOXE1	0.6242	0.0154	forkhead box E1 (thyroid transcription factor 2)
FOXE2	0.8277	0.1141	forkhead box E2
FOXH1	0.5873	0.1437	forkhead box H1
GATA1	0.7987	0.0039	GATA-binding protein 1 (globin transcription factor 1)
GATA3	0.8243	0.0236	GATA-binding protein 3
GBX2	0.6435		gastrulation brain homeobox 2
GLI2	0.8041	0.0112	GLI-Kruppel family member GLI2
GRLF1	0.7656	0.0850	glucocorticoid receptor DNA binding factor 1
GTF2A1	0.6452	0.0031	general transcription factor IIA, 1 (37kD & 19kD subunits)
GTF2E2	0.7368	0.0404	general transcription factor IIE, polypeptide 2 (beta subunit)
GTF2F2	0.6863	0.0150	general transcription factor IIF, polypeptide 2 (30kD subunit)
GTF2H3	0.7005	0.0375	general transcription factor IIH, polypeptide 3 (34kD subunit)
GTF3A	0.8322	0.0115	general transcription factor IIIA
HES2	0.8116	0.0190	hairy and enhancer of split 2 (Drosophila)
HIF1A	0.8173	0.2977	hypoxia-inducible factor 1, alpha subunit
HIRA	0.7871	0.1747	HIR (histone cell cycle regulation defective,) homolog A

HIVEP2	0.7573	0.0091	human immunodeficiency virus type I enhancer-binding protein 2
HNF4A	0.8265	0.1206	hepatocyte nuclear factor 4, alpha
HOXA11	0.7880	0.2358	homeobox A11
HOXB13	0.7188	0.0197	homeobox B13
HOXB7	0.7670	0.0537	homeobox B7
HOXC6	0.8061	0.0172	homeobox C6
HOXC8	0.8112	0.0245	homeobox C8
HOXD11	0.8264	0.1256	homeobox D11
HOXD12	0.5679	0.0005	homeobox D12
HOXD9	0.7417	0.0250	homeobox D9
HRIHFB2436	0.5497	0.0007	endocrine regulator
HS747E2A	0.7583	0.0970	hypothetical protein (RING domain)
HSA275986	0.8239	0.0121	transcription factor SMIF
HSF2BP	0.7699	0.0670	heat shock transcription factor 2 binding protein
HSHPX5	0.7452	0.0023	HPX-5
IRX7	0.7431		iroquois homeobox protein 7
JUN	0.8267	0.3185	v-jun avian sarcoma virus 17 oncogene homolog
JUNB	0.6858		Jun B proto-oncogene
KIAA0161	0.7553	0.0170	likely ortholog of mouse ubiquitin conjugating enzyme 7 interacting protein 4
KIAA0478	0.8072	0.0632	KIAA0478 protein
KIAA0798	0.7534	0.1017	KIAA0798 gene product
KIAA1528	0.8228	0.0049	deltex homolog 2 (Drosophila)
LDOC1	0.7480	0.1752	leucine zipper, down-regulated in cancer 1
LOC51036	0.8194	0.0218	retinoic acid receptor-beta associated open reading frame
LOC51087	0.7555	0.0977	germ cell specific Y-box binding protein
LOC51193	0.8141	0.0811	zinc finger protein ANC_2H01
LOC51270	0.6971	0.0005	E2F-like protein
LOC51290	0.7874	0.1382	CDA14
LOC55893	0.7595	0.0302	papillomavirus regulatory factor PRF-1
LRP5	0.6561		low density lipoprotein receptor-related protein 5
M96	0.6894	0.0607	likely ortholog of mouse metal response element binding transcription factor 2
MAPK8IP1	0.7504	0.0009	mitogen-activated protein kinase 8 interacting protein 1
MDS032	0.7492	0.0358	uncharacterized hematopoietic stem/progenitor cells protein MDS032
MED6	0.7994	0.0606	mediator of RNA polymerase II transcription, subunit 6
MEF2A	0.6718	0.0056	MADS box transcription enhancer factor 2, polypeptide A (myocyte enhancer factor 2A)
MEF2D	0.7647	0.0034	MADS box transcription enhancer factor 2, polypeptide D (myocyte enhancer factor 2D)
MLLT6	0.8169	0.0029	myeloid/lymphoid or mixed-lineage leukemia; translocated to 6
MYC	0.7181	0.0794	v-myc myelocytomatosis viral oncogene homolog (avian)
MYF5	0.7623	0.0005	myogenic factor 5
MYT2	0.6692		myelin transcription factor 2
NCOA3	0.7951	0.1199	nuclear receptor coactivator 3
NEUROD6	0.7679		neurogenic differentiation 6
NFIA	0.6079	0.0127	nuclear factor I/A
NFKB2	0.7379	0.0064	nuclear factor of kappa light polypeptide gene enhancer in B-cells 2 (p49/p100)
NR2E1	0.3774	0.0036	nuclear receptor subfamily 2, group E, member 1
NR2E3	0.7961	0.0571	nuclear receptor subfamily 2, group E, member 3

NR4A1	0.8013	0.0183	nuclear receptor subfamily 4, group A, member 1
P38IP	0.8285	0.0759	transcription factor (p38 interacting protein)
PAX1	0.8215	0.0883	paired box gene 1
PAX4	0.7296	0.0420	paired box gene 4
PHTF1	0.8305	0.0838	putative homeodomain transcription factor
PMX1	0.8142	0.0132	paired mesoderm homeo box 1
POU3F2	0.7978	0.0090	POU domain, class 3, transcription factor 2
POU5F1	0.8310	0.3282	POU domain, class 5, transcription factor 1
PRDM16	0.6946		PR domain containing 16
PREB	0.7659	0.0306	prolactin regulatory element binding
PROC	0.7611		protein C (inactivator of coagulation factors Va and VIIIa)
RARA	0.7570		retinoic acid receptor, alpha
RB1	0.7952	0.1100	retinoblastoma 1 (including osteosarcoma)
RNF10	0.7255	0.2588	ring finger protein 10
RNF15	0.7794	0.0088	ring finger protein 15
SIX1	0.8214	0.1050	sine oculis homeobox homolog 1 (Drosophila)
SNAPC4	0.8067	0.1564	small nuclear RNA activating complex, polypeptide 4,
SRY	0.5753	0.0023	sex determining region Y
TAF-172	0.7571	0.0931	BTAF1 RNA polymerase II, B-TFIID transcription factor-associated
TAF2H	0.6988		TATA box binding protein (TBP)-associated factor, RNA polymerase II, H
TBX15	0.7793	0.0147	T-box 15
TCFL1	0.6915	0.0140	transcription factor-like 1
TCFL5	0.7246	0.0396	transcription factor-like 5 (basic helix-loop-helix)
TEAD3	0.7372	0.0268	TEA domain family member 3
TNRC9	0.7971	0.0811	trinucleotide repeat containing 9
UBTF	0.6815	0.0002	upstream binding transcription factor, RNA polymerase I
ZFY	0.7807	0.0344	zinc finger protein, Y-linked
ZID	0.7884	0.1656	zinc finger protein with interaction domain
ZNF212	0.8219	0.0336	zinc finger protein 212
ZNF286	0.7934	0.2040	zinc finger protein 286
ZNF44	0.6739	0.0043	zinc finger protein 44 (KOX 7)
ZNF79	0.6225	0.0221	zinc finger protein 79 (pT7)
ZNF92	0.7837	0.0264	zinc finger protein 92 (HTF12)
ZNF93	0.7494	0.0672	zinc finger protein 93 (HTF34)
AF5Q31	2.0474	0.0018	ALL1 fused gene from 5q31
AR	1.2219	0.1342	androgen receptor (dihydrotestosterone receptor)
BAPX1	4.1942	0.0004	bagpipe homeobox (Drosophila) homolog 1
BHLHB3	2.3401	0.0002	basic helix-loop-helix domain containing, class B, 3
CBX4	1.4381	0.0119	chromobox homolog 4 (Drosophila Pc class)
CHES1	1.2411	0.0571	checkpoint suppressor 1
CITED1	1.8217	0.0016	Cbp/p300-interacting transactivator, with Glu/Asp-rich carboxy-terminal domain, 1
CROC4	1.2047	0.1696	transcriptional activator of the c-fos promoter
CSRP2	1.4438	0.0072	cysteine and glycine-rich protein 2
CUTL1	1.4946	0.0319	cut (Drosophila)-like 1 (CCAAT displacement protein)
DLX3	1.3874	0.0504	distal-less homeobox 3
E2F5	1.2441	0.1442	E2F transcription factor 5, p130-binding
ERF	1.2397	0.1802	Ets2 repressor factor
FLJ10298	1.2017	0.0342	hypothetical protein FLJ10298
FLJ11191	1.2044	0.2789	hypothetical protein FLJ11191
FLJ13659	2.6882	0.0000	hypothetical protein FLJ13659

FOG2	1.2901	0.0005	friend of GATA2
FOSB	1.3037	0.0025	FBJ murine osteosarcoma viral oncogene homolog B
FOXO3A	1.4111	0.0187	forkhead box O3A
GTF2F1	1.2986	0.0112	general transcription factor IIF, polypeptide 1 (74kD subunit)
GTF2H4	1.2810	0.0572	general transcription factor IIH, polypeptide 4 (52kD subunit)
HES7	1.3254	0.0167	hairy and enhancer of split 7 (Drosophila)
HLXB9	2.9249	0.0002	homeo box HB9
HNF3A	1.5346	0.0987	forkhead box A1
HNF3B	1.4838	0.0028	forkhead box A2
HOXA3	1.4433	0.0077	homeobox A3
HOXA5	1.2952	0.0129	homeobox A5
HOXA6	1.2746	0.0667	homeobox A6
HOXB6	1.5564	0.0352	homeobox B6
HOXB8	1.4677	0.0013	homeobox B8
HOXD8	1.3583	0.0185	homeobox D8
HRIHFB2122	1.6647	0.0002	Tara-like protein (Drosophila)
HSAJ2425	1.3633	0.0356	p65 protein
HSF1	1.3924	0.1268	heat shock transcription factor 1
HSPC189	1.1994	0.0313	HSPC189 protein
IRF6	1.2336	0.0677	interferon regulatory factor 6
KIAA0130	1.4508	0.0022	thyroid hormone receptor-associated protein, 100 kDa
KIAA0244	1.2167	0.0646	PHD finger protein 3
KIAA0293	1.4715	0.0017	cut-like 2 (Drosophila)
KIAA0306	1.2923	0.0003	capicua homolog (Drosophila)
KLF5	1.3190	0.2740	Kruppel-like factor 5 (intestinal)
LMX1B	1.9164	0.0001	LIM homeobox transcription factor 1, beta
MADH6	1.5716	0.0289	MAD, mothers against decapentaplegic homolog 6
MAFK	1.2018	0.0943	v-maf musculoaponeurotic fibrosarcoma oncogene family, protein K (avian)
MAX	1.4441	0.0010	MAX protein
MHC2TA	3.1476	0.0000	MHC class II transactivator
MNT	1.3232	0.1076	MAX binding protein
MTF1	1.3363	0.2090	metal-regulatory transcription factor 1
MYB	1.2024	0.3226	v-myb myeloblastosis viral oncogene homolog (avian)
MYBL1	1.3853	0.0029	v-myb myeloblastosis viral oncogene homolog (avian)-like 1
MYCN	1.2044	0.1913	v-myc myelocytomatosis viral related oncogene, neuroblastoma derived (avian)
MYT1L	1.2057	0.3442	myelin transcription factor 1-like
NEUROD4	1.3234	0.1390	neurogenic differentiation 4
NFKBIB	1.4357	0.0004	nuclear factor of kappa light polypeptide gene enhancer in B-cells inhibitor, beta
NHLH2	1.2274	0.2210	nescient helix loop helix 2
NKX2B	1.2271	0.0139	NK2 transcription factor related, locus 2 (Drosophila)
NR1I3	1.5821	0.0216	nuclear receptor subfamily 1, group I, member 3
NR3C2	1.2806	0.0147	nuclear receptor subfamily 3, group C, member 2
NR5A1	1.2864	0.2459	nuclear receptor subfamily 5, group A, member 1
OCT11	1.2063	0.0660	POU domain, class 2, transcription factor 3
ONECUT2	1.2188	0.0070	one cut domain, family member 2
PAX6	1.2382	0.0313	paired box gene 6 (aniridia, keratitis)
PER1	1.3376	0.2337	period homolog 1 (Drosophila)
PGR	3.1773	0.0019	progesterone receptor

POU2AF1	1.3992	0.0019	POU domain, class 2, associating factor 1
POU3F4	1.2155	0.0207	POU domain, class 3, transcription factor 4
POU4F2	1.2073	0.0918	POU domain, class 4, transcription factor 2
PRDM15	1.2129	0.0390	PR domain containing 15
PROP1	1.2345	0.0602	prophet of Pit1, paired-like homeodomain transcription factor
RNF24	1.2204	0.0485	ring finger protein 24
RREB1	1.2929	0.0567	ras responsive element binding protein 1
SAP30	1.2612	0.0665	sin3-associated polypeptide, 30kD
SCML2	1.2101	0.1133	sex comb on midleg-like 2 (Drosophila)
STAT1	1.3781	0.0152	signal transducer and activator of transcription 1, 91kDa
STAT2	1.2401	0.1082	signal transducer and activator of transcription 2, 113kDa
TAF2C1	1.6520	0.0005	TAF4 RNA polymerase II, (TBP)-associated factor
TAL2	1.2648	0.0574	T-cell acute lymphocytic leukemia 2
TCF17	1.2218	0.1615	zinc finger protein 354A
TCF2	1.2064	0.2923	transcription factor 2, hepatic; LF-B3;
TEL2	1.5012	0.0016	ets transcription factor TEL2
TFAP4	1.2065	0.0943	transcription factor AP-4 (activating enhancer binding protein 4)
THRA	1.2020	0.0728	thyroid hormone receptor, alpha
TIEG2	1.3265	0.0032	TGFB inducible early growth response 2
TRIP6	1.4745	0.0240	thyroid hormone receptor interactor 6
TZFP	1.7017	0.0313	testis zinc finger protein
USF2	1.2021	0.3106	upstream transcription factor 2, c-fos interacting
VENTX2	1.4963	0.0008	VENT-like homeobox 2
XBP1	2.1037	0.0172	X-box binding protein 1
YAF2	1.3955	0.0021	YY1 associated factor 2
ZF5128	1.2533	0.0181	zinc finger protein
ZFPL1	1.2479	0.0086	zinc finger protein-like 1
ZNF142	1.3880	0.0384	zinc finger protein 142 (clone pHZ-49)
ZNF144	1.2237	0.1094	zinc finger protein 144 (Mel-18)
ZNF147	1.5345	0.0107	zinc finger protein 147 (estrogen-responsive finger protein)
ZNF155	1.2101	0.1829	zinc finger protein 155 (pHZ-96)
ZNF162	1.3438	0.0813	splicing factor 1
ZNF174	1.2822	0.1634	zinc finger protein 174
ZNF207	1.2598	0.2283	zinc finger protein 207
ZNF216	1.2557	0.0288	zinc finger protein 216
ZNF219	1.3022	0.1623	zinc finger protein 219
ZNF225	1.2220	0.2076	zinc finger protein 225
ZNF239	1.2739	0.0300	zinc finger protein 239
ZNF259	1.3213	0.0447	zinc finger protein 259
ZNF261	1.1995	0.0447	zinc finger protein 261
ZNF288	1.1990	0.2924	zinc finger protein 288
ZNF38	1.8372	0.0017	zinc finger protein 38
ZNF6	1.6927	0.0011	zinc finger protein 6 (CMPX1)
ZNF8	1.2199	0.1054	zinc-finger protein 8 (clone HF.18)
ZNF80	1.4028	0.0025	zinc finger protein 80 (pT17)
ZNF81	1.3220	0.1084	zinc finger protein 81 (HFZ20)
ZNF83	1.3824	0.0135	zinc finger protein 83 (HPF1)
ZXDA	1.3909	0.0773	zinc finger, X-linked, duplicated A
ZXDA/B	1.2279	0.0773	zinc finger, X-linked, duplicated B

REFERENCES

- Adam, J., Myat, A., Le Roux, I., Eddison, M., Henrique, D., Ish-Horowicz, D. and Lewis, J. (1998) Cell fate choices and the expression of Notch, Delta and Serrate homologues in the chick inner ear: parallels with *Drosophila* sense-organ development. *Development*, **125**, 4645-4654.
- Ahmed, Z.M., Riazuddin, S., Bernstein, S.L., Ahmed, Z., Khan, S., Griffith, A.J., Morell, R.J., Friedman, T.B., Riazuddin, S. and Wilcox, E.R. (2001) Mutations of the protocadherin gene PCDH15 cause Usher syndrome type 1F. *Am J Hum Genet*, **69**, 25-34.
- Akoulitchchev, S., and Reinberg, D. (1998) The molecular mechanism of mitotic inhibition of TFIIH is mediated by phosphorylation of CDK7. *Genes Dev.* **12**, 3541-3550.
- Alagramam, K.N., Yuan, H., Kuehn, M.H., Murcia, C.L., Wayne, S., Srisailpathy, C.R., Lowry, R.B., Knaus, R., Van Laer, L., Bernier, F.P., Schwartz, S., Lee, C., Morton, C.C., Mullins, R.F., Ramesh, A., Van Camp, G., Hageman, G.S., Woychik, R.P., Smith, R.J., and Hageman, G.S. (2001) Mutations in the novel protocadherin PCDH15 cause Usher syndrome type 1F. *Hum Mol Genet*, **10**, 1709-1718.
- Aoki, H., Hayashi, J., Moriyama, M., Arakawa, Y., and Hino, O. (2000) Hepatitis C virus core protein interacts with 14-3-3 protein and activates the kinase Raf-1. *J Virology*, **74**, 1736-1741.
- Badea, T.C., Niculescu, F.I., Soane, L., Shin, M.L., and Rus, H. (1998) Molecular cloning and characterization of RGC-32, a novel gene induced by complement activation in oligodendrocytes. *J Biol Chem*, **273**, 26977-26981.
- Balak, K.J., Corwin, J.T., and Jones, J.E. (1990) Regenerated hair cells can originate from supporting cell progeny: evidence from phototoxicity and laser ablation experiments in the lateral line system. *J Neurosci*, **10**, 2502-2512.
- Ben-Yosef, T., Belyantseva, I.A., Saunders, T.L., Hughes, E.D., Kawamoto, K., Van Itallie, C.M., Beyer, L.A., Halsey, K., Gardner, D.J., Wilcox, E.R., Rasmussen, J., Anderson, J.M., Dolan, D.F., Forge, A., Raphael, Y., Camper, S.A., and Friedman, T.B. (2003) Claudin 14 knockout mice, a model for autosomal recessive deafness DFNB29, are deaf due to cochlear hair cell degeneration. *Hum Mol Genet*, **12**, 2049-2061.
- Bermingham, N.A., Hassan, B.A., Price, S.D., Vollrath, M.A., Ben-Arie, N., Eatock, R.A., Bellen, H.J., Lysakowski, A., and Zoghbi, H. (1999) *Math1*: An essential gene for the generation of inner ear hair cells. *Science*, **284**, 1837-1841.
- Bermingham, N.A., Hassan, B.A., Wang, V.Y., Fernandez, M., Banfi, S., Bellen, H.J., Fritsch, B., and Zoghbi, H.Y. (2001) Proprioceptor pathway development is dependent on MATH1. *Neuron*, **30**, 411-422.

- Bermingham-McDonogh, O., Stone, J.S., Reh, T.A., and Rubel, E.W. (2001) FGFR3 expression during development and regeneration of the chick inner ear sensory epithelia. *Dev Biol*, **238**, 247-259.
- Bernstein, E., Caudy, A.A., Hammond, S.M., and Hannon, G.J. (2001) Role for a bidentate ribonuclease in the initiation step of RNA interference. *Nature*, **409**, 363-366.
- Bitner-Glindzicz, M., Lindley, K.J., Rutland, P., Blaydon, D., Smith, V.V., Milla, P.J., Hussain, K., Furth-Lavi, J., Cosgrove, K.E., Shepherd, R.M., Barnes, P.D., O'Brien, R.E., Farndon, P.A., Sowden, J., Liu, X.Z., Scanlan, M.J., Malcolm, S., Dunne, M.J., Aynsley-Green, A., and Glaser, B. (2000) A recessive contiguous gene deletion causing infantile hyperinsulinism, enteropathy and deafness identifies the Usher type 1C gene. *Nat Genet*, **26**, 56-60.
- Blackshaw, S., Fraioli, R.E., Furukawa, T., and Cepko, C.L. (2001) Comprehensive analysis of photoreceptor gene expression and the identification of candidate retinal disease genes. *Cell*, **107**, 579-589.
- Boeda, B., El-Amraoui, A., Bahloul, A., Goodyear, R., Daviet, L., Blanchard, S., Perfettini, I., Fath, K.R., Shorte, S., Reiners, J., Houdusse, A., Legrain, P., Wolfrum, U., Richardson, G., and Petit, C. (2002) Myosin VIIa, harmonin and cadherin 23, three Usher I gene products that cooperate to shape the sensory hair cell bundle. *EMBO J*, **21**, 6689-6699.
- Bolouri, H. and Davidson, E.H. (2003) Transcriptional regulatory cascades in development: initial rates, not steady state, determine network kinetics. *Proc Natl Acad Sci USA*. **100**, 9371-9376.
- Bolz, H., von Brederlow, B., Ramirez, A., Bryda, E.C., Kutsche, K., Nothwang, H.G., Seeliger, M., del C-Salcedo, Cabrera, M., Vila, M.C., Molina, O.P., Gal, A., and Kubisch, C. (2001) Mutation of CDH23, encoding a new member of the cadherin gene family, causes Usher syndrome type 1D. *Nat Genet*, **27**, 108-112.
- Bonaldo, M.F., Lennon, G., and Soares, M.B. (1996) Normalization and subtraction: two approaches to facilitate gene discovery. *Genome Res*, **6**, 791-806.
- Bonnin, M.A., Edom-Vovard, F., Kefalas, P., and Duprez, D. (2002) CRP2 transcript expression pattern in embryonic chick limb. *Mech Dev*, **116**, 151-155.
- Bork, J.M., Peters, L.M., Riazuddin, S., Bernstein, S.L., Ahmed, Z.M., Ness, S.L., Polomeno, R., Ramesh, A., Schloss, M., Srisailpathy, C.R., Wayne, S., Bellman, S., Desmukh, D., Ahmed, Z., Khan, S.N., Kaloustian, V.M., Li, X.C., Lalwani, A., Riazuddin, S., Bitner-Glindzicz, M., Nance, W.E., Liu, X.Z., Wistow, G., Smith, R.J., Griffith, A.J., Wilcox, E.R., Friedman, T.B., and Morell, R.J. (2001) Usher syndrome 1D and nonsyndromic autosomal recessive deafness DFNB12 are caused by allelic mutations of the novel cadherin-like gene CDH23. *Am J Hum Genet*, **68**, 26-37.

- Bouchard, M., Pfeffer, P., and Busslinger, M. (2000) Functional equivalence of the transcription factors Pax2 and Pax5 in mouse development. *Development*, **127**, 3703-3713.
- Bryant, J., Goodyear, R.J., and Richardson, G.P. (2002) Sensory organ development in the inner ear: molecular and cellular mechanisms. *Br Med Bull*, **63**, 39-57.
- Burton, Q., Cole, L.K., Mulheisen, M., Chang, W., and Wu, D.K. (2004) The role of Pax2 in mouse inner ear development. *Dev Biol*, **272**, 161-175.
- Busca, R. and Ballotti, R. (2000) Cyclic AMP a key messenger in the regulation of skin pigmentation. *Pigment Cell Res*, **13**, 60-69.
- Cable, J. and Steel, K.P. (1991) Identification of two types of melanocytes within the stria vascularis of the mouse inner ear. *Pigment Cell Research*, **4**, 87-101.
- Cai, Y., Lechner, M.S., Nihalani, D., Prindle, M.J., Holzman, L.B., Dressler, G.R. (2002) Phosphorylation of Pax2 by the c-Jun N-terminal kinase and enhanced Pax2-dependent transcription activation. *J Biol Chem*, **277**, 1217-1222.
- Carreira, S., Liu, B., and Goding, C.R. (2000) The gene encoding the T-box factor Tbx2 is a target for the Microphthalmia-associated transcription factor in melanocytes. *J Biol Chem*, **275**, 21920-21927.
- Chen, P. and Segil, N. (1999) p27^{Kip1} links cell proliferation to morphogenesis in the developing organ of Corti. *Development*, **126**, 1581-1590.
- Chen, Z-Y. and Corey, D.P. (2002a) Understanding inner ear development with gene expression profiling. *J Neurobiol*, **53**, 276-285.
- Chen, Z-Y. and Corey, D.P. (2002b) An inner ear gene expression database. *J Assoc Res Otolaryngol*, **3**, 140-148.
- Chen, P., Zindy, F., Abdala, C., Liu, F., Li, X., Roussel, M.F., and Segil, N. (2003) Progressive hearing loss in mice lacking the cyclin-dependent kinase inhibitor Ink4d. *Nat Cell Biol*, **5**, 422-426.
- Chen, H., Chung, S., and Sukumar, S. (2004) HOXA5-induced apoptosis in breast cancer cells is mediated by caspases 2 and 8. *Mol Cell Biol*, **24**, 924-935.
- Chiba, S., Takeshita, K., Imai, Y., Kumano, K., Kurokawa, M., Masuda, S., Shimizu, K., Nakamura, S., Ruddle, F.H., and Hirai, H. (2003) Homeoprotein DLX-1 interacts with Smad4 and blocks a signaling pathway from activin A in hematopoietic cells. *Proc Natl Acad Sci USA*, **100**, 15577-15582.
- Cohen-Salmon, M., Ott, T., Michel, V., Hardelin, J.P., Perfettini, I., Eybalin, M., Wu, T., Marcus, D.C., Wangemann, P., Willecke, K., and Petit, C. (2002) Targeted ablation of

- connexin26 in the inner ear epithelial gap junction network causes hearing impairment and cell death. *Curr Biol*, **12**, 1106-1111.
- Corwin, J.T. and Cotanche, D.A. (1988) Regeneration of sensory hair cells after acoustic trauma. *Science*, **240**, 1772-1774.
- Cotanche, D.A. (1987) Regeneration of hair cell stereociliary bundles in the chick cochlea following severe acoustic trauma. *Hear Res*, **30**, 181-194.
- Couillard, M., Guillaume, R., Tangy, N., D'Amato, V., and Strudel, M. (2002) c-myc-induced apoptosis in polycystic kidney disease is independent of Falsifies interaction. *Cancer Res*, **62**, 2210-2214.
- Cruz, R.M., Lambert, P.R. and Rubel, E.W. (1987) Light microscopic evidence of hair cell regeneration after gentamicin toxicity in the chick cochlea. *Arch Otolaryngol* **113**, 1058-1062.
- Curtin, J.A., Quaint, E., Stupor, V., Ark ell, R.M., Cataract, B., Cop, A.J., Henderson, D.J., Spur, N., Stonier, P., Fisher, E.M., Nolan, P.M., Steel, K.P., Brown, S.D.M., Gray, I.C., and Murdoch, J.N. (2003) Mutation of *Celsr1* disrupts planar polarity of inner ear hair cells and causes severe neural tube defects in the mouse. *Curr Biol*, **13**, 1129-1133.
- Dabdoub, A., Donohue, M.J., Brennan, A., Wolf, V., Montcouquiol, M., Sassoon, D.A., Sheikh, J-C., Rubin, J.S., Salinas, P.C., and Kelley, M.W. (2003) Wnt signaling mediates reorientation of outer hair cell stereociliary bundles in the mammalian cochlea. *Development*, **130**, 2375-2384.
- Davies, A.C., eds. Littman, M.E. and Haggard, M.P. (1993) Hearing disorders in the population: first phase findings of the MRC National Study of Hearing. *Hearing Science and Hearing Disorders*. Academic Press, New York.
- Davydov, I.V., Bachmann, D., Kramer, P.H., and Li-Weber, M. (1995) Cloning of the cDNA encoding human C/EBP gamma, a protein binding to the PRE-I enhancer element of the human interleukin-4 promoter. *Gene*, **161**, 271-275.
- Denissova, N.G. and Liu, F. (2004) Repression of endogenous Smad7 by Ski. *J Biol Chem*, **279**, 28143-28148.
- Dhakshinamoorthy, S. and Jaiswal, A.K. (2000) Small Maf (Magi and Mark) proteins negatively regulate antioxidant response element-mediated expression and antioxidant induction of the NAD(P)H:quinone oxidoreductase1 gene. *J Biol Chem*, **275**, 40134-40141.
- Di Palma, F., Holme, R.H., Bryda, E.C., Belyantseva, I.A., Pellegrino, R., Kachar, B., Steel, K.P. and Noben-Trauth, K. (2001) Mutations in *Cdh23*, encoding a new type of cadherin,

- cause stereocilia disorganization in waltzer, the mouse model for Usher syndrome type 1D. *Nat Genet*, **27**, 103-107.
- Di Palma, T., Nitsch, R., Mascia, A., Nitsch, L., Di Lauro, R., and Zannini, M. (2003) The paired domain-containing factor Pax8 and the homeodomain-containing factor TTF-1 directly interact and synergistically activate transcription. *J Biol Chem*, **278**, 3395-3402.
- Domingos, P.M., Mlodzik, M., Mendes, C.S., Brown, S., Steller, H., and Mollereau, B. (2004) Spalt transcription factors are required for R3/R4 specification and establishment of planar cell polarity in the *Drosophila* eye. *Development*, **131**, 5695-5702.
- Dowdy, S.C., Mariani, A., and Janknecht, R. (2003) HER2/Neu- and TAK1-mediated up-regulation of the transforming growth factor beta inhibitor Smad7 via the ETS protein ER81. *J Biol Chem*, **278**, 44377-44384.
- Ebert, P.J., Timmer, J.R., Nakada, Y., Helms, A.W., Parab, P.B., Liu, Y., Hunsaker, T.L., and Johnson, J.E. (2003) Zic1 represses Math1 expression via interactions with the Math1 enhancer and modulation of Math1 autoregulation. *Development*, **130**, 1949-1959.
- Elbashir, S.M., Lendeckel, W., and Tuschl, T. (2001a) RNA interference is mediated by 21- and 22-nucleotide RNAs. *Genes Dev*, **15**, 188-200.
- Elbashir, S.M., Harborth, J., Lendeckel, W., Yalcin, A., Weber, K., and Tuschl, T. (2001b) Duplexes of 21-nucleotide RNAs mediate RNA interference in cultured mammalian cells. *Nature*, **411**, 494-498.
- Ellenrieder, V., Buck, A., Harth, A., Jungert, K., Buchholz, M., Adler, G., Urrutia, R., and Gress, T.M. (2004) KLF11 mediates a critical mechanism in TGF-beta signaling that is inactivated by Erk-MAPK in pancreatic cancer cells. *Gastroenterology*, **127**, 607-620.
- Endege, W.O., Steinmann, K.E., Boardman, L.A., Thibodeau S.N., and Schlegel, R. (1999) Representative cDNA libraries and their utility in gene expression profiling. *Biotechniques*, **26**, 542-550.
- Enomoto, Y., Enomoto, K., Kitamura, T., and Kanda, T. (2004) Keratinocyte-specific POU transcription factor hSkN-1a represses the growth of cervical cancer cell lines. *Oncogene*, **23**, 5014-5022.
- Erkman, L., McEvilly, R.J., Luo, L., Ryan, A.K., Hooshmand, F., O'Connell, S.M., Keithley, E.M., Rapaport, D.H., Ryan, A.F., and Rosenfeld M.G. (1996) Role of transcription factors Brn-3.1 and Brn-3.2 in auditory and visual system development. *Nature*, **381**, 603-606.
- Estivill, X., Fortina, P., Surrey, S., Rabionet, R., Melchionda, S., D'Agruma, L., Mansfield, E., Rappaport, E., Govea, N., Mila, M., Zelante, L., and Gasparini, P. (1998) Connexin-26 mutations in sporadic and inherited sensorineural deafness. *Lancet*, **351**, 394-398.

- Eudy, J.D., Weston, M.D., Yao, S., Hoover, D.M., Rehm, H.L., Ma-Edmonds, M., Yan, D., Ahmad, I., Cheng, J.J., Ayuso, C., Cremers, C., Davenport, S., Moller, C., Talmadge, C.B., Beisel, K.W., Tamayo, M., Morton, C.C., Swaroop, A., Kimberling, W.J., and Sumegi, J. (1998) Mutation of a gene encoding a protein with extracellular matrix motifs in Usher syndrome type IIa. *Science*, **280**, 1753-1757.
- Fantini, M.C., Becker, C., Monteleone, G., Pallone, F., Galle, P.R., and Neurath, M.F. (2004) Cutting edge: TGF-beta induces a regulatory phenotype in CD4+CD25- T cells through Foxp3 induction and down-regulation of Smad7. *J Immunol*, **172**, 5149-5153.
- Farrell, E.R. and Munsterberg, A.E. (2000) *csal1* is controlled by a combination of FGF and Wnt signals in developing limb buds. *Dev Biol*, **225**, 447-458.
- Fekete, D.M., Muthukumar, S., and Karagogeos, D. (1998) Hair cells and supporting cells share a common progenitor in the avian inner ear. *J Neurosci*, **18**, 7811-7821.
- Feo, S., Arcuri, D., Piddini, E., Passantino, R., and Giallongo, A. (2000) ENO1 gene product binds to the c-myc promoter and acts as a transcriptional repressor: relationship with Myc promoter-binding protein 1 (MBP-1). *FEBS*, **473**, 47-52.
- Ferrigno, O., Lallemand, F., Verrecchia, F., L'Hoste, S., Camonis, J., Atfi, A., and Mauviel, A. (2002) Yes-associated protein (YAP65) interacts with Smad7 and potentiates its inhibitory activity against TGF-beta/Smad signaling. *Oncogene*, **21**, 4879-4884.
- Forge, A., Li, L., Corwin, J.T., and Nevill G. (1993) Ultrastructural evidence for hair cell regeneration in the mammalian inner ear. *Science*, **259**, 1616-1619.
- Fujita, M., Kiyono, T., Hayashi, Y., and Ishibashi, M. (1996) hCDC47, a human member of the MCM family. Dissociation of the nucleus-bound form during S phase. *J Biol Chem*, **271**, 4349-4354.
- Fujita, N., Sato, S., Katayama, K., and Tsuruo, T. (2002) Akt-dependent phosphorylation of p27Kip1 promotes binding to 14-3-3 and cytoplasmic localization. *J Biol Chem*, **277**, 28706-28713.
- Fujitani, M., Yamagishi, S., Che, Y.H., Hata, K., Kubo, T., Ino, H., Tohyama, M., and Yamashita, T. (2004) P311 accelerates nerve regeneration of the axotomized facial nerve. *J Neurochem*, **91**, 737-744.
- Galibert, M.D., Yavuzer, U., Dexter, T.J., and Goding, C.R. (1999) Pax3 and regulation of the melanocyte –specific tyrosinase-related protein-1 promoter. *J Biol Chem*, **274**, 26894-26900.

- Gazit, R., Krizhanovsky, V., and Ben-Arie, N. (2004) Math1 controls cerebellar granule cell differentiation by regulating multiple components of the Notch signaling pathway. *Development*, **131**, 903-913.
- Geissler, E.N., Ryan, M.A., and Housman, D.E. (1988) The dominant-white spotting (W) locus of the mouse encodes the c-kit proto-oncogene. *Cell*, **55**, 185-192.
- Geloc, G.S. and Holt, J.R. (2003) Developmental acquisition of sensory transduction in hair cells of the mouse inner ear. *Nat Neurosci*, **6**, 1019-1020.
- Gibson-Brown, J.J., Agulnik, S.I., Silver, L.M., and Papaioannou, V.E. (1998) Expression of T-box genes Tbx2-Tbx5 during chick organogenesis. *Mech Dev*, **74**, 165-169.
- Goodyear, R.J., Gates, R., Lukashkin, A.N., and Richardson, G.P. (1999) Hair cell numbers continue to increase in the utricular macula of the early posthatch chick. *J Neurocytol*, **28**, 851-861.
- Gupta, S., Campbell, D., Derijard, B., and Davis, R.J. (1995) Transcription factor ATF2 regulation by the JNK signal transduction pathway. *Science*, **267**, 389-393.
- Haddon, C., Jiang, Y.J., Smithers, L., and Lewis, J. (1998) Delta-Notch signalling and the patterning of sensory cell differentiation in the zebrafish ear: evidence from the mind bomb mutant. *Development*, **125**, 4637-4644.
- Halmos, B., Basseres, D.S., Monti, S., D'Alo, F., Dayaram, T., Ferenczi, K., Wouters, B.J., Huettner, C.S., Golub, T.R., and Tenen, D.G. (2004) A transcriptional profiling study of CCAAT/enhancer binding protein targets identifies hepatocyte nuclear factor 3 beta as a novel tumor suppressor in lung cancer. *Cancer Res*, **64**, 4137-4147.
- Hawkins, R.D., Bashirades, S., Helms, C.A., Hu, L., Saccone, N.L., Warchol, M.E., and Lovett, M. (2003) Gene expression differences in quiescent versus regenerating hair cells of avian sensory epithelia: implications for human hearing and balance disorders. *Hum Mol Genet*, **12**, 1261-1272.
- Heanue, T.A., Davis, R.J., Rowitch, D.H., Kispert, A., McMahon, A.P., Mardon, G., and Tabin, C.J. (2002) Dach1, a vertebrate homologue of *Drosophila* dachshund, is expressed in the developing eye and ear of both chick and mouse and is regulated independently of Pax and Eya genes. *Mech Dev*, **111**, 75-87.
- Helms, A.W., Abney, A.L., Ben-Arie, N., Zoghbi, H.Y., and Johnson, J.E. (2000) Autoregulation and multiple enhancers control Math1 expression in the developing nervous system. *Development*, **127**, 1185-1196.
- Henrique, D., Adam J., Myat, A., Chitnis, A., Lewis, J., and Ish-Horowicz, D. (1995) Expression of a Delta homologue in prospective neurons in the chick. *Nature*, **375**, 787-790.

- Hertzano, R., Montcouquiol, M., Rashi-Elkeles, S., Elkon, R., Yucel, R., Frankel, W.N., Rechavi, G., Moroy, T., Friedman, T.B., Kelley, M.W., and Avraham, K.B. (2004) Transcription profiling of inner ears from Pou4f3(ddl/ddl) identifies Gfi1 as a target of the Pou4f3 deafness gene. *Hum Mol Genet*, **13**, 2143-2153.
- Hillier, L.W., Miller W., Birney, E., Warren, W., Hardison, R.C., Ponting, C.P., Bork, P., Burt, D.W., Groenen, M.A., Delany, M.E., et al., International Chicken Genome Sequencing Consortium. (2004) Sequence and comparative analysis of the chicken genome provide unique perspectives on vertebrate evolution. *Nature*, **432**, 695-716.
- Hirai, H. and Sherr, C.J. (1996) Interaction of D-type cyclins with a novel myb-like transcription factor, DMP1. *Mol Cell Biol*, **16**, 6457-6467.
- Holme, R.H., Kiernan, B.W., Brown, S.D.M., and Steel, K.P. (2002) Elongation of hair cell stereocilia is defective in the mouse mutant whirler. *J Comp Neurol*, **450**, 94-102.
- Hone, S.W. and Smith, R.J.H. (2001) Genetics of hearing impairment. *Semin Neonatal*, **6**, 531-541.
- Hudspeth, A.J. (1997) How Hearing Happens. *Neuron*, **19**, 947-950.
- Hutson, M.R., Lewis, J.E., Nguyen-Luu, D., Lindberg, K.H., and Barald, K.F. (1999) Expression of Pax2 and patterning of the chick inner ear. *J Neurocytol*, **28**, 795-807.
- Itoh, M., Kim, C.H., Palardy, G., Oda, T., Jiang, Y.J., Maust, D., Yeo, S.Y., Lorick, K., Wright, G.J., Ariza-McNaughton, L., Weissman, A.M., Lewis, J., Chandrasekharappa, S.C., and Chitnis, A.B. (2003) Mind bomb is a ubiquitin ligase that is essential for efficient activation of Notch signaling by Delta. *Dev Cell*, **4**, 67-82.
- Izumikawa, M., Minoda, R., Kawamoto, K., Batts, S.A., Crumling, M.A., Wang, C.H., Abrashkin, K.A., Swiderski, D.L., Brough, D.E., Dolan, D.F., and Raphael, Y. (2004) Auditory hair cell replacement and hearing improvement after *Math1* gene therapy in deaf guinea pigs. 5th *Molecular Biology of Hearing & Deafness Meeting Abstract* **147**.
- Jacobs, J.J., Keblusek, P., Robanus-Maandag, E., Kriste, I. P., Lingbeek, M., Nederlof, P.M., van Welsem, T., van de Vijver, M.J., Koh, E.Y., Daley, G.Q., and van Lohuizen, M. (2000) Senescence bypass screen identifies TBX2, which represses Cdkn2a (p19(ARF)) and is amplified in a subset of human breast cancers. *Nat Genet*, **26**, 291-299.
- Jeffrey, P.L., Capes-Davis, A., Dunn, J.M., Tolhurst, O., Seeto, G., Hannan, A.J., and Lin, S.L. (2000) CROC-4: a novel brain specific transcriptional activator of c-fos expressed from proliferation through to maturation of multiple neuronal cell types. *Mol Cell Neurosci*, **16**, 185-196.
- Jiang, B.H., Agani, F., Passaniti, A., and Semenza, G.L. (1997) V-SRC induces expression of Hypoxia-inducible factor 1 (HIF-1) and transcription of genes encoding Vascular

- endothelial growth factor and Enolase 1: Involvement of HIF-1 in tumor progression. *Cancer Res*, **57**, 5328-5335.
- Joensuu, T., Hamalainen, R., Yuan, B., Johnson, C., Tegelberg, S., Gasparini, P., Zelante, L., Pirvola, U., Pakarinen, L., Lehesjoki, A.E., de la Chapelle, A., and Sankila, E.M. (2001) Mutations in a novel gene with transmembrane domains underlie Usher syndrome type 3. *Am J Hum Genet*, **69**, 673-684.
- Johnson, K.R., Gagnon, L.H., Webb, L.S., Peters, L.L., Hawes, N.L., Chang, B., and Zheng, Q.Y. (2003) Mouse models of USH1C and DFNB18: phenotypic and molecular analyses of two new spontaneous mutations of the Ush1c gene. *Hum Mol Genet*, **12**, 3075-3086.
- Jorgensen, J.M. and Mathiesen, C. (1988) Continuous production of hair cells in vestibular sensory organs, but not in the auditory papilla. *Naturwissenschaften*, **75**, 319-320.
- Jorgensen, J.M. (1989) Number and distribution of hair cells in the utricular macula of some avian species. *J Morphol*, **201**, 187-204.
- Jorgensen, J.M. and Christensen, J.T. (1989) The inner ear of the common rhea (*Rhea americana* L.). *Brain Behav Evol*, **34**, 273-280.
- Karis, A., Pata, I., van Doornincj, J.H., Grosveld, F., de Zeeuw, C.I., de Caprona, D., and Fritsch, B. (2001) Transcription factor GATA3 alters pathways selection of olivocochlear neurons and affects morphogenesis of the ear. *J Comp Neurol*, **429**, 615-630.
- Katagiri, T., Imada, M., Yanai, T., Suda, T., Takahashi, N., and Kamijo, R. (2002) Identification of a BMP-responsive element in Id1, the gene for inhibition of myogenesis. *Genes Cells*, **7**, 949-960.
- Kataoka, K., Igarashi, K., Itoh, K., Fujiwara, K.T., Noda, M., Yamamoto, M., and Nishizawa, M. (1995) Small Maf proteins heterodimerize with Fos and may act as competitive repressors of the NF-E2 transcription factor. *Mol Cell Biol*, **15**, 2180-2190.
- Kataoka, K., Yoshitomo-Nakagawa, K., Shioda, S., and Nishizawa, M. (2001) A set of Hox proteins interact with the Maf oncoprotein to inhibit its DNA binding, transactivation, and transforming activities. *J Biol Chem*, **276**, 819-826.
- Kawakami, K., Sato, S., Ozaki, H., and Ikeda, K. (2000) Six family genes--structure and function as transcription factors and their roles in development. *Bioessays*, **22**, 616-626, Review.
- Kawamoto, K., Ishimoto, S-I., Minoda, R., Brough, D.E., and Raphael, Y. (2003a) *Math1* gene transfer generates new cochlear hair cells in mature guinea pigs *in vivo*. *J Neurosci*, **23**, 4395-4400.

- Kawamoto, K., Yagi, M., Stover, T., Kanzaki, S., and Raphael, Y. (2003b) Hearing and hair cells are protected by adenoviral gene therapy with TGF-beta1 and GDNF. *Mol Ther*, **7**, 484-492.
- Kelsell, D.P., Dunlop, J., Stevens, H.P., Lench, N.J., Liang, J.N., Parry, G., Mueller, R.F., and Leigh, I.M. (1997) Connexin 26 mutations in hereditary non-syndromic sensorineural deafness. *Nature*, **387**, 80-83.
- Khalili, K., Del Valle, L., Muralidharan, V., Gault, W.J., Darbinian, N., Otte, J., Meier, E., Johnson, E.M., Daniel, D.C., Kinoshita, Y., Amini, S., and Gordon, J. (2003) Puralpha is essential for postnatal brain development and developmentally coupled cellular proliferation as revealed by genetic inactivation in the mouse. *Mol Cell Biol*, **23**, 6857-6875.
- Kikkawa, Y., Shitara, H., Wakana, S., Kohara, Y., Takada, T., Okamoto, M., Taya, C., Kamiya, K., Yoshikawa, Y., Tokano, H., Kitamura, K., Shimizu, K., Wakabayashi, Y., Shiroishi, T., Kominami, R., and Yonekawa, H. (2003) Mutations in a new scaffold protein *Sans* cause deafness in Jackson shaker mice. *Hum Mol Genet*, **12**, 453-461.
- Kido, T., Sekitani T., Yamashita, H., Endo, S., Okami, K., Ogata, Y., and Hara, H. (1993) The otolithic organ in the developing chick embryo. Scanning electron microscopic study on the utricular macula. *Acta Oto-Laryngologica*, **113**, 128-136.
- Kil, J., Warchol, M.E., and Corwin, J.T. (1997) Cell death, cell proliferation, and estimates of hair cell life spans in the vestibular organs of chicks. *Hear Res*, **114**, 117-126.
- Kudo, T., Kure, S., Ikeda, K., Xia, A-P., Katori, Y., Suzuki, M., Kojima, K., Ichinohe, A., Suzuki, Y., Aoki, Y., Kobayashi, T., and Matsubara, Y. (2003) Transgenic expression of a dominant-negative connexin26 causes degeneration of the organ of Corti and non-syndromic deafness. *Hum Mol Genet*, **12**, 995-1004.
- Kuntz, A.L. and Oesterle, E.C. (1998) Transforming growth factor alpha with insulin stimulates cell proliferation in vivo in adult rat vestibular sensory epithelium. *J Comp Neurol*, **399**, 413-423.
- Kurebayashi, S., Ueda, E., Sakaue, M., Patel, D.D., Medvedev, A., Zhang, F., and Jetten, A.M. (2000) Retinoid-related orphan receptor gamma (RORgamma) is essential for lymphoid organogenesis and controls apoptosis during thymopoiesis. *Proc Natl Acad Sci USA*, **97**, 10132-10137.
- Lanford, P.J., Lan, Y., Jiang, R., Lindsell, C., Weinmaster, G., Gridley, T., and Kelley, M.W. (1999) Notch signalling pathway mediates hair cell development in mammalian cochlea. *Nat Genet*, **21**, 289-292.

- Lawoko-Kerali, G., Rivolta, M.N., and Holley, M. (2002) Expression of the transcription factors GATA3 and Pax2 during development of the mammalian inner ear. *J Comp Neurol* **442**, 378-391.
- Ledford, A.W., Brantley, J.G., Kemeny, G., Foreman, T.L., Quaggin, S.E., Igarashi, P., Oberhaus, S.M., Rodova, M., Calvet, J.P., and Vanden Heuvel, G.B. (2002) Deregulated expression of the homeobox gene Cux-1 in transgenic mice results in downregulation of p27(kip1) expression during nephrogenesis, glomerular abnormalities, and multiorgan hyperplasia. *Dev Biol*, **245**, 157-171.
- Lee, K.H. and Cotanche, D.A. (1996) Potential role of bFGF and retinoic acid in the regeneration of chicken cochlear hair cells. *Hear Res*, **94**, 1-13.
- Lee, T.K., Man, K., Ling, M.T., Wang, X.H., Wong, Y.C., Lo, C.M., Poon, R.T., Ng, I.O., and Fan, S.T. (2003a) Over-expression of Id-1 induces cell proliferation in hepatocellular carcinoma through inactivation of p16INK4a/RB pathway. *Carcinogenesis*, **24**, 1729-1736.
- Lee, H.J., Chang, J.H., Kim, Y.S., Kim, S.J., and Yang, H.K. (2003b) Effect of ets-related transcription factor (ERT) on transforming growth factor (TGF)-beta type II receptor gene expression in human cancer cell lines. *J Exp Clin Cancer Res*, **22**, 477-480.
- Lee, M.J., Kim, J.Y., Suk, K., and Park, J.H. (2004) Identification of the hypoxia-inducible factor 1 alpha-responsive HGTD-P gene as a mediator in the mitochondrial apoptotic pathway. *Mol Cell Biol*, **24**, 3918-3927.
- Lengler, J. and Graw, J. (2001) Regulation of the human SIX3 gene promoter. *Biochem Biophys Res Commun*, **287**, 372-376.
- Li, S., Price, S.M., Cahill, H., Ryugo, D.K., Shen, M.M., and Xiang, M. (2002a) Hearing loss caused by progressive degeneration of cochlear hair cells in mice deficient for the Barhl1 homeobox gene. *Development*, **129**, 3523-3532.
- Li, C., Zhu, N.L., Tan, R.C., Ballard, P.L., Derynck, R., and Minoo, P. (2002b) Transforming growth factor-beta inhibits pulmonary surfactant protein B gene transcription through SMAD3 interactions with NKX2.1 and HNF-3 transcription factors. *J Biol Chem*, **277**, 38399-38408.
- Li, X., Perissi, V., Liu, F., Rose, D.W., and Rosenfeld, M.G. (2002c) Tissue-specific regulation of retinal and pituitary precursor cell proliferation. *Science*, **297**, 1180-1183.
- Li, H., Liu, H., and Heller, S. (2003a) Pluripotent stem cells from the adult mouse inner ear. *Nat Med*, **9**, 1293-1299.
- Li, H., Roblin, G., Liu, H., and Heller, S. (2003b) Generation of hair cells by stepwise differentiation of embryonic stem cells. *Proc Natl Acad Sci USA*, **100**, 13495-13500.

- Li, X., Oghi, K.A., Zhang, J., Krones, A., Bush, K.T., Glass, C.K., Nigam, S.K., Aggarwal, A.K., Maas, R., Rose, D.W., and Rosenfeld, M.G. (2003c) Eya protein phosphatase activity regulates Six1-Dach-Eya transcriptional effects in mammalian organogenesis. *Nature*, **426**, 247-54.
- Ling, M.T., Wang, X., Ouyang, X.S., Xu, K., Tsao, S.W., and Wong, Y.C. (2003) Id-1 expression promotes cell survival through activation of NF-kappaB signalling pathway in prostate cancer cells. *Oncogene*, **22**, 4498-4508.
- Liu, W., Li, G., Chien, J.S., Raft, S., Zhang, H., Chiang, C., and Frenz, D.A. (2002) Sonic hedgehog regulates otic capsule chondrogenesis and inner ear development in the mouse embryo. *Dev Biol*, **248**, 240-250.
- Louis, H.A., Pino, J.D., Schmeichel, K.L., Pomies, P., and Beckerle, M.C. (1997) Comparison of three members of the cysteine-rich protein family reveals functional conservation and divergent patterns of gene expression. *J Biol Chem*, **272**, 27484-27491.
- Macias-Silva, M., Abdollah, S., Hoodless, P.A., Pirone, R., Attisano, L., and Wrana, J.L. (1996) MADR2 is a substrate of the TGFbeta receptor and its phosphorylation is required for nuclear accumulation and signaling. *Cell*, **87**, 1215-1224.
- Manne, U., Gary, B.D., Oelschlager, D.K., Weiss, H.L., Frost, A.R., and Grizzle, W.E. (2001) Altered subcellular localization of suppressin, a novel inhibitor of cell-cycle entry, is an independent prognostic factor in colorectal adenocarcinomas. *Clin Cancer Res*, **7**, 3495-3503.
- Maroon, H., Walshe, J., Mahmood, R., Kiefer, P., Dickson, C., and Mason, I. (2002) Fgf3 and Fgf8 are required together for formation of the otic placode and vesicle. *Development*, **129**, 2099-108.
- Marzluff, W.F., Gongidi, P., Woods, K.R., Jin, J., and Maltais, L.J. (2002) The human and mouse replication-dependent histone genes. *Genomics*, **80**, 487-498.
- Mburu, P., Mustapha, M., Varela, A., Weil, D., El-Amraoui, A., Holme, R.H., Rump, A., Hardisty, R.E., Blanchard, S., Coimbra, R.S., Perfettini, I., Parkinson, N., Mallon, A.M., Glenister, P., Rogers, M.J., Paige, A.J., Moir, L., Clay, J., Rosenthal, A., Liu, X.Z., Blanco, G., Steel, K.P., Petit, C., and Brown, S.D.M. (2003) Defects in whirlin, a PDZ domain molecule involved in stereocilia elongation, cause deafness in the whirler mouse and families with DFNB31. *Nat Genet*, **34**, 421-424.
- Messina, D.N., Glasscock, J., Gish, W., and Lovett, M. (2004) An ORFeome-based analysis of human transcription factor genes and the construction of a microarray to interrogate their expression. *Genome Res*, **14**, 2041-2047.

- Mo, Y., Vaessen, B., Johnston, K., and Marmorstein, R. (1998) Structures of SAP-1 bound to DNA targets from the E74 and c-fos promoters: insights into DNA sequence discrimination by Ets proteins. *Mol Cell*, **2**, 201-212.
- Modur, V., Nagarajan, R., Evers, B.M., and Milbrandt, J. (2002) FOXO proteins regulate tumor necrosis factor-related apoptosis inducing ligand expression. Implications for PTEN mutation in prostate cancer. *J Biol Chem*, **277**, 47928-47937.
- Montcouquiol, M. and Corwin, J.T. (2001a) Brief treatments with forskolin enhance s-phase entry in balance epithelia from the ears of rats. *J Neurosci*, **21**, 974-982.
- Montcouquiol, M., and Corwin, J.T. (2001b) Intracellular signals that control cell proliferation in mammalian balance epithelia: key roles for phosphatidylinositol-3 kinase, mammalian target of rapamycin, and S6 kinases in preference to calcium, protein kinase C, and mitogen-activated protein kinase. *J Neurosci*, **21**, 570-580.
- Montcouquiol, M., Rachel, R.A., Lanford, P.J., Copeland, N.G., Jenkins, N.A., and Kelley, M.W. (2003) Identification of *Vangl2* and *Scrb1* as planar polarity genes in mammals. *Nature*, **423**, 173-177.
- Moran, J.A., Dahl, E.L., and Mulcahy, R.T. (2002) Differential induction of mafF, mafG and mafK expression by electrophile-response-element activators. *Biochem J*, **361**, 371-377.
- Morrison, A., Hodgetts, C., Gossler, A., Hrabe de Angelis, M., and Lewis, J. (1999) Expression of Delta1 and Serrate1 (Jagged1) in the mouse inner ear. *Mech Dev*, **84**, 169-172.
- Morsli, H., Choo, D., Ryan, A., Johnson, R., and Wu, D.K. (1998) Development of the mouse inner ear and origin of its sensory organs. *J Neurosci*, **18**, 3327-3335.
- Motohashi, H., Katsuoka, F., Shavit, J.A., Engel, J.D., and Yamamoto, M. (2000) Positive or negative MARE-dependent transcriptional regulation is determined by the abundance of small Maf proteins. *Cell*, **103**, 865-875.
- Navaratnam, D.S., Su, H.S., Scott, S.P., and Oberholtzer, J.C. (1996) Proliferation in the auditory receptor epithelium mediated by a cyclic AMP-dependent signaling pathway. *Nat Med*, **2**, 1136-1139.
- Noben-Trauth, K., Zheng, Q.Y., and Johnson, K.R. (2003) Association of cadherin 23 with polygenic inheritance and genetic modification of sensorineural hearing loss. *Nat Genet*, **35**, 21-23.
- Oesterle, E.C. and Rubel, E.W. (1993) Postnatal production of supporting cells in the chick cochlea. *Hear Res*, **66**, 213-224.

- Oh, S.H., Johnson, R., and Wu, D.K. (1996) Differential expression of bone morphogenetic proteins in the developing vestibular and auditory sensory organs. *J Neurosci*, **16**, 6463-6475.
- Ohtsuka, T., Ishibashi, M., Gradwohl, G., Nakanishi, S., Guillemot, F., and Kageyama, R. (1999) Hes1 and Hes5 as notch effectors in mammalian neuronal differentiation. *EMBO J*, **18**, 2196-2207.
- Ozaki, H., Nakamura, K., Funahashi, J., Ikeda, K., Yamada, G., Tokano, H., Okamura, H., Kitamura, K., Muto, S., Kotaki, H., Sudo, K., Horai, R., Iwakura, Y., and Kawakami, K. (2003) Six1 controls patterning of the mouse otic vesicle. *Development*, **131**, 551-562.
- Pan, D., Zhe, X., Jakkaraju, S., Taylor, G.A., and Schuger, L. (2002) P311 induces a TGF-beta1-independent, nonfibrogenic myofibroblast phenotype. *J Clin Invest*, **110**, 1349-1358.
- Parient, R.K. and McGhee, J.D. (2002) The GATA Family (Vertebrates and Invertebrates). *Curr Opin Genet and Devel*, **12**, 416-422.
- Park, G.T. and Morasso, M.I. (2002) Bone morphogenetic protein-2 (BMP-2) transactivates Dlx3 through Smad1 and Smad4: alternative mode for Dlx3 induction in mouse keratinocytes. *Nucleic Acids Res*, **30**, 515-522.
- Patel, J.H., Loboda, A.P., Showe, M.K., Showe, L.C., and McMahon, S.B. (2004) Analysis of genomic targets reveals complex functions of MYC. *Nat Rev Cancer*, **4**, 562-568, Review.
- Pessah, M., Marais, J., Prunier, C., Ferrand, N., Lallemand, F., Mauviel, A., and Atfi, A. (2002) c-Jun associates with the oncoprotein Ski and suppresses Smad2 transcriptional activity. *J Biol Chem*, **277**, 29094-29100.
- Peters, C.S., Liang, X., Li, S., Kannan, S., Peng, Y., Taub, R., and Diamond, R.H. (2001) ATF-7, a novel bZIP protein, interacts with the PRL-1 protein-tyrosine phosphatase. *J Biol Chem*, **276**, 13718-13726.
- Pfeffer, P.L., Gerster, T., Lun, K., Brand, M., and Busslinger, M. (1998) Characterization of three novel members of the zebrafish Pax2/5/8 family: dependency of Pax5 and Pax8 expression on the Pax2.1 (noi) function. *Development*, **125**, 3063-3074.
- Pierantoni, G.M., Bulfone, A., Pentimalli, F., Fedele, M., Iuliano, R., Santoro, M., Chiariotti, L., Ballabio, A., and Fusco, A. (2002) The homeodomain-interacting protein kinase 2 gene is expressed late in embryogenesis and preferentially in retina, muscle, and neural tissues. *Biochem Biophys Res Commun*, **290**, 942-947
- Postigo, A.A. (2003) Opposing functions of ZEB proteins in the regulation of the TGFbeta/BMP signaling pathway. *EMBO J*, **22**, 2443-2452.

- Puppin, C., Presta, I., D'Elia, A.V., Tell, G., Arturi, F., Russo, D., Filetti, S., and Damante, G. (2004) Functional interaction among thyroid-specific transcription factors: Pax8 regulates the activity of Hex promoter. *Mol Cell Endocrinol*, **214**, 117-125.
- Quackenbush, J. (2002) Microarray data normalization and transformation. *Nat Genet*, **32**, supplement 496-501.
- Raphael, Y. (1992) Evidence for supporting cell mitosis in response to acoustic trauma in the avian inner ear. *J Neurocytol*, **31**, 663-671.
- Rau, A., Legan, P.K., and Richardson, G.P. (1999) Tectorin mRNA expression is spatially and temporally restricted during mouse inner ear development. *J Comp Neurol*, **405**, 271-280.
- Renn, S.C., Aubin-Horth, N., and Hofmann, H.A. (2004) Biologically meaningful expression profiling across species using heterologous hybridization to a cDNA microarray. *BMC Genomics*, **5**, 42.
- Resendes, B.L., Williamson, R.E., and Morton, C.C. (2001) At the speed of sound: gene discovery in the auditory system. *Am J Hum Genet*, **69**, 923-935.
- Reyes, J.C., Barra, J., Muchardt, C., Camus, A., Babinet, C., and Yaniv, M. (1998) Altered control of cellular proliferation in the absence of mammalian brahma (SNF2alpha). *EMBO J*, **17**, 6979-6991.
- Riccomagno, M.M., Martinu, L., Mulheisen, M., Wu, D.K., and Epstein, D.J. (2002) Specification of the mammalian cochlea is dependent on Sonic hedgehog. *Genes Dev*, **16**, 2365-2378.
- Riley, B.B., Chiang, M-Y., Farmer, L., and Heck, R. (1999) The *deltaA* gene of zebrafish mediates lateral inhibition of hair cells in the inner ear and is regulated by *pax2.1*. *Development*, **126**, 5669-5678.
- Rivolta, M.N. and Holley, M.C. (1998) GATA3 is downregulated during hair cell development in the mouse cochlea. *J Neurocytol*, **27**, 637-647.
- Rivolta, M.N., Halsall, A., Johnson, C.M., Tones, M.A., and Holley, M.C. (2002) Transcript profiling of functionally related groups of genes during conditional differentiation of a mammalian cochlear hair cell line. *Genome Res*, **12**, 1091-1099.
- Roberson, D.W., Weisleder, P., Bohrer, P., and Rubel, E.W. (1992) Ongoing production of sensory cells in the vestibular epithelium. *Hear Res*, **57**, 166-174.
- Roberson, D.W. and Rubel, E.W. (1994) Cell division in the gerbil cochlea after acoustic trauma. *Am J Otolaryngol*, **15**, 28-34.

- Rodrigo, I., Hill, R.E., Balling, R., Munsterberg, A., and Imai, K. (2003) Pax1 and Pax9 activate Bapx1 to induce chondrogenic differentiation in the sclerotome. *Development*, **130**, 473-82.
- Ryals, B.M. and Rubel, E.W. (1988) Hair cell regeneration after acoustic trauma in adult Coturnix quail. *Science*, **240**, 1774-1776.
- Sambrook, J. and Russell, D.W., eds. (2001) *Molecular Cloning: A Laboratory Manual*. Cold Spring Harbor Laboratory Press, New York.
- Saville, M.K. and Watson, R.J. (1998) The cell-cycle regulated transcription factor B-Myb is phosphorylated by cyclin A/Cdk2 at sites that enhance its transactivation properties. *Oncogene*, **17**, 2679-2689.
- Sekiya, T., Oda, T., Matsuura, K., and Akiyama, T. (2004) Transcriptional regulation of the TGF-beta pseudoreceptor BAMBI by TGF-beta signaling. *Biochem Biophys Res Commun*, **320**, 680-684.
- Serizawa, H., Makela, T.P., Conaway, J.W., Conaway, R.C., Weinberg, R.A., and Young, R.A. (1995) Association of Cdk-activating kinase subunits with transcription factor TFIIF. *Nature*, **374**, 280-282.
- Shaulian, E., Schreiber, M., Piu, F., Beeche, M., Wagner, E.F., and Karin, M. (2000) The mammalian UV response: c-Jun induction is required for exit from p53-imposed growth arrest. *Cell*, **103**, 897-907.
- Shaulian, E. and Karin, M. (2002) AP-1 as a regulator of cell life and death. *Nature Cell Bio*, **4**, E131-E136, Review.
- Sidi, S., Friedrich, R.W., and Nicolson, T. (2003) NompC TRP channel required for vertebrate sensory hair cell mechanotransduction. *Science*, **301**, 96-99.
- Siemens, J., Lillo, C., Dumont, R.A., Reynolds, A., Williams, D.S., Gillespie, P.G., and Muller, U. (2004) Cadherin 23 is a component of the tip link in hair-cell stereocilia. *Nature*, **428**, 950-954.
- Silverstein, H., Wolfson, R.J., and Rosenberg, S. (1992) Diagnosis and management of hearing loss. *Clin Symposia*, **44**, 1-32.
- Simmons, A.D. and Lovett, M. (1999) Direct cDNA selection using large genomic DNA targets. *Methods Enzymol*, **303**, 111-126.
- Sinclair, C.S., Adem, C., Naderi, A., Soderberg, C.L., Johnson, M., Wu, K., Wadum, L., Couch, V.L., Sellers, T.A., Schaid, D., Slezak, J., Fredericksen, Z., Ingle, J.N., Hartmann, L., Jenkins, R.B., and Couch, F.J. (2002) TBX2 is preferentially amplified in BRCA1- and BRCA2-related breast tumors. *Cancer Res*, **62**, 3587-3591.

- Skurk, C., Maatz, H., Kim, H.S., Yang, J., Abid, M.R., Aird, W.C., and Walsh, K. (2004) The Akt-regulated forkhead transcription factor FOXO3a controls endothelial cell viability through modulation of the caspase-8 inhibitor FLIP. *J Biol Chem*, **279**, 1513-1525.
- Smolders, J.W. (1999) Functional recovery in the avian ear after hair cell regeneration. *Audiol Neurotol*, **4**, 286-302, Review.
- Sollner, C., Rauch, G-J., Siemens, J., Geisler, R., Schuster, S.C., the Tübingen 2000 Screen Consortium, Müller, U., and Nicolson, T. (2004) Mutations in *cadherin 23* affect tip links in zebrafish sensory hair cells. *Nature*, **428**, 955-959.
- Spritz, R.A. and Beighton, P. (1998) Piebaldism with deafness: molecular evidence for an expanded syndrome. *Am J Med Genet*, **75**, 101-103.
- Stevens, C.B., Davies, A.L., Battista, S., Lewis, J.H., and Fekete, D.M. (2003) Forced activation of Wnt signaling alters morphogenesis and sensory organ identity in the chicken inner ear. *Develop Biol*, **261**, 149-164.
- Stone, J.S. and Cotanche, D.A. (1994) Identification of the timing of S phase and the patterns of cell proliferation during hair cell regeneration in the chick cochlea. *J Comp Neurol*, **341**, 50-67.
- Stone, J.S., Oesterle, E.C., and Rubel, E.W. (1998) Recent insights into regeneration of auditory and vestibular hair cells. *Curr Opin Neurol*, **11**, 17-24.
- Stone, J.S. and Rubel, E.W. (1999) *Delta1* expression during avian hair cell regeneration. *Development*, **126**, 961-973.
- Stone, J.S., Shang, J.L., and Tomarev, S. (2004) cProx1 immunoreactivity distinguishes progenitor cells and predicts hair cell fate during avian hair cell regeneration. *Dev Dyn*, **230**, 597-614.
- Su, D., Ellis, S., Napier, A., Lee, K., and Manley, N.R. (2001) Hoxa3 and pax1 regulate epithelial cell death and proliferation during thymus and parathyroid organogenesis. *Dev Biol*, **236**, 316-329.
- Subramaniam, S., Strelau, J., and Unsicker, K. (2003) Growth differentiation factor-15 prevents low potassium-induced cell death of cerebellar granule neurons by differential regulation of Akt and ERK pathways. *J Biol Chem*, **278**, 8904-8912.
- Suzuki, T., Blank, V., Sesay, J.S., and Crawford, D.R. (2001) Maf genes are involved in multiple stress response in human. *Biochem Biophys Res Commun*, **280**, 4-8.
- Tachibana, M. (2000) MITF: a stream flowing for pigment cells. *Pigment Cell Res*, **13**, 230-240.

- Taira, T., Maeda, J., Onishi, T., Kitaura, H., Yoshida, S., Kato, H., Ikeda, M., Tamai, K., Iguchi-Ariga, S.M., and Ariga, H. (1998) AMY-1, a novel C-MYC binding protein that stimulates transcription activity of C-MYC. *Genes Cells*, **3**, 549-565.
- Tan, B.C. and Lee, S.C. (2004) Nek9, a novel FACT-associated protein, modulates interphase progression. *J Biol Chem*, **279**, 9321-9330.
- Teubner, B., Michel, V., Pesch, J., Lautermann, J., Cohen-Salmon, M., Sohl, G., Jahnke, K., Winterhager, E., Herberhold, C., Hardelin, J-P., Petit, C., and Willecke, K. (2003) Connexin30 (Gjb6)-deficiency causes severe hearing impairment and lack of endocochlear potential. *Hum Mol Genet*, **12**, 13-21.
- Torres, M., Gomez-Pardo, E., and Gruss, P. (1996) Pax2 contributes to inner ear patterning and optic nerve trajectory. *Development*, **122**, 3381-3391.
- Tsai, H., Hardisty, R.E., Rhodes, C., Kiernan, A.E., Roby, P., Tymowska-Lalanne, Z., Mburu, P., Rastan, S., Hunter, A.J., Brown, S.D., and Steel, K.P. (2001) The mouse slalom mutant demonstrates a role for Jagged1 in neuroepithelial patterning in the organ of Corti. *Hum Mol Genet*, **10**, 507-512.
- Tsue, T.T., Watling, D.L., Weisleder, P., Coltrera, M.D., and Rubel, E.W. (1994) Identification of hair cell progenitors and intermitotic migration of their nuclei in the normal and regenerating avian inner ear. *J Neurosci*, **14**, 140-152.
- Van Esch, H., Groenen, P., Nesbit, M.A., Schuffenhauer, S., Lichtner, P., Vanderlinden, G., Harding, B., Beetz, R., Bilous, R.W., Holdaway, I., Shaw, N.J., Fryns, J.P., Van de Ven, W., Thakker, R.V., and Devriendt, K. (2000) GATA3 haplo-insufficiency causes human HDR syndrome. *Nature*, **406**, 419-422.
- Verpy, E., Leibovici, M., Zwaenepoel, I., Liu, X-Z., Gal, Z., Salem, N., Mansour, A., Blanchard, S., Kobayashi, I., Keats, B.J.B., Slim, R., and Petit, C. (2000) A defect in harmonin, a PDZ domain-containing protein expressed in the inner ear sensory hair cells, underlies usher syndrome type 1C. *Nat Genet*, **26**, 51-55.
- Wallis, D., Hamblen, M., Zhou, Y., Venken, K.J., Schumacher, A., Grimes, H.L., Zoghbi, H.Y., Orkin, S.H., and Bellen, H.J. (2003) The zinc finger transcription factor Gfi1, implicated in lymphomagenesis, is required for inner ear hair cell differentiation and survival. *Development*, **130**, 221-232.
- Wallis, J.W., Aerts, J., Groenen M.A., Crooijmans, R.P., Layman, D., Graves, T.A., Scheer, D.E., Kremitzki, C., Fedele, M.J., Mudd, N.K., et al. (2004) A physical map of the chicken genome. *Nature*, **432**, 761-764.
- Wakabayashi, Y., Inoue, J., Takahashi, Y., Matsuki, A., Kosugi-Okano, H., Shinbo, T., Mishima, Y., Niwa, O., and Kominami, R. (2003) Homozygous deletions and point mutations of

- the *Rit1/Bcl11b* gene in gamma-ray induced mouse thymic lymphomas. *Biochem Biophys Res Commun*, **301**, 598-603.
- Warchol, M.E. (1995) Supporting cells in isolated sensory epithelia of avian utricles proliferate in serum-free culture. *Neuroreport*, **6**, 981-984.
- Warchol, M.E. (2002) Cell density and N-cadherin interactions regulate cell proliferation in the sensory epithelia of the inner ear. *J Neurosci*, **22**, 2607-2616.
- Warchol, M.E., Lambert, P.R., Goldstein, B.J., Forge, A., and Corwin, J.T. (1993) Regenerative proliferation in inner ear sensory epithelia of adult guinea pigs and humans. *Science*, **259**, 1619-1622.
- Warchol, M.E. and Corwin, J.T. (1996) Regenerative proliferation in organ cultures of the avian cochlea: identification of the initial progenitors and determination of the latency of the proliferative response. *J Neurosci*, **16**, 5466-5477.
- Warchol, M.E. and Hu, L. (2003) The Transcription Factor GATA3 Identifies the Position of the Striola During Sensory Regeneration the Avian Utricle. Abstract. *Assoc Res Otolaryngol* 26th Research Meeting.
- Warner, S.J., Hutson, M.R., Oh, S-H., Gerlach-Bank, L.M., Lomax, M.I., and Barald, K.F. (2003) Expression of ZIC genes in the development of the chick inner ear and nervous system. *Dev Dyn*, **226**, 702-712.
- Weil, D., Blanchard, S., Kaplan, J., Guilford, P., Gibson, F., Walsh, J., Mburu, P., Varela, A., Levilliers, J., Weston, M.D., et al. (1995) Defective myosin VIIA gene responsible for Usher syndrome type 1B. *Nature*, **374**, 60-61.
- Weil, D., El-Amraoui, A., Masmoudi, S., Mustapha, M., Kikkawa, Y., Laine, S., Delmaghani, S., Adato, A., Nadifi, S., Zina, Z.B., Hamel, C., Gal, A., Ayadi, H., Yonekawa, H., and Petit, C. (2003) Usher syndrome type I G (USH1G) is caused by mutations in the gene encoding SANS, a protein that associates with the USH1C protein, harmonin. *Hum Mol Genet*, **12**, 463-471.
- Weisleder, P., Tsue, T.T., and Rubel, E.W. (1995) Hair cell replacement in avian vestibular epithelium: supporting cell to type I hair cell. *Hear Res*, **82**, 125-133.
- Wiggins, A.K., Wei, G., Doxakis, E., Wong, C., Tang, A.A., Zang, K., Luo, E.J., Neve, R.L., Reichardt, L.F., and Huang, E.J. (2004) Interaction of Brn3a and HIPK2 mediates transcriptional repression of sensory neuron survival. *J Cell Biol*, **167**, 257-267.
- Wilkins, H.R., Presson, J.C., and Popper, A.N. (1999) Proliferation of vertebrate inner ear supporting cells. *J Neurobiol*, **39**, 527-535.

- Williams, S.C., Cantwell, C.A., and Johnson, P.F. (1991) A family of C/EBP-related proteins capable of forming covalently linked leucine zipper dimers in vitro. *Genes Dev*, **5**, 1553-1567.
- Wistow, G.J., Lietman, T., Williams, L.A., Stapel, S.O., de Jong, W.W., Horwitz, J., and Piatigorsky, J. (1988) Tau-crystallin/alpha-enolase: one gene encodes both an enzyme and a lens structural protein. *J Cell Biol*, **107**, 2729-2736.
- Wittwer, C.T., Herrmann, M.G., Moss, A.A., and Rasmussen, R.P. (1997) Continuous fluorescence monitoring of rapid cycle DNA amplification. *BioTechniques*, **22**, 130-138.
- Wolfinger, R.D., Gibson, G., Wolfinger, E.D., Bennett, L., Hamadeh H., Bushel P., Afshari C., and Paules R.S. (2001) Assessing gene significance from cDNA microarray expression data via mixed models. *J Comput Biol*, **8**, 625-637.
- Wong, G.K., Liu, B., Wang, J., Zhang, Y., Yang, X., Zhang, Z., Meng, Q., Zhou, J., Li, D., Zhang, J, et al. (2004) A genetic variation map for chicken with 2.8 million single-nucleotide polymorphisms. *Nature*, **432**, 717-722.
- Wright, T.J. and Mansour, S.L. (2003) Fgf3 and Fgf10 are required for mouse otic placode induction. *Development*, **130**, 3379-3390.
- Wu, K., Yang, Y., Wang, C., Davoli, M.A., D'Amico, M., Li, A., Cveklova, K., Kozmik, Z., Lisanti, M.P., Russell, R.G., Cvekl, A., and Pestell, R.G. (2003) DACH1 inhibits transforming growth factor-beta signaling through binding Smad4. *J Biol Chem*, **278**, 51673-51684.
- Xiang, M., Gan, L., Li, D., Chen, Z., Zhou, L., O'Malley, B.W. Jr., Klein, W., and Nathans, J. (1997) Essential role of POU-domain factor Brn-3c in auditory and vestibular hair cell development. *Proc Natl Acad Sci USA*, **94**, 9445-9450.
- Yamashita, H. and Oesterle, E.C. (1995) Induction of cell proliferation in mammalian inner-ear sensory epithelia by transforming growth factor-alpha and epidermal growth factor. *Proc Natl Acad Sci USA*, **92**, 3152-3155.
- Yang, X., Menon, S., Lykke-Andersen, K., Tsuge, T., Di, Xiao, Wang, X., Rodriguez-Suarez, R.J., Zhang, H., and Wei, N. (2002) The COP9 signalosome inhibits p27(kip1) degradation and impedes G1-S phase progression via deneddylation of SCF Cul1. *Curr Biol*, **12**, 667-672.
- Zelante, L., Gasparini, P., Estivill, X., Melchionda, S., D'Agruma, L., Govea, N., Mila, M., Monica, M.D., Lutfi, J., Shohat, M., Mansfield, E., Delgrosso, K., Rappaport, E., Surrey, S., and Fortina, P. (1997) Connexin26 mutations associated with the most common form of non-syndromic neurosensory autosomal recessive deafness (DFNB1) in Mediterraneans. *Hum Mol Genet*, **6**, 1605-1609.

- Zenner, H.P. (1986) K⁺-induced motility and depolarization of cochlear hair cells. Direct evidence for a new pathophysiological mechanism in Meniere's disease. *Arch Otorhinolaryngol*, **243**, 108-111.
- Zenner, H.P., Reuter, G., Zimmermann, U., Gitter, A.H., Fermin, C., and LePage, E.L. (1994) Transitory endolymph leakage induced hearing loss and tinnitus: depolarization, biphasic shortening and loss of electromotility of outer hair cells. *Eur Arch Otorhinolaryngol*, **251**, 143-153.
- Zhao, Y., Yamoah, E.N., and Gillespie, P.G. (1996) Regeneration of broken tip links and restoration of mechanical transduction in hair cells. *Proc Natl Acad Sci USA*, **93**, 15469-15474.
- Zheng, J.L., Helbig, C., and Gao, W.Q. (1997) Induction of cell proliferation by fibroblast and insulin-like growth factors in pure rat inner ear epithelial cell cultures. *J Neurosci*, **17**, 216-226.
- Zheng, J.L., Keller, G., and Gao, W.Q. (1999) Immunocytochemical and morphological evidence for intracellular self-repair as an important contributor to mammalian hair cell recovery. *J Neurosci*, **19**, 2161-2170.
- Zheng, J.L., Shou, J., Guillemot, F., Kageyama, R. and Gao, W-Q. (2000a) *Hes1* is a negative regulator of inner ear hair cell differentiation. *Development*, **127**, 4551-4560.
- Zheng, J.L. and Gao, W-Q. (2000b) Overexpression of *Math1* induces robust production of extra hair cells in postnatal rat inner ears. *Nature*, **3**, 580-586.
- Zheng, W., Huang, L., Wei, Z-B., Silvius, D., Tang, B., and Xu, P-X. (2003) The role of *Six1* in mammalian auditory system development. *Development*, **130**, 3989-4000.
- Zhou, S., Zawel, L., Lengauer, C., Kinzler, K.W., and Vogelstein, B. (1998) Characterization of human FAST-1, a TGF beta and activin signal transducer. *Mol Cell*, **2**, 121-127.
- Zhou, J., Ma, J., Zhang, B.C., Li, X.L., Shen, S.R., Zhu, S.G., Xiong, W., Liu, H.Y., Huang, H., Zhou, M., and Li, G.Y. (2004) BRD7, a novel bromodomain gene, inhibits G1-S progression by transcriptionally regulating some important molecules involved in ras/MEK/ERK and Rb/E2F pathways. *J Cell Physiol*, **200**, 89-98.
- Zine, A., Van De Water, T.R., and de Ribaupierre, F. (2000) Notch signaling regulates the pattern of auditory hair cell differentiation in mammals. *Development*, **127**, 3373-3383.
- Zine, A., Aubert, A., Qui, J., Therianos, S., Guillemot, F., Kageyama, R., and de Ribaupierre, F. (2001) *Hes1* and *Hes5* activities are required for the normal development of the hair cells in the mammalian inner ear. *J Neurosci*, **21**, 4712-4720.

Website References

ATCC Library/Clone resource: www.atcc.org

BBSRC (University of Delaware) chicken finished cDNAs (July 2004, 19,626 sequences):
<http://www.chickest.udel.edu/>

GeneCluster 2.0 (MIT) for Self-Organizing Maps: www.broad.mit.edu

Gene Ontology (GO): www.geneontology.org

Hereditary Hearing Loss Homepage (HHH): <http://webhost.ua.ac.be/hhh/>

Human Unigene Build #175 (54,560 unique sequences):
<ftp://ftp.ncbi.nlm.nih.gov/repository/UniGene/>

KEGG: www.genome.jp/kegg/

Lovett Laboratory website: <http://hg.wustl.edu>

Microarray gene list: <http://hg.wustl.edu/lovett/projects/nohr/TFarray.html>

Microarray control tag sequences: <http://hg.wustl.edu/lovett/projects/nohr/intlctrl.html>

National Institute on Deafness and Other Communication Disorders:
<http://www.nidcd.nih.gov/health/statistics/hearing.asp>

NCBI chicken ESTs (492,640 G. gallus sequences extracted from):
<ftp://ftp.ncbi.nlm.nih.gov/blast/db/FASTA>

NCBI Genbank Per-organism statistics: <ftp://ftp.ncbi.nih.gov/genbank/gbrel.txt>

NCBI Entrez Gene : www.ncbi.nlm.nih.gov/entrez/query.fcgi?db=gene

SAS code from Wolfinger et al.: <http://statgen.ncsu.edu/ggibson/Manual.html>

Subtraction sequence and contigs: http://hg.wustl.edu/lovett/Gg_utr/

The Institute for Genome Research (TIGR) chicken gene index: <http://www.tigr.org/tdb/tgi/gggi/>

TIGR BLAST: <http://tigrblast.tigr.org/tgi/>

TIGR TMEV2.2 and MIDAS2.17 Programs for array analysis: <http://www.tigr.org>

VITA

Raymond David Hawkins was born in Greenville, Texas, on October 24, 1973, the son of Carol Jane Hawkins and Hershel Dean Hawkins. He graduated from DeSoto High School, DeSoto, Texas in May of 1992. After attending the University of Oklahoma for two years, majoring in chemical engineering, he transferred to the University of Texas at Austin. He graduated from UT with a Bachelor of Science in Biochemistry in May of 1997. He became the first person in his family to obtain a college degree. In the Fall of 1997, he entered the Graduate School of Biological and Biomedical Sciences at the University of Texas Southwestern Medical Center at Dallas. After two years in Dallas, he relocated with his mentor to Washington University School of Medicine in St. Louis to finish his dissertation research. He will be awarded the degree of Doctor of Philosophy in Genetics and Development in June of 2005. In October of 2004, he married Tandi Louise Collisson.

Permanent Address: 125 E. 5th Street
Lancaster, Texas 75146